A MODAL APPROACH TO INDUCTION MOTOR DYNAMICS

Boon-Teck Ooi, B.E.Hons. (U. of Adelaide), S.M., E.E. (M.I.T.)

A MODAL APPROACH TO INDUCTION MOTOR TRANSIENTS

Electrical Boon-Teck Ooi, B.E. Hons. (U. of Adel.) S.M.E.E. (M.I.T) Ph.D.

ABSTRACT

The acceleration transients and the asymptotic stability of the balanced 3 - phase induction motor operating from a balanced single frequency voltage supply have been investigated by a combination of numerical techniques and analytical methods. A critical review is given for the various reference frame formulations of the induction motor dynamics and the efficiency of the methods for solving the dynamic equations has been assessed. The modal approach is presented as a comprehensive framework around which the numerical results are systematically organized and such disparate subjects as acceleration transients, asymptotic stability and nonsimultaneous switching are unified.

Detailed attention is given to the identification of the physical modes and to understanding their behavioral changes as a function of rotor speeds. Asymptotic stability is studied by linearization through small signal perturbations. Quadratic Liapunov Functions are proposed and it is shown that a Liapunov Function associated with the Total Energy can be used to prove Asymptotic Stability in the Large. Eigenvalue sensitivity with respect to system parameters is also presented. The m.m.f. spacevector viewpoint is presented to give a physical description of the modes, the airgap magnetic field interactions in the production of transient torque, and the possibility of supersynchronous speeds during transients.

A MODAL APPROACH TO INDUCTION MOTOR DYNAMICS

by

Boon-Teck Ooi, B.E. (Hons.), (U.of Adel.), S.M. (M.I.T.)

Department of Electrical Engineering

McGill University,

Montreal, Quebec.

A MODAL APPROACH TO INDUCTION MOTOR DYNAMICS

by

Boon-Teck Ooi, B.E. (Hons.), (U. of Adelaide), S.M. (M.I.T.)

A thesis submitted to the Faculty of Graduate Studies and Research in partial fulfillment of the requirements for the degree of Doctor of Philosophy.

Department of Electrical Engineering,

McGill University,

Montreal, Quebec,

February, 1970.

[ⓒ] Boon-Teck Ooi 1970

CLAIM OF ORIGINALITY

To the best of the author's knowledge the following contributions are original.

- 1. The application of modal analysis to solve and classify the constant speed transients of the induction motor and an explanation of controlled nonsimultaneous switching in terms of mode suppression.
- 2. Investigation of the behaviour of the induction motor modes as they interact with rotor speed; and proof for the damping coefficients sum invariance with respect to rotor speed.
- 3. Identification of the physical modes through sub-primitive approximations; and proof that the induction motor modes approximate asymptotically the modes of the loss-less sub-primitive at high rotor speeds.
- 4. Proof for the Eigenvector Rotational Property; and representation of the physical modes through m.m.f. space-vectors associated with the eigenvector.
- 5. Derivation of a formula which expresses the damping coefficient as components of energy storage and power dissipation associated with the mode.
- The application of the Direct Method of Liapunov to explore the region of asymptotic stability, and proof that whenever the total energy of the induction motor can be shown to be a Liapunov Function, then the equilibrium point is asymptotically stable in the large.

- 7. Unification of switching transient studies with stability studies through eigenvalues identification.
- 8. Investigation of eigenvalue sensitivities with respect to motor parameters and development of efficient computer methods for the calculation of the sensitivity indices.
- 9. The physical interpretation of switching transients, supersynchronous rotor speeds, and modes through m.m.f. space
 vectors; and the definition of the instantaneous airgap
 power in terms of the angular velocity of the resultant airgap
 magnetization space vector.

ABSTRACT

The acceleration transients and the asymptotic stability of the balanced 3 - phase induction motor operating from a balanced single frequency voltage supply have been investigated by a combination of numerical techniques and analytical methods. A critical review is given for the various reference frame formulations of the induction motor dynamics and the efficiency of the methods for solving the dynamic equations has been assessed. The modal approach is presented as a comprehensive framework around which the numerical results are systematically organized and such disparate subjects as acceleration transients, asymptotic stability and nonsimultaneous switching are unified.

Detailed attention is given to the identification of the physical modes and to understanding their behavioral changes as a function of rotor speeds. Asymptotic stability is studied by linearization through small signal perturbations. Quadratic Liapunov Functions are proposed and it is shown that a Liapunov Function associated with the Total Energy can be used to prove Asymptotic Stability in the Large. Eigenvalue sensitivity with respect to system parameters is also presented. The m.m.f. spacevector viewpoint is presented to give a physical description of the modes, the airgap magnetic field interactions in the production of transient torque, and the possibility of supersynchronous speeds during transients.

ACKNOWLEDGEMENTS

My sincere appreciation is extended to the following persons:

Dr. T.H. Barton, who is my research supervisor. He has expedited this research with substantial assistance and has guided and encouraged me with a wise and nice mix of direction and latitude.

Drs. Belanger, R.E. Burridge, T.E. Dy Liacco, T.C. Lim and Peter Morrison, for many helpful and fruitful discussions.

The Nakra's, the Hamblin's, the Taal's and the Yu's, for their friendship and good counsel.

Mrs. P. Hyland and Mrs. Soulellis for their patience and skill in the preparation of this manuscript.

TABLE OF CONTENTS

			Page
ABSTRACT			i
ACKNOWLE	DGEMEN.	тѕ	ii
TABLE OF C	○ NITENITS		
			iii
LIST OF ILLU	JSTRATIO1	NS	vii
NOMENCLA	TURE		×
CHAPTER	I	INTRODUCTION	1
	1-1	Induction Motor Dynamic Problems in Industry	1
	1 <i>-</i> 2 1 <i>-</i> 3	Historical Review Outline of the Problem	2 4
	, ,	Comme of the Problem	4
CHAPTER	11	REFERENCE FRAMES	8
	2-1	Basic Induction Motor Equations – abc Frame	9
	2-2 2-3	3 - Phase Digital Model	12
	2-4	Three–Phase to Two–Phase Transformations The α – β Reference Frame	12
	2-5	The d - q Reference Frame	14 16
	2-6	Common Reference Frame Transformations	18
	2-7	The Synchronously Rotating Frame	19
	2-8	The Complex Transformations	22
	2-9	Instantaneous Symmetrical Components	22
	2-10	Cylindrical Symmetry	24
	2-11	Space – Vector Representation	25
	2-12 2-13	Space–Vector Viewpoint of Electromagnetic Torque Space Vector Viewpoint in Synchronously Rotat–	28
		ing Frame	29
CHAPTER	111	NONLINEAR SWITCHING TRANSIENTS	30 .
	3-1	Statement of the Problem	
	3-2	Nature of Dynamic Equations	30
	3-3	Constant Speed Approximations	31 32
	3-4	Approximations for Variable Speed Torques	32 32
	3-5	Analogue Computer Solutions	33
	3-6	Solutions by Numerical Integration	34
	3-7	Numerical Integration with Digital Computers	36

			ÌΥ
			Page
	3-8	Choice of Reference Frame	36
	3-9	Choice of Integration Subroutines	40
	3-10	Choice of Strategy in Integration Step-Size Control	45
	3-11	Modified Integration Algorithms	50
	3-12	Terminal Voltage and Initial Value Problems	51
	3-13	Numerical Examples	59
	3-14	Torque Transients in Synchronous Switching	60
	3-15	Supersynchronous Motoring Torque	66
	3-16	Instantaneous Airgap Power	67
CHAPTER	IV	MODAL ANALYSIS OF CONSTANT SPEED INDUCTION MOTOR EQUATIONS	70
		INDUCTION MOTOR EQUATIONS	72
	4-1	Introduction , ,	72
	4-2	Constant Speed Linearization	73
	4-3	The Constant Speed Induction Motor Equations	74
	4-4	The Modal Analysis	77
	4-5	Eigenvalues and Eigenvectors	80
	4-6	Eigenvalue and Eigenvector Subroutines	82
	4-7	Constant Speed Transients in Induction Motors	83
	4-8	A Numerical Example	83
	4-9	Transient Solutions	87
	4-10	Components of Electromechanical Torque	92
	4-11	Constant Speed Eigenvalue Loci	96
	4-12	Patterns of Constant Speed Transient Torques	98
	4-13	Modal Excitation Due to Initial Currents	107
	4-14	Modal Excitation by Voltage Supply	110
	4-15	Mode Suppression and Nonsimultaneous Switching	110
CHAPTER	V	IDENTIFICATION, BEHAVIOUR AND INTERPRE-	
		TATION OF INDUCTION MOTOR MODES	115
	5-1	Introduction	115
	5-1-1	Damping Coefficients Sum Invariance	119
	5-2	Natural Frequencies of Oscillation Sum	119
	5- 3	The Transient Subprimitives	121
	5-4	The Transformer Subprimitive	123
	5-5	The Magnetization Subprimitive	125
	5-6	The Lossless Subprimitive	128
	5-6-1	Asymptotic Approximation	133
	5 - 7	Eigenvector Rotational Property	135
	5- 8	Mode Representation by Eigenvectors	136
	5-8-1	Space Vector Diagrams	138
	5-9	Modal Representation in Free Motion	146
	5-10	Damping Factor Structure	147
	5-10-1	Negative Dissipation	148

			Page
	5-10-2 5-11 5-11-1	Damping Factor Variations with Speed Structure of Natural Frequency of Oscillation Natural Frequency Variation with Speed	149 154 158
CHAPTER	٧ı	INDUCTION MOTOR STABILITY	162
	6-1 6-2 6-3 6-4 6-5 6-6 6-7 6-8 6-9	Introduction Induction Motor Equation for Stability Study Small Signal Linear Approximation Stability of the Operating Point Stability of Operating Points Over Speed Range Eigenvalue Identification The Direct Method of Liapunov Total Energy as a Liapunov Function Asymptotic Stability in the Large in Induction Motors Stability Bounds from Quadratic Liapunov Functions	162 163 167 167 168 176 183 186
CHAPTER	VII	PARAMETRIC SENSITIVITY	198
	7-1 7-2 7-3 7-4 7-5	Introduction Eigenvalue Sensitivity Calculation of Eigenvalue Sensitivity Numerical Example Significance of Eigenvalue Sensitivity Indices	198 198 199 201 204
CHAPTER	VIII	SUMMARY AND CONCLUSIONS	207
	8-1 8-2 8-3	Summary Conclusions Suggestions for Future Work	207 208 213
APPENDIX	Α	INDUCTION MOTOR POWER EQUATION	215
APPENDIX	В	INSTANTANEOUS AIR-GAP POWER	217
APPENDIX	С	EIGENVALUE ROTATIONAL PROPERTY	220
APPENDIX	D	MODE OSCILLATOR FREQUENCY	223
APPENDIX	Е	A METHOD OF CONSTRUCTING THE POSITIVE DEFINITE [P] MATRIX	225
APPENDIX	F	SIMULTANEOUS EQUATIONS FOR SOLVING	227

•

LIST OF ILLUSTRATIONS

Figure No.	Title	Page
2-1 (a), (b), (c)	M. M. F. Space Vectors	27
3-1	Reswitching Sequences	56
3-2	Torque and Speed Transients in Simultaneous Switching for $J_1 = 0.0006 \text{ Kg.} - \text{m}^2$.	61
3-3	Switching Current Referred to $d-q$ Frame and Synchronously Rotating $\chi-\delta$ Frame	62
3-4(a)	Simultaneous Switching Transients for $J_1 = 0.06 \text{ Kgm}^2$	63
3-4 (b)	Magnitudes of Space–Vectors in Simultaneous Switching Transient	64
3-4(c)	Space-Vector Angles Referred to Synchronous Reference Frame	65
3-5(a)	Switching Transients Showing the Occurrence of Supersynchronous Speed and Motoring Torque	68
3-5(b)	Rotor Angular Velocity and Instantaneous Angu- lar Velocity of Magnetization Flux Vector	69
3-5(c)	Airgap Power and Electromechanical Power Output	70
4-1	Flow Chart of Program to Solve for Induction Motor Transient at a Constant Speed	84
4-2	d – q Axes Eigenvalue Loci of Induction Motor	97
4-3(a)	Electromechanical Torque at Simultaneous Switching – Rotor at Standstill	99
4-3(b)	Components of Torque - Rotor at Standstill	100
4-4 (a)	Electromechanical Torque in Simultaneous Switching - Rotor at 0.5 p.u. Synchronous Speed	102

Figure No.	Title		
4-4 (b)	Components of Torque Rotor at 0.5 p.u. Synchronous Speed		
4-5(a)	Electromechanical Torque in Simultaneous Switching – Rotor at 0.9 p.u. Synchronous Speed	105	
4-5(b)	Components of Torque – Rotor at 0.9 p.u. Synchronous Speed	106	
4-6	Free Motion of Induction Motor Modes at Rotor Standstill (a) Magnetization Mode (λ_2) , (b) Leakage Inductance Mode $(\ \lambda_1)$	108	
4-7	Switching Torque and Speed Pattern when the Magnetization Mode is Suppressed by Non-simultaneous Switching	113	
5-1.	Variation of Damping Factors with Rotor Speed	118	
5-2	Variation of Natural Frequencies with Rotor Speed	120	
5- 3	(a) Equivalent Circuit of Transformer Subprimitive		
	(b) The Leakage Inductance Mode	124	
	(c) The Magnetization Inductance Mode		
5-4	M.M.F. Vector Representation of Modes		
•	(a) Rotor Speed = 0.0 rad./sec.	139	
	(b) Rotor Speed = 0.04 p.u.	140	
	(c) Rotor Speed = 0.1 p.u.	141	
	(d) Rotor Speed = 0.4 p.u.	142	
	(e) Rotor Speed = 0.48 p.u.	143	
	(f) Rotor Speed = 1.0 p.u.	144	
5-5(a)	Dissipative Components of σ_1	150	
5-5(b)	Energy Storage Components of σ_1	1.51	
5-6 (a)	Dissipative Components of σ_2	152	
5-6(b)	Energy Storage Components of σ_2	153	

		i×
Figure No.	<u>Title</u>	Page
5-7	Structural Components of ω_1 / ω_m	159
5-8	Structural Components of ω_2/ω_m	160
6-1	Small Perturbation Eigenvalues in Stationary Reference Frame	169
6-2	Induction Motor Torque – Speed Characteristics of Different Supply Frequencies	170
6-3(a)	Damping Factor of Heavily Damped Electrical Mode as a Function of Operating Point	172
6-3 (b)	Natural Frequency of Heavily Damped Electrical Mode as Function of Operating Point	173
6-4(a)	Damping Factor of Lightly Damped Magnetization Mode as Function of Operating Point	174
6-4 (b)	Natural Frequency of Lightly Damped Magnetiza- tion Mode as Function of Operating Point	175
6-5	Damping Factor of Mechanical Mode as Function of Operating Point	177
6-6	Estimate of Mechanical Damping Factor from Tangent of Torque Speed Curve	178
6-7 (a)	Dependence of the Damping Factors of the Electrical Modes on the Moment of Inertia	181
6-7(b)	Dependence of the Natural Frequencies of Oscillation of the Electrical Modes on the Moment of Inertia	182
6-8	Operating Points M. N. Defined by Intersection of Motor Torque – Speed Curve and Load Line	190

NOMENCLATURE

Matrices

__

Complex conjugate.

 $[]^T$

Transpose.

[]

Inverse.

a, b, c

Subscripts of 3 - phase quantities.

a =

 $(-\frac{1}{2} + i\frac{\sqrt{3}}{2})$

Equation 2 - 17

[A]

 5×5 matrix of linearized perturbation equations of induction motor about an operating point.

[Adq], [Ay8]

 4×4 matrix of the induction motor at a constant speed referred to d - q axes, χ - δ axes.

[B]

 5×5 matrix of energy storage elements defined in Equation 6 - 25.

[B_{dq}], [B ₈₈]

 4×4 matrix coupling state to forced excitation, in d - q axes (Equation 4 - 3), in $\chi - \delta$ axes (Equation 4 - 7).

[c]

 5×5 matrix defined in Equation 6 - 30.

 $\begin{bmatrix} C^{abc} \end{bmatrix}, \begin{bmatrix} C^{\alpha\beta} \end{bmatrix}, \\ 0_{\alpha\beta} \qquad dq \end{bmatrix}$

Connection matrices defined in Equations .2 - 5, .2 - 9, .2 - 12.

[Cdq]

d q

Subscripts for direct and quadrature axes.

 e^{s} , e^{r} abc

Vectors of stator and rotor voltages in a, b, c frame.

e^s , e^r , ...

Instantaneous voltage in stator direct axis, in rotor \mathcal{X} - axis.

 $\frac{e}{-}\alpha\beta$, $\frac{e}{-}dq$, $\frac{e}{-}$ $\delta\delta$

Vector of voltages in $\alpha - \beta$, d - q and $\chi - \delta$ axes frames.

Ep

Peak of sinusoidal time varying voltage excitation.

Eγδ

Steady-state voltage vector in 3-8 frame.

f

Supply frequency Hertz.

f

Viscous damping.

 $\frac{f}{n}$

Vector of nonlinear terms of perturbation variables, Equation 6 – 11.

3, 3, 3mm

Magnitudes of space vectors representing the stator, the rotor and the resultant airgap m.m.fs. (Equations 2-19, 2-20, 2-21).

 \underline{F} (\underline{Y}, t)

Vector of a general function in \underline{Y} and t .

[G w_m]

 4×4 motional inductance matrix (Equation 6 - 2).

[H₁₁],[H₁₂],

Submatrices of [A] (Equation 6 - 6).

 $[H_{21}], [H_{22}]$

h

Integration stepsize.

<u>|</u> 88

Vector of steady-state currents in &- & frame.

Ī

Instantaneous current.

Ĭ

General current vector.

i (0) General current vector at t = 0. i = 1, 2, 3 ...Numerical index. [I]Unit square matrix. Moment of inertia of motor $(Kg - m^2)$ J k^s , k^r Coefficient of coupling between two coils of the stator, rotor. Stator, rotor self inductance of one phase in abc frame. Ls, Lr Stator, rotor self inductance in 2 phase equivalents. [[] General inductance matrix. Is, Ir Stator, rotor leakage inductance. M^1 Maximum mutual inductance between a stator phase and a rotor phase in a b c frame. M Maximum mutual inductance between one phase and a rotor phase in 2 - phase equivalent. Subscript for mechanical quantities. m Number of pole - pairs. n Subscript for negative sequence (Equation 2 - 16).

Subscript for zero sequence (Equation 2 - 16).

0

p

Subscript for positive sequence (Equation 2 - 16).

p

$$=\frac{d}{dt}$$
.

[P]

 5×5 positive definite matrix (Equation 6 - 35) .

pa;

The ith parameter of the system.

Pag

Airgap power.

P_{rk} , P_{sk}

Defined Equation 5 - 57, Equation 5 - 58.

q

Subscript for quadrature axis.

91 , 92 , 93, 94

Modal variables.

 Q_{1t} Q_{2t} Q_{ss}

Modal vector of solutions in 1st mode, 2nd mode and steady-state.

 R^{s} , R^{r}

Stator, rotor resistance of phase.

[R]

General resistance matrix.

r

Subscript for rotor

S

Subscript for stator.

[S ₈], [S_{dq}]

Eigenvector matrix in χ -8 frame, d-q frame.

 \mathbf{T}_{em}

Electromechanical torque (Newton-metre).

TL

Load torque (Newton-metre).

T

Superscript denotes transpose.

 T_1 , T_2 ... T_6

6 components of transient torque.

Time (second). †]-'[†]]+ Instant before, after disconnection. Instant before, after reconnection. [T]Matrix defined in Equation 4 - 39. ΔT Differential change of torque in torque speed curve. Eigenvector of the kth eigenvalue. $\frac{U}{k}$ Û Eigenvector of the transpose of [A]. U_-1 Unit step function. V (x) Liapunov Function. ٧٥ Minimum value of $V(\underline{x})$ on $W(\underline{x}) = 0$. [\] 5 x 5 symmetric matrix proposed for Liapunov Function Equation 6 - 33. Ľ General voltage vector. W (x) Time derivative of Liapunov Function Equation 6 - 27. [w] Matrix defined in Equation 4 - 41. 5×1 column of perturbation state variables obtained × from small signal linearization about equilibrium operating point. Y (t) General time function vector.

the nth sequence of Y.

Υn

<u>z</u> (†) General time function vector. Z (x) Scalar function defined in Equation 6 - 40. Subscript for a - axis. α Switching angle at which two phases of the motor are connected to the three-phase supply. The Kth coefficient. αK · Subscript for β -axis. β Delay angle in nonsimultaneous switching at which the β_s third phase of the moror is connected to the three-phase supply. β_k , β_{ik} Constant coefficients. Subscript for 8-axis. X Subscript for δ - axis. δ Rotor position (radians). ith eigenvalue. λ $[\Lambda_{8}], [\Lambda_{dq}]$ Diagonal matrix of eigenvalues in $\chi - \delta$, d - q frame. Constant. μ ρ [A] Spectral radius of the matrix A. Real part of λ_i , damping factor. σ_{i} Total dissipation of kth mode.

$\sum_{\mathbf{sk}}$	Total energy storage of kth mode.
T	Dummy variable.
ø _s , ø _r , ø _m	Space phase angles of the stator, the rotor and the resultant airgap m.m.f. vectors.
ø _m	Angular velocity of resultant airgap m.m.f. space vector.
[Φ]	Rotational matrix defined in Equation 5 - 36.
$\underline{\psi}$	General flux linkage vector.
ω_{m}	Rotor angular velocity.
− ω m	Operating rotor angular velocity.
$\omega_{ extsf{f}}$	Line frequency.
·ω _c	Angular velocity of rotating common reference frame.
Δ ω _m	Differential change in rotor angular velocity in

torque-speed curve.

CHAPTER I

INTRODUCTION

1-1 Induction Motor Dynamic Problems in Industry

At least two recent developments have made the study of the induction motor dynamics both relevant and important:

- (a) The increasing use of large horse-power induction motors with direct-on-line switching.
- (b) The development of solid-state variable frequency inverters which make variable speed induction motor operation economically feasible.

The problem associated with the first application is the existence of large pulsating transient torques. For example, strain gauge measurements on a 200 H P experimental pulp refiner at the Pulp and Paper Research Institute, Pointe Claire, have recorded torques which are as high as 20 times the rated torque of the motor. Undoubtedly, these large transient torques have contributed to the frequent shaft key failures in pulp refiners.

The problem related to the use of the induction motor as a variable speed drive is one of stability. Although the induction motor is known to be highly stable at 60 Hz operation, there have been reports of unstable or very lightly damped operating points at low frequency operations.

Because of the topical and the practical nature of the problems, research on the dynamics of the induction motor has been an area of active interests.

1-2 Historical Review

The patent for the induction motor was granted to Nikolai Tesla in 1888. The study of its dynamic characteristics, however, had to wait until the development of dynamic circuit theory of electric machinery by Kron [1], his precursors [2-3] and successors [4-7]. Unfortunately, dynamic circuit theory merely formulates the problem in the differential form and the ensuing task of solving the non-linear equations had to await the development of powerful digital computers.

Attempts at solving the nonlinear differential equation in its entire form were made since the 1940's, at first using the differential analysers [8–11], then using the analogue computers [12–14], and in the late 1960's using numerical techniques in conjunction with the digital computer [15–18]. Those who favoured the analytical solution have found it possible to linearise the system equations by making the constant speed assumption and subsequently using the Laplace Transform to solve for the electrical transients [16 and 19–22]. Solution of the variable speed problem has also been found to be analytically possible by assuming the stator resistance to be negligible, an assumption which corresponds to using the constant flux linkage theorem [23].

Most of the papers have been of a theoretical nature and have been concerned with the speed and current transients. It is not until around 1965 that

suitable torque recording equipment produced confirmable experimental results which establish the dynamic induction equations with confidence, especially in respect to the pattern of transient torques.

To date, the experimentally confirmable knowledge on switching torque transients resides mainly in the publications of three research groups, Wood et al [15, 22, 29], Enslin et al [21] and Smith et al [16,17]. Their research which followed almost on identical lines, consisted of:

- (a) producing experimental transient torque patterns which correlated closely with the digital computer solutions and
- (b) using the characteristic roots of the constant speed linear equations to classify and explain the torque components.

It was around 1965 that the stability problem becomes of interest. Motivated by a practical problem involving the stability of mill-motors, G.J. Rogers [24] analysed the small-perturbation linearised dynamic equations using the root-locus technique. He found that the motor understudy becomes very lightly damped at low frequency operation but is still stable. Since then, Nelson Lipo and Krause [25] and Fallside and Wortley [26] have found parameter combinations for which the induction motor can be truly electrically unstable. The paper by Fallside and Wortley contains correlated experimental and theoretical stability boundaries. This paper together with the experimental and theoretical studies on power synchro dynamics by Burridge and Barton [27] confirm the soundness of using small perturbation linearization for stability studies in induction motors.

In closing this historical survey, it is worthwhile itemizing some of the important physical phenomena which have been discovered in the dynamic studies throughout the years, but for which there has been no adequate explanation in existing induction motor theory.

- (a) Since 1941 [28], it has been noted that during a switching transient, the induction motor may exceed the synchronous speed.
- (b) By controlled nonsimultaneous switching, it is possible to suppress undesirable transient torque components. [13,21, 22, 29].
- c) The characteristic roots of the linearised constant speed equations change with the rotor speed. [21, 22]. In particular the damping factor of the dominant root decreases with speed suggesting its inter-relationship with instability at low frequency operation and prolonged switching transients.

1-3 Outline of the Problem

Although the literature shows that there has been extensive research on induction motor dynamics, much of the results exist in the raw, undigested and fragmentary form. Different facets of the problem have been solved in isolation, each unrelated to the other. The methods employed are of varying merits and there is a

need to review their effectiveness from points of view of efficiency, accuracy and modern practice. There is need to find a mathematical formulation with sufficient scope to provide a unifying viewpoint. Furthermore there are still vast patches of ignorance to be explored especially with respect to the curious dynamic phenomena itemized above. Finally, there has been a general lack of physical interpretation.

In an attempt to remedy some of these deficiencies and to contribute towards the development of the theory of induction motor dynamics, there are four objectives which are interwoven in the chapters of this thesis.

(a) Review

The existing literature is reviewed with the purpose of evaluating the merits of each reference frame formulation of the dynamic equations (Chapter II) and assessing the efficacy of the methods for solving them (Chapter III).

(b) Presenting a Unified Viewpoint

Throughout this thesis, the results of modern control theory are used as the unifying mathematical language for the description, classification and analysis of the induction motor dynamics. The state-space formulations, the modal approach, the concepts of eigenvalues and eigenvectors have served as a comprehensive frame-work on which such disparate studies as nonlinear transients (in Chapter III) and stability studies (in Chapter VI) can be unified.

(c) Contributions to Knowledge

This thesis has sought to map the following areas of ignorance:

- (i) A basic understanding of the dependence of the eigenvalues on the rotor speed. (Chapter V is devoted entirely to the clarification of this problem).
- (ii) The dependence of dynamic characteristics and performance
 with each of the motor parameters. (Chapter VII develops
 the eigenvalue sensitivity indices to provide the supplementary information otherwise concealed by the numerical methods).
- turbations. (The Direct Method of Liapunov is applied to the stability studies in Chapter VI with limited success).

Because of the many predecessors on this problem, many of the contributions consist of filling in gaps which are the necessary connectives between established areas of knowledge. An example of this, is the physical identification of the eigenvalues in Chapter VI which enable stability studies to be related to the transient torque studies in Chapters III and IV.

(d) Physical Interpretation

In the discussion on "Transient Effects on Induction Motors", M.G. Say [30] made a just criticism that "a defect common to all papers" is "the lack of a physical explanation". In pursuance of this remedy, the magnetic field viewpoint of Fitzgerald and Kingsley [31] is adopted and developed to provide a physical understanding of the electromechanical interactions as they occur in the motor airgap. By

developing the concepts of the space-vectors which represent the airgap m.m.f.s, it is possible to obtain a comprehensive picture for

- (i) the production of transient torque and
- (ii) the physical interpretation of the damping factors and the oscillating frequency of the transient modes.

Besides the physical interpretations, the m.m.f. space-vectors have also proved to be theoretically fruitful in clarifying the interesting transient phenomenon of the existence momentary motoring torque with the rotor at super-synchronous speed.

Note that in this thesis, details of computer programs used have not been included because of space limitations.

CHAPTER II

REFERENCE FRAMES

The purpose of this chapter is to review the many reference frames in which the induction motor dynamic equations can be expressed and to assess their suitability with respect to the methods for solving them. Thus, whenever the analogue computer is used, it is necessary to formulate the equations so that they can be easily simulated by the standard hardware such as adders, multipliers and integrators. On the other hand, whenever the digital computer is used the preferred formulation is one which offers minimum computation time for maximum accuracy.

The first desirable feature is to be able to reduce the order of the system equations. In the most general form the industrial wound-rotor induction motor is dynamically described by an 8-order system of differential equations: 3 for the 3-phase stator currents, 3 for the 3-phase rotor currents, and 2 additional equations for mechanical motion.

In the squirrel cage motor, the number of phases in the rotor is equal to the number of rotor bars per pole pair. This increases the dimensionality of the system equations. However, it has been shown by Barton and Dunfield [32] that the squirrel cage is dynamically equivalent to a set of ideal, short-circuited 2-phase windings. This fact enables an otherwise high-order system to be reduced to a 7-order system.

In many industrial applications, the stator and the rotor neutral points are not connected so that the zero sequence component cannot exist. In such cases, it is possible to specialize the equations by transforming from a 3-phase system to a

2-phase system, and ultimately reducing the 8-order to a 5-order system - such as in the d-q and α - β frames.

2-1 Basic Induction Motor Equations - a b c Frame

Making the usual assumptions of

- (a) uniform airgap;
- (b) negligible core losses, saturation and hysteresis effects;
- (c) distributed windings producing only a fundamental sinsoidal distribution of airgap flux;

the dynamic equations of the 3-phase induction motor are described by Equations 2-1(a) and (b).

$$\begin{bmatrix} e^{s} \\ e^{abc} \end{bmatrix} = \begin{bmatrix} r^{s} \\ abc \end{bmatrix} + p \begin{bmatrix} r^{s} \\ abc \end{bmatrix} - p \begin{bmatrix} r^{s} \\ abc \end{bmatrix} - p \begin{bmatrix} r^{s} \\ abc \end{bmatrix}$$

$$\begin{bmatrix} r^{r} \\ abc \end{bmatrix} + p \begin{bmatrix} r^{s} \\ abc \end{bmatrix}$$

$$\begin{bmatrix} r^{r} \\ abc \end{bmatrix} - r \begin{bmatrix} r^{s} \\ abc \end{bmatrix}$$

where

$$\frac{e^{s}}{-abc} = \begin{bmatrix} e^{s} \\ a \\ e^{s} \\ b \\ e^{s} \\ c \end{bmatrix}, \quad e^{r}_{-abc} = \begin{bmatrix} e^{r} \\ a \\ e^{r} \\ b \\ e^{r} \\ c \end{bmatrix}$$

$$\begin{vmatrix}
i_{abc}^{s} & = \begin{bmatrix} i_{a}^{s} \\ i_{b}^{s} \\ \vdots \\ i_{c}^{s} \end{bmatrix} \qquad \begin{vmatrix}
i_{abc}^{r} & = \begin{bmatrix} i_{a}^{r} \\ i_{b}^{r} \\ \vdots \\ i_{c}^{r} \end{bmatrix} \qquad 2-1 (a)$$

$$\begin{bmatrix} r_{abc} \\ 0 & R^s & 0 \\ 0 & 0 & R^s \end{bmatrix} , \begin{bmatrix} r_{abc} \\ 0 & R^r & 0 \\ 0 & 0 & R^r \end{bmatrix}$$

$$\begin{bmatrix} L_{abc}^{s} \end{bmatrix} = L_{s}^{s} \begin{bmatrix} 1 & -k^{s} & -k^{s} \\ -k^{s} & 1 & -k^{s} \\ -k^{s} & -k^{s} & 1 \end{bmatrix} \begin{bmatrix} L_{abc}^{r} \end{bmatrix} = L_{s}^{r} \begin{bmatrix} 1 & -k^{r} & -k^{r} \\ -k^{r} & 1 & -k^{r} \\ -k^{r} & -k^{r} & 1 \end{bmatrix}$$

$$\begin{bmatrix} L_{abc}^{sr} \end{bmatrix} = M' \begin{bmatrix} \cos n \theta_m & \cos \left(n \theta_m + \frac{2\pi}{3}\right) & \cos \left(n \theta_m - \frac{2\pi}{3}\right) \\ \cos \left(n \theta_m - \frac{2\pi}{3}\right) & \cos n \theta_m & \cos \left(n \theta_m + \frac{2\pi}{3}\right) \\ \cos \left(n \theta_m + \frac{2\pi}{3}\right) & \cos \left(n \theta_m - \frac{2\pi}{3}\right) & \cos n \theta_m \end{bmatrix}$$

$$\begin{bmatrix} L_{abc}^{sr} \end{bmatrix} = \begin{bmatrix} L_{abc}^{rs} \end{bmatrix}^{T}$$

$$\begin{split} J_{1} & p \; \omega_{m} \; + \; f_{1} \; \omega_{m} \; + \; T_{L} \; = \; T_{em} \\ & T_{em} \; = \; - \; nM \; (\; i_{\alpha}^{s} \; i_{\alpha}^{r} \; + \; i_{b}^{s} \; i_{b}^{r} \; + \; i_{c}^{s} \; i_{c}^{r}) \; \sin n \; \theta_{m} \\ & - \; nM \; (\; i_{\alpha}^{s} \; i_{b}^{r} \; + \; i_{b}^{s} \; i_{c}^{r} \; + \; i_{c}^{s} \; i_{\alpha}^{r}) \; \sin (n \; \theta_{m} \; + \; \frac{2\pi}{3}) \\ & - \; nM \; (\; i_{\alpha}^{s} \; i_{c}^{r} \; + \; i_{b}^{s} \; i_{\alpha}^{r} \; + \; i_{c}^{s} \; i_{b}^{r}) \; \sin (n \; \theta_{m} \; - \; \frac{2\pi}{3}) \\ & p \; \theta_{m} \; = \; \omega_{m} \; \; . \end{split}$$

Because of the complex coupling and the dependence on trigonometric functions, these equations are not suited for the analogue computer. If they have to be solved, then the digital computer is more suitable.

Because the six electrical equations in Equation 2-1 (a) and the two mechanical equations in Equation 2-1 (b) bear a direct relationship to the real machine, a general computer program based on it can handle all conceivable applications of the induction motor. This is particularly attractive in transient studies of the composite inverter -induction motor system where successive phases can be open circuit and complicated terminal current constraints have to be matched. Unfortunately a program based on Equation 2-1 is inherently slow since it requires the matrix inversion of the [L] matrix (which is position dependent) at each integration step. This is because Equation 2-1 must be expressed in the standard form of Equation 2-3 so that it can be handled by a numerical integration subroutine.

Equation 2-1 is rewritten as

$$\underline{\nu} = [R] \underline{i} + [L] P \underline{i}$$

which yields the standard form

$$P_{\underline{i}} = [L]^{-1} \underline{\nu} + [L]^{-1} [R]_{\underline{i}}$$
 2-3

2-2 3-Phase Digital Model

It is possible to eliminate the position dependence of the [L] matrix and at the same time retain the direct relationship of the stator currents with the real machine by transforming the rotor equations from the 3-phase slip-ring to the 3-phase commutator equivalent. This 3-phase commutative model has been proposed by Barton [33], and Robertson and Hebbar [34].

Essentially, the 3-phase commutator equivalent is obtained by using a power invariant transformation of the type relating the α - β frame to the d-q frame in which the trigonometric functions of rotor positions in Equation 2-1 are replaced by speed voltages. Hence the [L] matrix is a constant matrix and the advantage of this model is that repeated matrix inversion is not necessary at each integration step.

2-3 <u>Three-Phase to Two-Phase Transformations</u>

Since the airgap flux from the balanced three phase motor can be reproduced by a combination of

(a) an equivalent set of currents in a two-phase (α , β) wind-ing in space quadrature, together with

(b) a zero sequence component, it is often times convenient to transform from the a b c variables to the $0 \alpha \beta$ variables by use of the following transformation [36]:

where the orthogonal connection matrix is

$$\begin{bmatrix} c_{0\alpha\beta}^{abc} \end{bmatrix} = \sqrt{\frac{2}{3}} \begin{bmatrix} \sqrt{2} & \sqrt{2} & \sqrt{2} \\ \frac{1}{2} & -\frac{1}{2} & -\frac{1}{2} \\ 0 & \sqrt{\frac{3}{2}} & -\frac{\sqrt{3}}{2} \end{bmatrix}$$
2-5

In a large number of applications, there is no zero sequence components since the neutral of the stator windings and that of the rotor windings are not connected to a return wire. Consequently it is possible to reduce the order of the electrical equations from 6 to 4 by transforming to the 2 - phase $\alpha - \beta$ system. From the $\alpha - \beta$ frame it is possible to perform further power invariant two-phase transformations, e.g. to the d - q and the synchronously rotating frames. The theory behind these power invariant axis frame transformations are fully described in many excellent texts [1], [5-7] and will not be discussed here. It is useful to be reminded that the three-phase and two-phase parameters under such orthogonal transformation are related as follows:

Two – Phase		<u>Three</u> – Phase
R ^s	= .	R ^s
R ^r	=	R ^r
l ^s	=	l _L
i ^r	=	ır
M	<u></u>	$\frac{3}{2}$ M^1

and that the two-phase quantities can be obtained directly from the per-phase values calculated from the standard no-load and locked rotor tests [35].

2-4 The $\alpha - \beta$ Reference Frame

When there is no zero-sequence component, the 3 to 2-phase transformation yields the α - β frame equations [36]:

$$\begin{bmatrix} e_{d}^{s} \\ e_{q}^{s} \\ e_{\alpha}^{r} \end{bmatrix} = \begin{bmatrix} R^{s} + L^{s} p & 0 & p & (M \cos n \theta_{m}) & p & (M \sin n \theta_{m}) \\ 0 & R^{s} + L^{s} p & -p & (M \sin n \theta_{m}) & p & (M \cos n \theta_{m}) \\ p & (M \cos n \theta_{m}) - p & M \sin n \theta_{m} & R^{r} + L^{r} p & 0 \\ e_{\alpha}^{r} \\ e_{\beta}^{r} \end{bmatrix} \begin{bmatrix} i_{d}^{s} \\ i_{q}^{r} \\ i_{\alpha}^{r} \\ i_{\beta}^{r} \end{bmatrix}$$

$$J_{1} P \omega_{m} + f_{1} \omega_{m} + T_{L} = n M \left[\left(i_{\beta}^{r} i_{d}^{s} - i_{\alpha}^{r} i_{q}^{s} \right) \cos n \theta_{m} \right]$$

$$- \left(i_{\alpha}^{r} i_{d}^{s} + i_{\beta}^{r} i_{q}^{s} \right) \sin n \theta_{m}$$

$$2-6(b)$$

$$P \theta_{m} = \omega_{m}$$

Because of the trigonometric functions of rotor angles, these equations are difficult to simulate in the analogue computer and consequently have not been widely used. When these equations are considered in the context of the digital computer, the positional dependence of the [L] matrix in Equation 2-6(a) means that at each integration-step, the [L] - matrix inversion has to be performed so that the standard form of Equation 2-3 can be obtained. So, at first sight, it seems that the $\alpha - \beta$ frame would suffer the same disadvantage as the basic motor equation, Equation 2-1. However, because the [L] matrix is now a 4 x 4 matrix with certain symmetric properties, it can be inverted by hand in an algebraic form to give

$$[L]^{-1} = \frac{1}{L^{s} L^{r} - M^{2}}$$

$$\begin{bmatrix} L^{r} & 0 & -M \cos n \theta_{m} & -M \sin n \theta_{m} \\ 0 & L^{r} & M \sin n \theta_{m} & -M \cos n \theta_{m} \end{bmatrix}$$

$$-M \cos n \theta_{m} & M \sin n \theta_{m} & L^{s} & 0$$

$$-M \sin n \theta_{m} & -M \cos n \theta_{m} & 0 & L^{s}$$

Because this matrix inversion is solved algebraically before hand, the evaluation of the right hand side of Equation 2-3 is a matter of straight-forward sum and product computer operations. As Table 3-1 shows, the computation time in the $\alpha-\beta$ frame is only marginally slower than in the d-q frame because of the additional time required to evaluate the trigonometric functions of rotor positions.

The rotor position dependence and the trigonometric functions can be eliminated by transforming to one of the common reference frames. As will be seen, the d-q axis frame and the synchronously rotating reference frame are two important particular cases of the common reference frames.

2-5 The d - q Reference Frame

The d-q axis frame or the commutative primitive is the historical and logical next step from the $\alpha-\beta$ frame or the slip-ring primitive. This is obtained by the transformations [3], [38]:

$$\frac{i}{-dq} = \left[C_{dq}^{\alpha\beta} \right] \frac{i}{-\alpha\beta}$$
 2-8(\alpha)

$$\frac{e}{-dq} = \left[C_{dq}^{\alpha\beta} \right] \frac{e}{-\alpha\beta}$$
 2-8 (b)

where the connection matrix is

This transformation yields the system equations listed as Equation 2-10(a) and (b).

$$\begin{bmatrix} e_d^s \\ e_d^s \\ e_q^s \\ e_d^r \\ e_d^r \\ e_q^r \end{bmatrix} = \begin{bmatrix} R^s + L^s p & 0 & Mp & 0 \\ 0 & R^s + L^s p & 0 & Mp \\ -Mn \omega_m & R^r + L^r p & -L^r n \omega_m \\ Mn \omega_m & Mp & L^r n \omega_m & R^r + L^r p \end{bmatrix} \begin{bmatrix} i_d^s \\ i_q^r \\ i_d^r \\ i_q^r \end{bmatrix}$$

2-10(a)

$$J_1 p \omega_m + f_1 \omega_m + T_L = n M (i_d^s i_q^r - i_d^r i_q^s)$$
 2-10(b)

There are two important features to note about the d - q reference frame.

(i) When Equation 2-10(a) is written in the form of Equation 2-2, the inductance matrix [L] is a constant matrix. Thus an integration routine using this frame would save time since [L] would have to be evaluated only once and no trigonometric functions are involved.

(ii) Whereas in the basic motor equations (Equation 2-1 (b)) and in the α - β frame (Equation 2-6 (b)), it takes two equations to describe the mechanical dynamics, the d- q frame needs only a single equation (Equation 2-10 (b)). This reduction of system order does not imply a loss or degeneracy of information when transforming to the d- q frame. It implies that the rotor angle position θ_m is merely a description of the rotor α - β frames in Equation 2-6 and unlike the velocity ω_m , θ_m does not enter into the dynamics of electromechanical interaction. This system reduction represents an important result arising from the cylindrical symmetry of the motor and will be discussed more fully in Section 2-10.

2-6 Common Reference Frame Transformations

Equation 2-10 in the d-q frame can be transformed to a moving frame [39] which rotates at electrical radians ω_c by the following power invariant transformations.

$$i_{\gamma\delta} = [C_{\gamma\delta}^{dq}] i_{dq}$$
 2-11(a)

$$\frac{e}{-18} = \left[C_{18}^{dq} \right] \frac{1}{-dq}$$
 2-11(b)

where

$$\begin{bmatrix} C_{\mathbf{y}\delta}^{\mathbf{dq}} \end{bmatrix} = \begin{bmatrix} \cos \omega_{\mathbf{c}} t & -\sin \omega_{\mathbf{c}} t & 0 & 0 \\ \sin \omega_{\mathbf{c}} t & \cos \omega_{\mathbf{c}} t & 0 & 0 \\ 0 & 0 & \cos \omega_{\mathbf{c}} t & -\sin \omega_{\mathbf{c}} t \\ 0 & 0 & \sin \omega_{\mathbf{c}} t & \cos \omega_{\mathbf{c}} t \end{bmatrix}$$

which yield

$$\begin{bmatrix} e_{\delta}^{s} \\ e_{\delta}^{s} \\ e_{\delta}^{s} \end{bmatrix} = \begin{bmatrix} R^{s} + p L^{s} & L^{s} \omega_{c} & M p & M \omega_{c} \\ -L^{s} \omega_{c} & R^{s} + p L^{s} & -M \omega_{c} & M p \\ M p & M (\omega_{c} - n \omega_{m}) & R^{r} + p L^{r} & L^{r} (\omega_{c} - n \omega_{m}) \\ e_{\delta}^{r} \end{bmatrix} \begin{bmatrix} i_{\delta}^{s} \\ i_{\delta}^{s} \\ i_{\delta}^{r} \\ i_{\delta}^{r} \end{bmatrix}$$

$$\begin{bmatrix} e_{\delta}^{s} \\ e_{\delta}^{r} \end{bmatrix} = \begin{bmatrix} R^{s} + p L^{s} & L^{s} \omega_{c} & M p & M \omega_{c} \\ M p & M (\omega_{c} - n \omega_{m}) & R^{r} + p L^{r} & L^{r} (\omega_{c} - n \omega_{m}) \\ -M (\omega_{c} - n \omega_{m}) & M p & -L^{r} (\omega_{c} - n \omega_{m}) & R^{r} + p L^{r} \end{bmatrix}$$

$$\begin{bmatrix} e_{\delta}^{s} \\ i_{\delta}^{r} \\ i_{\delta}^{r} \end{bmatrix}$$

$$\begin{bmatrix} e_{\delta}^{s} \\ e_{\delta}^{r} \end{bmatrix} = \begin{bmatrix} R^{s} + p L^{s} & L^{s} \omega_{c} & M p & M \omega_{c} \\ M p & M (\omega_{c} - n \omega_{m}) & R^{r} + p L^{r} & L^{r} (\omega_{c} - n \omega_{m}) \\ -M (\omega_{c} - n \omega_{m}) & M p & -L^{r} (\omega_{c} - n \omega_{m}) & R^{r} + p L^{r} \end{bmatrix}$$

$$J_1 p \omega_m + f_1 \omega_m + T_L = n M (i^s i^r_{\delta} - i^s_{\delta} i^r) - i^s_{\delta} i^r)$$
 2-13(b)

Of the infinite number of common reference frames [25] which may be chosen, only two are of practical interest:

(i) $\omega_c = 0$. This reverts back to the d-q axis frame in Section 2-5.

(ii)
$$\omega_{\rm c}=\omega_{\rm f}$$
. This is the synchronously rotating reference frame of Section 2-7 where the frames rotate at the supply frequency $\omega_{\rm f}$.

2-7 The Synchronously Rotating Frame

The synchronously rotating frame is most advantageously used in solving switching transients with balanced symmetrical voltage supplies which in the $\,\mathrm{d}$ - $\,\mathrm{q}$ frame is expressed as

$$\frac{e}{-dq} = \begin{bmatrix} E_p \cos(\omega_f t + \alpha_s) \\ -E_p \sin(\omega_f t + \alpha_s) \\ 0 \\ 0 \end{bmatrix} \quad v_{-1} (t)$$
 2-14

By transforming to the synchronously rotating frame, the sinusoidally time varying voltage sources of Equation 2-14 are now expressed as d.c. voltages:

$$\frac{e}{-\chi_{\delta}} = \begin{bmatrix} E_{p} \cos \alpha_{s} \\ -E_{p} \sin \alpha_{s} \\ 0 \\ 0 \end{bmatrix}$$
2-15

Consequently, the steady-state current solutions to Equation 2-13 are d.c. currents. There are three important results which follow from this:

- (i) The transient current solutions are less oscillatory than these in the d q frame. Hence it becomes possible to use larger integration step-size for the same computation accuracy and in our experience its solutions is at least twice as fast as in the other frames. In the limiting case when the transients are damped out and the constant steady state solutions are reached, the step-size can be infinite.
- (ii) In Section 6-2, the local stability of the induction motor at each operating point will be studied by linearizing the system equations through a method of small signal perturbation which produces a dynamic system equation of the form $\dot{x} = [A]x$. The synchronously rotating frame is the only frame which yields a constant [A] matrix for symmetrical balanced voltage sources.
- (iii) The synchronously rotating frame offers a clearer physical insight to the electromechanical interaction than the other frames. This is because their solutions are slowly time varying quantities which consist of (a) the steady-state solutions which are d.c. quantities and (b) the transient solutions superimposed on them. In contrast the d q solutions are in a maze of sinusoids with the transients being barely distinguishable as envelopes.

In Section 3-15-2 by combining the concepts of m.m.f. space vectors and the synchronously rotating reference frames, it becomes possible to follow the sequence of electromechanical interaction during an induction motor transient.

2-8 Complex Transformations

Hitherto all the frame transformations have been real transformations to which can be attached some physical significance. The next task is to review the complex transformations such as the instantaneous symmetric component transformation introduced by W.Y. Lyon in his book [9], and like-wise examine their merits in terms of numerical integration.

2-9 Instantaneous Symmetrical Components

The method of instantaneous symmetrical component has been used by

I.R. Smith and S. Sriharan [16] to transform the induction motor equations from

three-phase to a form which is efficient for solving the transients numerically. Thus,

by using the complex transformation

$$\begin{bmatrix} \mathbf{i}_{p} \\ \mathbf{i}_{n} \\ \mathbf{i}_{o} \end{bmatrix} = \frac{1}{3} \begin{bmatrix} 1 & \alpha & 2 \\ 1 & \alpha^{2} & \alpha \\ 1 & 1 & 1 \end{bmatrix} \begin{bmatrix} \mathbf{i}_{\alpha} \\ \mathbf{i}_{b} \\ \mathbf{i}_{c} \end{bmatrix}$$

$$(2-16)$$

where
$$\alpha = \exp\left(i\frac{2\pi}{3}\right)$$
 2-17

it is possible to decompose the induction motor equations to zero sequence, positive sequence and negative sequence component equations. For motors with unconnected star points, there is no zero-sequence components. Also, the negative sequence equations are the complex conjugate of those in the positive sequence. Consequently, it is possible to retain only the positive sequence components without loss of information. The positive sequence equations are:

$$\begin{bmatrix} e_{p}^{s} \\ e_{p}^{s} exp \mid \theta \end{bmatrix} = \begin{bmatrix} R^{s} + L^{s}p & Mp \\ M (p - i n \omega_{m}) & R^{r} + L^{r} (p - i n \omega_{m}) \end{bmatrix} \begin{bmatrix} i_{p}^{s} \\ i_{p}^{r} exp \mid \theta \end{bmatrix}$$

$$2-18$$

where the voltage and the current vectors are complex quantities.

Although Equation 2-18 appears compact, it in fact embodies 4 electrical system equations which are obtained by equating the real and the imaginary parts of Equation 2-18. On expansion Equation 2-18 yields Equation 2-10 which is the d-q frame equations. As such there is no computational advantage in using complex transformations for numerical integration of the induction motor transients.

It can be concluded that the equations in the common reference frames (e.g. the d-q and the synchronously rotating frame) represent the very bare essentials in the description of the induction motor dynamics. Since the digital computer programmes based on these would not contain redundancies in the formulation, they can at best be equaled by using the complex transformations.

2-10 Cylindrical Symmetry

In the transformation from the α - β frame (Section 2-4) to the d - q frame in (Section 2-5) it has been observed that the two mechanical equations in Equation 2-6(b) reduces to a single equation in Equation 2-10(b). This result is a consequence of the cylindrical symmetry arising from the idealised model in Section 2-1 which assumes (a) a uniform airgap and (b) balanced, symmetrical sinusoidally distributed windings. Because of this idealization, one rotor position θ_{m_1} is electromagnetically indistinguishable from another position θ_{m_2} .

A corollary of the cylindrical symmetry is that the starting torque pattern is independent of the assigned initial rotor positions θ_m when using the α - β equations, Equation 2-6. This has been verified by digital computer runs of the transient torque using different initial values for θ_m .

A second corollary is that when the inert induction motor is simultaneously switched (i.e. all the line contactors close simultaneously on the balanced symmetrical voltage source), the transient torque pattern is independent of the switching angle α_s . In the 2-phase common reference frame, the simultanous switching and the switching angle α_s are the mathematically expressed as the step-forcing functions of Equation 2-14 or Equation 2-15. Because of the uniform airgap and the idealised windings, the rotating electromagnetic fields set up in the airgap by the symmetrical voltage source always follow the same time and space pattern except for an angular position shift of α_s electrical radians. Since the electromechanical torque is dependent on the stator m.m.f., the rotor m.m.f. and the space-phase angle between them, the angle α_s merely represents a shift of the reference axis and does not affect the torque pattern at all. This result has also been verified by digital computer runs.

2-11 Space - Vector Representation

Hitherto this study has been engrossed in reviewing the reference frames with the purpose of finding formulations which lend themselves to easy solutions.

Once the solutions are found it becomes necessary to interpret and organize them into a comprehensible body of knowledge. Left in their original form the inter-relations of the solutions are difficult to follow. Thus, the solutions in the d - q frame are a tangle of sinusoidal currents and their relationship with the torque pattern are difficult to discern.

It is found that the m.m.f.space vector representation yields the most meaningful presentation of the output solution. The m.m.f. space vector viewpoint is an extention of the concepts developed in Fitzgerald and Kingsley [31] and it is applied here to dynamic studies.

Basically three quantities are defined: the stator, the rotor and the magnetization current vectors which are at all instants of time related directly to the spatial m.m.f. and flux-density waves which occur in the uniform airgap of the induction motor. This vector representation is possible because

- (a) the airgap is uniform,
- (b) the orthogonal windings are sinusoidally distributed at a fundamental space harmonic and as such vector additions are permissible.

In the d - q reference frame, the three space-vectors are defined as follows:

Stator Current Vector 3 49 s

$$\mathcal{Z}_{s} = \left[i \frac{s^{2}}{d} + i \frac{s^{2}}{q} \right]^{1/2}$$

$$\mathcal{Q}_{s} = \arctan \frac{i \frac{s}{d}}{i \frac{s}{d}}$$
2-19

Rotor Current Vector 3 L 9 r

$$\mathfrak{F}_{r} = \left[i \frac{r^{2}}{d} + i \frac{r^{2}}{q} \right]^{1/2}$$

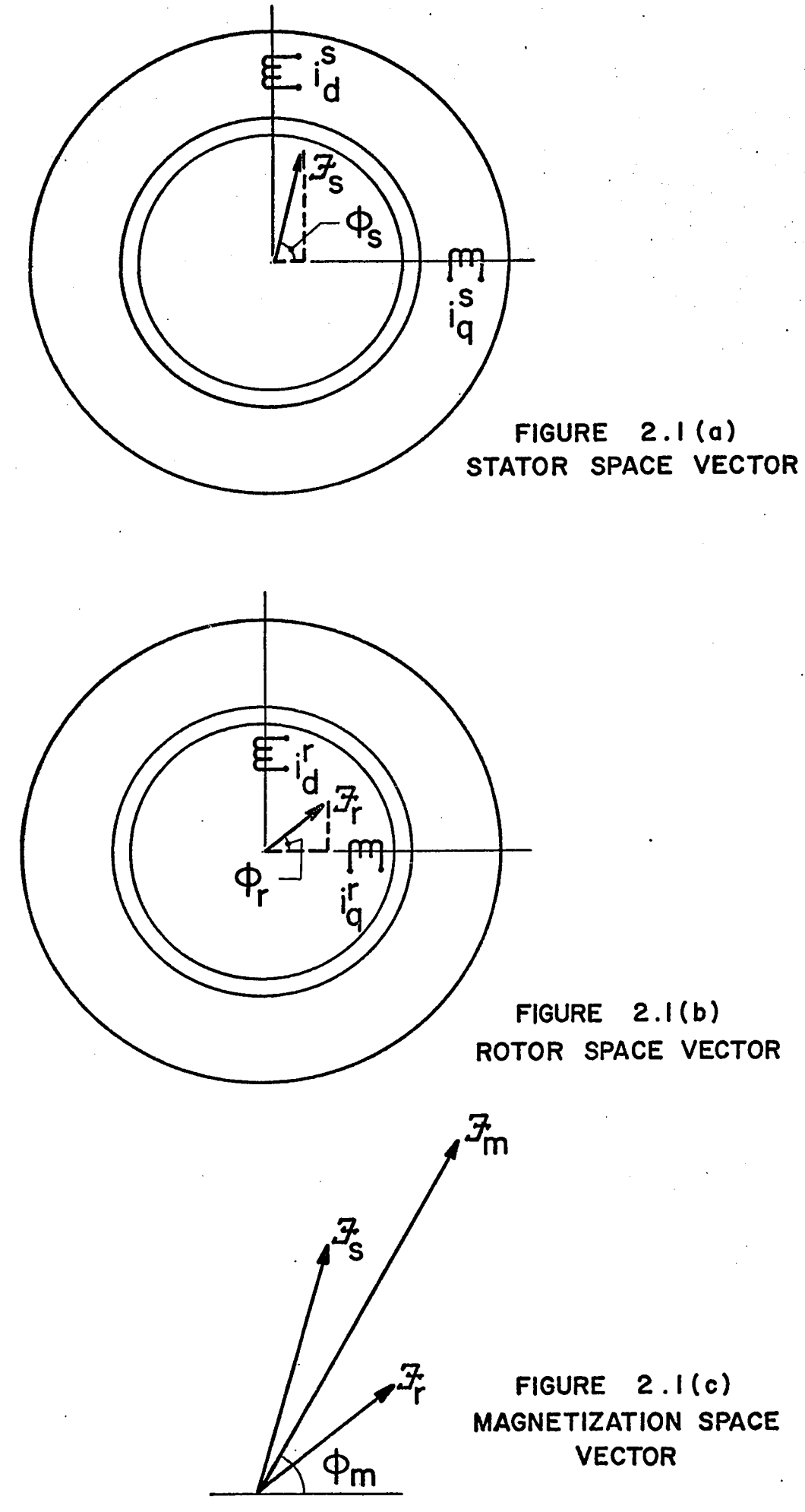
$$\mathfrak{G}_{r} = \arctan \frac{i \frac{r}{d}}{i \frac{r}{q}}$$
2-20

Magnetization Current Vector 3 40 m

$$\mathcal{F}_{m} = \left[\left(i_{d}^{s} + i_{d}^{r^{2}} \right) + \left(i_{q}^{s} + i_{q}^{r} \right)^{2} \right]^{1/2}$$

$$\mathcal{O}_{m} = \arctan \frac{i_{d}^{s} + i_{d}^{r}}{i_{q}^{s} + i_{q}^{r}}$$
2-21

These vectors have each a magnitude and a space-angle with respect to the coil windings as illustrated in Figure 2-1 (a) to (c). Note that of the six quantities defined in Equations 2-19 to 2-21, only four quantities are independent. Thus as shown in Figure 2-1 (c) the magnetization current vector is the resultant of the stator and the rotor vectors.



Furthermore, it should be noted that Equations 2-19 to 2-21 imply that both the stator and the rotor currents are referred to the stator and consequently the turns ratio have been taken care of .

2-12 Space Vectors Viewpoint of Electromagnetic Torque

The importance of the space-vector viewpoint is established when the electromechanical torque can be expressed in terms of the space vectors. The electromechanical torque of Equation 2-13(b)

$$T_{em} = n M (i_{\chi}^{s} i_{\delta}^{r} - i_{\delta}^{s} i_{\gamma}^{r})$$
 2-22

are written for orthogonal axes frames. On transformation to the polar co-ordinate frames of the space-vector representation it becomes:

$$T_{em} = n M \mathcal{F}_{m} \mathcal{F} \sin (\mathcal{O}_{m} - \mathcal{O}_{r})$$
 2-23(a)

or
$$T_{em} = n M \mathcal{F}_{sm} \sin (\mathcal{O}_{sm} - \mathcal{O}_{m})$$
 2-23(b)

or
$$T_{em} = n M \mathcal{F}_{s} \mathcal{F}_{r} \sin (\mathcal{G}_{s} - \mathcal{G}_{r})$$
 2-24

Thus the electromechanical torque is n M times the area contained in the vector parallelogram of Figure 2-1 (c). The torque is positive whenever $(\mathcal{O}_m - \mathcal{O}_r)$ and $(\mathcal{O}_s - \mathcal{O}_r)$ lie in the first and second quadrant and negative when these angles exceed 180° .

2-13 Space Vector Viewpoint in Synchronously Rotating Frame

wectors 3, 3 and 3 rotate with an average speed which is the synchronous speed of the supply frequency. As such the synchronously rotating frame is the best frame to view the interactions of the space-vectors in producing the motor torque.

CHAPTER III

NONLINEAR SWITCHING TRANSIENTS

3-1 Statement of the Problem

In industrial applications of the induction motor, electrical and mechanical transients occur when the machine is switched from one steady state to another.

Some examples of transient occurrences are:

- (a) The inert motor at standstill is accelerated to full speed after being switched on to the power source.
- (b) The induction motor with load operating at rated speed is transferred from one busbar to another.
- (c) Two of the line voltages are reversed so as to reverse the direction of rotation or to "plug" the motor to standstill.
- (d) The induction motor is dynamically braked by injecting ad. c. voltage into the stator windings.

All these, and miscellaneous induction motor transient problems can be viewed comprehensively in terms of the differential equation, Equation 2-1(a) and (b) and of finding the solutions to a particular forcing function $\begin{bmatrix} e^s \\ abc \end{bmatrix}$ and a particular

set of initial currents

3–2 Nature of Dynamic Equations

The Equations 2-1 (a) and 2-1 (b) are not at all easy to handle and whenever the induction motor is of the Y connection with unconnected neutral, a transformation to one of the common frames (as discussed in Chapter II) is favoured because of the advantage in system order reduction from 8 to 5. Thus in the d-q axis frame, the problem consists of finding the solutions to the differential equations of Equation 2-10 (a) and 2-10 (b) for a specification of forcing function voltages

Reduced to this most simplified form, the induction motor equation remains intractable to analytic solution because of the mathematical nonlinearity.

This nonlinearity consists of quadratic products of the state-variables, i.e. of the kind ω_{m} is in the electrical equations, Equation 2-10(a) and of the kind is in the mechanical equations, Equation 2-10(b).

Faced with this analytical impasse, past engineering practice has been to use approximations.

3-3 Constant Speed Approximations

A good approximation consists of assuming a constant rotor speed $\omega_{\rm m}$ in which case the electrical equations of Equation 2-10(a) are linear and can be solved by the Laplace Transform techniques. The solutions of the current variables are used in Equation 2-10(b) to calculate the torque.

This is a very good approximation in the first few cycles of the switching transients especially in cases of very large inertia and the motor torque can only produce low accelerations. Furthermore, since the most severe torque occurs in the first few cycles of switching, a good estimate of the maximum torque can be made from such an approximate solution.

Because of the importance of this linear approximation, Chapter IV will be devoted to its discussion.

3-4 Approximations for Variable Speed Torques

An analytical method [23] which computes the motor torque while taking the variable speed into account is possible by assuming:

- (a) negligible stator resistance which results in using the "constant flux linkage theorem",
- (b) a specification of the rotor speed.

This method has been used to study the effect of an abrupt change in slip, sinusoidal change in slip, rotor oscillation about a mean position and motor dynamic stability.

3-5 Analogue Computer Solutions

Essentially the analogue computer solutions consist of simulating the differential equations of the induction motor by the electronic integrators, adders, multipliers and function generators of the analogue computer. Most previous studies [12 - 14] have used the d - q axes frame which has the advantages (a) of being easily simulated and (b) being versatile enough to include study of the induction motor under unconventional operation.

When the induction motor transients are to be studied under balanced symmetrical voltage supplies only, then the synchronously rotating frame equations of Equation 2-13 offers the added advantage that the supplies are the d.c. voltages of Equation 2-15 and time sinusoidal function generators need not be used to simulate the d - q axis voltages of Equation 2-14. Once again versatility can be exchanged for economy.

The analogue computer is readily "plugged" together and fast. However its serious defect is in the poor accuracy. Although the speed and the current transient solutions are themselves tolerably accurate, the formulation of the torque expression in Equation 2-10(b) inherently prevents high accuracy for the torque solution. This is because by Lenz's Law, $i_d^s \approx -i_d^r$ and $i_q^s \approx -i_q^r$ and hence the torque expression is the

difference of two nearly equal terms. As such unless the current solutions are accurate to many significant figures (which is not usually achieved by the analogue computer) the percentage error in the torque prediction is necessarily quite high.

3-6 Solutions by Numerical Integration

Because of the general availability of fast, large memory computers, it has become feasible to solve a system of nonlinear differential equations by numerical integration algorithms. Generally the numerical integration methods of solving a set of first order non-linear differential equations

$$p \underline{Y} (t) = \underline{F} (\underline{Y}, t)$$
 3-5

with the initial conditions \underline{Y} (o) fall under two broad classifications.

(a) One Step Methods

The algorithm for evaluating the (n + 1)th integration step is

$$\frac{Y}{-n+1} = \frac{Y}{-n} + h \frac{g'}{n}$$

where $\underline{\mathscr{G}}_n$ is calculated from information based only on \underline{Y}_n , t_n , and h is the step-size. When $\underline{\mathscr{G}}_n$ is calculated from m evaluations of \underline{F} (. .) this method is called m substitution method. Thus the fourth-order Runge-Kutta is a 4 - substitution method.

The Runge-Kutta methods and the method developed by Wiederholt, Fath and Wertz [40] belong to this category. The theory of the Runge-Kutta methods are described in the standard numerical analysis texts [41], [43]. In the digital computer applications, the Gill's modification to the Runge-Kutta method is most favoured since (a) the Runge-Kutta constants for evaluating $\underline{\emptyset}_n$ can be solved recursively and (b) the storage requirements and accumulated round-off errors are small.

(b) Multi-Step Methods

In the multi-step methods, numerical integration is achieved through a formula of the kind

$$\underline{Y}_{n+1} = \sum_{k=0}^{I} \alpha_k \ \underline{Y}_{n-k} + h \sum_{k=-1}^{I} \beta_K \underline{F} \ (\underline{Y}_{n-k}, t_{n-k})$$
 3-7

When $\beta_{-1}=0$, Equation 3-7 is explicit, which means to say that the desired function at the (n+1) integration step is predicted from available information from the previous increments, i.e. n, n-1, n-2, ..., n-1.

This predicted value is subsequently combined in Equation 3-7 for the implicit case, i.e. $\beta_{-1} \neq 0$ to improve the estimate of Y_{n+1} . Generally the formula is used iteratively in the predictor – corrector process. Each time Equation 3-7 is used, only one re-evaluation of \underline{F} () is necessary and consequently an algorithm which makes use of R iterations is faster than an m – substitution one step method if $(R+1) \leq m$, i.e. provided the increment h remains the same for both methods. However there is no assurance that to achieve the same accuracy, both the one-step and the multi-step methods will use the same increment size h.

The Hamming's Predictor – Corrector Method [44], [45], the Adams – Moulton Method [42], [46] fall under this classification and the theory is covered in standard texts on numerical integration.

3-7 Numerical Integration with Digital Computers

The constraints placed on digital computer usage are (a) economy of computational time and (b) economy of memory storage. In the studies of a single machine in transient, the system order is at most of 8 variables and over-concern with these economies are not justifiable. Nevertheless economy practised in the single machine case can be extended to multi-machine studies.

Generally, the following three-factors determine such economies in the numerical solution of a single motor in transient.

- (a) Choice of Reference Frames.
- (b) Choice of Integration Subroutines.
- (c) Choice of strategy in integration step-size control.

3-8 Choice of Reference Frame

Chapter II has discussed the many reference frames in which the system dynamics of the induction motor can be written. The following observations can be made:

- (a) The computation time at each integration step can be economised when the inductance matrix [L] Equation 2-2 is not a function of position or time (as it is in Equation 2-1 and Equation 2-6) so that it is not necessary to invert it by the computer each time. Thus the digital model based on the 3-phase commutator equivalent is preferred to the a-b-c frame, Equation 2-1 in the three-phase equations. Likewise, the common axes frame equations (d q in Equation 2-10 and \$\chi\$ \$\delta\$ in Equation 2-13) are preferred to \$\alpha\$ \$\beta\$ frame Equation 2-6 in the two phase model.
- (b) Whenever the induction motor has an unconnected neutral in the Y connection, system reduction (from 8 to 15) can be achieved by transforming Equation 2-1 to a common reference 2-phase frame (Equation 2-10, Equation 2-13).
- gration step-size and thus hasten the numerical integration process.

 Thus in the cases where the voltage supply is balanced, symmetrical and at a single fundamental frequency, the synchronous reference frame (Section 2-7) is very much faster than the solutions in the d q axis.

3-8-1 Comparison of Two-Axis Frame Transformations

Table 3-1 gives the computation times for solving an identical induc-

tion motor switching problem by the three reference frames. The problem consists of an acceleration run from standstill by simultaneous switching to a balanced symmetrical voltage source at a single supply frequency. The programs for each frame are written so as to minimise computer time. Thus for example the first line in Equation 2-3 in the d-q frame is programmed in FORTRAN IV as

where the constant coefficients D (1), D (2), D (3) are clusters of motor parameters which are written algebraically and evaluated by a separate sub-program beforehand. Thus for example

$$D(2) = \frac{R^{s} L^{s}}{L^{s} L^{r} - M^{2}}$$

In comparing the merits of the reference frames, it should be noted that the α - β frame is only marginally slower than the d - q frame. This is because, the position dependence [L] matrix of Equation 2-6(a) can be inverted by hand al-

TABLE 3-1. AXES FRAME COMPUTATIONAL TIME.

Axes Frame	Computation * Time (minutes)	Steady-State Stator Frequency	Steady-State Rotor Frequency	Maximum Integration Step-size Used
α - β	0.61	ω	ω× slip	0.0005 sec.
d - q	0.54	ω	ω	0.0005
synchronous ¥ - δ	0.24	d.c	d.c.	0.005 sec.

^{*} HPCG Subroutine: Switching from 0 - 1.0 sec. Initial step-size 0.001 sec.

gebraically to give Equation 2-7. Thus it is possible to write Equation 2-3 in the form of Equations 3-8 and 3-9. Consequently, the $\alpha - \beta$ frame is slower only by the necessity to evaluate the trigonometric functions of angular position.

The computation time for the synchronous reference frame is less than half that of the d-q reference frame. This is because, given the same accuracy tolerance, the numerical integration is performed at a larger integration step-size. Thus as has been presented in Table 3-1, a maximum of 0.005 sec. increment has been used in the synchronously rotating frame.

Figure 3-3 shows graphically why a larger integration step-size is possible. Figure 3-3 plots a typical current solution for the d-q axis frame and the synchronously rotating frame. In the d-q axis the current solution is highly oscillatory. In contrast there is a large steady state d.c. component in the transient solutions in the synchronously rotating frame. As such, for the same percentage accuracy, it is possible to take a larger step-size since the instantaneous gradients are lower.

3-9 Choice of Integration Subroutines

Since the development of integration subroutines is not the purpose of this study, reliance has been placed on the IBM Scientific Subroutine Packages viz the RKGS and the HPCG which are general programs for solving a system of first order nonlinear differential equations. It should be pointed out that the system nonlinearities which appear in the induction motor are of the quadratic product form and it may be

possible to develop specialised integration subroutines for the induction motor which exploit this structural property. In fact L.F. Wiederholt, A.F. Fath and H.J. Wertz [40] have developed a numerical solution technique based on this insight and for which they claimed "a time reduction of about ten" over the convention routines. Accordingly this study has examined and developed such a quadratic nonlinearity program and compared it with the RKGS and the HPCG.

As a subroutine package, the HPCG and the RKGS have important internal differences which are of no consequence to the users. The RKGS uses the Runge-Kutta method with Gill's modification and is described in Reference [47]. The HPCG uses the Hamming's modified predictor – corrector method and is described in Reference [48]. As in all multi-step methods it is not self starting and it uses a special Runge-Kutta procedure to obtain the starting values.

3-9-1 Comparison of Subroutines

From the user's viewpoint, the following observations can be made with respect to the merits of the SSP - RKGS and the SSP - HPCG.

Computational Time

Test runs whose results are listed in Table 3-2 show that the RKGS is as fast and sometimes faster than the HPCG in solving an identical problem. This is surprising in view of the fact that the RKGS is a 4-substitution method and requires 4 evaluations of the state functions per integration step when compared to 2 evalua-

TABLE 3 - 2. PERFORMANCE FIGURES OF INTEGRATION SUBROUTINES.

Subroutines	Computation Time	Step Size Taken	Auxiliary Storage Array
IBM SSP - HPCG	0.54 minutes	0.0005 sec.	16 × 5
IBM SSP - RKGS	0.49 minutes	0.001 sec.	8 × 5

Test runs based on

- (a) Solution of induction motor transient in d q frame.
- (b) Test run 0 1.0 sec. with initial step-size of 0.001 sec.
- (c) Computer IBM 360.

obvious when the step-sizes for an integration run are printed out. It is found that for the same accuracy and strategy in step-size control, the RKGS can take a larger step-size (sometimes twice as large) than the HPCG. This fact has also been reported by Prabhashanker and Janischewsyi [45].

Because the RKGS does not have any formula estimates relating local truncation error with the step-size, the reason why the RKGS can take a larger step-size is not apparent. This can be an interesting subject for research by the numerical analysts.

Whilst the subroutine packages such as the HPCG and the RKGS have proved to be fast, reliable and accurate, it may be possible to develop faster integration subroutines based on the special nature of the problem. One such attempt is outlined in Reference [40] and has the objective of enabling small digital computers to solve problems of induction motor transients.

3-9-2 Special Integration Subroutines for Quadratic Nonlinearity

The algorithm developed in Reference [40] exploits the fact that the induction motor nonlinearity consists of quadratic products of the state-variables, i.e. each of the first order differential equations can be written in the form

$$p Y_1 = a_1 Y_1 + b_1 Y_2 Y_3$$
 3-10

where $a_1 = constant coefficient of linear term,$

b₁ = constant coefficient of nonlinear quadratic product term,

and I denotes the first row.

The method consists using a truncated Taylor series expansion of the state variables about a given time instant. Thus, for a third order system, the Taylor series expansion of each of the state variables is

$$Y_{i} = \sum_{k=0}^{\infty} \beta_{ik} h^{k}$$
 3-11

for
$$i = 1, 2, 3$$

where $\beta_{ik} = K$ th order Taylor coefficient of x_i .

The method consists of substituting the Taylor series expansions of Equation 3-11 into the system dynamic equations of the form in Equation 3-10 and evaluating the Taylor coefficients by equating the coefficients of the same powers of h. The success of this method lies in the nonlinearity being quadratic, in which case it is possible to obtain a recursion formula where every Taylor coefficient can be found from the preceding terms. The recursion formula based on Equation 3-10 is

$$\beta_{1,k+1} = \frac{1}{k+1} [\alpha_1 \beta_{1,K} + b_1 \sum_{l=0}^{K} \beta_{2,K-l} \beta_{3,l}]$$
 3-12

The recursion formula starts from the 0 - order Taylor coefficients which is the initial condition and all the other coefficients up to any order can be

obtained from it. By choosing the step size h and the approximate truncated series, the solution for the (n+1) increment is obtained from the n - increment solutions which are used as the 0 - order Taylor coefficients.

A program based on this principle has been developed in this study. For comparison purposes, the same step-size control as the HPCG and the RKGS sub-routines has been used. Unfortunately, it is found that the RKGS and the HPCG are far superior in speed and in accuracy to this program. This does not necessarily reflect on the merit of the method, but rather on the relative skill of the programmers. Although no definite conclusions can be drawn, the following observations can be made:

- (a) The IBM SSP packages are efficiently programmed. For example in the RKGS, the Gill's version is used and as such the Runge-Kutta constants are solved in a recursive manner. Hence the recursive formula of Equation 3-12 does not have a competitive edge over the RKGS.
- (b) It is found that in order to achieve comparable accuracy at the RKGS, for the same-step size, fairly high orders of the Taylor series in Equation 3-11 have to be used.

3-10 Choice of Strategy in Integration Step-Size Control

In practice, the economical step-size is determined by the kind of accuracy desired for the solutions. Since the total computation time is dependent

on the step-size, it is important to ensure that the step-size is not smaller than is demanded by the accuracy. Generally speaking, the step-size needs to be very small when the time rate of change of the solution is very large and conversely when the solutions have small gradients, it is possible to take large step-sizes. In Section 3-8 and in Figure 3-3 it has been shown that by choosing the synchronously rotating frame it is possible to obtain a solution which has less curvature than the solution in the d - q axis and as such the step-sizes can increase to the extent of halving the integration time.

In continuing to examine the current solution is in Figure 3-3, it can be noted that from the curvature argument, the integration step-size needs to be very small in the first few milliseconds. However as soon as this leakage inductance mode (see Section 5-4) becomes damped out, it is possible to increase the step-size because the curvature is lower. As such, the strategy of step-size control should be able to decrease and increase the step-size as the need arises.

3-10-1 Accuracy and Step-Size Control

A grave disadvantage of the One-Step Method such as the Runge-Kutta algorithms and of the special integration subroutines of Section 3-9-2) is that the truncation error cannot be estimated in the course of the calculations. The accuracy is estimated by comparing the results obtained from a step size 2 h and the results from twice the step-size h.

The multi-step method such as the HPCG have formulae for the local truncation error and the calculation procedure includes an estimate of the accuracy.

In both the HPCG and the RKGS the step-size control is as follows:

- (a) When the estimated truncation error for a step-size h is excessive of the accuracy tolerance, the result is rejected, the step size is halved and the computation is repeated and successively tested and halved until the accuracy tolerance is met.
- (b) When the truncation error is less than the accuracy tolerance, the result is accepted as correct. Whenever the truncation error is less than $\frac{1}{50}$ x accuracy tolerance, the next step is computed for a doubled increment, i.e. 2 h.

This strategy has proved to be reliable and stable, although the stepsize increase based on $\frac{1}{50}$ x accuracy tolerance may be on the conservative side.

The strategy used by Wiederholt, Fath and Wertz in Reference [40] is more complex. It consists of changing (a) the step-size and (b) the order of the Taylor series approximation, in response to accuracy requirements at each integration step. Besides simple logic tests as to whether the step-size and the order of the Taylor series need to be increased or decreased, there are memory statements as to whether the step-size and the Taylor series expansion were changed in the previous step.

3-10-2 Step-Size and the Spectral Radius

Hitherto, the term "curvature" in the solution has been used to express intuitive notions as to why the integration step-size needs to be large or small.

Mathematically a measure of this curvature is known as "spectral radius".

In a dynamic linear system of equations

$$p Y = [A] Y$$
 3-13

where [A] is a constant square matrix with eigenvalues in the left half of the complex plane only, the spectral radius is defined as

$$p([A]) = max | \lambda_i |$$
 3-14
 $i = 1, 2, ..., m$

where λ_1 , λ_2 , ..., λ_m are the eigenvalues of [A]

It is possible to prove [50] that in solving the linear system Equation,

3-14 by numerical integration, the solution would be numerically unstable if the step
size h is excessively large, i.e.

$$h > \frac{2}{p([A])}$$
 3-15

Equation 3-15 can be interpreted to mean that when a component of the solution is a highly damped and/or oscillatory mode, the step size must be very small.

Returning to Figure 3-3 again, the first few milliseconds correspond to a highly damped

leakage inductance mode for which the spectral radius is very high and consequently the h must be small.

Of course Figure 3-3 corresponds to the solution of the nonlinear equations, Equation 3-5 and not to the linear equations, Equation 3-13. Nevertheless it is possible to extend the concept of spectral radius to the nonlinear equations by replacing the constant $\begin{bmatrix} A \end{bmatrix}$ matrix with the Jacobian of F(Y), to give the spectral radius $P(\frac{\partial F}{\partial Y})$. As the numerical integration proceeds, $P(\frac{\partial F}{\partial Y})$ changes and ideally the step-size can lengthen or contract in unison with the spectral radius.

It must be emphasized that in actual fact, the step-size is usually limited by the accuracy tolerance before the numerical stability constraint is violated. Hence the spectral radius is only a rough guide based on a spacious argument that if the numerical stability constraint permits an increase in step-size, then a step-size increase is also likely to be permitted by the accuracy constraint.

Many times, it is permissible to increase the step-size based on accuracy constraint although the spectral radius point of view would argue against it. Thus for example, we take again the linear equations, Equation 3-13 to which Equation 3-15 sets a bound on the step-size. It is possible that (a) the mode of the eigenvalue from which p([A]) is taken is not excited and (b) that this mode is highly damped. In such a situation, the step-size h can be increased when (a) this particular mode is unexcited or (b) when the mode is damped out. Equation 3-15 assumes a fixed step-size strategy for the entire numerical integration run and of course is inferior to the dynamic strategies described in Section 3-10-1.

In spite of the lack of rigour and other limitations the spectral radius remains an important tool as (a) a plausible measure by which step-size changes can be discussed and more importantly (b) in showing how new and faster integration algorithms can be derived.

3-11 Modified Integration Algorithms

In Section 3-9, it has been found that by transforming from the d-q to the synchronously rotating \(\chi - \text{8} \) frame, it is possible to increase the integration step-size and hence improve that computation time. K.N. Stanton and S.N. Talukdar [50] have presented both theoretical and preliminary investigations of a general method of obtaining larger step-sizes through suitable mathematical transformations. Basically the method consists of transforming Equation 3-5 to

$$p \underline{Z} (t) = \underline{F}^{1} (\underline{Z} (t), t)$$
3-16

where a larger step-size can be used because the spectral radius $p(\lceil \frac{\partial F^{1}}{\partial Z} \rceil)$ of F^{1} is smaller than that of F^{2} in Equation 3-5.

The authors showed how this mathematical transformation can be achieved and have incorporated the transformation into modified Runge-Kutta and modified "Adams type" algorithms for which they claim five to ten times improvements in step-size.

3-12 Terminal Voltage and Initial Value Problems

Hitherto, only the methods of solving the nonlinear induction motor equations have been discussed. In this section, it will be shown how the methods and the system equations (as presented in Chapter II) can be used to study the variety of switching and reswitching problems (as listed in Section 3-1). Because of its simplicity only the d-q frame equations will be used.

In the literature, the problems have been classified as: the switching and the reswitching problems. As used by many authors [16], [29], the switching problem is used to describe the closing of a three-phase line to an inert induction motor at standstill. When the three contactors close simultaneously, the name simultaneous switching is given to it. Otherwise it is called nonsimultaneous switching.

The reswitching problem is used to describe the case when the induction motor operating under steadystate is interrupted and then a reswitching voltage is applied to it. This may occur in transferring the supply to another bus-bar (reconnection), or in bringing the motor to a halt by dynamic braking or plugging. Since the reswitching operation cannot be performed instantaneously, it consists of two interruptions: (a) at the point of disconnection and (b) at a point of reconnection. Between these two interruptions, the induction motor equations become degenerate and the transients need to be solved separately.

Essentially at each interruption, the following situations have to be dealt with:

(a) circuit topology changes,

- (b) terminal voltage constraint changes,
- (c) the matching of physically continuous quantities, this may be mechanical velocity, winding currents or magnetic flux.

3-12-1 Simultaneous Switching

(b) are

The electrically inert induction motor is described by the initial values

$$[i_d^s, i_q^s, i_d^r, i_q^r, \omega_m]^T = [0, 0, 0, 0, \omega_m]^T$$
 3-16

In simultaneous switching, the driving functions for Equations 2–10(a) and

$$\begin{bmatrix} e_{d}^{s} \\ e_{q}^{s} \\ e_{q}^{r} \\ e_{d}^{r} \end{bmatrix} = \begin{bmatrix} \cos (\omega_{c} + \alpha_{s}) \\ -\sin (\omega_{c} + \alpha_{s}) \\ 0 \\ e_{q}^{r} \\ 0 \\ T_{L} \end{bmatrix} \begin{bmatrix} U_{-1} & (t) \\ U_{-1} & (t) \\$$

As discussed in Section 2–10, as a consequence of the cylindrical symmetry, the torque pattern is independent of the switching angle α_s and the rotor position in simultaneous switching.

3-12-2 Nonsimultaneous Switching

In most practical cases, the switching contactors do not close simultaneously. At the time the second contactor closes, it forms a continuous electrical circuit with the first contactor and activates a system of dynamic equations which is a degenerate form of Equations 2-10 (a) and (b), i.e.

$$\begin{bmatrix} e_{q}^{s} \\ e_{d}^{r} \\ e_{q}^{r} \end{bmatrix} = \begin{bmatrix} R^{s} + L^{s} p & 0 & M p \\ -M n \omega_{m} & R^{r} + L^{r} p & -L^{r} n \omega_{m} \\ M p & L^{r} n \omega_{m} & R^{r} + L^{r} p \end{bmatrix} \begin{bmatrix} i_{q}^{s} \\ i_{d}^{r} \\ i_{q}^{r} \end{bmatrix}$$

$$3-18(a)$$

$$J_1 p \omega_m + f_1 \omega_m + T_L = -n M i_d^r i_q^s$$
 3-18(b)

These equations are solved for the initial conditions

$$[i_q^s, i_d^r, i_q^r, \omega_m] = [0, 0, 0, \omega_m]$$
 3-19

and for the driving functions

$$\begin{bmatrix} e_q^s \\ e_d^r \\ e_d^r \end{bmatrix} = \begin{bmatrix} -\sin(\omega_c t + \alpha_s) \\ 0 \\ 0 \\ T_L \end{bmatrix} U_{-1} (t)$$
3-20
$$T_L$$

Equation 3-18 describes a degeneracy which consists of the d-axis stator winding being in the open circuit. By the time the third contactor closes, at a phase angle β_s after the switching described by Equation 3-20, the solution of Equation 3-18 is

$$[i_{q}^{s}(t_{1}), i_{d}^{r}(t_{1}), i_{q}^{r}(t_{1}), \omega_{m}(t_{1})]^{T}$$
 3-21

where
$$t_{1-} = \frac{\beta_s}{\omega_c}$$
 3-22

At the point of the closing of the third contactor, the complete system equations of Equation 2-10 will be used. Shifting the time origin to this instant, the forcing function is described by

$$\begin{bmatrix} e_{d}^{s} \\ e_{d}^{s} \\ e_{q}^{s} \\ e_{q}^{r} \\ e_{d}^{r} \\ e_{d}^{r} \\ e_{d}^{r} \\ T_{L} \end{bmatrix} = \begin{bmatrix} \cos (\omega_{c} t + \alpha_{s} + \beta_{s}) \\ -\sin (\omega_{c} t + \alpha_{s} + \beta_{s}) \\ 0 \\ T_{L} \end{bmatrix} = \begin{bmatrix} \cos (\omega_{c} t + \alpha_{s} + \beta_{s}) \\ 0 \\ T_{L} \end{bmatrix}$$

$$3-23$$

From continuity considerations, the initial conditions of Equation 2–10 are the final values described by Equation 3–21, i.e.

$$\begin{bmatrix} i_{d}^{s} (t_{1+}), i_{q}^{s} (t_{1+}), i_{d}^{r} (t_{1+}), i_{q}^{r} (t_{1+}) \omega_{m} (t_{1+}) \end{bmatrix}^{T} = \begin{bmatrix} 0, i_{q}^{s} (t_{1-}), i_{d}^{r} (t_{1-}), i_{q}^{r} (t_{1-}) \omega_{m} (t_{1-}) \end{bmatrix}^{T}$$

$$3-24$$

Depending on the switching angles α_s and β_s a family of torque patterns will be produced. The influence of the switching angles has been studied by Enslin [21], Wood, Flynn and Shanmugasundaram [29].

3-12-3 Reswitching Problems

The reswitching problem in the induction motor is pictorially described in Figure 3-1 where the disconnect and the reconnect switching interruptions at time instants t_1 and t_2 break the problem into 3-piece-wise time segments.

(a) Before Disconnection $t < t_1$

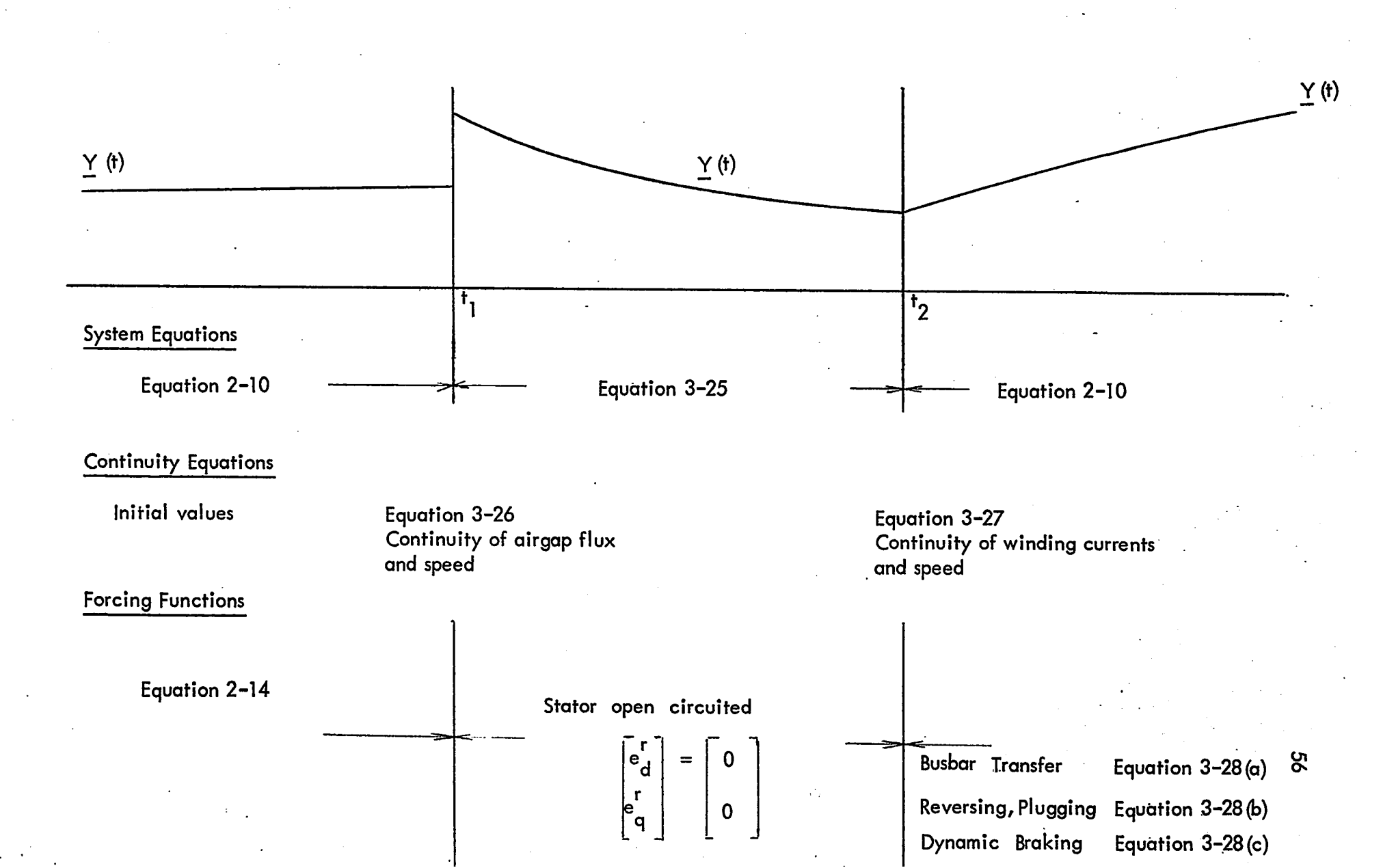
Prior to this disconnection the induction motor operates at a particular voltage specification $\begin{bmatrix} e^{sr} \\ dq \end{bmatrix}^1$ to which the complete system equation, Equation 2-10 is applicable. In many applications, this voltage specification is Equation 2-14 and by the time t_1 the system has arrived at the electro-mechanical steady-state. At the point of disconnection, the state is describable by the vector

$$\begin{bmatrix} i_{d}^{s} (t_{1}) & i_{q}^{s} (t_{1}) & i_{d}^{r} (t_{1}) & i_{q}^{r} (t_{1}) & \omega_{m} (t_{1}) \end{bmatrix}^{T}$$

(b) Disconnected Interval t₁ < t < t₂

In the disconnected interval, the stator windings are in open circuit because of the finite time it takes to switch on the second voltage supply $\left[e^{sr}_{dq}\right]^{11}$ after the first one has been removed. Since $i_d^s = i_q^s = 0$, the system equations

FIGURE 3-1. RESWITCHING SEQUENCES.



degenerate to

$$\begin{bmatrix} 0 \\ 0 \end{bmatrix} = \begin{bmatrix} R^{r} + L^{r} p & -nL^{r} \omega_{m} \\ nL^{r} \omega_{m} & R^{r} + L^{r} p \end{bmatrix} \begin{bmatrix} i_{d}^{r} \\ i_{q}^{r} \end{bmatrix}$$
3-25(a)

$$J_1 p \omega_m + f_1 \omega_m + T_1 = 0$$
 3-25(b)

In this interval, the magnetic flux associated with the rotor currents decays and likewise the rotor decelerates because of the load $\,T_L\,$ and viscous friction $\,f_1\,$.

Before the numerical integration of Equation 3-25 can proceed, it is necessary to know the initial values of the system. Arguing that the airgap flux cannot change instantaneously, we have the initial conditions as

$$\begin{bmatrix} i_{d}^{r} & (t_{1+}) \\ i_{q}^{r} & (t_{1+}) \\ \omega_{m} & (t_{1+}) \end{bmatrix} = \begin{bmatrix} i_{d}^{s} & (t_{1-}) + i_{d}^{r} & (t_{1-}) \\ i_{q}^{s} & (t_{1-}) + i_{q}^{r} & (t_{1-}) \\ \omega_{m} & (t_{1-}) \end{bmatrix}$$
3-26

At the instant of reswitching, the state-vector after decay is

3-27

(c) Reconnection $t > t_2$

At the instant of reconnection t_2 , the initial values are

$$\begin{bmatrix} i_{d}^{s} (t_{2+}) \\ i_{q}^{s} (t_{2+}) \\ i_{d}^{r} (t_{2+}) \\ i_{q}^{r} (t_{2+}) \\ \vdots \\ \omega_{m} (t_{2+}) \end{bmatrix} = \begin{bmatrix} 0 \\ 0 \\ i_{d}^{r} (t_{2-}) \\ i_{q}^{r} (t_{2-}) \\ \vdots \\ \omega_{m} (t_{2-}) \end{bmatrix}$$

The system equations, Equation 2-10 are then solved for the forcing functions described by the supply voltages $\begin{bmatrix} e^{sr} \\ dq \end{bmatrix}^{11}$. The different specifications of the reswitching voltages are :

Busbar Transfer

$$\begin{bmatrix} e_{dq}^{sr} \end{bmatrix}^{1} = \begin{bmatrix} E_{p} \cos (\omega_{c} t + \alpha_{s1}) \\ -E_{p} \sin (\omega_{c} t + \alpha_{s1}) \end{bmatrix} \quad U_{-1} (t - t_{2}) \quad 3-28(a)$$

$$0 \quad 0$$

Reversing and Plugging

$$\begin{bmatrix} e_{dq}^{sr} \end{bmatrix}^{11} = \begin{bmatrix} E_{p} \cos(\omega_{c} t + \alpha_{s}) \\ E_{p} \sin(\omega_{c} t + \alpha_{s}) \\ 0 \end{bmatrix} \quad U_{-1} \quad (t - t_{2})$$
 3-28(b)

Dynamic Braking

$$\begin{bmatrix} e_{dq}^{sr} \end{bmatrix}^{11} = \begin{bmatrix} E_{d.c.}^{1} \\ U_{-1} & (t - t_{2}) \end{bmatrix}$$

$$\begin{bmatrix} e_{dq}^{sr} \end{bmatrix}^{11} = \begin{bmatrix} E_{d.c.}^{1} \\ E_{d.c.}^{11} \\ 0 \\ 0 \end{bmatrix}$$
3-28(c)

3-13 <u>Numerical Examples</u>

Programs have been written which solve the dynamic equations of the induction motor under switching and reswitching constraints. The rest of this chapter will be concerned with presenting the solutions for a few practical examples related to synchronous switching.

Since this thesis has interests in discovering the physical nature of the transients, subroutines have been incorporated which analyse and display the solutions in terms of power exchange, energy storage and m.m.f. space-vectors. It is found that the m.m.f. space-vectors viewpoint has been most rewarding, especially in correlating the production of transient torque from current solutions.

The solutions presented are for a typical induction motor, the parameters of which are listed in Appendix G.

3–14 Torque Transients in Synchronous Switching

3-14-1 d - q Currents Viewpoint

Figures 3-2 and 3-3 show examples of synchronous switching transients for $E_p = 300 \text{ volts}$, $f_1 = 0.01 \text{ newton-metre-sec.}$, $T_L = 0.0$. Figure 3-2, which is for a moment of inertia $J_1 = 0.006$, shows the acceleration torque pattern consisting of two parts: (a) the electrical transient portion 0 - 0.1 sec., which has a 60 Hz oscillating component and (b) a mechanical transient portion 0.1 - 0.2 sec., which indicates that the acceleration is in accordance to the static torque-speed characteristics of conventional theory.

Figure 3-3 which is a larger moment of inertia $J_1 = 0.06$ shows on an enlarged time scale, (a) the electromechanical torque, (b) the rotor speed and (c) a typical stator current i_d^s , for the first portion of the transient. All the other state-variables are not presented because they are similar except for phase shifts and besides they cannot reveal the relationship of torque to the motor currents. Visually it is baffling that although the stator currents seem to have subsided by the first or second cycle, the transient torque persists in oscillating. A complete explanation of this is given in Chapter IV where the nonlinear equations are linearised by assuming a constant speed. For the present, the m.m.f. viewpoint is instructive.

3-14-2 Space-Vector Viewpoint of Transient Torque

Figure 3-4(b) displays the magnitude of $_{\rm s}$, $_{\rm r}$ and M $_{\rm m}$ which are constructed from the state-currents solutions of the numerical integration subroutines.

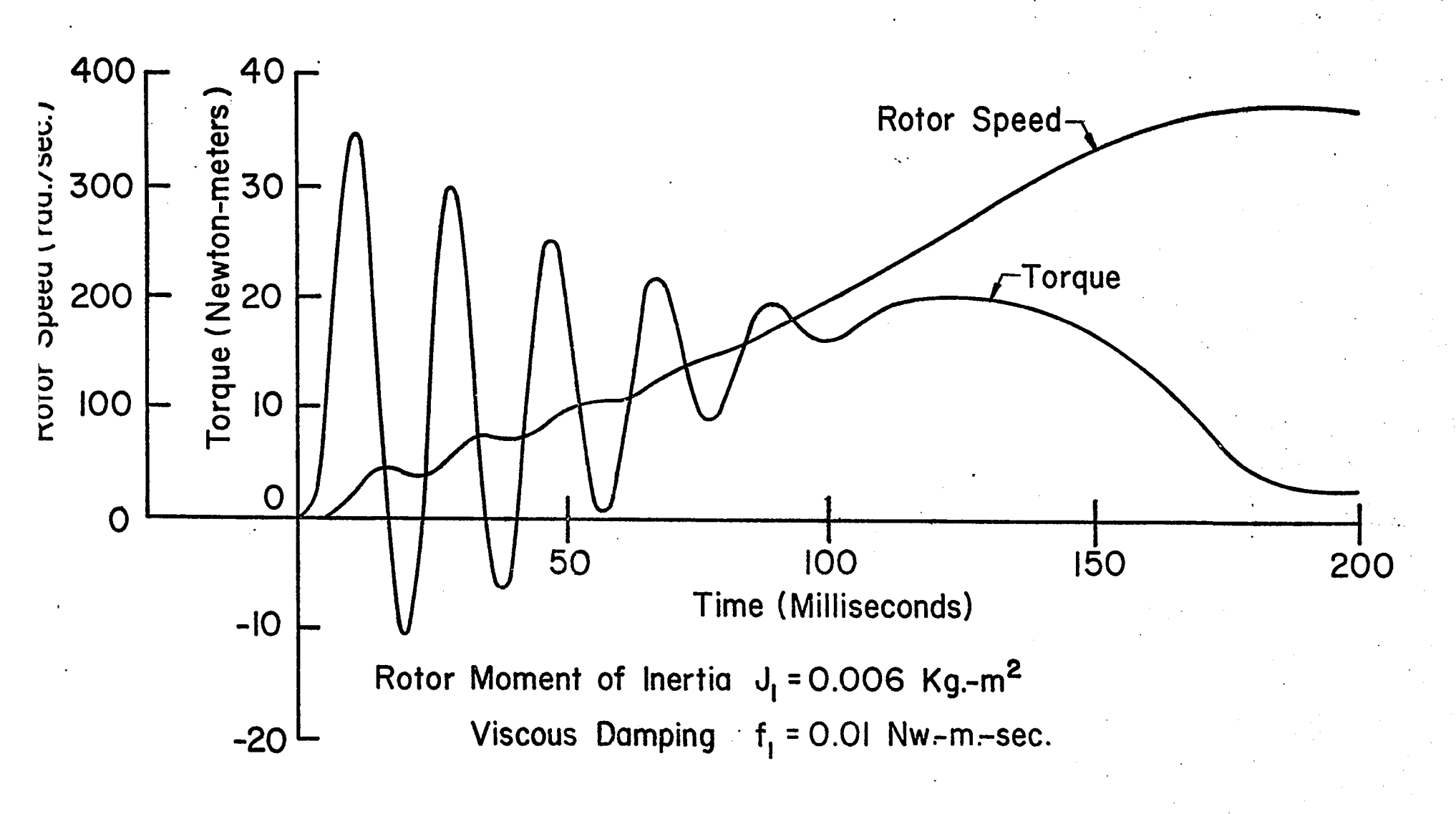
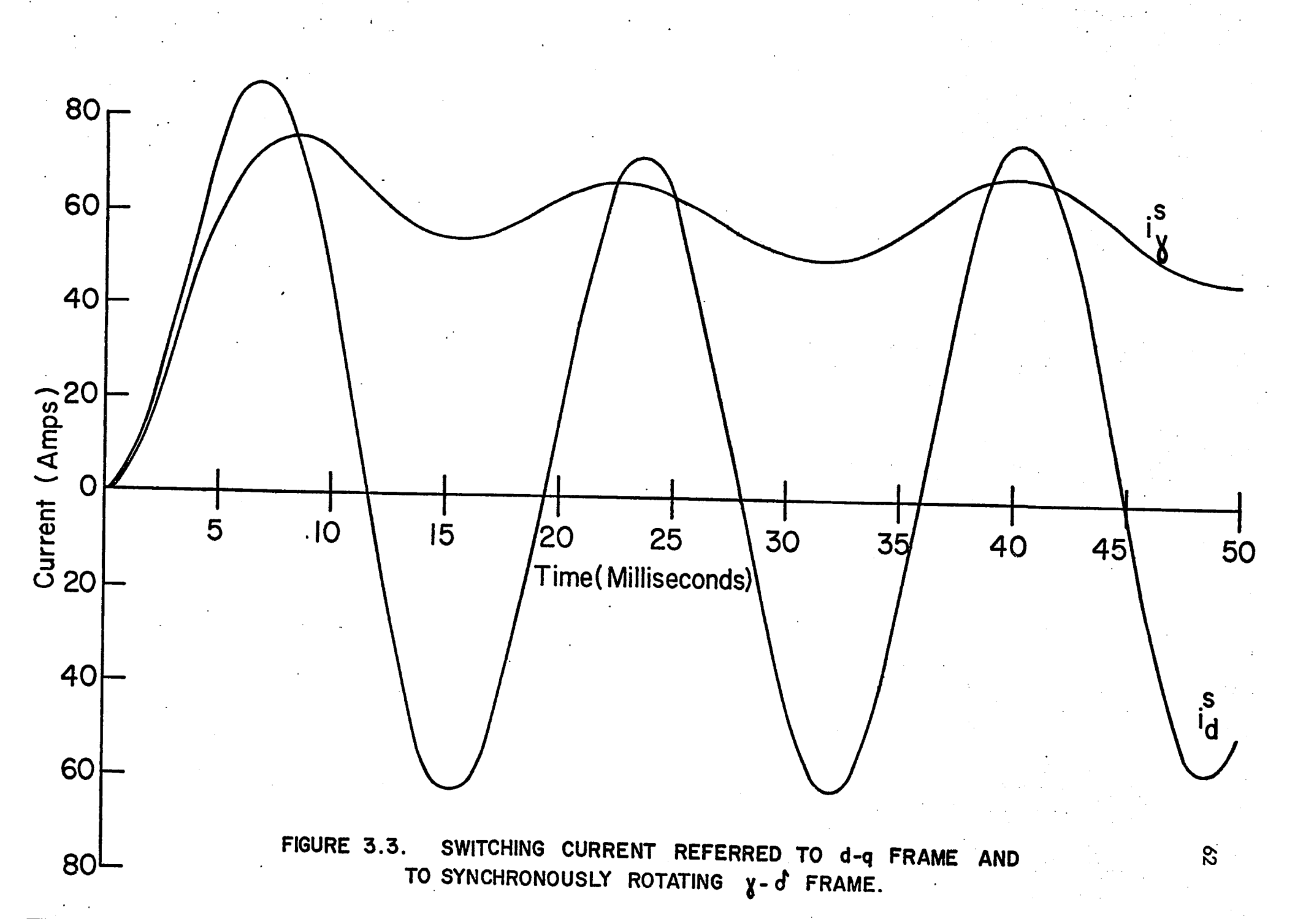
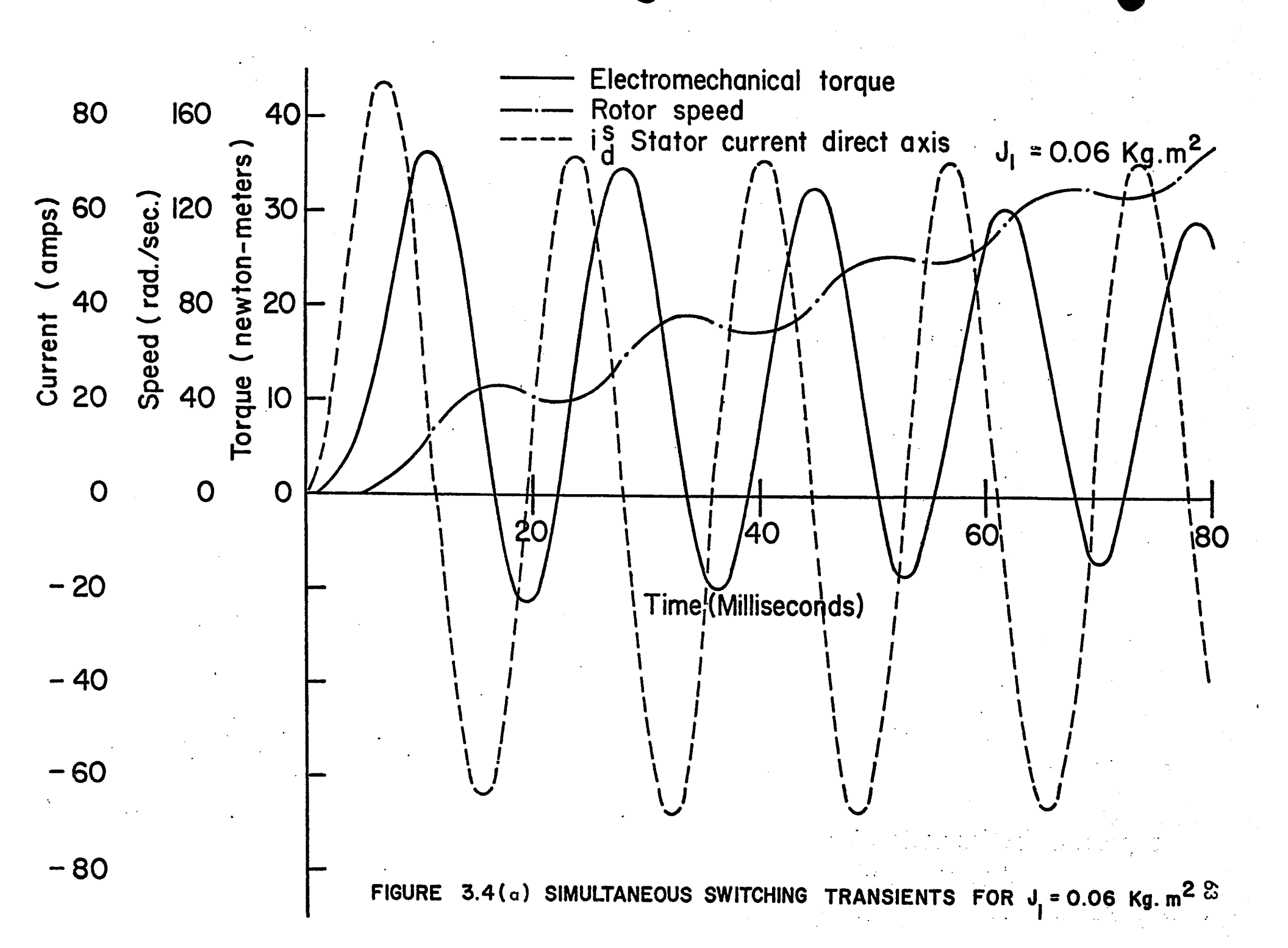


FIGURE 3.2. TORQUE AND SPEED TRANSIENTS IN SIMULTANEOUS SWITCHING FOR $J_1 = 0.006 \, \text{Kg.-m}^2$





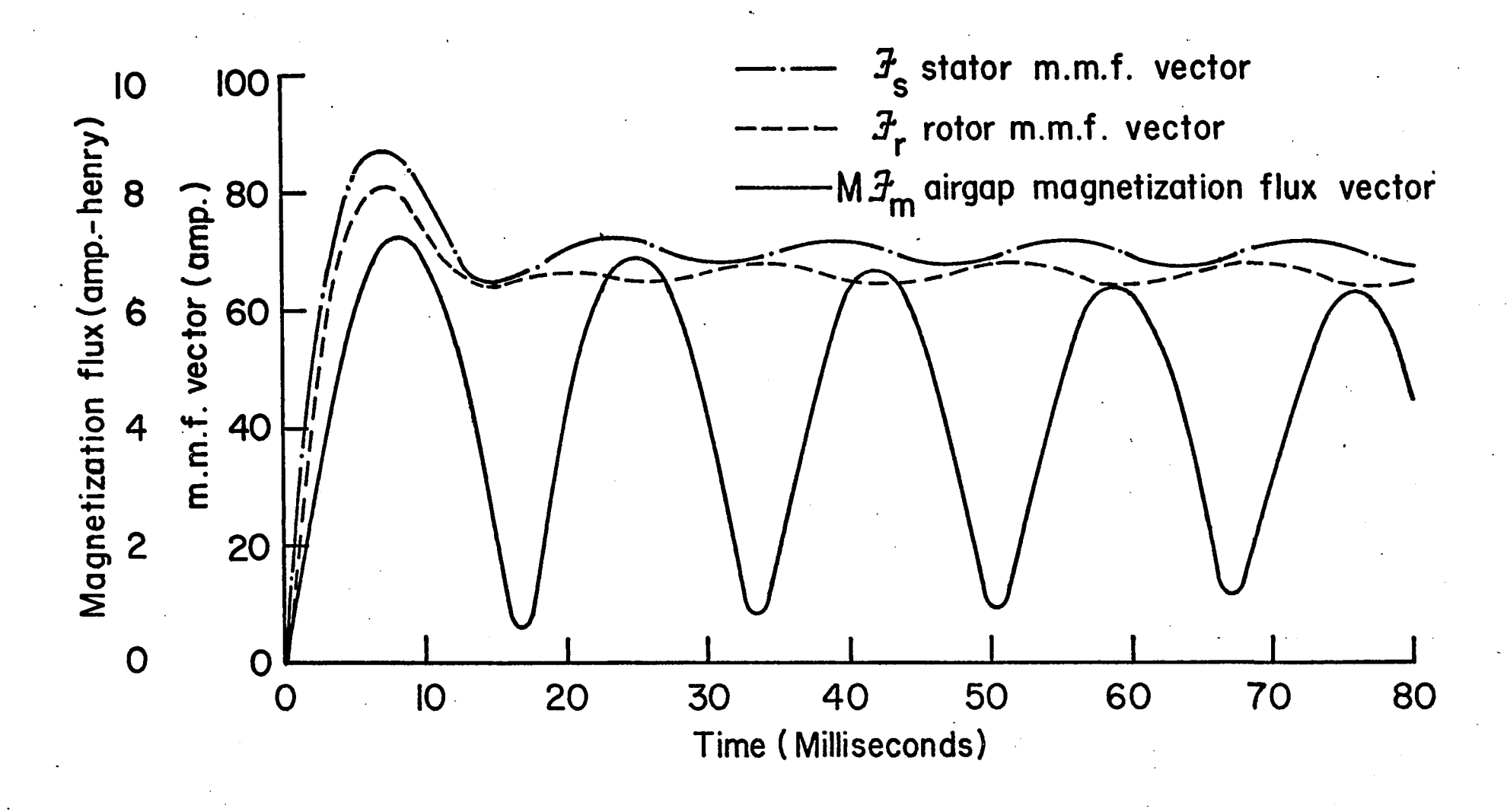


FIGURE 3.4 (b) MAGNITUDES OF SPACE-VECTORS IN SIMULTANEOUS SWITCHING TRANSIENT FOR J,= 0.06

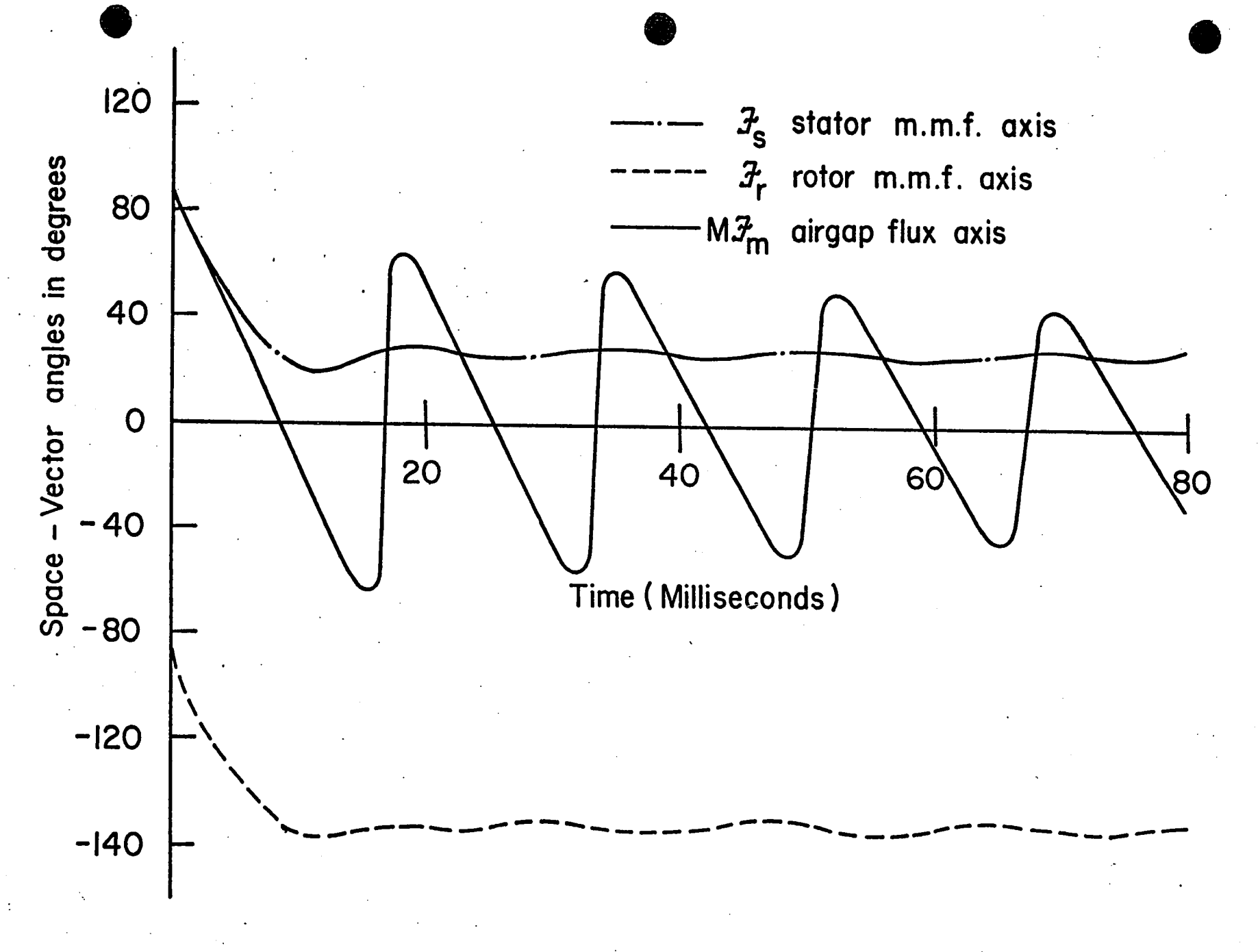


FIGURE 3.4 (c). SPACE - VECTOR ANGLES REFERRED TO SYNCHRONOUS REFERENCE FRAME

5

Figure 3-4(c) displays the phase-angles \mathscr{G}_r , \mathscr{G}_s , \mathscr{G}_m as viewed from the synchron-ously rotating frame. The space vector quantities are defined in Equations 2-19 to 2-21. With these space-vectors and using the electromagnetic equation, Equations 2-22 to 2-23, it is possible to relate the production of transient torque with the physical quantities as they occur in the airgap of the induction motor.

On a qualitative basis, it can be said that as soon as the voltage is switched on, the stator currents build up very quickly to produce a stator m.m.f. which remains roughly constant in magnitude and which rotates synchronously with the supply. In response to Lenz's law the induced rotor currents flow to produce a rotor m.m.f. which is slightly less in magnitude and in an opposite direction to the stator m.m.f. vector. Thus the displays show $|\mathcal{F}_s| \approx |\mathcal{F}_r|$ and $\mathcal{F}_s - \mathcal{F}_r \approx 180^\circ$ electrical. The difference between the vector \mathcal{F}_s and \mathcal{F}_r is the magnetization current vector \mathcal{F}_m . Magnetization flux in the airgap space and in the period of the oscillating electromagnetic torque, it is this quantity which oscillates in magnitude and in angle with respect to the synchronously rotating frame. Using the torque equations, Equation 2-23 or Equation 2-24, the torque pattern of Figure 3-4(a) can be correlated with the spacevectors of Figure 3-4(b) and Figure 3-4(c). In particular it is interesting to note the negative torques occur when $\sin(\mathcal{F}_s - \mathcal{F}_m)$ becomes negative.

3-15 Supersynchronous Motoring Torque

A well-documented and interesting fact in acceleration transients of the induction motor is that the mechanical speed can exceed the supply synchronous speed

[28], [30]. This phenomenon is investigated in the numerical example in which $J_1=0.0006$ is assigned to the rotor inertia and the rotor exceeds the synchronous speed in the second cycle. The surprising fact here is that the torque $T_{\rm em}$ can be positive when $\omega_{\rm m}>\omega_{\rm c}$. This appears in the numerical integration solution shown in Figure 3-7(a) in time segment 0.018< t<0.025 sec.

This existence of a super-synchronous motoring torque requires fundamental revision of established induction motor theory. In conventional theory, the airgap power is associated with the synchronous speed, $\omega_{\rm c}$ and a conventional argument against the possibility of $T_{\rm em} > 0$ when $\omega_{\rm m} > \omega_{\rm c}$ is summarised by the question : Where would the power come from ?

In answering this question it is proposed that the airgap power be associated with 0, the instantaneous angular velocity of the magnetization airgap flux, rather than the synchronous speed ω_{C} .

3-16 Instantaneous Airgap Power

The angular velocity of the airgap flux vector \mathcal{G}_{m} can be obtained by differentiating Equation 2–21 (b)

and the airgap power is defined as

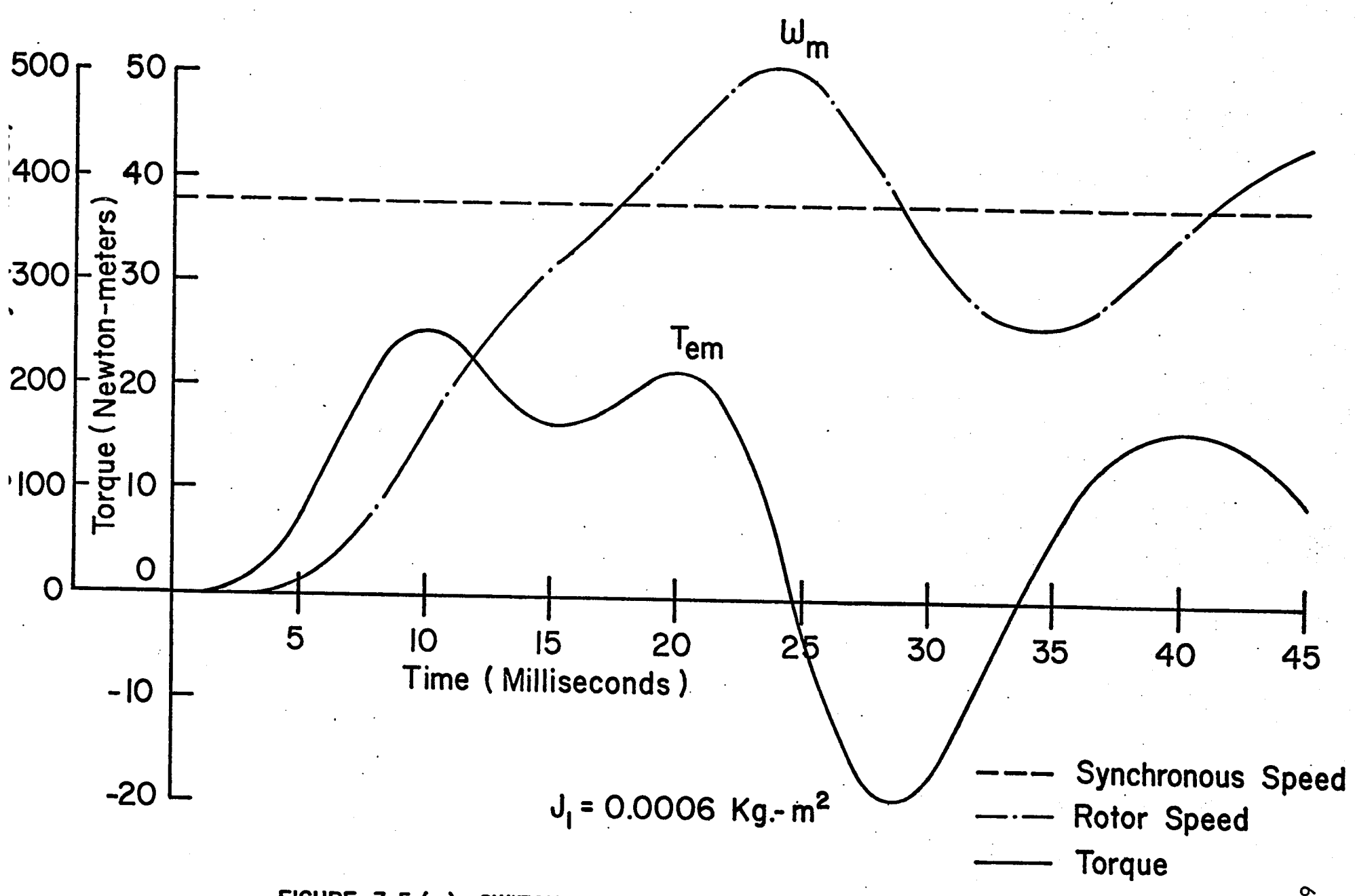


FIGURE 3.5 (a). SWITCHING TRANSIENTS SHOWING THE OCCURENCE OF SUPERSYNCHRONOUS ROTOR SPEED AND MOTORING TORQUE

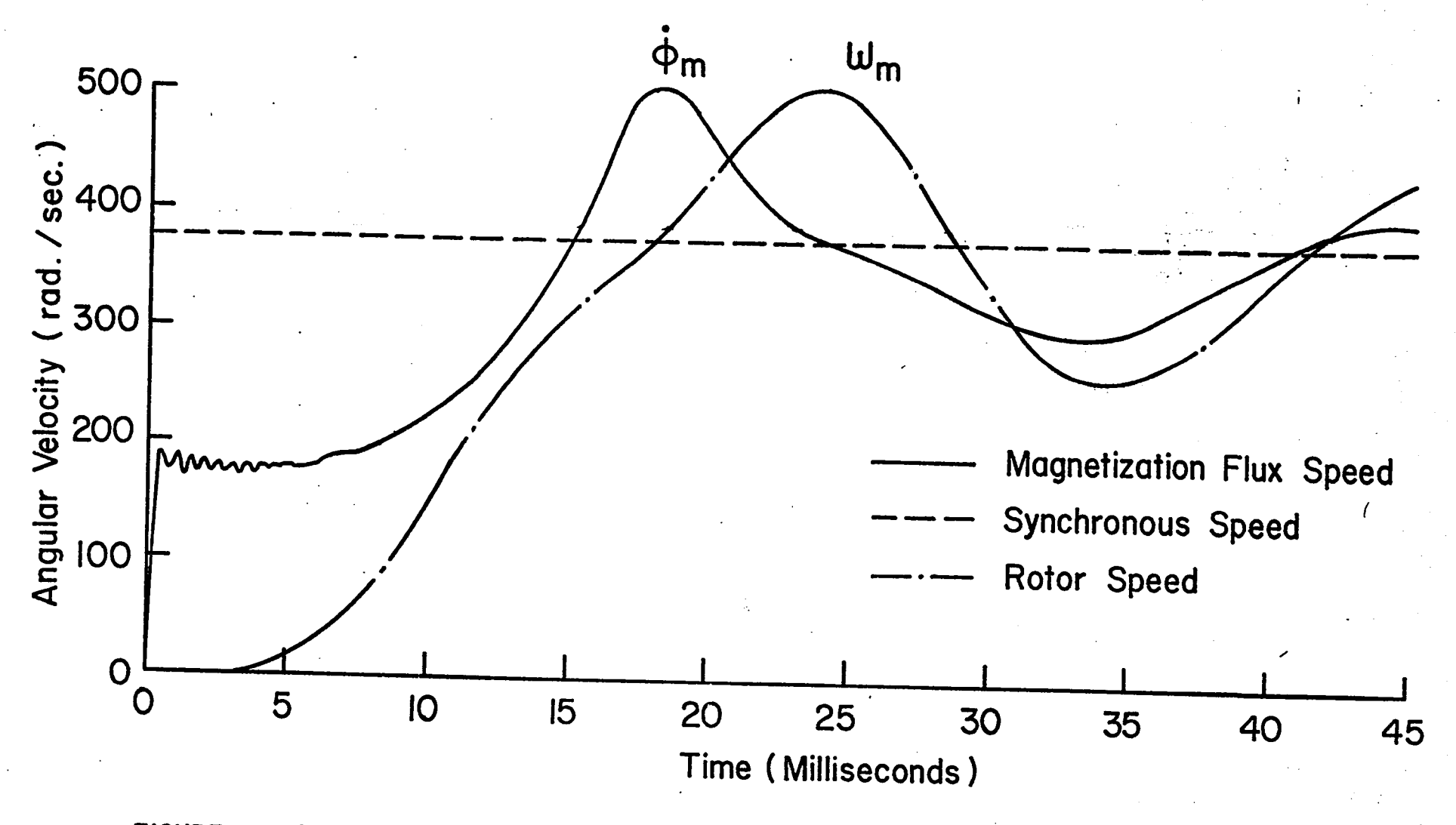
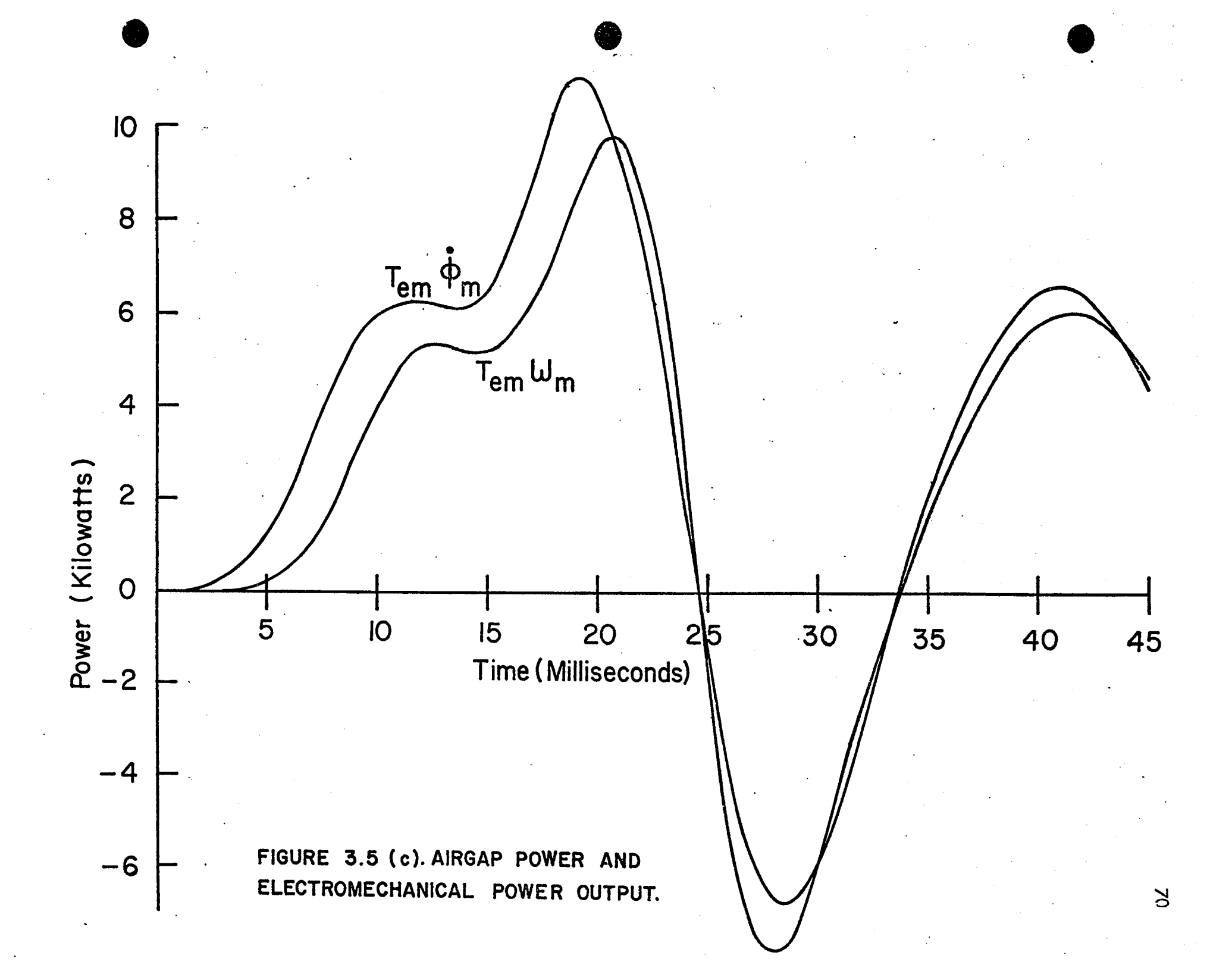


FIGURE 3.5(b). ROTOR ANGULAR VELOCITY AND INSTANTANEOUS ANGULAR VELOCITY OF MAGNETIZATION FLUX VECTOR



$$P_{ag} = T_{em} p_{m}$$
 3-30

This definition comprehends the conventional definition because in the steady state $g_m' = \omega_c$.

Figure 3-5(b) shows the time sequence of ω_m and \emptyset_m' for the same acceleration transient as in Figure 3-5(a). Although ω_m exceeds the synchronous speed ω_c , the airgap flux can still have a higher velocity.

More convinving still, Figure 3-5(c) shows the airgap power $T_{em} \mathcal{D}_{m}$ besides the mechanical power output $T_{em} \omega_{m}$. In the regions of negative torque, the direction of airgap power transfer is reversed, i.e. the kinetic energy in the rotor inertia is transferred back to the stator. Although, $T_{em} \mathcal{D}_{m} - \omega_{m}$ can be negative at many instants, the time integral is always positive, i.e.

$$\int_{0}^{t} T_{em} (p'_{m} - \omega_{m}) d C \ge 0$$
3-31

Figures 3-5(b) and (c) illustrate the feasibility of the definition of airgap power. In Appendix B, it will be demonstrated that the induction motor differential equations imply such a definition for the airgap power. Finally by translating the lumped parameter formulation of the induction motor into an electromagnetic field problem, it can be shown that the definition of Equation 3-30 is required by airgap power transfer considerations using the Poynting's Theorem.

CHÁPTER IV

MODAL ANALYSIS OF CONSTANT SPEED

INDUCTION MOTOR EQUATIONS

4-1 Introduction

Although the numerical solutions generated by the digital computer subroutines described in Chapter III are accurate, their lack of analytical insight is a serious disadvantage. It is possible to sacrifice accuracy for insight if the induction motor equations are linearised by making the constant speed assumption. Many studies [16], [21], [22], have usefully pursued this line of attack and have characterised the dynamic behaviour of the induction motor from the roots of the constant speed linear equations. These studies employ the Laplace Transform technique which reduces the linear differential equations into an algebraic characteristic equation of the fourth order. Typically it is not possible to find the 4 characteristic roots $\sigma_1 \pm i \omega_1$, $\sigma_2 \pm i \omega_2$ explicitly in terms of the system parameters. Since the roots are ultimately solved numerically, much of the advantages claimed for the analytical solution are in fact lost.

The modal approach which is presented here is mathematically equivalent to the Laplace Transform method. It has the advantage that it offers a compact and elegant matrix formulation, exploits fully the capabilities of the digital computer, and present the eigenvector matrix and its inverse as tools for understanding the inter-relation-ship of modes and excitations.

The modal analysis consists essentially of transforming the linear system equations from the current-coordinates to a set of fictitious normal coordinates which are in the directions of the system eigenvectors. The theory of such a transformation is described in many standard texts of the state space approach to linear systems [51 - 53].

4-2 Constant Speed Linearization

By assuming that the rotor shaft speed $\omega_{\rm m}$ is constant, the electrical system equation, Equation 2-10(a) becomes mathematically linear. The mechanical equation, Equation 2-10(b), is considered to be decoupled, i.e. although the electrical currents produce an electromechanical torque, the rotor shaft speed cannot change since an infinite inertia is implicitly assumed.

In many switching transients where the angular acceleration is small by virtue of the large mechanical inertia, it is instructive to divide the accelerating transient into as many time segments as the accuracy demands. In each of the time segment, the rotor speed ω_m is incremented to a constant value representative of the rotor speed. The electrical equations are solved as linear equations in that time segment for the representative ω_m . The connection between the two adjacent time segments are: the final state of the previous time segment becomes the initial values of the present time segment. Although this method will not be as efficient and as accurate as the numerical integration subroutines, it offers valuable qualitative insight because the roots of the linearized electrical equations form a very useful basis for characterizing the induction motor dynamics.

The importance of these roots will be apparent again in Chapter VI which is a study of the stability of the induction motor at each operating point. There, it will be shown that of the 5 eigenvalues which characterize the dynamic properties of a steady-state operating point, 4 of them are identifiable with those of the constant speed electrical equations.

The Constant Speed Induction Motor Equations

The electrical equation, Equation 2-10(a) expressed in the standard statevariable form is:

$$P i_{dq} = [A_{dq}] i_{dq} + [B_{dq}] e_{dq}$$
4-1

where

here
$$\begin{bmatrix} A_{dq} \end{bmatrix} = -\frac{1}{L^{s}L^{r} - M^{2}} \begin{bmatrix} L^{r}R^{s} & n M^{2} \omega_{m} & -M R^{r} & nM L^{r} \omega_{m} \\ -n M^{2}\omega_{m} & L^{r}R^{s} & -n M L^{r}\omega_{m} & -M R^{r} \\ -M R^{s} & -n M L^{s}\omega_{m} & L^{s}R^{r} & -n L^{s}L^{r}\omega_{m} \\ n M L^{s}\omega_{m} & -M R^{s} & nL^{s}L^{r}\omega_{m} & L^{s}R^{r} \end{bmatrix}$$

and

$$[B_{dq}] = [L]^{-1} = \frac{1}{L^{s} L^{r} - M^{2}} \begin{bmatrix} L^{r} & 0 & -M & 0 \\ 0 & L^{r} & 0 & -M \\ -M & 0 & L^{s} & 0 \\ 0 & -M & 0 & L^{s} \end{bmatrix}$$
4-3

Since $\begin{bmatrix} A_{dq} \end{bmatrix}$ is a constant matrix when ω_m is assumed constant, the dynamic system behaviour is determined by its eigenvalues. It is possible to proceed directly to the modal frame from a knowledge of the eigenvectors of $\begin{bmatrix} A_{dq} \end{bmatrix}$. However, after setting up the d-q axis frame equations, it is preferable to proceed to the synchronous reference frame for two reasons.

- (a) For motor standstill transients $\omega_m=0$, $[A_{dq}]$ contains two pairs of coincident real roots. These represent complications and require separate treatment in the modal analysis. It will be assumed throughout this study that the eigenvalues are distinct where the treatment is simpler. Although the synchronously rotating frame does not guarantee that the eigenvalues are always distinct for all ω_m , it does guarantee it for the very important practical case of switching from rotor standstill, i.e. $\omega_m=0$.
- (b) For a symmetrical single frequency voltage supply, the synchronously rotating reference frame voltages are d.c. voltages (see Equation 2-15) and the algebraic solutions can be solved very simply.

The synchronous reference frame equation, Equation 2-13(a) is written in the standard form as:

$$p \stackrel{i}{=} \chi_{\delta} = [A_{\chi_{\delta}}] \stackrel{i}{=} \chi_{\delta} + [B_{\chi_{\delta}}] \stackrel{e}{=} \chi_{\delta}$$

where

where the slip S is defined as

$$S = \frac{\omega_f - n \omega_m}{\omega_f}$$

and

$$\begin{bmatrix} B_{\chi\delta} \end{bmatrix} = \begin{bmatrix} C_{\chi\delta}^{dq} \end{bmatrix}^T \begin{bmatrix} L \end{bmatrix}^{-1} \begin{bmatrix} C_{\chi\delta}^{dq} \end{bmatrix}$$
$$= \begin{bmatrix} L \end{bmatrix}^{-1}$$

It must be noted that there is one slight disadvantage in considering the modes of $[A_{Y\delta}]$ viz: the eigenvalues are not physical. Although the real part

corresponds to the damping coefficient of the measured currents (in the stationary d - q frame), the imaginary part of the eigenvalue of [A 38] must be interpreted as the natural frequency of oscillation with respect to the synchronously rotating reference frame. The dependence of the imaginary part of the eigenvalues on the velocity of the reference frame can be viewed as a Doppler effect phenomenon.

4-4 The Modal Analysis

In Equation 4-1 and Equation 4-4, one sees that in spite of the fact that they are linear differential equations they are still difficult to solve because neither $\begin{bmatrix} A_{dq} \end{bmatrix}$ nor $\begin{bmatrix} A_{\chi\delta} \end{bmatrix}$ is a diagonal matrix and there is intercoupling between all the state-variables. Essentially the modal approach consists of a linear transformation which achieves this diagonalization and hence decoupling. This is possible if we can find $\begin{bmatrix} A_{\chi\delta} \end{bmatrix}$ and $\begin{bmatrix} S_{\chi\delta} \end{bmatrix}$ such that:

$$[A_{\chi_{\delta}}] = [S_{\chi_{\delta}}][\Lambda_{\chi_{\delta}}][S_{\chi_{\delta}}]^{-1}$$
 4-8

$$[\Lambda_{\delta\delta}] = [S_{\delta\delta}]^{-1} [A_{\delta\delta}] [S_{\delta\delta}]$$
 4-9

where

$$[S_{\chi_{\delta}}][S_{\chi_{\delta}}]^{-1} = [I]$$
 4-10

and

$$\begin{bmatrix} \Lambda_{\delta} \delta \end{bmatrix} = \begin{bmatrix} \lambda_1 & & & \\ & \lambda_2 & & \\ & & \lambda_3 & & \\ & & & \lambda_4 \end{bmatrix}$$

where only the diagonal terms λ_1 , λ_2 , λ_3 , λ_4 are non-zero and distinct.

Hence defining a set of modal state-variables, $\frac{q}{2} \delta$ which are related to the current variables by the transformations,

$$\underline{q}_{\chi\delta} = [S_{\chi\delta}]^{-1} \quad \underline{i}_{\chi\delta} \qquad 4-12(\alpha)$$

$$\frac{i}{2} \chi_{\delta} = [S_{\chi_{\delta}}] \underline{q}_{\chi_{\delta}}$$
 4-12(b)

Equation 4-4 can be transformed to

$$P \underline{q}_{\chi\delta} = [\Lambda_{\chi\delta}] \underline{q}_{\chi\delta} + \underline{\nu}_{\chi\delta}$$
 4-13

where the modal driving function is

$$\frac{\nu}{2} \delta = \left[S \delta S \right]^{-1} \left[L \right]^{-1} = \delta S$$

and the modal initial condition is

$$\underline{q}_{\chi\delta}$$
 (o) = $[S_{\chi\delta}]^{-1}$ $\underline{i}_{\chi\delta}$ (o) 4-15

For simplicity, numerical notations will be used, in describing the modal quantities:

$$\underline{q}_{\chi\delta}^{T} = [q_1, q_2, q_3, q_4]$$
4-16

$$\frac{\nu}{2} \chi_{8}^{T} = [\nu_{1}, \nu_{2}, \nu_{3}, \nu_{4}] \qquad 4-17$$

Equation 4-13. which is the system equation written in the modal frame, constitutes the objective of our transformations. Since $[\Lambda_{\delta\delta}]$ is a diagonal matrix, the modal co-ordinates are decoupled and Equation 4-13 can be solved separately row by row. Each row is of the form:

$$p q_{K} = \lambda_{K} q_{K} + \nu_{K} (t)$$
 4-18

for
$$K = 1, 2, 3, 4$$
.

The solution of Equation 4-18 for an initial modal value q_K (o) is

$$q_K(t) = q_K(0) \exp \lambda_K t + \int_{-\infty}^{t} \exp \lambda_K(t - \tau) \nu_K(\tau) d\tau$$
 4-19

The first term of Equation 4-19 is the transient response excited by the initial conditions. The second term is a convolution integral of the impulse response of the Kth mode with the modal driving function $\nu_{\rm K}$ (t).

In the restricted case of the balanced single frequency voltage supply, $\nu_{\rm K} \ ({\rm t}) \ = \ \overline{\rm E}_{\rm K} \ \ {\rm is \ a \ constant \ complex \ number \ when \ using \ the \ synchronously \ rotating \ re-}$

ference frame. As such, the formidable expression of the convolution integral can be avoided and Equation 4-19 simplifies to:

$$q_{K}(t) = [q_{K}(0) + \frac{\overline{E}_{K}}{\lambda_{K}}] \exp \lambda_{K} t - \frac{\overline{E}_{K}}{\lambda_{K}}$$

$$4-20$$

Closed form expressions of Equation 4-19 can be obtained for a large class of practical voltage supplies especially when they can be expressed as sinusoidally time varying functions and their harmonics.

Once the modal solutions of Equation 4-19 or Equation 4-20 have been solved, the solutions in the original reference frame can be transformed back through Equation 4-12.

The key to the modal analysis is the possibility of finding the matrices [Λ_{δ}] and [S_{δ}] which satisfy the equations, Equations 4-8 to 4-11.

4-5 Eigenvalues and Eigenvectors

In many standard text-books on linear systems using the state-space approach [51], [52], the basic mathematical relationships of Equation 4-8 to Equation 4-11 are discussed. It suffices only to restate the important definitions and results.

The Eigenvalue Matrix

[$\Lambda_{\gamma\delta}$] is the eigenvalue matrix of [A $_{\gamma\delta}$] and each of the diagonal elements λ_1 , λ_2 , λ_3 , λ_4 are the eigenvalues. It is to be recalled that each of the eigenvalues λ_K is a complex number which satisfies the determinant equation

$$\det \left(\left[A \right]_{8} \right] - \lambda_{K} \left[\right] = 0$$
 4-21

It is assumed that the eigenvalues are distinct.

The Eigenvector Matrix

[S χ_{δ}] is the eigenvector matrix of [A χ_{δ}]. Each of the columns of [S χ_{δ}] is the corresponding eigenvector of λ_1 , λ_2 , λ_3 , λ_4 , that is

$$[s_{\delta\delta}] = [\underline{U}_1 : \underline{U}_2 : \underline{U}_3 : \underline{U}_4] \qquad 4-22$$

and by definition, the eigenvector is the non-zero vector which satisfies the equation

$$[A_{KS}] \underline{U}_{K} = \lambda_{K} \underline{U}_{K}$$
 4-23

In assuming that all the 4 eigenvalues λ_K of [A $_8\delta$] are distinct, then all the 4 eigenvectors \underline{U}_K are linearly independent.

4-6 Eigenvalue and Eigenvector Subroutines

The modal analysis would have been an academic exercise had it not been for the existence of fast digital computer subroutines which can solve for the eigenvalues and the eigenvectors of a general matrix, quickly and accurately.

The program used throughout this study is the DAL 4 which is available in the SHARE Program Library (SDA 3385). This program computes in double precision the eigenvalues, and optionally the eigenvectors of a real general matrix of size up to 30×30 . By adapting the input and output statements, the DAL 4 has been changed into a subroutine well suited to the induction motor problem. The numerical method in the subroutine consists of using the Leverrier method of finding the coefficients of a characteristic polynomial and the roots are calculated by means of Newton-Raphson Method [54].

It is found that double-precision is essential to acceptable results. For example, attempts have been made to use the single precision ALLMAT subroutine which is available in the McGill Computer Library. Although the eigenvalues are acceptable, the eigenvectors are insufficiently accurate because the complex eigenvectors do not come out in complex conjugate pairs.

To give an estimate of the computation time, it takes altogether 2.4 seconds in the IBM 7094 (a) to calculate $\begin{bmatrix} A & \chi & \delta \end{bmatrix}$ from the system parameters, (b) to use the DAL 4 to solve for the eigenvalue matrix $\begin{bmatrix} A & \chi & \delta \end{bmatrix}$ and the eigenvector matrix $\begin{bmatrix} S & \chi & \delta \end{bmatrix}$, (c) to use a complex inversion matrix to obtain $\begin{bmatrix} S & \chi & \delta \end{bmatrix}^{-1}$ and (d) finally to reconstruct $\begin{bmatrix} A & \chi & \delta \end{bmatrix}$ from Equation 4-8 to test for accuracy.

4-7 Constant Speed Transients in Induction Motor

the same constant speed induction motor transients as previous workers [16], [21] and [22] have done. But unlike the Laplace Transform methods, a minimum of algebra is required of the programmer. Furthermore because of the unwieldy algebraic expressions of the Laplace Transform methods, previous workers have been daunted from solving any but the simplest switching problems. However the modal method enables a combination of initial value and voltage problems to be solved, by reading in the appropriate initial values into the computer. The treatment of the initial conditions is especially significant in considering accelerating transients from the viewpoint of constant speed linear equations. The initial currents enable one set of linearised solutions to be related to the next set solved for an incremented speed.

4-8 A Numerical Example

The foregoing concepts will now be illustrated by a numerical example. The analysis is presented for the locked rotor transients of a typical induction motor whose parameters are listed in Appendix G. At rotor standstill ($\omega_{\rm m}=0$), Equation 4-4 for a two pole machine becomes :

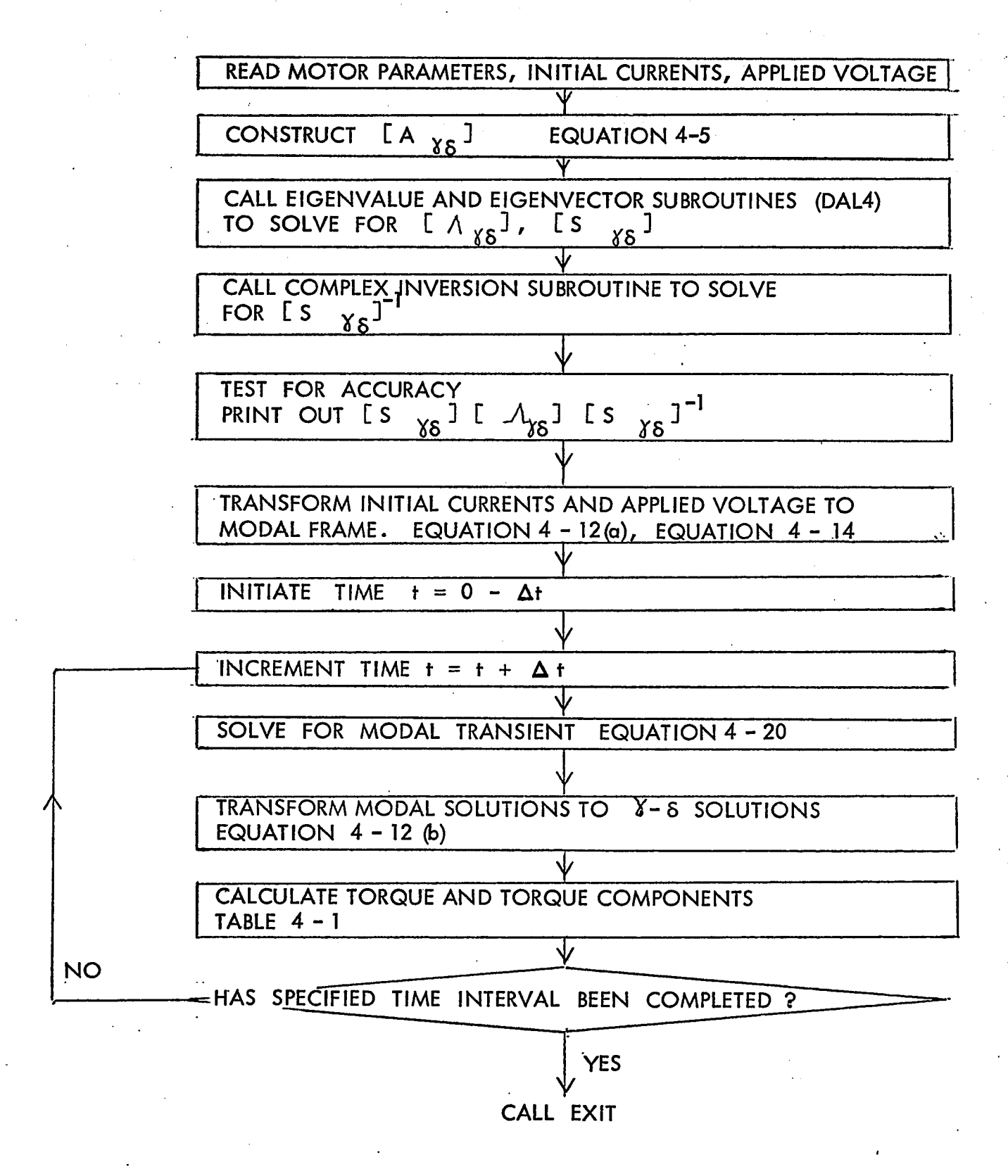


FIGURE 4 - 1. FLOW CHART OF PROGRAM TO SOLVE FOR INDUCTION MOTOR TRANSIENT AT A CONSTANT ROTOR SPEED.

1

4-25

$$P\begin{bmatrix} i_{\delta}^{s} \\ i_{\delta}^{s} \\ i_{\delta}^{r} \\ i_{\delta}^{r} \end{bmatrix} = \begin{bmatrix} -96.6 & -377.0 & 92.0 & 0.0 \\ 377.0 & -96.6 & 0.0 & 92.0 \\ 92.0 & 0.0 & -96.6 & -377.0 \\ 0.0 & 92.0 & 377.0 & -96.6 \end{bmatrix} \begin{bmatrix} i_{\delta}^{s} \\ i_{\delta}^{r} \\ i_{\delta}^{r} \\ i_{\delta}^{r} \end{bmatrix}$$

$$+ \begin{bmatrix} 96.6 & 0.0 \\ 0.0 & 96.0 \\ -92.0 & 0.0 \\ 0.0 & -92.0 \end{bmatrix} \begin{bmatrix} E_{p} \cos \alpha_{s} \\ -E_{p} \sin \alpha_{s} \end{bmatrix}$$

$$-92.0 & 0.0 \\ 0.0 & -92.0 \end{bmatrix}$$

This problem becomes complete when the initial values $\frac{i}{-}$ $\chi \delta^{(0)}$, E_p and α_s are specified.

In transforming to the modal frame, Equation 4-24 becomes

The transformations to and from the modal frame in accordance to

Equation 4-12, are:

$$\begin{bmatrix} q_1 \\ q_2 \\ q_3 \\ q_4 \end{bmatrix} = \begin{bmatrix} i \ 0.5 & -0.5 & -i \ 0.5 & 0.5 \\ -i \ 0.5 & 0.5 & -i \ 0.5 & 0.5 \\ -i \ 0.5 & -0.5 & i \ 0.5 & 0.5 \end{bmatrix} \begin{bmatrix} i_{\delta}^{s} \\ i_{\delta}^{r} \\ i_{\delta}^{r} \\ i_{\delta}^{r} \end{bmatrix}$$

4-26

where the rows are the reciprocal base vectors and

$$\begin{bmatrix} i_{\delta}^{s} \\ i_{\delta}^{s} \\ i_{\delta}^{r} \\ i_{\delta}^{r} \end{bmatrix} = \begin{bmatrix} 0.0 - i \ 0.5 & 0.0 + i \ 0.5 & 0.0 - i \ 0.5 & 0.0 + i \ 0.5 \\ -0.5 + i \ 0.0 & 0.5 + i \ 0.0 & 0.5 + i \ 0.0 & -0.5 + i \ 0.0 \\ 0.0 + i \ 0.5 & 0.0 + i \ 0.5 & 0.0 - i \ 0.5 & 0.0 - i \ 0.5 \\ 0.5 + i \ 0.0 & 0.5 + i \ 0.0 & 0.5 + i \ 0.0 & 0.5 + i \ 0.0 \end{bmatrix} \begin{bmatrix} q_{1} \\ q_{2} \\ q_{3} \\ q_{4} \end{bmatrix}$$

where the columns are the eigenvectors.

The decoupling of the state variables in the modal frame becomes quite apparent in Equation 4-25. For example, the second row

$$p q_2 = (-4.60 + j 377) q_2 - 2.3 E_p (j cos \alpha_s + sin \alpha_s)$$
 4-28

consists only of the state variable q_2 and the constant forcing function. Its solution is well known as:

$$q_{2}(t) = [q_{2}(t) - \frac{2.3 E_{p}(\sin \alpha_{s} + j \cos \alpha_{s})}{(-4.60 + j 377)}] \exp(-4.60 + j 377) + \frac{2.3 E_{p}(\sin \alpha_{s} + j \cos \alpha_{s})}{(-4.60 + j 377)}$$

$$+ \frac{2.3 E_{p}(\sin \alpha_{s} + j \cos \alpha_{s})}{(-4.60 + j 377)}$$

$$4-29$$

In this numerical example, it is interesting and important to note that the eigenvalues, the eigenvectors and the reciprocal base vectors exist in complex conjugate pairs. Like-wise, the modal frame initial conditions \underline{q}_{δ} (o) and the forcing functions $\underline{\nu}_{\delta}$ are also in complex conjugate pairs. As such the digital computer language should be capable of handling complex numbers. It should also be noted that when the modal solutions are transformed back to the current frame through Equation 4-27, the imaginary parts are mutually self-cancelling and disappear, thus leaving the real parts for the current solutions.

4-9 <u>Transient Solutions</u>

Since it is desirable to gain some analytical insight into the solutions, a systematic method of classifying the transient components according to the modes will be presented here.

4-9-1 Modal Frame Solutions

It can be recognized from the numerical examples listed from Equation 4-25 to Equation 4-29 that each complex conjugate pair of eigenvalues should be treated as a single entity and the modal solution of Equation 4-13 should be classified as follows:

$$\underline{q}_{\delta}(t) = \underline{Q}_{1t}(t) + \underline{Q}_{2t}(t) + \underline{Q}_{ss}(t)$$
 4-30

The modal transient components Q_{1t} (t) and Q_{2t} (t) are

$$Q_{1t}(t) = \begin{bmatrix} q_{1t}(t) \\ 0 \\ 0 \\ q_{1t}(t)^* \end{bmatrix}$$
Eq. 4-31(a) and $Q_{2t}(t) = \begin{bmatrix} 0 \\ q_{2t}(t) \\ 0 \\ 0 \end{bmatrix}$

$$q_{1t}(t)^* = \begin{bmatrix} 0 \\ q_{2t}(t)^* \\ 0 \end{bmatrix}$$
4-31(b)

where

$$q_{1\dagger}(t) = [q_{1\dagger}(0) + \frac{\overline{E}_1}{\lambda_1}] \exp \lambda_1 t$$
 4-32

$$q_{2t}(t) = \left[q_{2t}(0) + \frac{\overline{E}_2}{\lambda_2}\right] \exp \lambda_2(t)$$
 4-33

The steady-state component of the total solution is

4-34

$$Q_{ss}(t) = \begin{bmatrix} q_{1ss}(t) \\ q_{2ss}(t) \\ q_{2ss}(t) * \\ q_{1ss}(t) * \end{bmatrix}$$

$$q_{1ss}(t) = -\frac{\overline{E}_1}{\lambda_1} \text{ and } q_{2ss}(t) = -\frac{\overline{E}_2}{\lambda_2}$$

The modal frame solutions are complex numbers and it is difficult to attach physical significance to them. A physical interpretation can be sought by transferring Equation 4–30 into the real current frames.

Using the inverse transformation of Equation 4-12 (b), the &-8 solution is :

$$\frac{\mathbf{i}}{\mathbf{i}} \chi_{\delta}(t) = [S \chi_{\delta}] \underline{Q}_{1t}(t) + [S \chi_{\delta}] \underline{Q}_{2t}(t) + [S \chi_{\delta}] \underline{Q}_{ss}(t)$$

$$4-35$$

For the numerical example of Section 4-8, Equation 4-35 becomes

$$\frac{i}{-8.8} (t) = k_1 \exp (-189 t)$$

$$- \cos (377 t + \theta_1)$$

$$- \sin (377 t + \theta_1)$$

$$\cos (377 t + \theta_1)$$

$$\sin (377 t + \theta_1)$$

where k_1 , k_2 . . . k_7 are constant coefficients and θ_1 and θ_2 are the phase angles .

The current frame solutions are real and admit of physical interpretation. The real part of the eigenvalue becomes the damping factor and the imaginary part becomes the natural frequency of oscillation. Each of the current solutions consists of two transient components (for the fourth order system) and a steady-state term. It is significant to note that in the synchronously rotating frame, the steady-state term is d. c. and for a constant rotor speed $\omega_{\rm m}=0$, the transient components have a natural frequency of $\omega_{\rm l}=\omega_{\rm l}=377$ rad/sec., i.e. the synchronous angular velocity. Furthermore, the δ and the δ axis components of the same mode are δ 0 out of phase in time and the space-vector associated with each mode is rotating physically with respect to the reference frames at δ 1 radians per second in a direction opposite to that of the supply frequency.

4-9-3 d-q Current Solutions

to

Using the connection matrix $\begin{bmatrix} C_{dq} \end{bmatrix}$, Equation 4–36 is transformed

The stator currents in the stationary d - q reference frame correspond to those which are measured in the induction motor itself and hence the interpretation of the eigenvalues and modes from this frame has more engineering significance.

It is recalled that the eigenvalues in Equation 4-25 correspond to the $\delta-\delta$ frame $[A_{\delta}]$. By comparing the eigenvalues, Equations 4-36 and 4-37, it can be concluded that the real part of the eigenvalue corresponds to the damping factor for all common reference frames. However, the imaginary parts of the eigenvalue require some careful interpretation. Whereas the $\delta-\delta$ transient modes have a natural frequency at 377 rad/sec., the corresponding d - q transient components are

non-oscillatory. It is also important to note that the %-8 steady-state components are direct currents and conversely the d-q steady-state components oscillate at supply frequency. These indicate that the imaginary part of the eigenvalue is in fact the natural frequency, but as in all frequency quantities there is the Doppler effect related to the velocity reference frame.

The imaginary parts of the eigenvalues in Equation 4-25 make physical sense because the 377 radians/sec. natural frequency in the χ -8 frame corresponds to the stator and the rotor mmfs rotating at the 377 radians/sec. in the backward direction. But the χ -8 axes are themselves rotating at a synchronous speed in the forward direction. Therefore the mmfs have a net zero speed with respect to the stationary frame. This of course agrees with Equation 4-37 where the transient components are non-oscillatory.

From this physical argument, it can be concluded that if $\lambda_1 = \sigma_1 + i \omega_1$ is an eigenvalue of $\begin{bmatrix} A & & \\ & & & \end{bmatrix}$ which has ω_c as the speed of the reference frame, the corresponding eigenvalue for the d-q stationary frame matrix $\begin{bmatrix} A_{dq} \end{bmatrix}$ is $\lambda_1^1 = \sigma_1 + i (\omega_c \pm \omega_1)$. Whether ω_1 should have the positive sign or the negative sign is evident only in examining the direction of rotation of the eigenvectors. This will be treated in Chapter V.

4-10 Components of Electromechanical Torque

Section 4-9 has considered the total solution of the currents as the sum of the steady-state component and the two transient components which are associated with the two natural modes. Since the electromechanical torque consists of quadratic products of the winding currents, it can be analysed into 6 independent components along the modal classification as shown in Table 4-1.

The purpose here is to derive a formulation which enables the digital computer to handle the torque component analysis directly from the modal frame. Firstly, the torque equation

$$T_{em} = n M (i_{\delta}^{s} i_{\delta}^{r} - i_{\delta}^{s} i_{\delta}^{r})$$
 4-38

is written in the matrix form

$$T_{em} = \frac{i}{1} \gamma \delta^{T} [T] \underline{i} \gamma \delta$$
 4-38(a)

where

$$\begin{bmatrix} T \end{bmatrix} = \begin{bmatrix} 0 & 0 & 0 & 0 \\ 0 & 0 & 0 & 0 \\ 0 & -nM & 0 & 0 \\ nM & 0 & 0 & 0 \end{bmatrix}$$
4-39

Substituting Equation 4-12(b)

$$T_{em} = \underline{q} \chi_{\delta} [W] \underline{q} \chi_{\delta}$$
 4-40

where

$$[W] = [S_{\chi\delta}]^{T} [T] [S_{\chi\delta}]$$
 4-41

TABLE 4-1

CONSTANT SPEED INDUCTION MOTOR TORQUE COMPONENTS

Torque	Mode Classification	Formulae for Instantaneous
Component		Value
T ₁	steady-state	Q _{ss} [w] Q _{ss}
т2	exp 2 σ ₂ t	Q_{2t}^{T} [W] Q_{2t}
т ₃	exp 2 σ ₁ t	Q _{It} [w]Q _{It}
т ₄	[exp $(\sigma_1 + \sigma_2 +] [\cos (\omega_1 - \omega_2) +]$	Q_{1t}^{T} [W] $Q_{2t} + Q_{2t}^{T}$ [W] Q_{1t}
T ₅	[exp σ ₂ t] [cos ω ₂ t]	\underline{Q}_{2t}^{T} [W] \underline{Q}_{ss} + \underline{Q}_{ss}^{T} [W] \underline{Q}_{2t}
T ₆	[exp σ ₁ t] [cos ω ₁ t]	Q_{1t}^{T} [W] $Q_{ss} + Q_{ss}^{T}$ [W] Q_{1t}
	·	

The formula for the 6 torque components listed in Table 4-1 is obtained by substituting Equation 4-30 into Equation 4-40 and thereafter grouping the terms in their appropriate classifications. The importance of this classification lies in that the damping factors σ_1 , σ_2 and the natural frequencies of oscillations ω_1 , ω_2 (which are the real and the imaginary parts of the eigenvalues λ_1 , λ_2) constitute a common language which is familiar to everyone knowledgeable in dynamic linear systems theory. It is interesting to note that this classification is independent of the chosen reference frame. Thus if the currents in the stationary d - q frame are used, the torque equation is

$$T_{em} = i_{-dq}^{T} [T] i_{-dq}$$
 4-42

But
$$\frac{\mathbf{i}}{-dq} = \begin{bmatrix} \zeta_{dq} \end{bmatrix} \begin{bmatrix} \zeta_{\chi \delta} \end{bmatrix} \underline{q} \chi_{\delta}$$
 4-43

and substituting Equation 4-43 into Equation 4-42,

$$T_{em} = \underline{q} \chi \delta [W] \underline{q} \chi \delta$$
 4-44

because

$$\begin{bmatrix} C_{dq} \end{bmatrix}^T \begin{bmatrix} T \end{bmatrix} \begin{bmatrix} C_{dq}^{\delta \delta} \end{bmatrix} = \begin{bmatrix} T \end{bmatrix}$$
 4-45

Thus Equation 4-44 is identical to Equation 4-40.

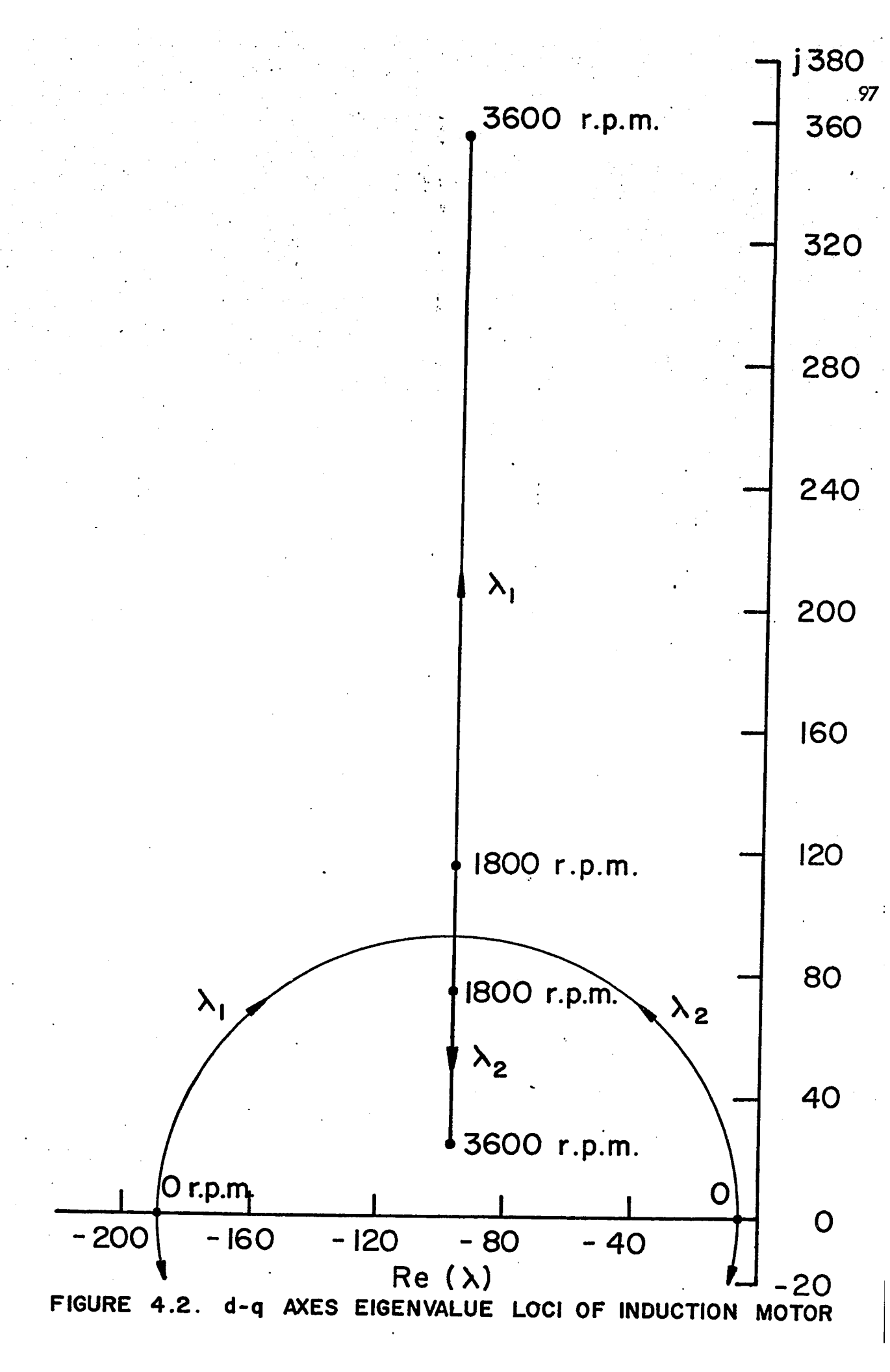
It is instructive to examine how a particular torque component, say T_5 , is constituted from the currents in each of the reference frames. T_5 consists of the

scalar products of Q_{2t} and Q_{ss} in Equation 4-35. In the $N-\delta$ synchronously rotating reference frame solution of Equation 4-36, both the damping factor σ_2 and the natural frequency of oscillation ω_2 (= 377 rad/sec.) belong to the transient solution of the first complex mode. The corresponding steady-state terms are d. c. currents.

In contrast, the same torque component T_5 when viewed from the stationary d - q reference frame is formed from the product of (a) the transient solution term which carries the damping factor σ_2 only, and (b) the steady-state component which oscillates with the supply frequency (377 rad/sec.). Thus from this viewpoint, the frequency shift of the eigenvalues with respect to the velocity of the reference frame ($\omega_k^1 = \omega_c^- \pm \omega_k^-$) is necessary to preserve the invariance of the component torques and hence is a consequence of the power invariance transformation $\delta \delta C_{dq}^-$.

4-11 Constant Speed Eigenvalue Loci

Figure 4-2 shows the continuous plots of two of the eigenvalues for rotor speed from standstill to $\omega_m=377~\text{rad/sec.}$ The other two eigenvalue loci are merely conjugate images in the lower half of the complex s-plane and have been omitted. The stationary d - q frame has been used and as such, at rotor standstill, the eigenvalues are real and the complex conjugate pairs are coincident. Because a numerical example has been chosen in which $R^S=R^\Gamma$ and $L^S=L^\Gamma$ some sort of symmetry in the loci



appears. In particular around $\omega_{\rm m}=0.49~{\rm p.u.}$, $\lambda_{\rm l}$ appears to coincide with $\lambda_{\rm l}$. For simplicity, this very interesting case will be isolated from this study. The occurrence, the treatment and the implications of such coincident eigenvalues should in itself be an interesting and important subject for further investigation.

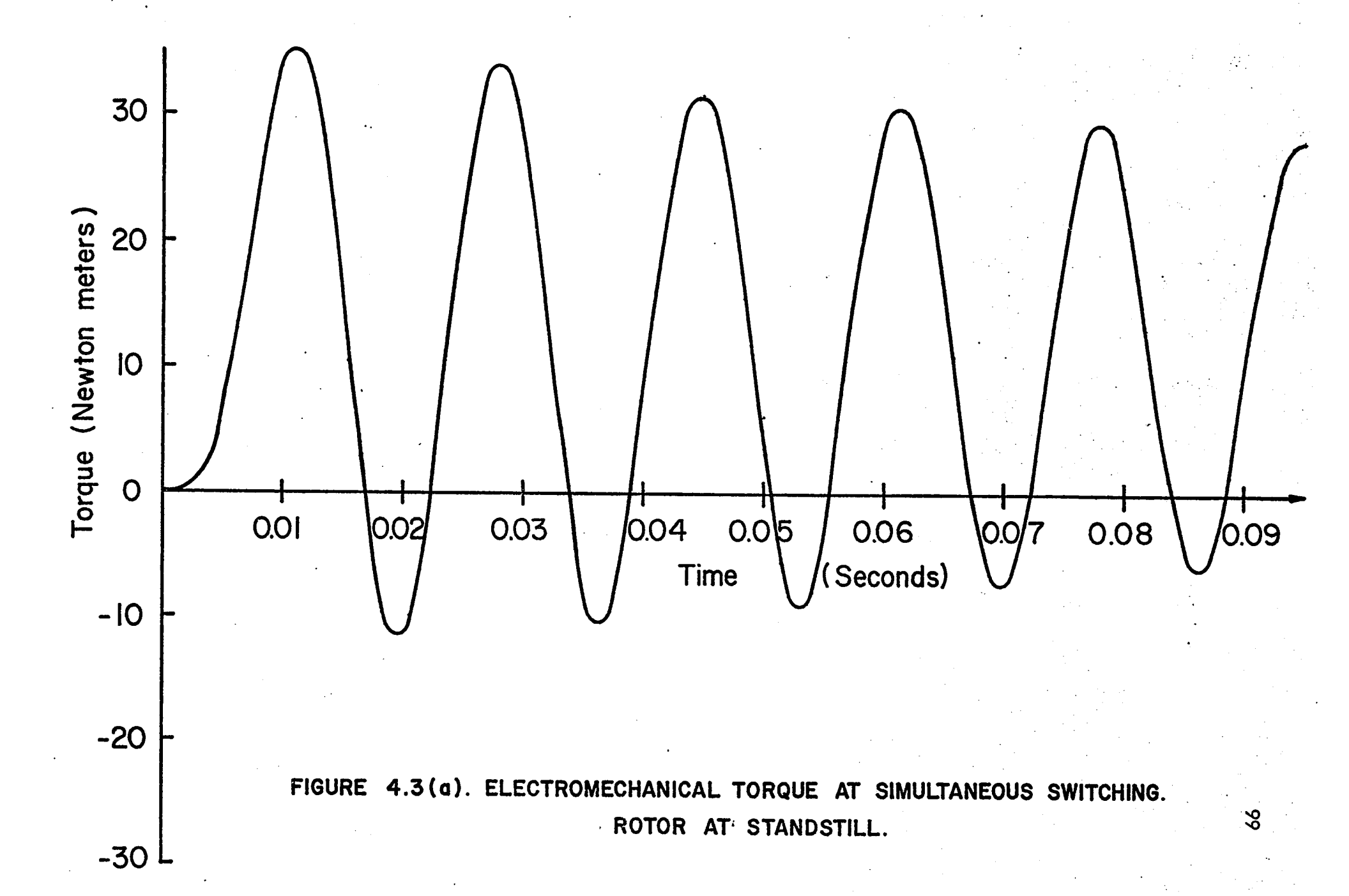
In Chapter V, a physical understanding of the speed dependence of the eigenvalues will be developed. In this section, interest is focussed on the relationship of the eigenvalue loci on the torque patterns. As such, the simultaneous switching torque patterns will be considered for: (a) the very important case of rotor standstill, i.e. $\omega_{\rm m} = 0.0$, (b) $\omega_{\rm m} = 0.5$ p. u. and (c) $\omega_{\rm m} = 0.9$ p. u.

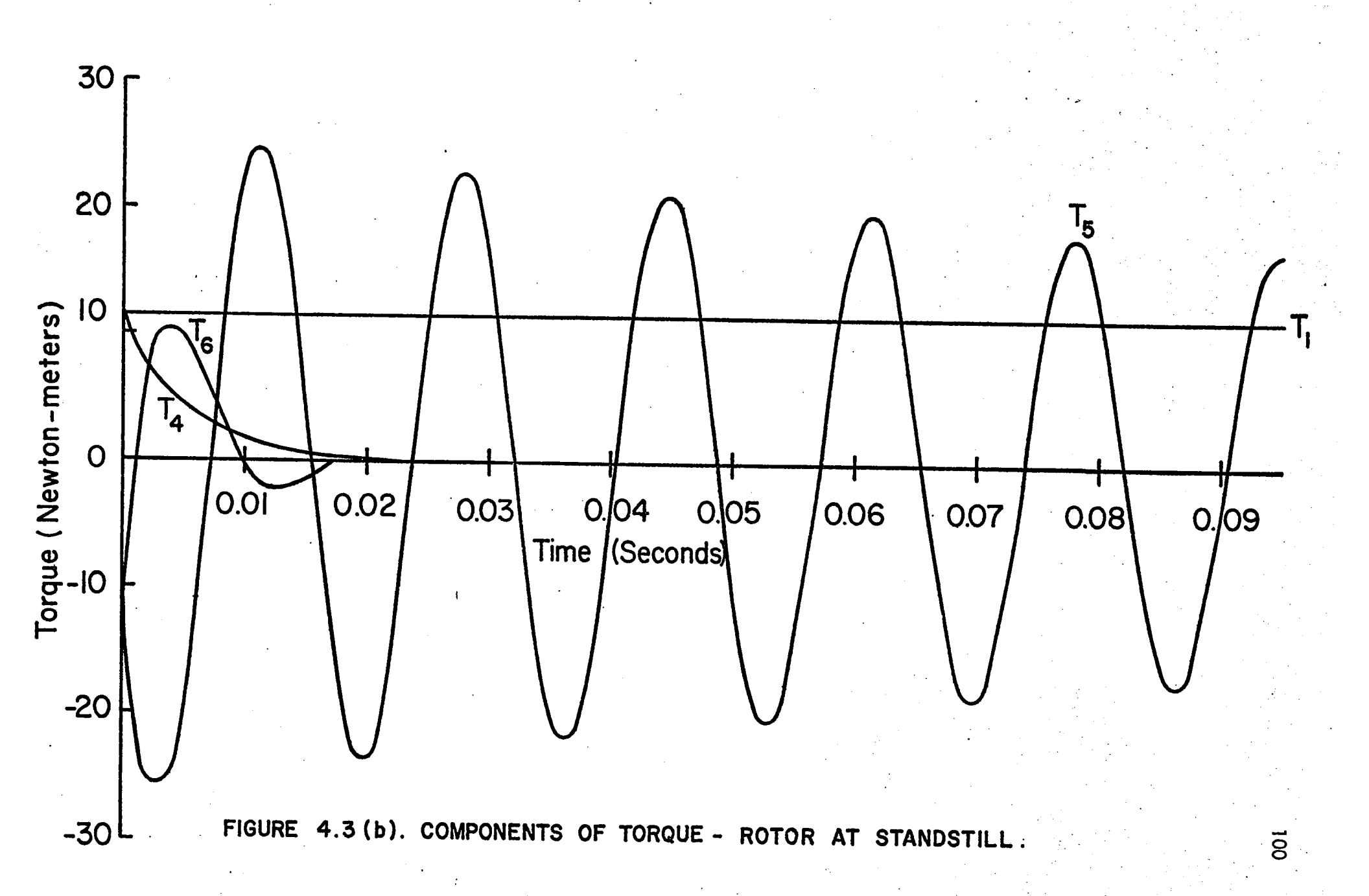
4-12 Patterns of Constant Speed Transient Torques

Figure 4-3(a) to Figure 4-5(a) show the simultaneous switching torque patterns produced when the rotor is kept at a constant speed: (i) $\omega_{\rm m}=0$, (ii) $\omega_{\rm m}=0.5$ p. u., (iii) $\omega_{\rm m}=0.9$ p. u. Figure 4-3(b) to Figure 4-5(b) show the torque analysed into the component classification of Table 4-1.

Case (i) $\omega_{m} = 0.0$

With $\omega_m=0$, the d- and the q- axis of Equation 4-1 are decoupled and each decoupled axis equation is that of a transformer. As such, the modes are all real and as will be shown in Chapter V, the eigenvalues $\lambda_2=-4.60$ correspond to the magnetization mode associated with the mutual inductance M. The very heavily





damped mode $\lambda_1 = -189$ can be identified with the leakage inductances $I^s = I^r = L^s - M$.

Figure 4-3(b) shows that the important torque components are the steady-state component T_1 and the 60 Hz component T_5 associated with the magnetization flux. The magnetization mode is very lightly damped because of the large mutual inductance with respect to the winding resistances. In contrast the components T_4 and T_6 which are associated with the leakage inductance mode are damped away within 0.02 sec. This is because the leakage inductances are small in comparison with the winding resistances. In this instance of simultaneous switching T_2 and T_3 are relatively too small to be shown in the graph.

By comparing Figure 4-3(a) with the case for the accelerating rotor in Figure 3-2, it can be seen that the linear modal is a good approximation for the first few cycles of switching. The discrepancies become serious thereafter because as the rotor picks up speed, both the eigenvalues (see Figure 4-2) and the eigenvectors (see Figure 5-4) change with speed.

Case (ii)
$$\omega_{\rm m} = 0.5 \, \rm p. \, \upsilon.$$

At 1800 r.p.m. (0.5 p. u.), the eigenvalues are $\lambda_2 = -96.6 \pm \text{j} 73.8$ and $\lambda_1 = -96.6 \pm \text{j} 114$. Because of the speed interactions, the cross axes windings are coupled together and both the damping factors are very large. It is significant to contrast the relative time period within which the transient torques are damped out in Figure 4-3(a) and Figure 4-4(a). As this result is related to the accelerating transients

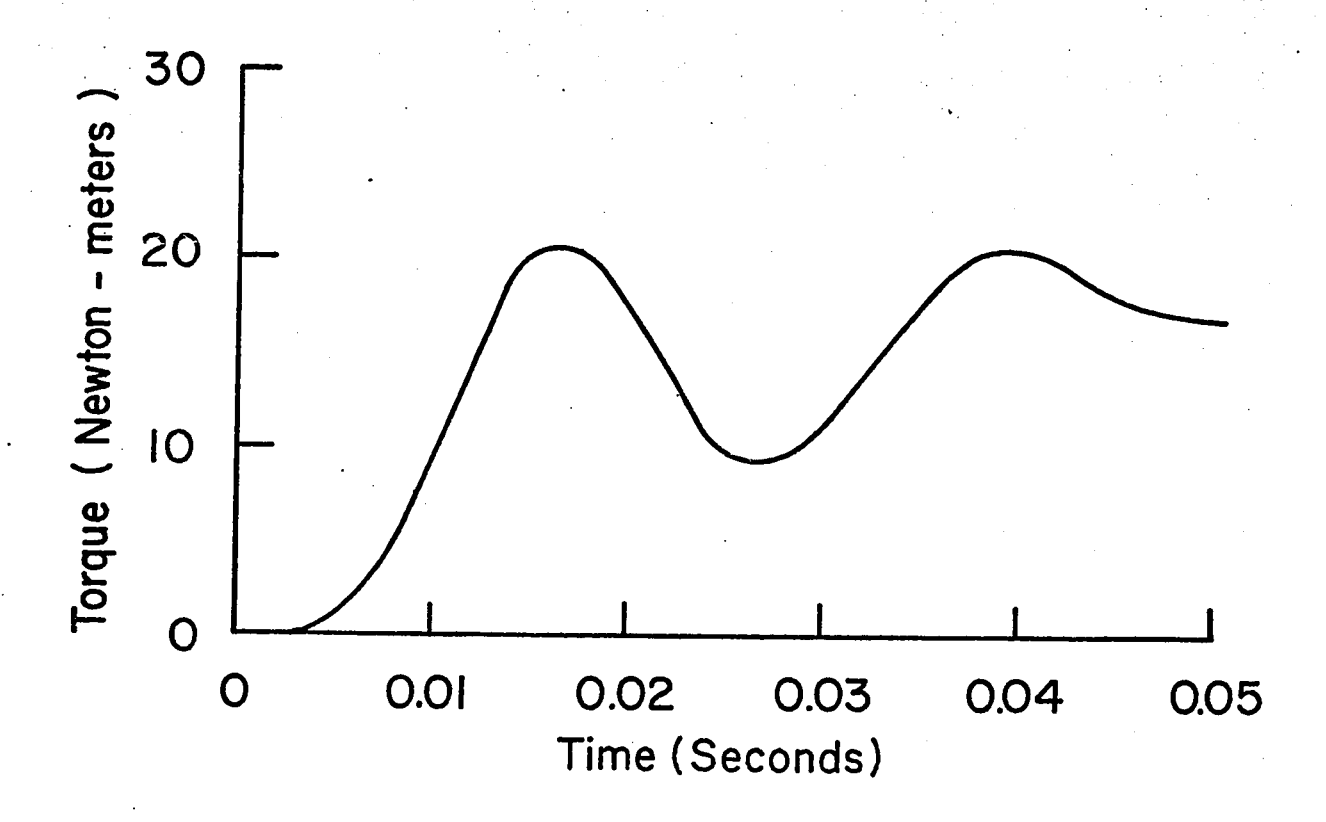
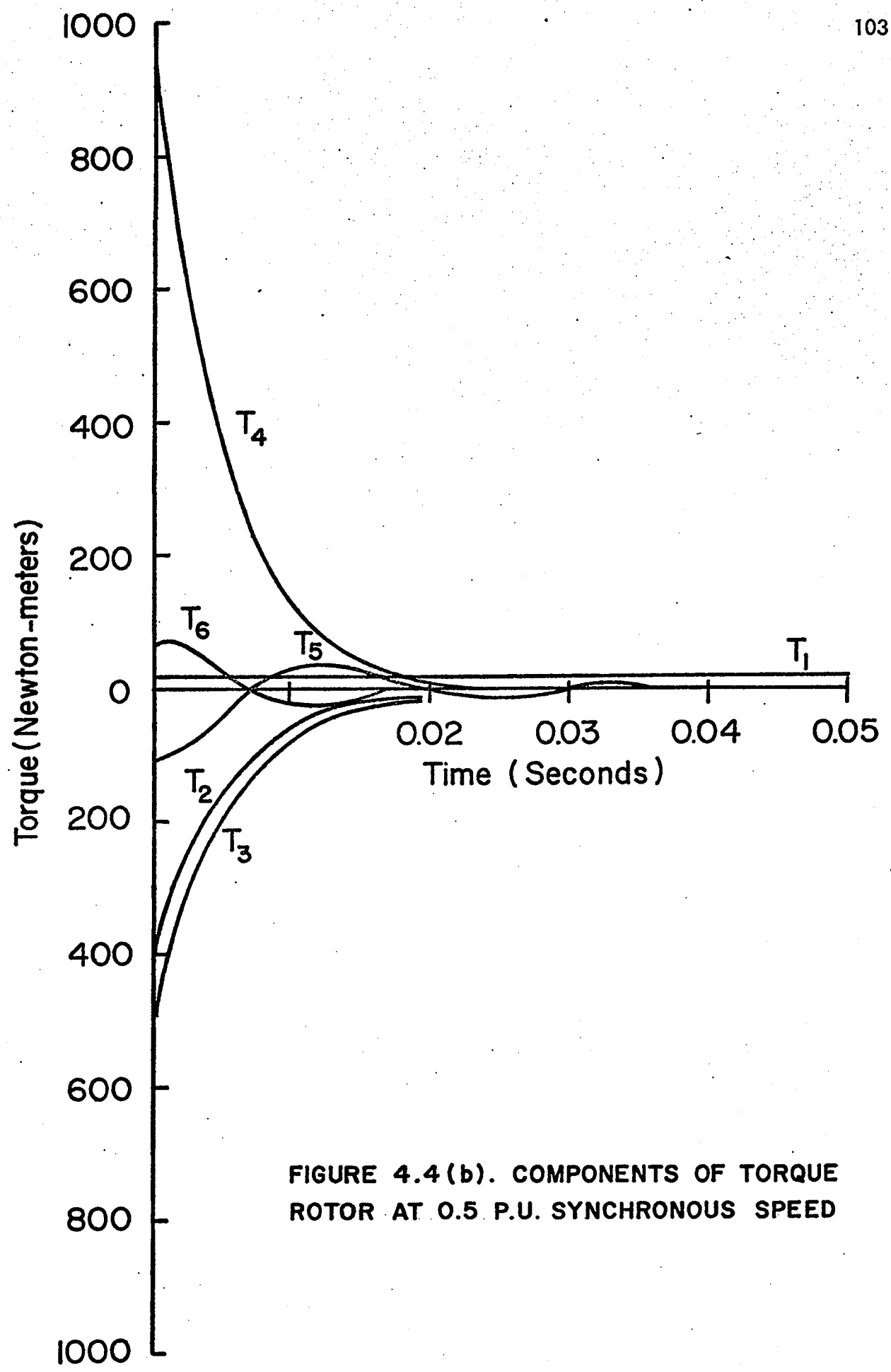


FIGURE 4.4(a). ELECTROMECHANICAL TORQUE IN SIMULTANEOUS SWITCHING. ROTOR AT 0.5 P.U. SYNCHRONOUS SPEED





of Figure 3-2, it can be concluded that the speed interactions contribute to damp out the initial 60 Hz transient torque component.

It is important to note that the vertical scale in Figure 4-4(b) has been changed to accommodate the large components of T_2 , T_3 and T_4 . Roughly speaking, the large component T_4 is cancelled by the sum of T_2 and T_3 ; and T_5 and T_6 are in opposite phase. These leave a resultant which is of the same order of magnitude as in Figure 4-3 (a) and Figure 4-5(a).

Case (iii)
$$\omega_{\rm m} = 0.9 \, \rm p. \, u.$$

At 3240 r.p.m. (0.9 p. u.), the eigenvalues are $\lambda_2 = -96.6 \pm \mathrm{i}$ 27.1 and $\lambda_1 = -96.6 \pm \mathrm{i}$ 312. The initial negative torque in Figure 4-5(a) is typical for simultaneous switching at high rotor speeds. [4],[5].

The damping factors for the two modes have remained constant and equal. The interesting departures arise from the frequencies of the two modes, i.e. $\omega_1 \rightarrow 0$ and $\omega_2 \rightarrow \omega_m$, which make T_4 and T_5 highly oscillatory.

Each of the three cases studied have illustrated the kinds of transient components which can exist. As the rotor speed changes, the eigenvalues move along the loci as shown in Figure 4-2 and these significantly change the damping factors and the natural frequency of oscillation of the torque component. But the details concerning the relative contributions of a torque component would have to depend on the excitation voltage $\overline{\mathbb{E}}_p$, the switching angle α_s , the initial currents $\frac{1}{2}$ (o) and in what

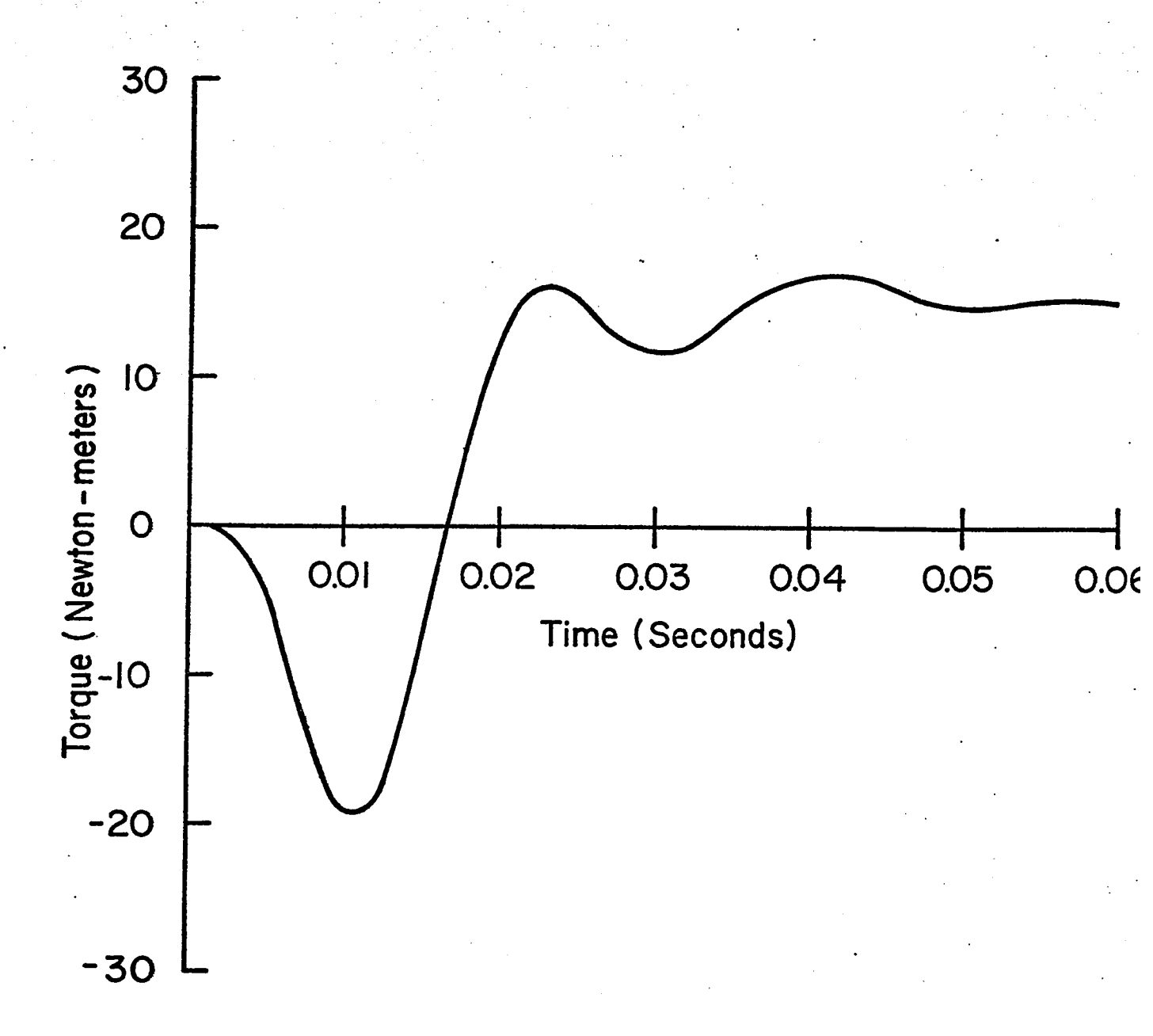
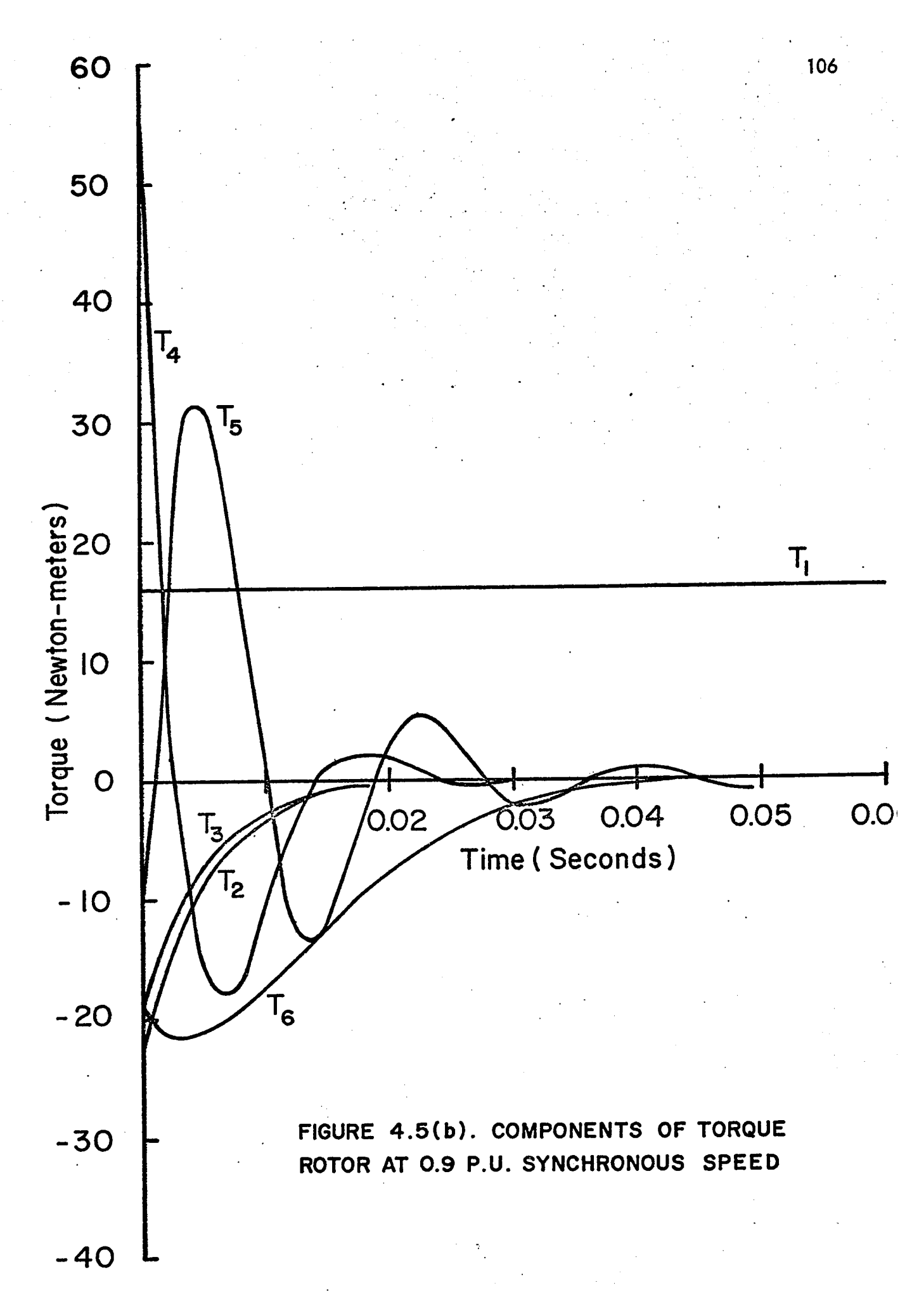


FIGURE 4.5(a). ELECTROMECHANICAL TORQUE IN SIMULTANEOUS SWITCHING. ROTOR AT 0.9 P.U. SYNCHRONOUS SPEED



manner they become coupled to the modes. The information with respect to the coupling is borne by the eigenvector matrix $[S_{\chi\delta}]$.

Since the system equation is linear, the two forms of modal excitations will be treated spearately: (a) initial current excitation and (b) switching voltage excitation. Thereafter it is possible to combine both forms of excitations using the principle of superposition. The case of the standstill rotor will be used as an illustrative example and it will be shown how the magnetization mode can be suppressed by a combination of initial currents and switching voltages.

4-13 Modal Excitation Due to Initial Currents

The physical model consists of all the motor windings short-circuited and the voltage sources removed. At the switching instant, it will be assumed that the coil windings bear a set of currents $\frac{1}{2} \delta \delta (0)$. The interest is centred on the behavior of the winding currents as they decay with time. The initial currents would excite the kth mode if q_{L} (o) is non-zero. Since

$$\underline{q}_{\chi\delta}(o) = [S_{\chi\delta}]^{-1} \underline{i}_{\chi\delta}(o)$$
 4-46

both the structure of $[S_{\delta\delta}]^{-1}$ and the relationship of $i_{\delta\delta}$ (o) with it are important in understanding the excitation of the modes.

It is possible, using the property of the linear independence of the eigenvectors of [S 38], to excite preferentially a mode in exclusion to the others. It is

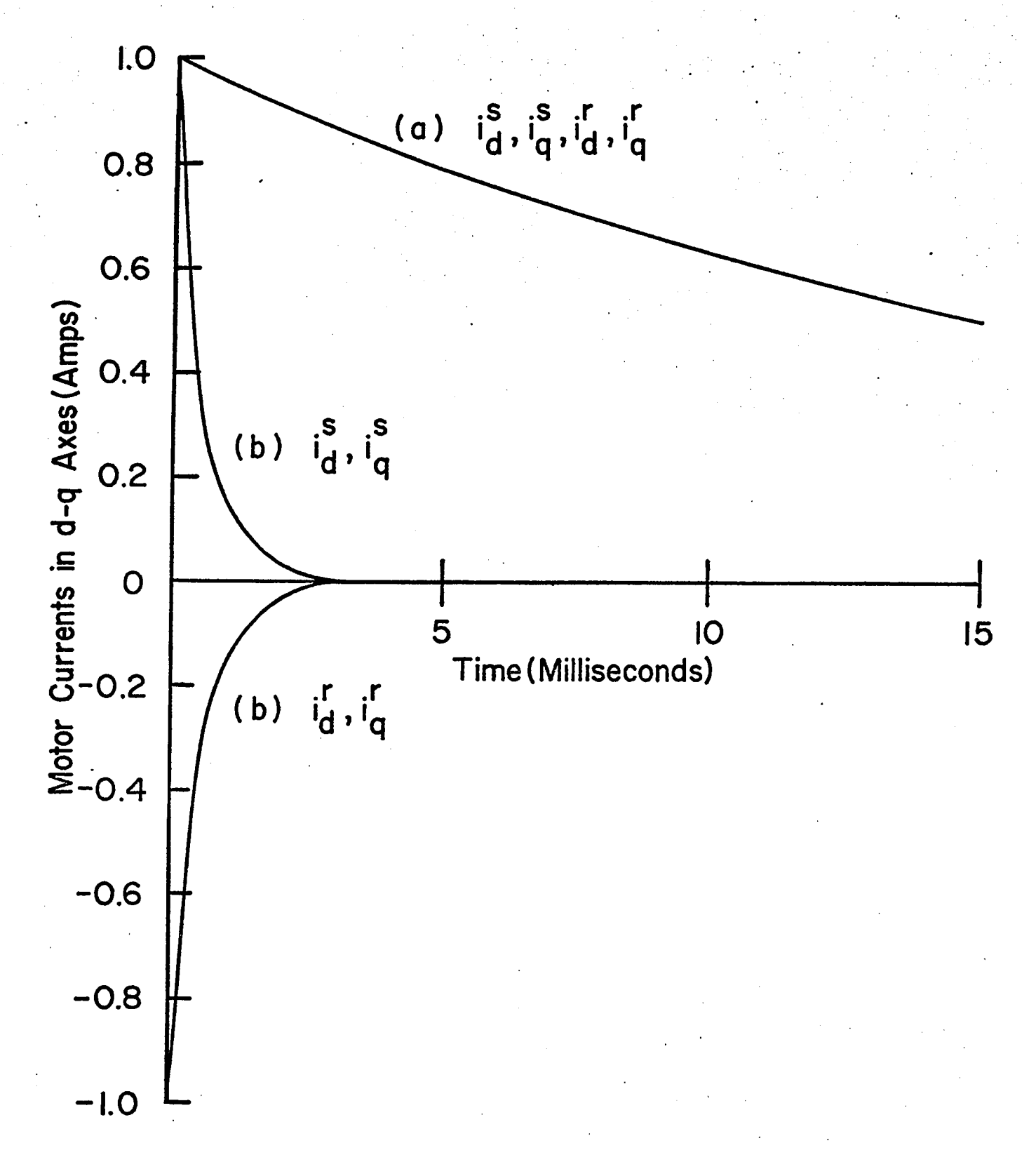


FIGURE 4.6. FREE MOTION OF INDUCTION MOTOR MODES AT ROTOR STANDSTILL (a) MAGNETIZATION MODE (λ_2) (b) LEAKAGE INDUCTANCE MODE (λ_1)

a well known fact from the standard textbooks on linear theory [51-52] that the kth mode is exclusively excited if $\frac{1}{2} \% 8$ (o) lie in the plane defined by the vector representing the real part and the vector representing the imaginary part of the kth eigenvector.

Thus, the oscillatory mode corresponding to $-189 \pm j$ 377 of Equation 4-24 will be exclusively excited by initial currents

$$\frac{i}{4} \times 6 = m_1 = 0 + m_2 = 0.5 \\
0 \\
0.5 = 0.5$$
0.0
0.5
0.0

where m₁ and m₂ are any arbitrary real numbers which are multiplied to the real and the imaginary parts of the eigenvectors of Equation 4-26.

The free-motion of this leakage inductance mode as viewed from the stationary d-q axes is shown in Figure 4-6(a). In the d-q frame, the free modal motion is damped and non-oscillatory.

Likewise Figure 4-6(b) shows the exclusive excitation of the magnetization mode (-4.60 \pm j 377) by the initial currents.

$$\frac{i}{-8}$$
 (o) = m_1 $\begin{bmatrix} 0.5 \\ 0.0 \\ 0.5 \\ 0.0 \end{bmatrix}$ + m_2 $\begin{bmatrix} 0.0 \\ 0.5 \\ 0.0 \\ 0.5 \end{bmatrix}$ 4-48

4-14 Modal Excitation By Voltage Supply

From Equation 4-18, the kth eigenvalue is excited if $\frac{\nu}{-k}$ (t) is non-zero. In general the modal driving function $\frac{\nu}{-k}$ δ is related to $\frac{\nu}{-k}$ by Equation 4-14. For the particular example of the rotor at standstill

$$\frac{\nu}{5} = \begin{bmatrix} i & 94.3 & -94.3 \\ -i & 2.3 & 2.3 \\ i & 2.3 & 2.3 \\ -i & 94.3 & -94.3 \end{bmatrix} \begin{bmatrix} E_{p} \cos \alpha_{s} \\ -E_{p} \sin \alpha_{s} \end{bmatrix}$$

$$4-49$$

It can be concluded that in the simultaneous switching of the inert motor, all the modes are excited and no matter what switching angle α_s is used, it is impossible to make any row zero. As such mode suppression can only be achieved by a combination of voltage and initial currents.

4-15 Mode Suppression

From Equation 4–20, the transient component of the kth eigenvalue can be suppressed if it is possible to design for a q_k (o) and a \overline{E}_k such that

$$q_{k}(0) + \frac{\overline{E}_{k}}{\lambda_{k}} = 0 4-50$$

This modal suppression has many important applications. Thus if in switching from standstill, it is desirable (a) to lower the peak of the transient torque and / or (b) to eliminate the 60 Hz oscillating torque component (because the shaft has mechanical resonant frequency around 60 Hz), then a suitable method consists of suppressing the slowly decaying magnetization mode. This is the mode of $\lambda_2 = -4.60 \pm i$ 377 in Equation 4-24 of the example.

From Equation 4-29, the necessary condition for this is

$$q_2 (o) = \frac{2.3 E_p (\sin \alpha_s + i \cos \alpha_s)}{(-4.60 + i 377)}$$
4-51

For the switching angle $\alpha_{_{S}}=0$, and because 4.60 is negligible compared to 377,

$$q_2$$
 (o) = q_3 (o) $\approx \frac{2.3 \text{ E}}{377}$ 4-52

This corresponds to the switching condition

$$\frac{1}{1} = \frac{2.3 E_{p}}{377} = \begin{bmatrix} 0 \\ 1 \\ 0 \\ 1 \end{bmatrix}$$
 4-53(a)

$$\begin{array}{ccc}
e & \delta \delta & = & \begin{bmatrix}
E_p \\
0 \\
0 \\
0
\end{bmatrix}$$
4-53(b)

The conditions of Equation 4-53 can be realised physically by injecting an initial set of currents and switching on the supply at the correct phase. The circuitry required to accomplish it, however, would be expensive. An approximate although engineeringly more satisfying method consists of nonsimultaneous switching of the supplies at the correct sequence as proposed by Wood, Flynn and Shanmugasundaram [29].

4-15-1 Mode Suppression by Non-simultaneous Switching

Non-simultaneous switching is accomplished in two switching sequences. In the first sequence, two of the three stator terminals are switched on to two of the three-phase lines at the appropriate phase of the supply cycle such that no magnetization transient is produced.

Thus if the three-phase voltages are

$$\begin{bmatrix} \nu_{\alpha} \\ \nu_{b} \\ \nu_{c} \end{bmatrix} = \sqrt{3} \quad \sqrt{p} \quad \begin{bmatrix} \sin (\omega_{f} t + \alpha_{s}) \\ \sin (\omega_{f} t + \alpha_{s} - \frac{2\pi}{3}) \\ \sin (\omega_{f} t + \alpha_{s} + \frac{2\pi}{3}) \end{bmatrix}$$

$$4-54$$

and the terminals A and C are switched at t = 0, then $a_s = 90^\circ$ is the approximate switching angle to cancel the magnetization flux.

The second switching sequence occurs at ω_f t = β_s when the B phase is switched on. For the magnetization mode to be suppressed in this second switching

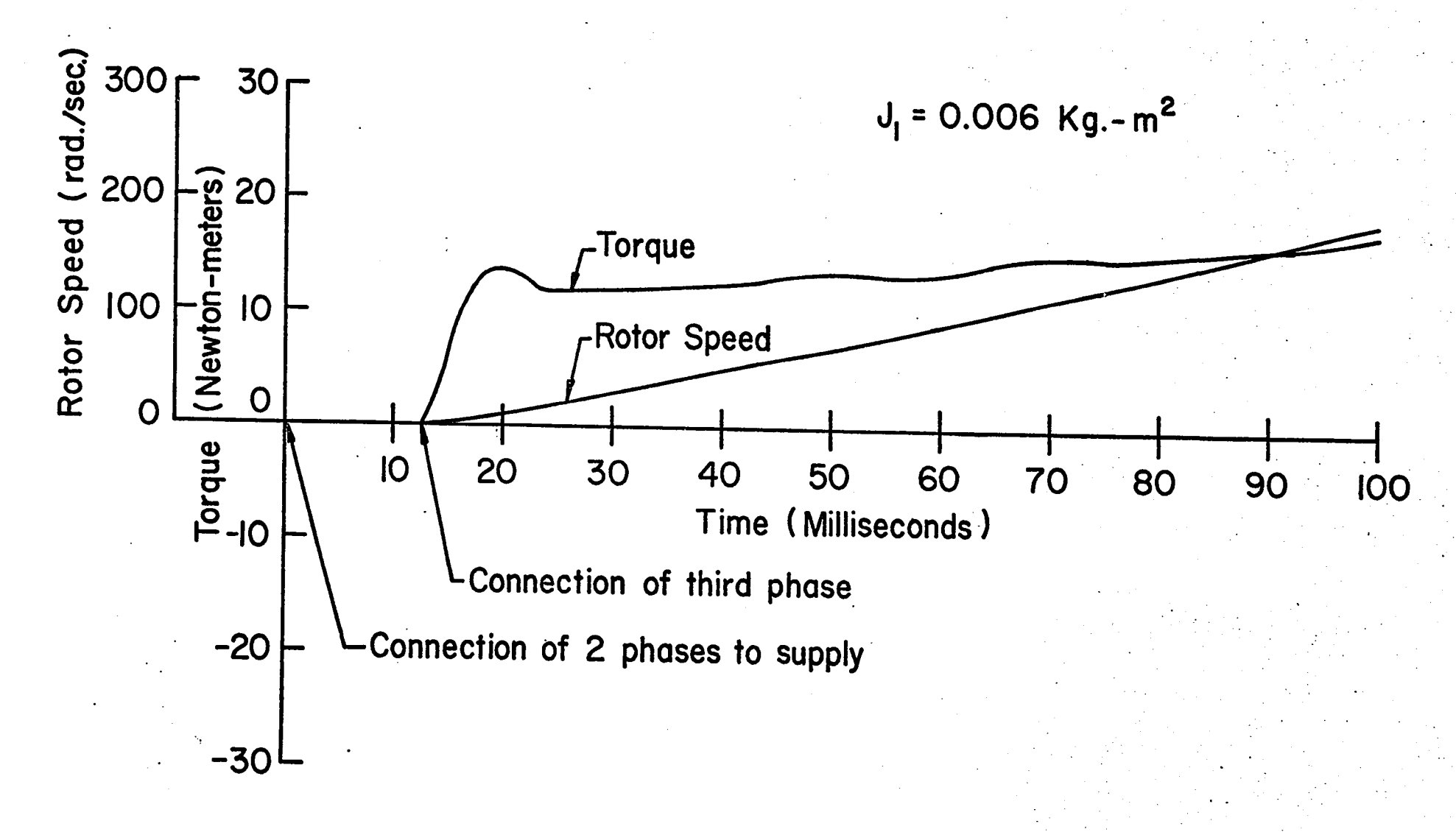


FIGURE 4.7. SWITCHING TORQUE AND SPEED PATTERN WHEN THE MAGNETIZATION MODE IS SUPPRESSED BY NON SIMULTANEOUS SWITCHING

sequence, the approximate switching angle is $\beta_s = 90^{\circ}$. Figure 4-7 shows the torque pattern using this form of non-simultaneous switching.

Although this method of mode suppression is only mathematically approximate, the switching circuitory would be easier to accomplish.

CHAPTER V

OF INDUCTION MOTOR MODES

5-1 Introduction

Chapter IV has described a method of characterising the induction motor transient torques based on analysing the linear constant speed induction equations along the natural modes of behavior of the system. It has been shown through the eigenvalues loci of Figure 4-2 that the damping and the natural frequency of oscillation of each mode change with the rotor speed. By following the eigenvalues loci, it is possible to understand, qualitatively at least, the torque pattern of an accelerating transient as in Figure 3-2. At this point, a number of questions present themselves: What are the physical meaning of these modes? Are there any physical explanations for their behavior?

Unfortunately because of the complex intercoupling of the system equations it is impossible to obtain an explicit expression of the eigenvalues in terms of the system parameters and the rotor speed ω_m . All frontal attacks are met with a fourth order algebraic characteristic equation which is surmountable only by numerical techniques. Once the numerical method is used, all physical relationships become lost.

In the face of this impasse, this study has resorted to three indirect approaches, each of which has yielded some fruitful fragments of knowledge.

CHAPTER V

OF INDUCTION MOTOR MODES

5-1 Introduction

Chapter IV has described a method of characterising the induction motor transient torques based on analysing the linear constant speed induction equations along the natural modes of behavior of the system. It has been shown through the eigenvalues loci of Figure 4-2 that the damping and the natural frequency of oscillation of each mode change with the rotor speed. By following the eigenvalues loci, it is possible to understand, qualitatively at least, the torque pattern of an accelerating transient as in Figure 3-2. At this point, a number of questions present themselves: What are the physical meaning of these modes? Are there any physical explanations for their behavior?

Unfortunately because of the complex intercoupling of the system equations it is impossible to obtain an explicit expression of the eigenvalues in terms of the system parameters and the rotor speed ω_m . All frontal attacks are met with a fourth order algebraic characteristic equation which is surmountable only by numerical techniques. Once the numerical method is used, all physical relationships become lost.

In the face of this impasse, this study has resorted to three indirect approaches, each of which has yielded some fruitful fragments of knowledge.

(a) Eigenvalue Invariance with Rotor Speed

Inspection of the eigenvalue loci in Figure 4-2 yields some simple conclusions with respect to the sum invariance properties of the damping factors and the natural frequencies at all rotor speeds, viz:

(i)
$$\sigma_1 + \sigma_2 = constant$$
 5-1

(ii)
$$\omega_1 + \omega_2 = \omega_m$$
 5-2

The results from this typical motor has led to finding the proofs of the general case from the characteristic equations.

(b) Mode Identification from Sub-primitives

The second method consists of investigating the dynamic characteristics of the many degenerate forms of the Kron's commutator primitive. Each degenerate form consists of assuming one or more of the system parameters to be negligible. Thus, in what shall be called the <u>magnetization sub-primitive</u>, it is assumed that both the stator and the rotor leakage inductances (l_s, l_r) are zero and thereby some simplification is achieved. By this artifice, attention is focussed on the interaction of rotor speed and the airgap magnetization flux. Consequently, it is possible to peer into the "physical mechanism" which produces the oscillation in the magnetization modes. The philosophy of this approach is: degeneracy enables the order of complexity of the interacting parameters to be reduced sufficiently for a simple physical picture to appear. Each of

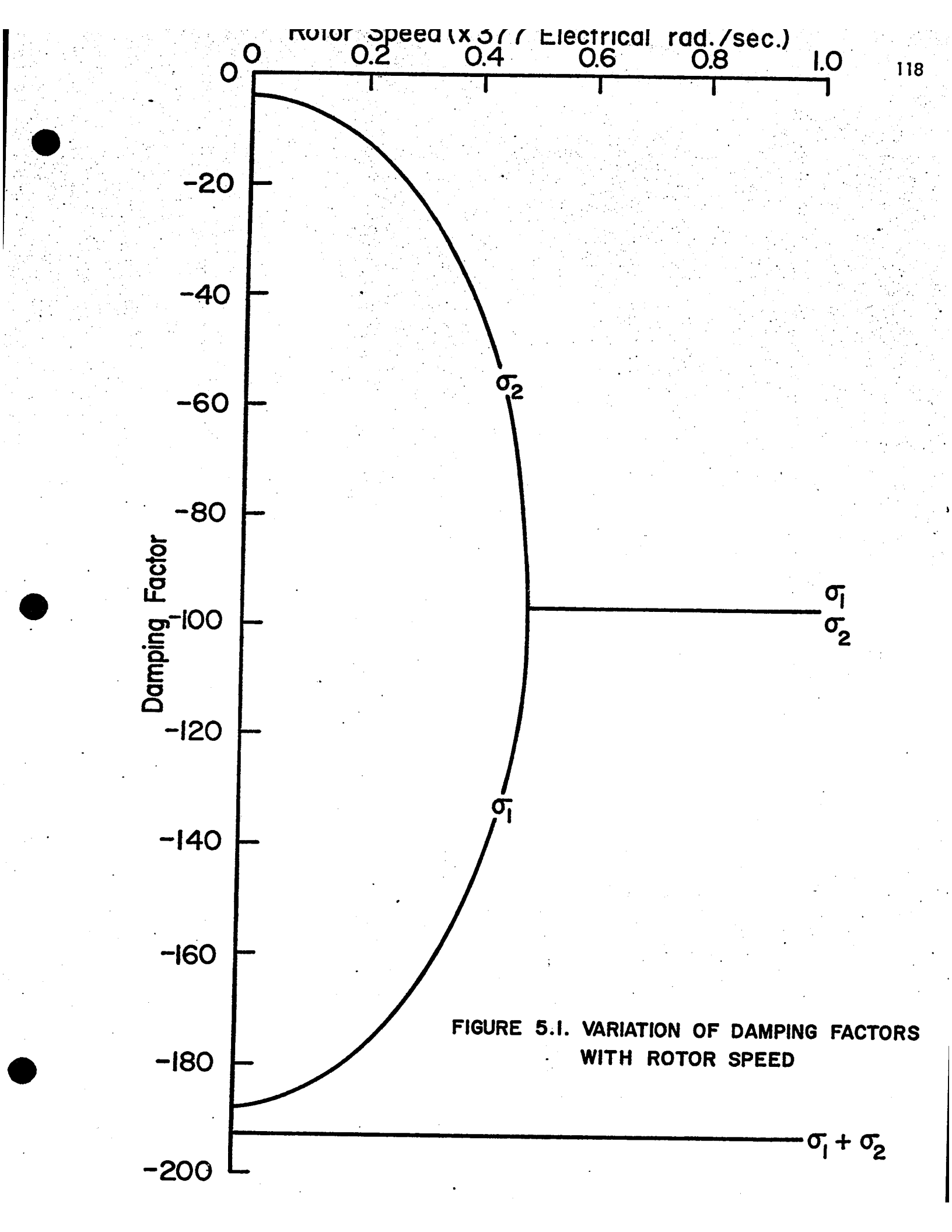
the simple physical pictures is, of course, only valid and approached asymptotically under restricted conditions in the real machine. In spite of these restrictions, one finds that (i) the lossless sub-primitive, (ii) the transformer modes and (iii) the magnetization sub-primitive have proved to be important sign-posts in the studies of the modes.

(c) Eigenvector Interpretation

The last method consists of using the complex numerical values in the eigenvector columns to interpret the behavior and to construct the physical picture of a mode. From a basic rotational symmetry in the complex numbers in the eigenvectors, it is possible to admit of a physical picture of a mode in terms of modal space vectors $\frac{3}{5}$, $\frac{3}{5}$ and $\frac{3}{5}$ rotating spirally in the airgap space under free motion. These space vectors are attenuated exponentially with a damping factor $\frac{3}{5}$ and the angular velocity of rotation is $\frac{3}{5}$. The rotational property, furthermore, enables a physical correlation of the damping factor $\frac{3}{5}$ in terms of the magnetic storage energy and the dissipative power associated with the mode. Likewise the natural frequency of oscillation $\frac{3}{5}$ can be correlated with the modal space vectors although a physical interpretation is less obvious.

By a combination of these three methods, it is possible to obtain a physical picture which correlates with the eigenvalue loci of Figure 4-2.

Throughout this chapter, the study has adhered to the d-q reference frames because (a) the eigenvalue loci in the d-q reference frame are closer to laboratory experience and (b) the algebra in the many proofs which will be presented here are less complicated in the d-q axes formulation.



5-1-1 Damping Coefficients Sum Invariance

Figure 5-1 shows a plot of the damping coefficients σ_1 , σ_2 and their sum σ_1 + σ_2 as a function of the rotor speed for the same induction motor as described in Chapter IV. The constant sum σ_1 + σ_2 is not restricted to a fortuitous choice of motor parameters in the numerical example but is a general result which can be expressed as

$$\sigma_1 + \sigma_2 = \frac{R^s L^r + R^r L^s}{L^s L^r - M^2}$$

This result is obtained by equating the characteristic equation to the determinant equation as shown in Equation 5-4

$$\begin{array}{l} (\lambda + \sigma_1 + i \omega_1) \; (\lambda + \sigma_1 - i \omega_1) \; (\lambda + \sigma_2 + i \omega_2) \; (\lambda + \sigma_2 - i \omega_2) \\ \\ = \; \det \; (\lambda \; [\; i \;] \; - \; [\; A_{dq} \;]) \end{array} \qquad \qquad 5-4$$

The coefficient of λ^3 in the left-hand side of Equation 5-4 is $2~(~\sigma_1~+~\sigma_2^{})~\text{and Equation 5-3 follows by equating it to the coefficient of}~\lambda^3~\text{in the determinant equation}.$

5-2 Natural Frequencies of Oscillation Sum

Likewise Figure 5-2 shows a plot of the natural frequencies of oscillation ω_1 , ω_2 and their sum ω_1 + ω_2 . The frequency sum

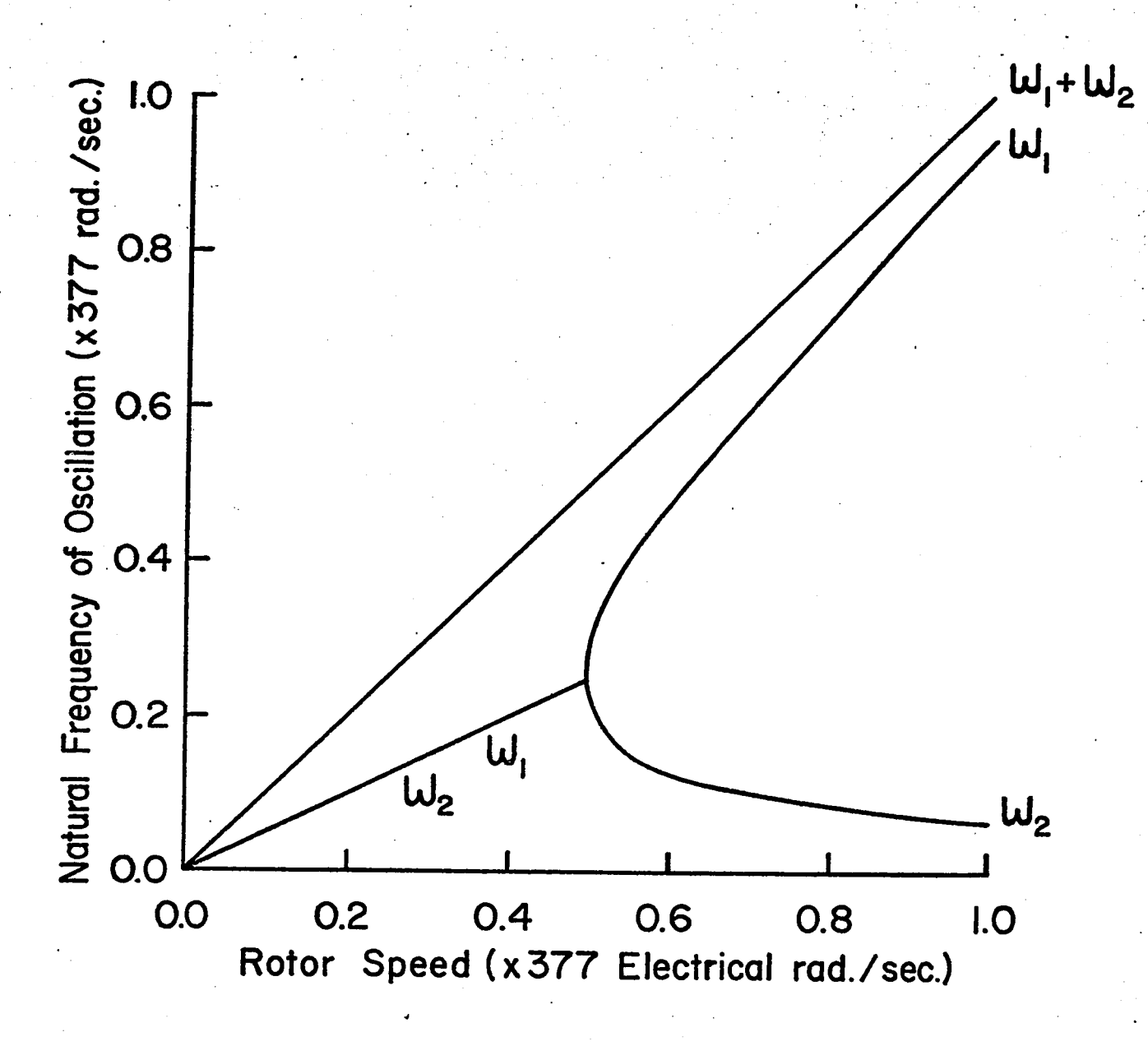


FIGURE 5.2. VARIATION OF NATURAL FREQUENCIES WITH ROTOR SPEED

$$\omega_1 + \omega_2 = \omega_m \qquad 5-5$$

$$|\omega_1| < \omega_m$$
 and $|\omega_2| < \omega_m$ 5-6

is a significant and simple relationship which has been reported and proved by Slater and Wood [22].

The inequalities of Equation 5-6 have an important theoretical significance which will be discussed fully in Section 5-10-1. It implies that since the speed of the magnetic flux of each mode is always slower than the mechanical speed of the rotor, then there is a generating countertorque associated with each of the constant speed modes.

5-3 The Transient Sub-Primitives

Because of the many parameters and the intercoupling of the four current equation in Equation 4-2, the commutator primitive in its entirety is too complicated to yield any physical insight. However by judiciously dropping out selected parameters, it is possible to simplify the system equations sufficiently to reveal some basic physics. It is found that the following three such degenerate systems have been extremely meaningful in identifying the modes:

- (i) the transformer sub-primitive,
- (ii) the magnetization sub-primitive,
- (iii) the loss-less sub-primitive.

The transformer sub-primitive describes and identifies the magnetization and the leakage inductance modes for the case of the rotor at standstill ($\omega_{\rm m}=0$). Referring to Figure 5-1 and Figure 5-2, the magnetization mode (σ_2) is very lightly damped whilst the leakage inductance mode, (σ_1) is heavily damped, and neither of them has an oscillatory component.

It can be seen that as the speed increases the damping factors change and the modes now become oscillatory. Initially the natural frequencies of oscillation is half the angular velocity of the rotor. What is it in the rotor speed interactions which "cause" the original transformer modes to break into oscillations? The magnetization sub-primitive is created to understand the rotor speed interaction with the magnetization mode in "causing" the oscillations.

The loss-less sub-primitive is proposed to identify the modes in the other end of the speed range and in fact as $\omega_{\overline{m}} > \infty$, Kron's commutator primitive approaches the loss-less sub-primitive asymptotically. The features distinguishing the modes in the fast speed range are now the frequencies. As Figure 5-2 suggests that as $\omega_{\overline{m}} > \infty$, $\omega_{\overline{m}} > 0$ and $\omega_{\overline{m}} > \omega_{\overline{m}}$.

Thus broadly speaking, it is possible to think of the induction motor modes as changing with speed from those of the transformer sub-primitive to those of the loss-less sub-primitive. The transition from one sub-primitive to the other is followed and described in detail using eigenvector representations in Sections 5-10 and 5-11.

5-4 The Transformer Sub-Primitive

At $\omega_m=0$, Equation 4-1 decouple into two sets of transformer equations, one set each for the d-axis windings and the q-axis windings. Assuming for simplicity that $R^S=R^\Gamma=R$ and $I^S=I^\Gamma=I$, the equations of the d-axis unexcited short-circuited transformer is:

$$\begin{bmatrix} M + I & M \\ M & M + I \end{bmatrix} p \begin{bmatrix} i_d^s \\ i_d^r \end{bmatrix} = \begin{bmatrix} -R & 0 \\ 0 & -R \end{bmatrix} \begin{bmatrix} i_d^s \\ i_d^r \end{bmatrix}$$
 5-6

The q - axis transformer is, of course, identical and it suffices to discuss Equation 5-6 only.

The eigenvector columns in Equation 4-26 suggest an odd and even symmetry for the modes in Equation 5-6, and a transformation based on the following steps can be made:

- (i) subtract the second row from the first row,
- (ii) add the second row to the first row.

This yields

$$\begin{bmatrix} I & 0 & p & \begin{bmatrix} i_d^s - i_q^s \\ i_d^s + i_q^s \end{bmatrix} = \begin{bmatrix} -R & \begin{bmatrix} i_d^s - i_q^s \\ i_d^s + i_q^s \end{bmatrix}$$

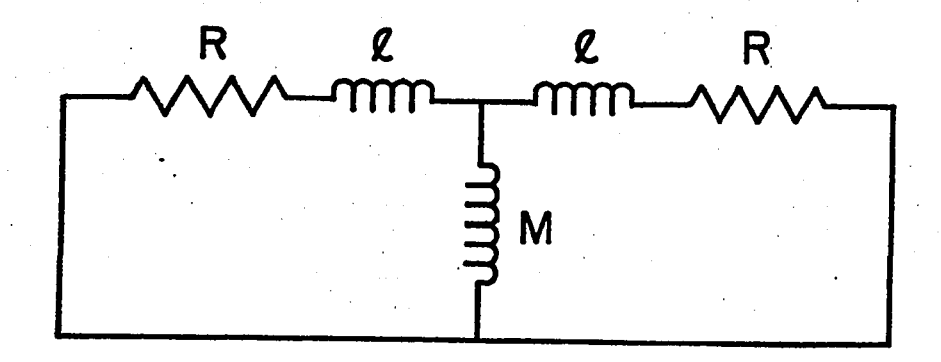


FIGURE 5.3(a). EQUIVALENT CIRCUIT OF TRANSFORMER SUBPRIMITIVE

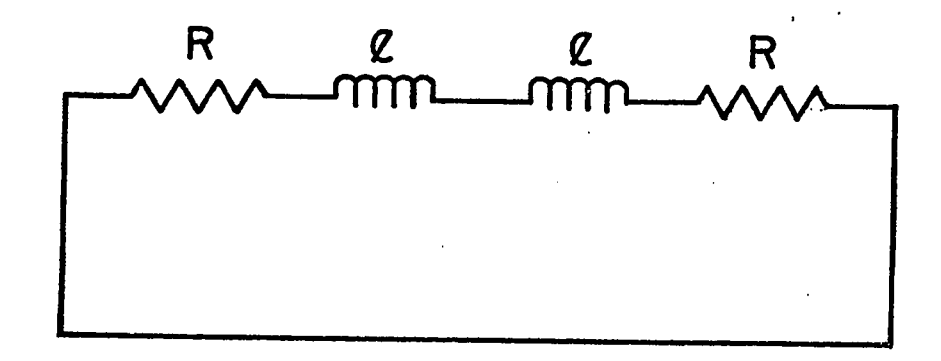


FIGURE 5.3(b). THE LEAKAGE INDUCTANCE MODE

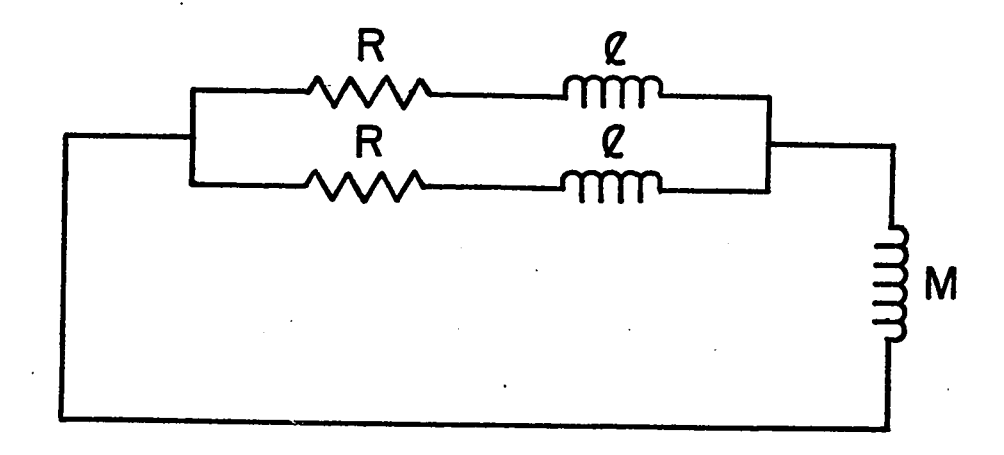


FIGURE 5.3(c). THE MAGNETIZATION INDUCTANCE MODE

Defining the modal variables

$$\begin{bmatrix} q_1 \\ q_2 \end{bmatrix} = \begin{bmatrix} 1 & -1 \\ 1 & 1 \end{bmatrix} \begin{bmatrix} i_d^s \\ i_d^r \end{bmatrix}$$
 5-8

and substituting into Equation 5-7, the decoupled modal equations are:

$$\mathbf{p} \begin{bmatrix} \mathbf{q}_1 \\ \mathbf{q}_2 \end{bmatrix} = \begin{bmatrix} \frac{-R}{T} \\ \frac{-R}{2M+1} \end{bmatrix} \begin{bmatrix} \mathbf{q}_1 \\ \mathbf{q}_2 \end{bmatrix} \qquad 5-9$$

The physical identification of each of the modes can be obtained from the modal transformation equation of Equation 5-8 in conjunction with the transformer equivalent circuit of Figure 5-3(a). The mode of q_1 consists of current flowing in the circuit topology as shown in Figure 5-3(b). It is a heavily damped mode because the storage elements consist of the leakage inductances only. In contrast the damping factor for the mode of q_2 is very lightly damped, because as shown in Figure 5-3(c), this mode is associated with the large mutual inductance M.

5-5 The Magnetization Sub-Primitive

The leakage inductances are assumed to be zero in the magnetization sub-primitive, and therefore $L^s=L^r=M$. Assuming $R^s=R^r=R$, the sub-primitive dynamic equation is :

$$\begin{bmatrix} R + Mp & 0 & Mp & 0 \\ 0 & R + Mp & 0 & Mp \\ Mp & -M \omega_{m} & R + Mp & -M \omega_{m} \\ M \omega_{m} & Mp & M \omega_{m} & Mp \end{bmatrix} \begin{bmatrix} i_{d}^{s} \\ i_{d}^{r} \\ i_{d}^{r} \end{bmatrix} = \begin{bmatrix} 0 \\ 0 \\ 0 \\ 0 \end{bmatrix}$$

$$\begin{bmatrix} i_{d}^{s} \\ i_{d}^{r} \\ i_{d}^{r} \end{bmatrix} = \begin{bmatrix} 0 \\ 0 \\ 0 \\ 0 \end{bmatrix}$$

Equation 5-10 is a degenerate set of equations and should be reduced to a second order system in terms of the d - and the q - axis magnetization currents as follows:

$$\begin{bmatrix} i_{md} \\ i_{mq} \end{bmatrix} = \begin{bmatrix} i_{d}^{s} + i_{d}^{r} \\ i_{q}^{r} + i_{q}^{r} \end{bmatrix}$$
5-11

Adding the first to the third row of Equation 5-10 and the second to the fourth row and thereafter substituting Equation 5-11, the magnetization subprimitive equations in terms of the magnetization currents are

The eigenvalues of Equation 5-12 are $\lambda = -\frac{R}{M} \pm i\frac{\omega_m}{2}$.

Figure 5-2 shows that the oscillating frequency of the sub-primitive term agrees very well with the magnetization mode of the real machine. The damping term, however,

is in serious error and the reason lies in the assumption of $l^s = l^r = 0$.

Since the objective here is to gain a physical "feel" for the production of the oscillating term, the resistance R will now be dropped from Equation 5-12. This leaves the differential equations of the harmonic oscillator of a natural frequency at $\frac{\omega}{2}$:

$$\mathbf{p} \begin{bmatrix} \mathbf{i}_{md} \\ \mathbf{i}_{mq} \end{bmatrix} = \begin{bmatrix} 0 & \frac{\omega_{m}}{2} \\ -\frac{\omega_{m}}{2} & 0 \end{bmatrix} \begin{bmatrix} \mathbf{i}_{md} \\ \mathbf{i}_{mq} \end{bmatrix}$$
 5-13

Equation 5-13 focusses on the interactions of the magnetization flux with the speed voltage in the production of the harmonic oscillations.

It is important to note that there is a directionality of rotation in the magnetization m.m.f., associated with these currents:

$$\begin{bmatrix} \mathbf{i}_{md} \\ \mathbf{i}_{mq} \end{bmatrix} = \begin{bmatrix} \cos \frac{\omega_{m}}{2} + \\ -\sin \frac{\omega_{m}}{2} + \end{bmatrix}$$
5-14

is a solution to Equation 5–13 while the solution

$$\begin{bmatrix} \mathbf{i}_{md} \\ \mathbf{i}_{md} \end{bmatrix} = \begin{bmatrix} \cos \frac{\omega_m}{2} + \\ \sin \frac{\omega_m}{2} + \end{bmatrix}$$

Using Equations 5-13 and 5-14 it is possible to obtain a qualitative description of the oscillation of the magnetization mode in terms of storage energy exchanges between the cross-axis mutual inductances. The medium of power transfer is through the speed voltages. The directionality of rotation of the magnetization flux is determined by the sign coefficients of $\frac{\omega_m}{2}$ in Equation 5-13 which expresses the polarity of induced voltage with respect to direction of the flux and the direction of the rotor speed.

5-6 The Lossless Sub-Primitive

In the lossless sub-primitive, the stator and the rotor resistances are assumed to be zero. As there is no dissipative component, the modes are never damped away, and as in Section 5-5 the usefulness of the sub-primitive comes from using the natural frequencies to identify the modes.'

The dynamic equations of the lossless sub-primitive are:

$$\begin{bmatrix} \mathbf{L}^{s} \mathbf{p} & 0 & M \mathbf{p} & 0 \\ 0 & \mathbf{L}^{s} \mathbf{p} & 0 & M \mathbf{p} \\ M \mathbf{p} & -M \omega_{m} & \mathbf{L}^{r} \mathbf{p} & -\mathbf{L}^{r} \omega_{m} \\ M \omega_{m} & M \mathbf{p} & \mathbf{L}^{r} \omega_{m} & \mathbf{L}^{r} \mathbf{p} \end{bmatrix} \begin{bmatrix} \mathbf{i}_{d}^{s} \\ \mathbf{i}_{q}^{r} \\ \mathbf{i}_{d}^{r} \\ \mathbf{q} \end{bmatrix} = \begin{bmatrix} 0 \\ 0 \\ 0 \\ 0 \end{bmatrix}$$

$$5-16$$

The eigenvalues found from the roots of the characteristic equation of Equation 5–16

$$\det \left[\lambda \left[L \right] + \omega_{m} \left[G \right] \right] = 0$$
 5-17

are $\lambda=0$, 0, $\omega_{\rm m}$ and $-\omega_{\rm m}$. Referring to Figure 5-2 it can be seen the frequencies of the lossless sub-primitive are approached asymptotically by the real machine in the region of large rotor speeds, i.e. as $\omega_{\rm m} \to \infty$, $\omega_2 \to 0$ and $\omega_1 \to \omega_{\rm m}$.

The physical modes can be identified for the sub-primitive by rewriting Equation 5-16 as a flux-linkage equation. Thus using the following transformation:

$$\frac{\Psi}{dq} = [L] \frac{i}{dq}$$
 5-18(a)

or

$$\begin{bmatrix} \psi_{d}^{s} \\ \psi_{q}^{s} \\ \psi_{d}^{r} \\ \psi_{d}^{r} \end{bmatrix} = \begin{bmatrix} L^{s} & 0 & M & 0 \\ 0 & L^{s} & 0 & M \\ M & 0 & L^{r} & 0 \\ 0 & M & 0 & L^{r} \end{bmatrix} \begin{bmatrix} i_{d}^{s} \\ i_{q}^{r} \\ i_{d}^{r} \\ i_{q}^{r} \end{bmatrix}$$

$$\begin{bmatrix} v_{d}^{s} \\ v_{d}^{r} \\ v_{d}^{r} \end{bmatrix} \begin{bmatrix} v_{d}^{r} \\ v_{d}^{r} \\ v_{d}^{r} \end{bmatrix}$$

and Equation 5-16 becomes

which can be expressed in the diagonalised form

$$\mathbf{P} \ \underline{\Psi}_{dq} = [S][\Lambda][S]^{-1} \ \underline{\Psi}_{dq}$$
 5-20

where the eigenvalue matrix is

the eigenvector matrix is

$$\begin{bmatrix} S \end{bmatrix} = \begin{bmatrix} 1 & 0 & 0 & 0 \\ 0 & 1 & 0 & 0 \\ 0 & 0 & \frac{1}{\sqrt{2}} & \frac{1}{\sqrt{2}} \\ 0 & 0 & -\frac{i}{\sqrt{2}} & \frac{i}{\sqrt{2}} \end{bmatrix}$$
5-22

and the reciprocal base vector matrix is

$$\begin{bmatrix} 5 \end{bmatrix}^{-1} = \begin{bmatrix} 1 & 0 & 0 & 0 \\ 0 & 1 & 0 & 0 \\ 0 & 0 & \frac{1}{\sqrt{2}} & \frac{-i}{\sqrt{2}} \\ 0 & 0 & \frac{1}{\sqrt{2}} & \frac{i}{\sqrt{2}} \end{bmatrix}$$
5-23

Using the knowledge of the eigenvectors in Equation 5-22 and Section 4-13, the following two flux-vectors

$$\frac{\Psi_{dq}}{dq} = \begin{bmatrix} 1 \\ 1 \\ 0 \\ 0 \end{bmatrix}$$
 5-24

$$\frac{\Psi_{dq}}{\sqrt{2}} = \begin{bmatrix}
0 & & & \\
0 & & \\
\sqrt{2} & \cos(\omega_{m} t + \frac{\pi}{4}) \\
\sqrt{2} & \sin(\omega_{m} t + \frac{\pi}{4})
\end{bmatrix}$$
5-25

are two possible free motion solutions associated with each of the modes of eigenvalues ± 0.0 and $\pm i \omega_m$ respectively. Transforming these modal solutions from the d - q

frame to the slip-ring primitive $\alpha-\beta$ frame using the connection matrix $[C_{\alpha\beta}^{\mbox{dq}}]$, i.e.

$$\Psi_{\alpha\beta} = [C_{\alpha\beta}^{dq}] \Psi_{dq}$$
 5-26

Equations 5-24 and 5-25 become

$$\begin{bmatrix}
\psi & s \\
d \\
\psi & s \\
q \\
\psi & r \\
\psi & \alpha \\
\psi & r \\
0 \\
0
\end{bmatrix}$$
5-27

$$\begin{bmatrix} \psi & s \\ d \\ \psi & s \\ q \\ \psi & r \\ \psi & \alpha \\ \psi & r \\ \beta & 1 \end{bmatrix} = \begin{bmatrix} 0 \\ 0 \\ 1 \\ 1 \end{bmatrix}$$
5-28

The flux-linkage solutions in the α - β frame identify the lossless sub-primitive modes as the stator mode (Equation 5-27) and the rotor mode (Equation 5-28). In the free motion of each mode, the winding currents flow so as to preserve the constant flux linkage theorem. The rotor mode when viewed from the stationary windings of the stator has of course a frequency of $\omega_{\rm m}$, which is the speed at which the constant rotor flux is "cutting" the stator windings.

Translating Equation 5-20 back to the current d - q axis frame

$$p_{i-dq} = [L]^{-1} [S] [A] [S]^{-1} [L]_{i-dq}$$
 5-29

the eigenvector matrix is

$$[L]^{-1}[S] = \frac{1}{L^{S}L^{T} - M^{2}} \begin{bmatrix} L^{T} & 0 & -\frac{M}{\sqrt{2}} & -\frac{M}{\sqrt{2}} \\ 0 & L^{T} & i\frac{M}{\sqrt{2}} & -i\frac{M}{\sqrt{2}} \\ -M & 0 & \frac{L^{S}}{\sqrt{2}} & \frac{L^{S}}{\sqrt{2}} \\ 0 & -M & -i\frac{L^{S}}{\sqrt{2}} & i\frac{L^{S}}{\sqrt{2}} \end{bmatrix}$$
 5-30

It will be shown subsequently in Section 5-11 that just as the modal oscillating frequencies of the induction motor approach those of the lossless subprimitive, likewise the eigenvectors Equation 5-30 are also approached asymptotically at high speeds.

5-6-1 Asymptotic Approximation

The asymptotic approximation of the induction motor modes to those of lossless, sub-primitive at high rotor speed can be demonstrated analytically. Firstly, since $\lambda = i \omega_m$ is an eigenvalue of the lossless sub-primitive, it is a solution to the

characteristic equation, Equation 5-17, i.e.

$$\det \left[i \omega_{m} \left[L \right] + \omega_{m} \left[G \right] \right] = 0$$
 5-31

Since $\omega_{\mathbf{m}}$ is a nonzero scalar, it can be factored out, leaving

The eigenvalues of the complete first commutator primitive must satisfy the characteristic equation, Equation 5-4, i.e.

$$\det \left[\lambda \left[L \right] + \left[R \right] + \omega_{m} \left[G \right] \right] = 0$$
 5-33

Substituting $\lambda = i\,\omega_m$ and again factoring out ω_m , Equation 5–33 becomes

$$\det \left[\frac{1}{\omega_{m}}\left[R\right]+i\left[L\right]+\left[G\right]\right] \longrightarrow \det \left[i\left[L\right]+\left[G\right]\right]=0$$
5-34

as
$$\omega_{m} \rightarrow \infty$$
.

This asymptotic property is borne out by the eigenvalues and the eigenvectors numerically solved from the digital computer subroutines.

5-7 <u>Eigenvector Rotational Property</u>

Since each of the eigenvectors consists a column of 4 complex numbers, there are altogether 8 real numbers defining their real parts and the imaginary parts. However, because of a rotational symmetry in [A_{dq}] of Equation 4-2, there are actually 4 independent real numbers, and the kth eigenvector can be written as

$$\underline{U}_{k} = \underline{U}_{r} + i \left[\Phi \right] \underline{U}_{r}$$
 5-35

and
$$\underline{U}_{r}^{T} = [U_{1}, U_{2}, U_{3}, U_{4}]$$
 5-37

where U_1 , U_2 , U_3 , U_4 are any real numbers .

The square matrix $[\Phi]$ bears the information of the forward rotation of the mode. The transpose of $[\Phi]$ describes a backward rotation, and the synchronous frame eigenvectors in the matrix of Equation 4-26 is a good example which states that the modes are rotating backwards with respect to the %- % reference frame.

The basic rotational property of the eigenvector in Equation 5-35 is is proved in Appendix C. It is a significant result which enables the mode representation and interpretation based on the eigenvector to follow.

5-8 Mode Representation by Eigenvectors

The geometrical interpretation of an oscillatory mode is the plane in a multi-dimensional sub-space supported by U_r and U_i which are respectively the real parts and the imaginary parts of the eigenvector. The free motion of the excited mode is described by a state-point in the modal plane spiralling towards the origin. Besides this mathematical interpretation, the modes of the induction motor admit of a physical interpretation in terms of the m.m.f.'s in the motor airgap space. In Section 2-11, the airgap m.m.f.'s have been represented in magnitudes and directions by the space-vectors $\frac{3}{5}$, $\frac{3}{7}$ and $\frac{3}{m}$. The objective here is, therefore, to present the space vectors as a physical representation of the modes.

The geometrical state-point lying on the modal plane of the kth mode of $\begin{bmatrix} A_{\mathbf{dq}} \end{bmatrix}$ is

$$i_{-dq} = b \underline{U}_r + d \underline{U}_i$$
 5-38

where b and d are any real constants. Substituting Equation 5–35 into

$$\frac{i}{-dq} = b \begin{bmatrix} U_1 \\ U_2 \\ U_3 \\ U_4 \end{bmatrix} + d \begin{bmatrix} -U_2 \\ U_1 \\ -U_4 \\ U_3 \end{bmatrix}$$
 5-39

Using the stator and rotor current vectors representation of Equation 2–19 and defining vector magnitudes and phases as

$$\begin{bmatrix} U_1 \\ U_2 \\ U_3 \\ U_4 \end{bmatrix} = \begin{bmatrix} \Im_{sk} & \sin \emptyset_{sk} \\ \Im_{sk} & \cos \emptyset_{sk} \\ \Im_{rk} & \sin \emptyset_{sk} \\ \Im_{rk} & \cos \emptyset_{sk} \end{bmatrix}$$
5-40

Equation 5-39 can be expressed as

$$\frac{i}{dq} = C_{1} \begin{bmatrix} 3_{sk} & \sin (\%_{sk} - \%_{o}) \\ 3_{sk} & \cos (\%_{sk} - \%_{o}) \\ 3_{rk} & \sin (\%_{rk} - \%_{o}) \end{bmatrix} 5-41$$

$$\frac{3_{rk}}{r_{k}} \cos (\%_{rk} - \%_{o})$$

where C_1 and \emptyset'_0 are the magnitudes and the reference angle of the polar representations of the arbitrary constants b and d, i.e.

$$C_{1} = (b^{2} + d^{2})^{1/2}$$

$$b = C_{1} \cos \varphi_{0}$$

$$d = C_{1} \sin \varphi_{0}$$

$$5-42$$

Using Equation 5-41 and Figure 2-1 it becomes possible to identify a mode in terms of the space-vectors in the motor airgap. As the point in the eigenvector modal plane is shifted, b and d take on other arbitrary values. This has the effect of changing the multiplying constant C_1 and the reference angle \mathscr{G}_0 in Equation 5-41, but essentially the parallelogram defined by \mathscr{F}_{sk} and \mathscr{F}_{rk} retains its similar geometry in Figure 2-1 despite the changes in magnification and orientation.

Now that a representation is possible, the next section will be devoted to examining the space-vectors of the modes for different speeds of the induction motor.

5-8-1 Space Vector Diagrams

Figure 5-4(a) to (f) show a series of space vector diagrams of the two modes of the induction motor described in Appendix G. The p. u. speed for a 60 Hz supply is 377 electrical radians per second and the rotor speeds in the diagrams are for 0.0, 0.04, 0.1, 0.4, 0.48 and 1.0 p.u. respectively.

Figure 5-4(a) shows the vectors for the magnetization and the leakage inductance modes for the motor at standstill. In the magnetization mode the three vectors, \mathfrak{F}_{s2} and \mathfrak{F}_{r2} are co-linear and pointing in the same direction thus giving a very large resultant \mathfrak{F}_{m2} . In contrast the leakage inductance vectors \mathfrak{F}_{s1} and \mathfrak{F}_{r1} are equal and opposite so that their sum $\mathfrak{F}_{m1}=0$.

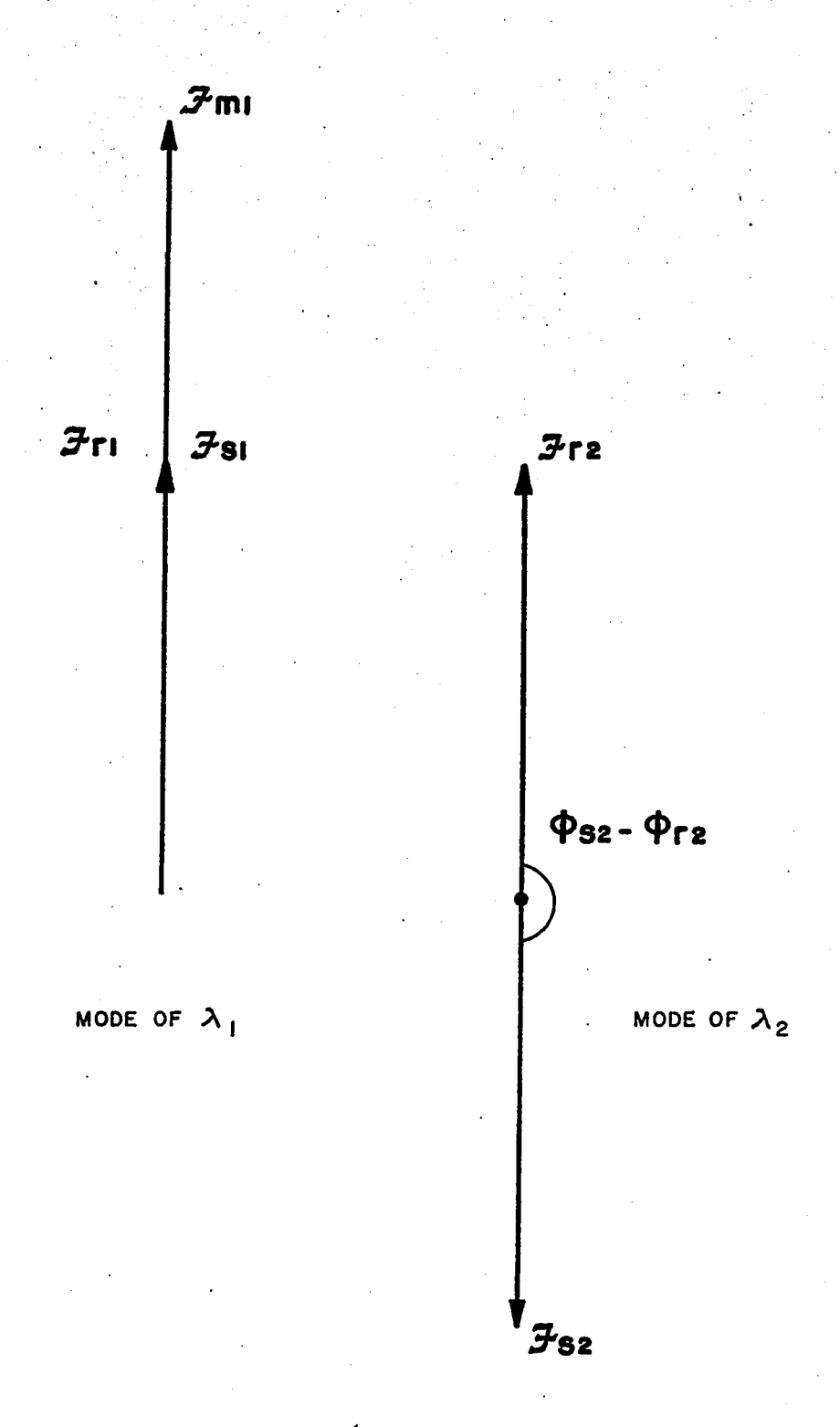


Fig. 5-4(a). M.M.F. Vector Representation of Modes
Rotor Speed=0.0 Rad./Sec.

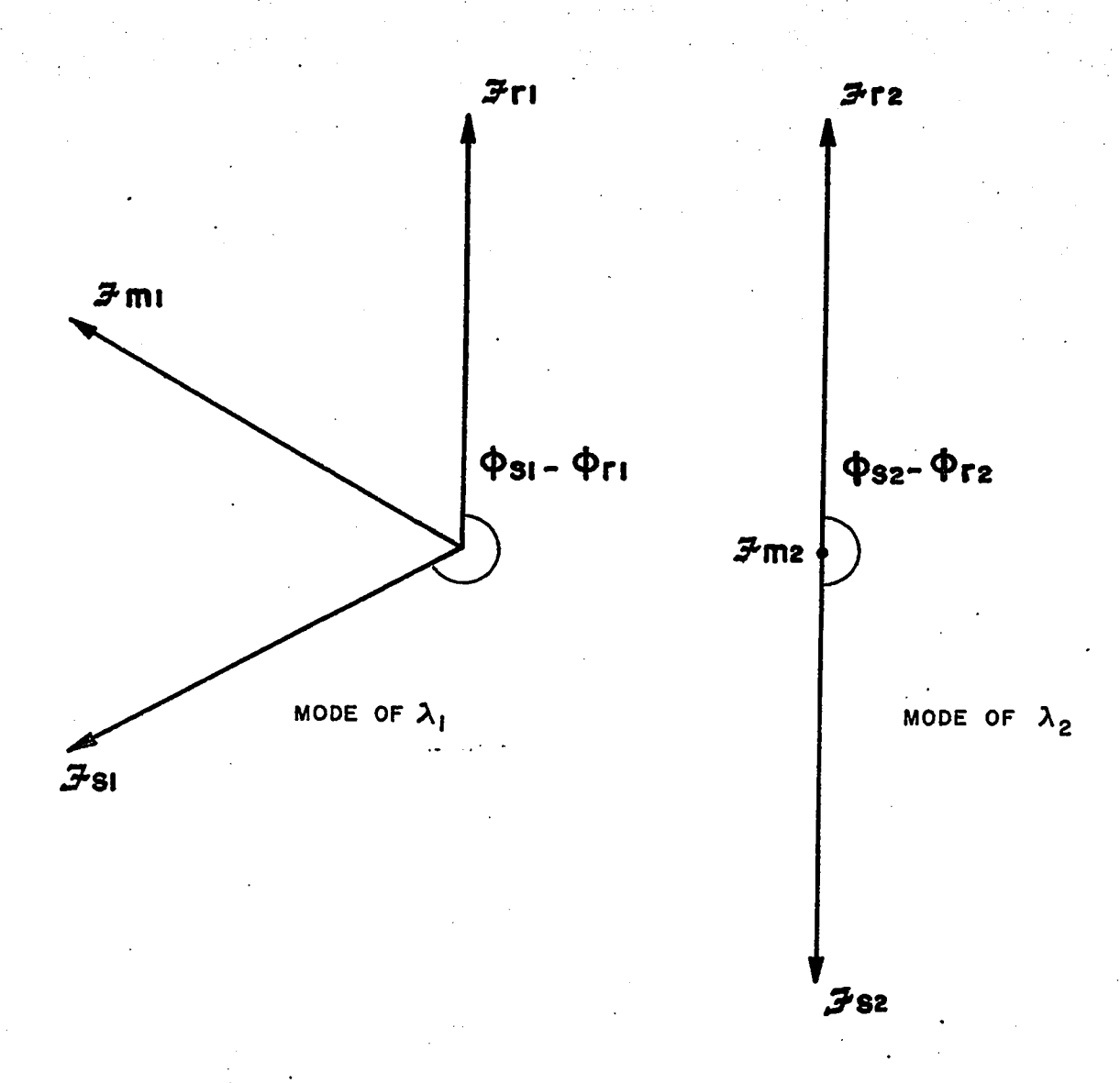


Fig. 5-4 (b) Rotor Speed = 0.04 p.u.

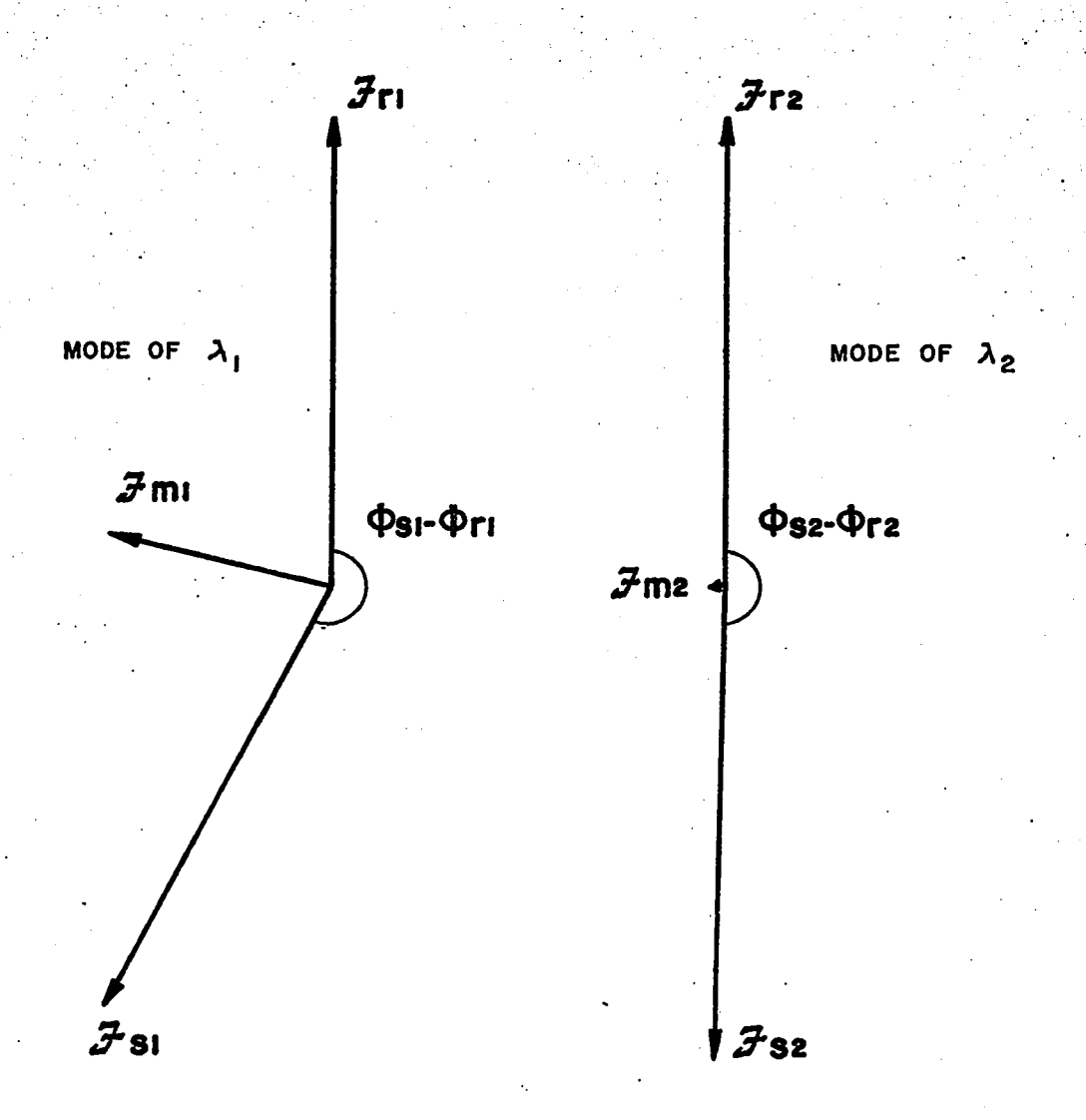


Fig. 5-4(c).Rotor Speed=O.l p.u.

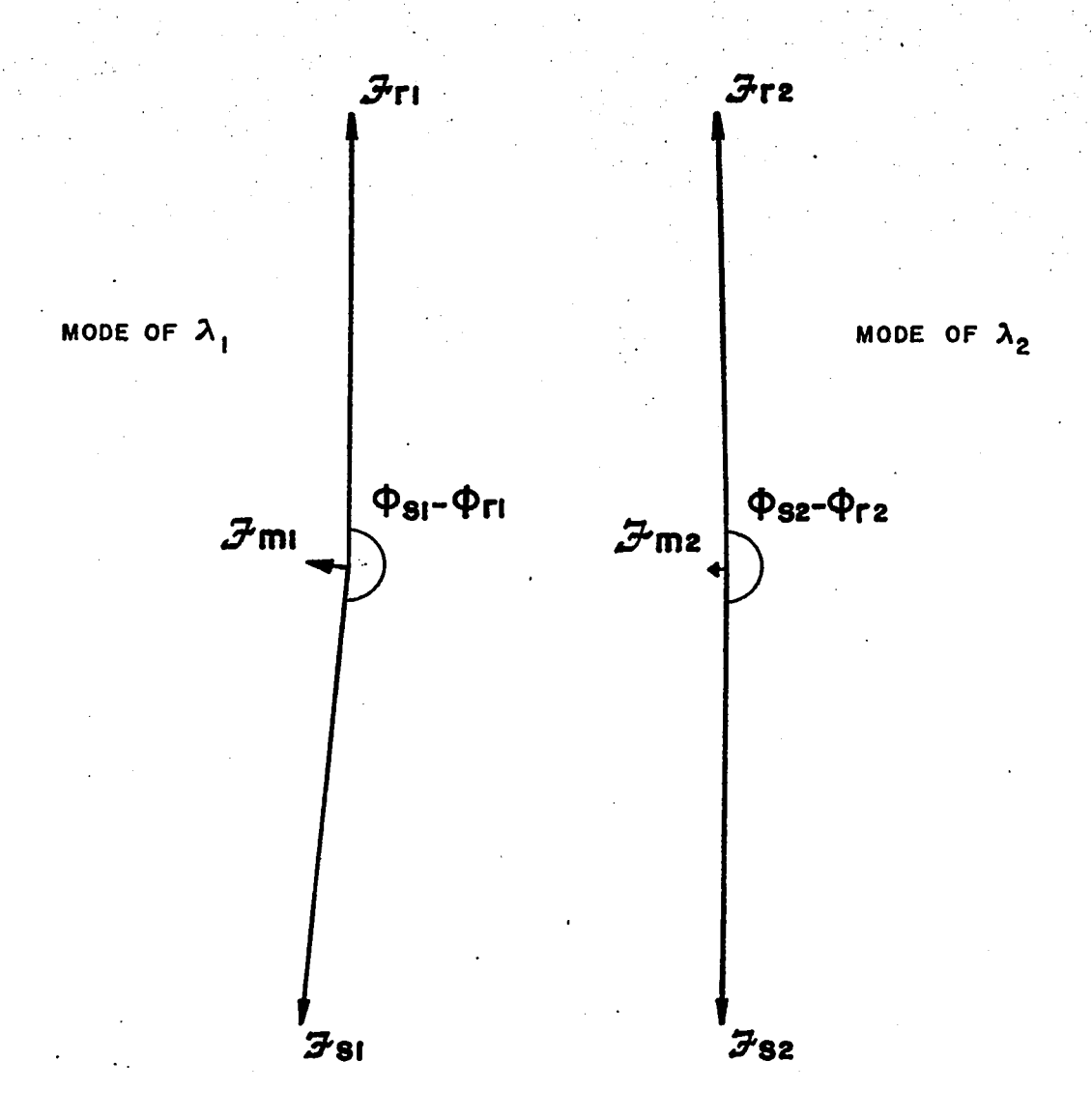


Fig. 5-4 (d). Rotor Speed = 0.4 p.u.

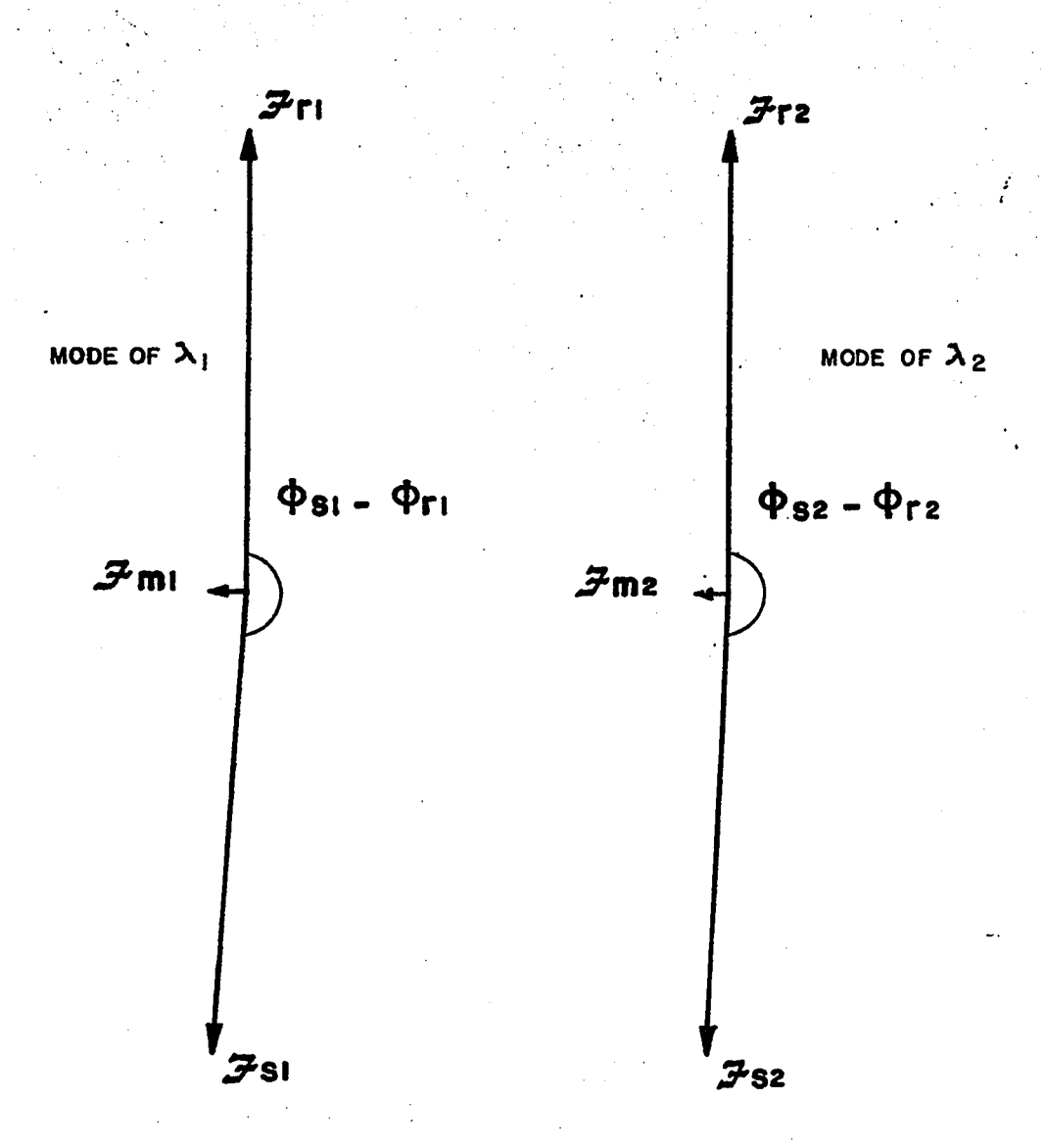


Fig. 5-4 (e). Rotor Speed = 0.48 p.u.

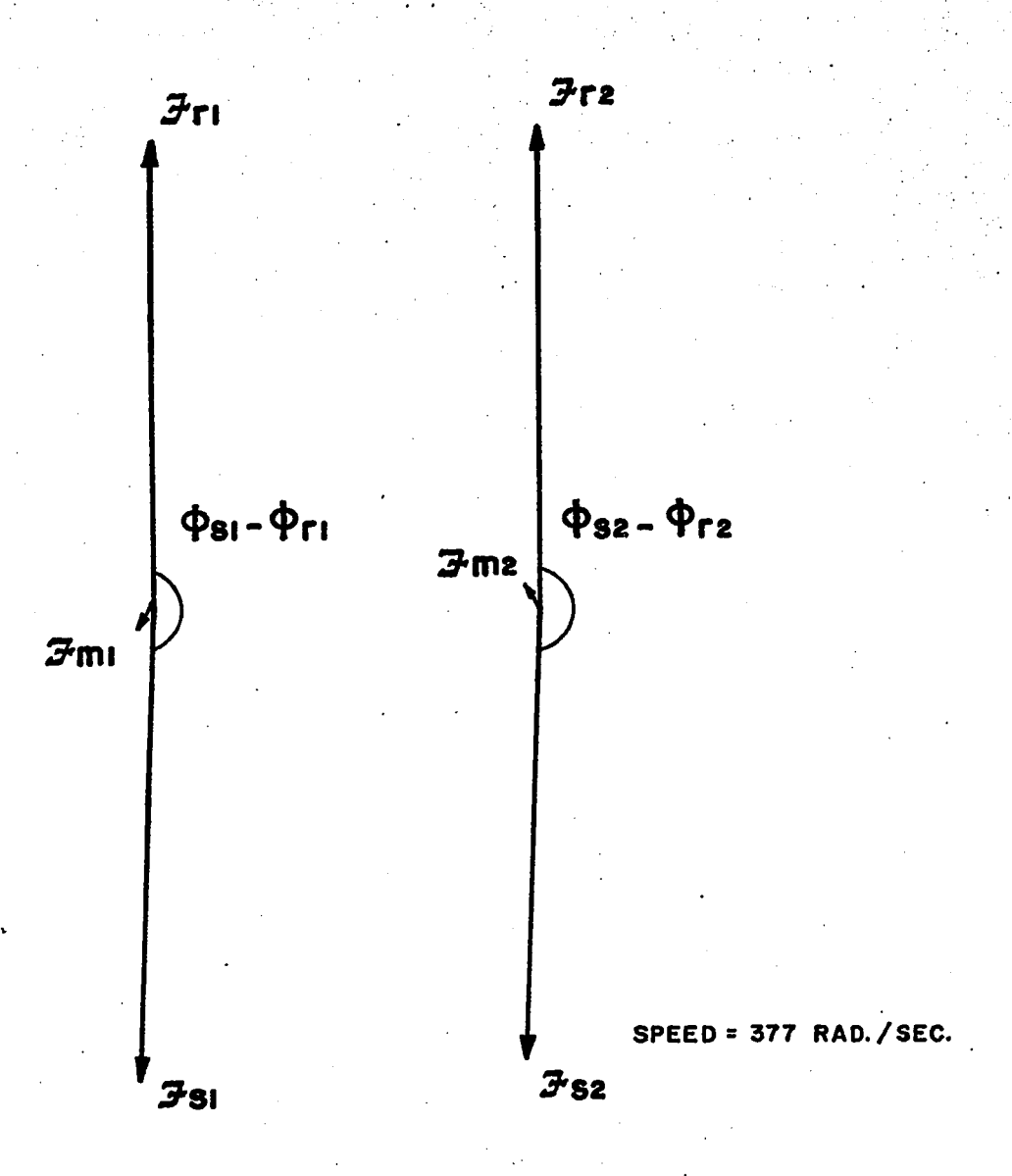


Fig. 5-4 (f). Rotor Speed = i.0 p.u.

Figure 5-4(f), on the other hand, shows the two modes at 1.0 p.u. speed and these approach the stator and the rotor modes of the lossless sub-primitive. The feature which distinguishes them are the relative directions of $\frac{3}{m1}$ which points towards $\frac{3}{r1}$ and $\frac{3}{m2}$ which points towards the stator space-vector $\frac{3}{s2}$.

It is instructive to follow the vector diagrams from Figure 5-4(a) to Figure 5-4(f) as a continuous change with rotor speed. From $\omega_m=0.0$ to $\omega_m=0.48$ p.u. the leakage inductance mode which has $\mathfrak{F}_{m1}=0.0$ at $\omega_m=0.0$ develops a finite \mathfrak{F}_{m1} and $(\mathfrak{F}_{s1}-\mathfrak{F}_{r2})$ moves from 180° into the third quadrant. Meanwhile \mathfrak{F}_{m2} in the magnetization mode collapses as $(\mathfrak{F}_{s2}-\mathfrak{F}_{r2})$ decreases from 360° to the third quadrant. Around $\omega_m=0.48$ p.u., the two modes become coincident and likewise the space-vectors of the two modes are indistinguishable. From $\omega_m=0.49$ p.u. speed upwards one mode moves towards the stator mode of the lossless sub-primitive and the other develops into the rotor mode. Because of the coincident eigenvalues in this numerical example it is not possible to identify whether the rotor mode is continuous from the magnetization or from the leakage inductance mode.

Hitherto the space-vector diagrams have been used as physical interpretation and representation of each mode. The next section will further show that the space-vectors can also be used to describe the dynamics of an excited mode.

5-43

5-9 Modal Representation in Free Motion

A set of initial currents which satisfy Equation 5-38 would excite the kth mode exclusively. On release, the currents would oscillate in the short-circuited windings and would ultimately be damped up as the state follows a trajectory described by:

$$\begin{split} \mathbf{i}_{-dq} &= \frac{1}{2} \exp \ \sigma_{k} t \left[\cos \omega_{k} \ t + i \sin \omega_{k} t \right] \left\{ \underbrace{U}_{r} + i \left[\Phi \right] \underbrace{U}_{r} \right\} \\ &+ \frac{1}{2} \exp \ \sigma_{k} t \left[\cos \omega_{k} t - i \sin \omega_{k} t \right] \left\{ \underbrace{U}_{r} - i \left[\Phi \right] \underbrace{U}_{r} \right\} \\ &= \exp \sigma_{k} t \cos \omega_{k} t \left[\underbrace{U}_{1} \right] \\ \underbrace{U}_{2} \\ \underbrace{U}_{3} \\ \underbrace{U}_{4} \end{aligned} \qquad \qquad - \exp \sigma_{k} t \sin \omega_{k} t \left[- \underbrace{U}_{2} \right] \\ \underbrace{U}_{1} \\ - \underbrace{U}_{4} \\ \underbrace{U}_{3} \end{aligned}$$

Using the space-vector representation in Equation 5-41, the modal currents can be expressed as

The magnitudes of the space-vectors in Equation 5-44 are damped exponentially at a rate σ_k and the axes rotate physically in the airgap space at an angular velocity ω_k in the forward direction. A picture of the vector parallelograms of Figure 5-4: spirally in the airgap space is a valid physical interpretation.

5-10 Damping Factor Structure

This section is devoted to establishing a physical correlation between the damping factor and the modal space-vectors. The damping factor is, of course, related to energy stored in the winding inductances and how quickly this energy is dissipated away by the stator and the rotor resistances. At any given instant in the trajectory of an exclusively excited mode, described by Equation 5-44, damping occurs because the net dissipated power is depleting the energy storage.

Under free-motion, the power balance equation derived in Appendix A is

$$R^{s} \mathcal{J}_{s}^{2} + R^{r} \mathcal{J}_{r}^{2} + n M \omega_{m} \mathcal{J}_{s} \mathcal{J}_{r} \sin (\mathcal{J}_{s} - \varphi_{r})$$

$$+ p \frac{1}{2} (I^{s} \mathcal{J}_{s}^{2} + I^{r} \mathcal{J}_{r}^{2} + M \mathcal{J}_{m}^{2}) = 0$$
5-45

Substituting Equation 5-44 into Equation 5-45, and performing the differentiation p = $\frac{d}{dt}$, it is possible to factor out the damping factor σ_k ,

$$\sigma_{k} = -\frac{1}{2} \frac{R^{s} \mathcal{S}_{sk}^{2} + R^{r} \mathcal{S}_{rk}^{2} + n \omega_{m} M \mathcal{S}_{sk} \mathcal{S}_{rk} \sin(0 - 0)}{\frac{1}{2} I^{s} \mathcal{S}_{sk}^{2} + \frac{1}{2} I^{r} \mathcal{S}_{rk}^{2} + \frac{1}{2} M \mathcal{S}_{mk}^{2}}$$

$$= -\frac{1}{2} \frac{\Sigma_{dk}}{\Sigma_{sk}}$$
5-46

where Σ_{dk} and Σ_{sk} are respectively the sum of the dissipative and storage components.

The denominator consists of the sum of the energy stored in the leakage inductances and the mutual inductance and the numerator consists of dissipation in the stator and rotor resistance and mechanical power. Each of the space vector magnitudes \mathbf{x}_{sk} , \mathbf{x}_{rk} , \mathbf{x}_{mk} is obtained from the eigenvector components \mathbf{U}_r , and Equation 5-46 is a display of the structure of the damping in terms of the distribution of the modal currents flowing in each system parameter. All the components of Equation 5-46 are positive except the mechanical power term which does become negative.

5-10-1 Negative Dissipation

The term in M $_{sk}^{s}$ $_{rk}^{s}$ $_{sin}^{s}$ $(_{s}^{s} - _{r}^{g})$ in Equation 5-46 is the space-vector expression of electromechanical torque. Whenever $(_{s}^{s} - _{r}^{g})$ lies in the 3rd or 4th quadrant, a negative torque exists and power is fed from the constant speed source into the short-circuited motor windings. There is effectively mechanical power converted into electrical power. In circuit theory this is represented by a negative resistance and the power associated with it is the negative dissipation. It has been remarked in Section 5-2 that since $|_{\omega_k}$ $|_{short}$ $|_{shor$

rotating airgap flux of the mode and roughly from the conventional steady-state theory the generating counter-torque always exist.

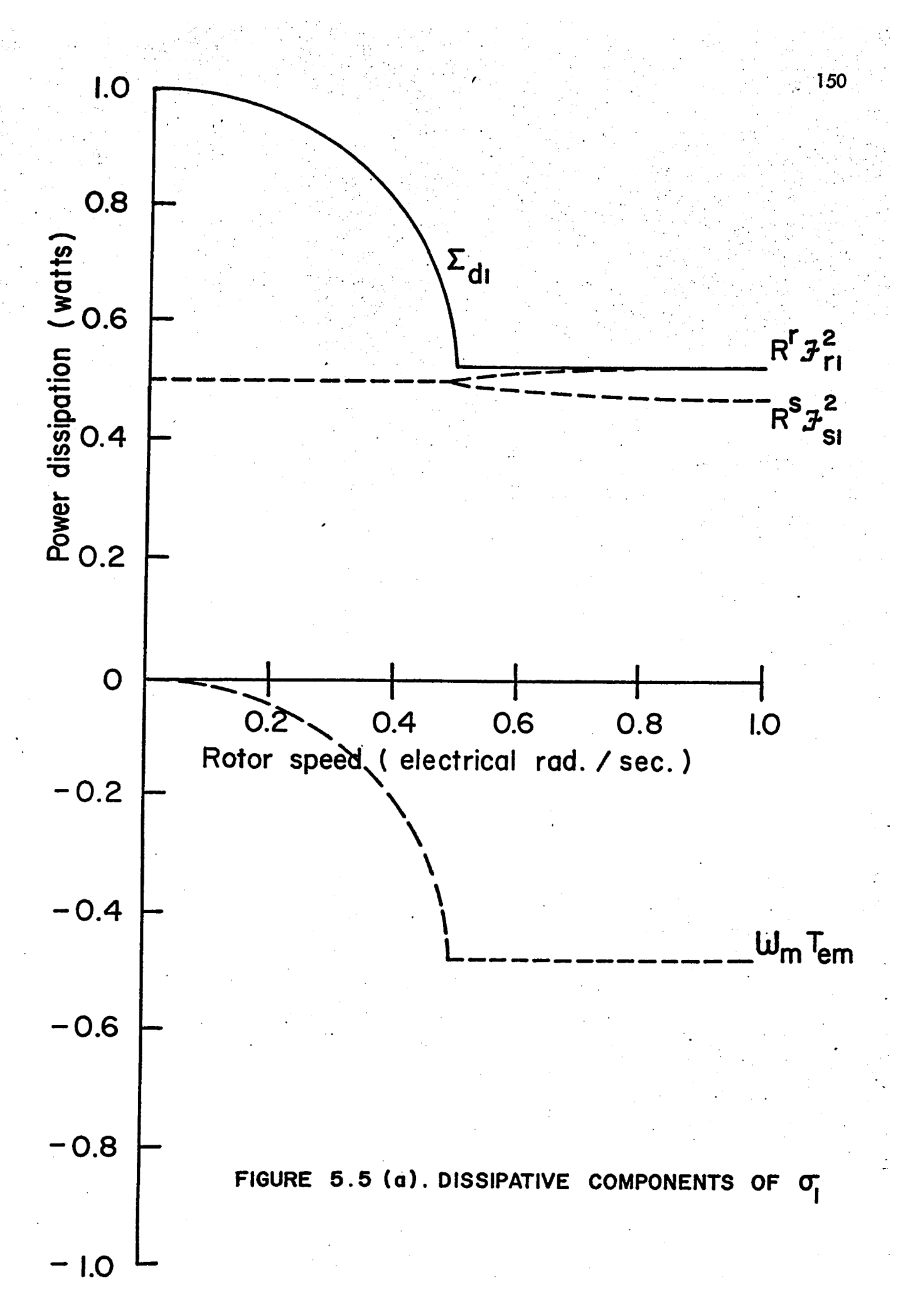
This negative dissipation is borne out in the structural analysis in Section 5-10-2. Furthermore from the space-vector diagrams in Figure 5-4 (a) to Figure 5-4 (f) $(\varphi_s - \varphi_r)$ always lie in the 3rd or 4th quadrant.

5-10-2 Damping Factor Variations with Speed

It is intended that by the study of the structural components of Equation 5-46, some physical understanding can be gained for the variation of σ_k with speed as shown in Figure 5-1. Figure 5-5 (a) and (b) display the dissipative and the stored energy components respectively of the mode $\lambda = \sigma_1 \pm i \omega_1$; and likewise Figure 5-6 (a) and (b) display those for the mode, $\lambda = \sigma_2 \pm i \omega_2$.

Figure 5-5(b) shows that the total energy stored in the windings is substantially constant for the mode of $\sigma_{\rm l}$. It should be noted that the contributions due to the mutual inductance is negligible and the stored energy resides in mainly the leakage inductances. Figure 5-5(a) shows that the sum of the stator and the rotor dissipative components remain constant with speed. The factor which contributes principally to the change from the highly damped $\sigma_{\rm l}=-188$ (at $\omega_{\rm m}=0$) to $\sigma_{\rm l}=-96.5$ (for $\omega_{\rm m}>0.49$ p.u.) in Figure 5-1 is the negative dissipation.

The behavior of the components of σ_2 is displayed in Figure 5-6. At rotor standstill, the bulk of the energy of the magnetization mode is stored mutual in-



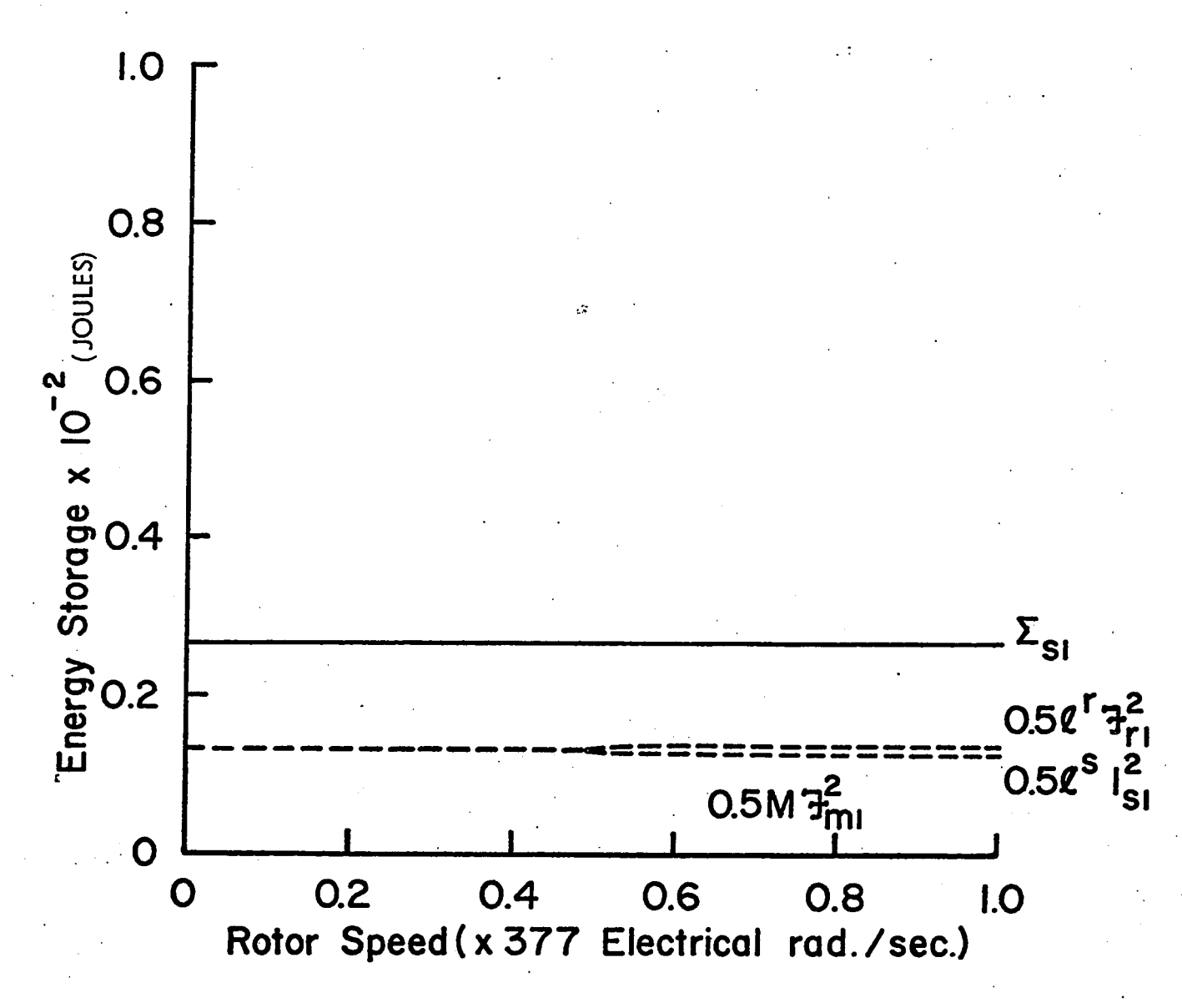
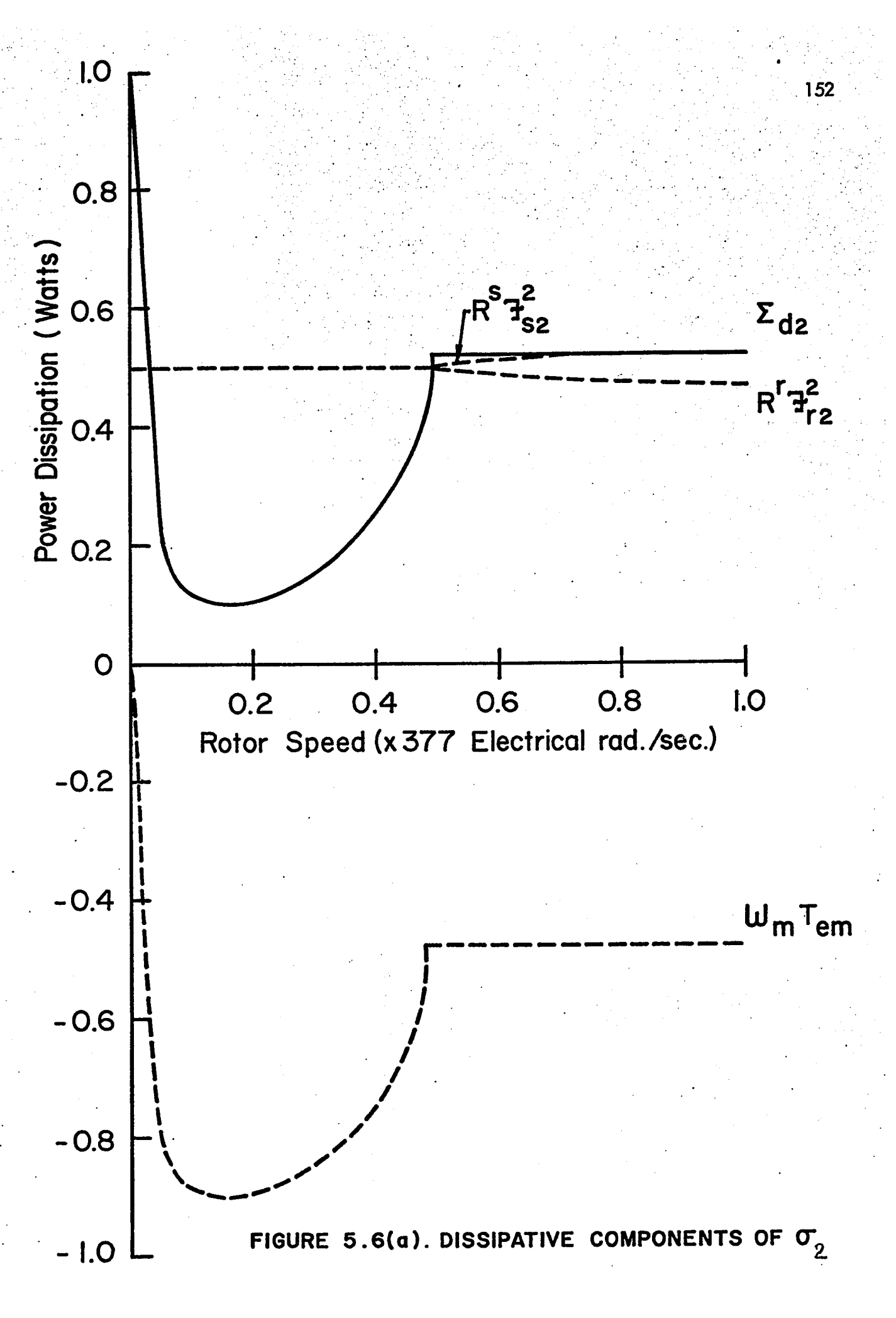


FIGURE 5.5(b). ENERGY STORAGE COMPONENTS OF σ_{i}



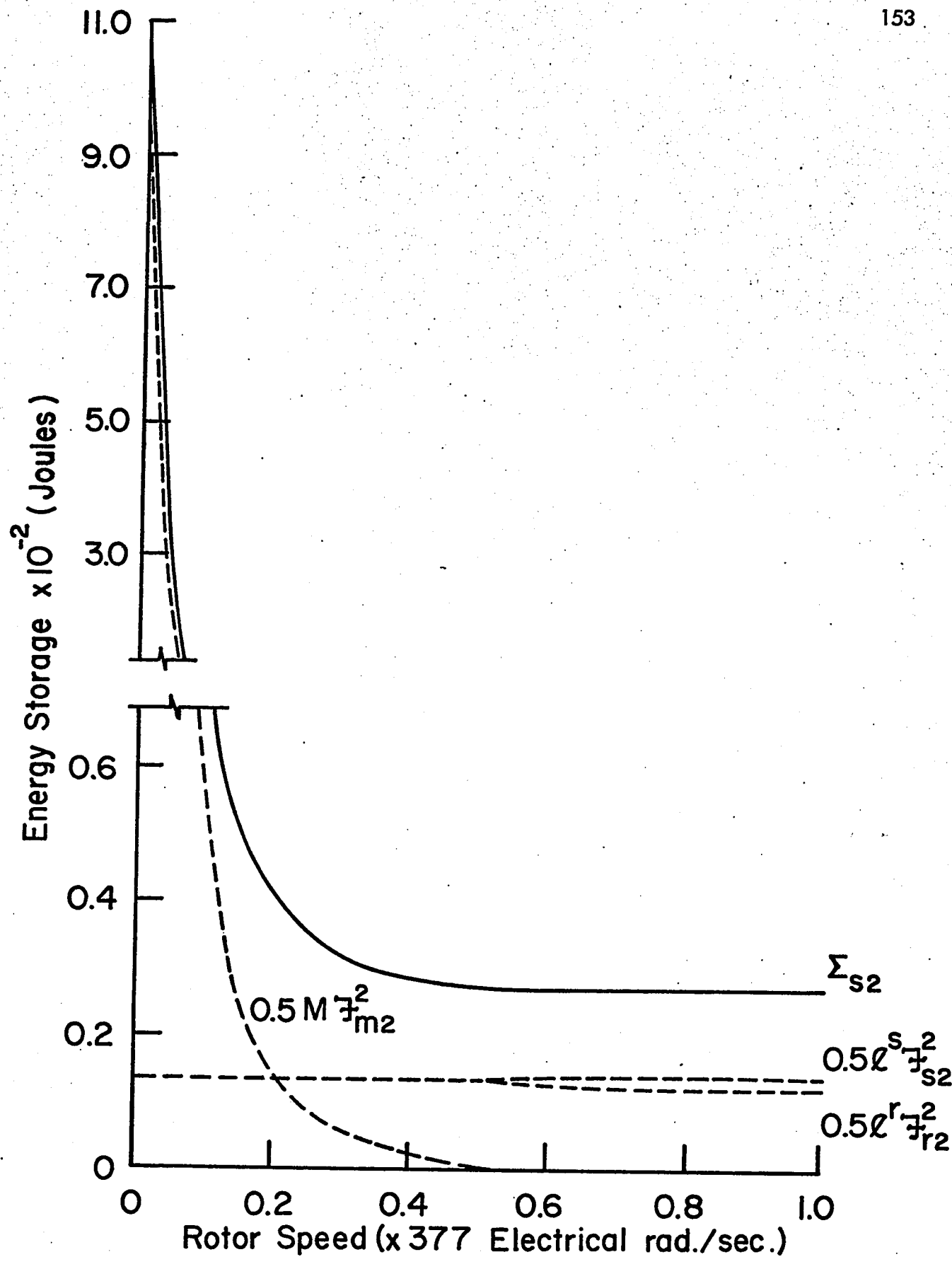


FIGURE 5.6(b). ENERGY STORAGE COMPONENTS OF σ_2

ductance. As the speed increases, the magnetization vector $\frac{3}{m2}$ collapses and the energy stored in the mutual inductance decreases to negligible values for $\omega_{m} > 0.49 \, \text{p.u.}$ Thereafter the energy of the leakage inductances predominates. Figure 5-6(a) shows that the sum of the resistive components is substantially constant, and for $0 \le \omega_{m} < 0.49$, the negative dissipation becomes important. In all, the collapse of $\frac{3}{m2}$ overwhelms the influence of negative dissipation and the net result is the increase in damping with speed from $\omega_{m} = 0$ to $\omega_{m} = 0.49$ as is shown in Figure 5-1.

The components of Equation 5-46 are evaluated from the eigenvector components U_1 , U_2 , U_3 and U_4 which solved by the eigenvector subroutine of DAL4. Since the eigenvector is not unique it has been necessary to "normalize" it so that the continuous curves of Figure 5-4 and Figure 5-5 can be plotted.

5-11 Structure of Natural Frequency of Oscillation in Mode

associated with it is continuously being exchanged among the various storage elements. The frequency of oscillation is related to the rate of this exchange. The magnetization sub-primitive is simplified enough to offer a view of the physical details of the interaction of the speed voltages and the magnetization flux. In the induction motor, the details of the energy exchanges are more complicated, but as the modal representation in Section 5-9 shows, this is the energy of the magnetic fields associated with the rotating space vectors $\frac{3}{5}$ and $\frac{3}{7}$ k.

At any time instant in the free motion of the kth mode, the velocity of the stator and the rotor current space vectors must each be equal to the natural frequency, i.e.

$$\omega_{k} = p \mathscr{Q}_{sk} = p \mathscr{Q}_{rk}$$
 5-47

Using the definitions in Equations 2-19 and 2-20

$$\omega_{k} = p \, \mathcal{O}_{sk} = \frac{i_{q}^{s} \, p \, i_{d}^{s} - i_{d}^{s} \, p \, i_{q}^{s}}{\left(i_{d}^{s}\right)^{2} + \left(i_{q}^{s}\right)^{2}}$$
5-48

$$\omega_{k} = p \, \mathscr{O}_{rk} = \frac{i_{q}^{r} \, p \, i_{d}^{r} - i_{d}^{r} \, p \, i_{q}^{r}}{(i_{d}^{r})^{2} + (i_{q}^{r})^{2}}$$
 5-49

Combining Equations 5-48 and 5-49 into Equation 5-47

$$\omega_{k} = \frac{i_{q}^{s} p i_{d}^{s} - i_{d}^{s} p i_{q}^{s} + i_{q}^{r} p i_{d}^{r} - i_{d}^{r} p i_{q}^{r}}{(i_{d}^{s})^{2} + (i_{q}^{s})^{2} + (i_{d}^{r})^{2} + (i_{q}^{r})^{2}}$$
5-50

Equation 5-50 is valid only when i_{-dq} is of the form of Equation 5-39, i.e. it is an instantaneous value in the free motion of the mode. The time differential quantities pi_d^s , pi_q^r etc. can be obtained from

$$p_{idq} = [A_{dq}]_{idq} = 5-51$$

Substituting Equation 4-2 and Equation 5-39 into Equation 5-50 and making the

normalization of the eigenvector components $(U_1^2 + U_2^2 + U_3^2 + U_4^2) = 1$

$$\omega_{k} = \frac{1}{L^{s} L^{r} - M^{2}} \left[(R^{s} - R^{r}) M (U_{1} U_{4} - U_{2} U_{3}) + n \omega_{m} \left\{ L^{s} L^{r} (U_{3}^{2} + U_{4}^{2}) - M^{2} (U_{1}^{2} + U_{2}^{2}) + M (L^{s} - L^{r}) (U_{1} U_{3} + U_{2} U_{4}) \right\} \right]$$

5-52

or expressed in the space vector forms

$$\omega_{k} = \frac{1}{L^{s} L^{r} - M^{2}} [(R^{s} - R^{r}) M \mathcal{F}_{sk} \mathcal{F}_{rk} \sin (\mathcal{G}_{sk} - \mathcal{G}_{rk})]$$

$$+ n \omega_{m} \left\{ L^{s} L^{r} \mathcal{F}_{rk}^{2} - M^{2} \mathcal{F}_{sk}^{2} + \frac{M}{2} (L_{s} - L_{r}) (\mathcal{F}_{mk}^{2} - \mathcal{F}_{sk}^{2} - \mathcal{F}_{rk}^{2}) \right\}$$
5-53

or

$$\omega_{k} = \frac{1}{L^{s} L^{r} - M^{2}} \left[(R^{s} - R^{r}) M \mathcal{F}_{sk} \mathcal{F}_{rk} \sin (\emptyset_{sk} - \emptyset_{rk}) + n \omega_{m} \left\{ \mathcal{F}_{rk}^{2} (M^{2} + \frac{1}{2} M . \overline{I^{s} + 3 I^{r}} + I^{s} I^{r} - \mathcal{F}_{sk}^{2} (M^{2} + \frac{1}{2} M . \overline{I^{s} - I^{r}}) + \mathcal{F}_{sk}^{2} (M^{2} + \frac{1}{2} M . \overline{I^{s} - I^{r}}) \right\}$$

$$+ \mathcal{F}_{mk}^{2} (\frac{1}{2} M (I^{s} - I^{r}))$$

$$= 5-54$$

These expressions show that the natural frequency arises from the interaction of the rotor speed ω_m and the electromechanical torque.

For the numerical example presented throughout this thesis, $R^s = R^r = R$ and $L^s = L^r = L$, and Equation 5–53 simplifies to

$$\omega_{k} = \frac{\omega_{m}}{L^{2} - M^{2}} \left(L^{2} \mathfrak{F}_{rk}^{2} - M^{2} \mathfrak{F}_{sk}^{2} \right)$$
 5-55

or

$$\omega_{\mathbf{k}} = \omega_{\mathbf{m}} \left(P_{\mathbf{r}\mathbf{k}} - P_{\mathbf{s}\mathbf{k}} \right)$$
 5-56

where

$$P_{rk} = \frac{L^2 \, \mathfrak{F}_{rk}^2}{L^2 - M^2}$$
 5-57

$$P_{sk} = \frac{M^2 \frac{3}{sk}^2}{1^2 - M^2}$$
 5-58

In this specialised case, ω_k is solely dependent on ω_m . Thus at rotor standstill, both the eigenvalues have zero imaginary parts since $\omega_m=0$.

At very high rotor velocities, the modes approach those of the lossless sub-primitive. Using the eigenvector components of Equation 5-30, the natural frequencies as calculated from Equation 5-55 correlate with the asymptotic values approached in Figure 5-2. Thus Table 5-1 lists the "normalised" $\frac{2}{s_k}$ and $\frac{2}{r_k}$ as calculated from the Equation 5-30 and ω_k as evaluated from Equation 5-37.

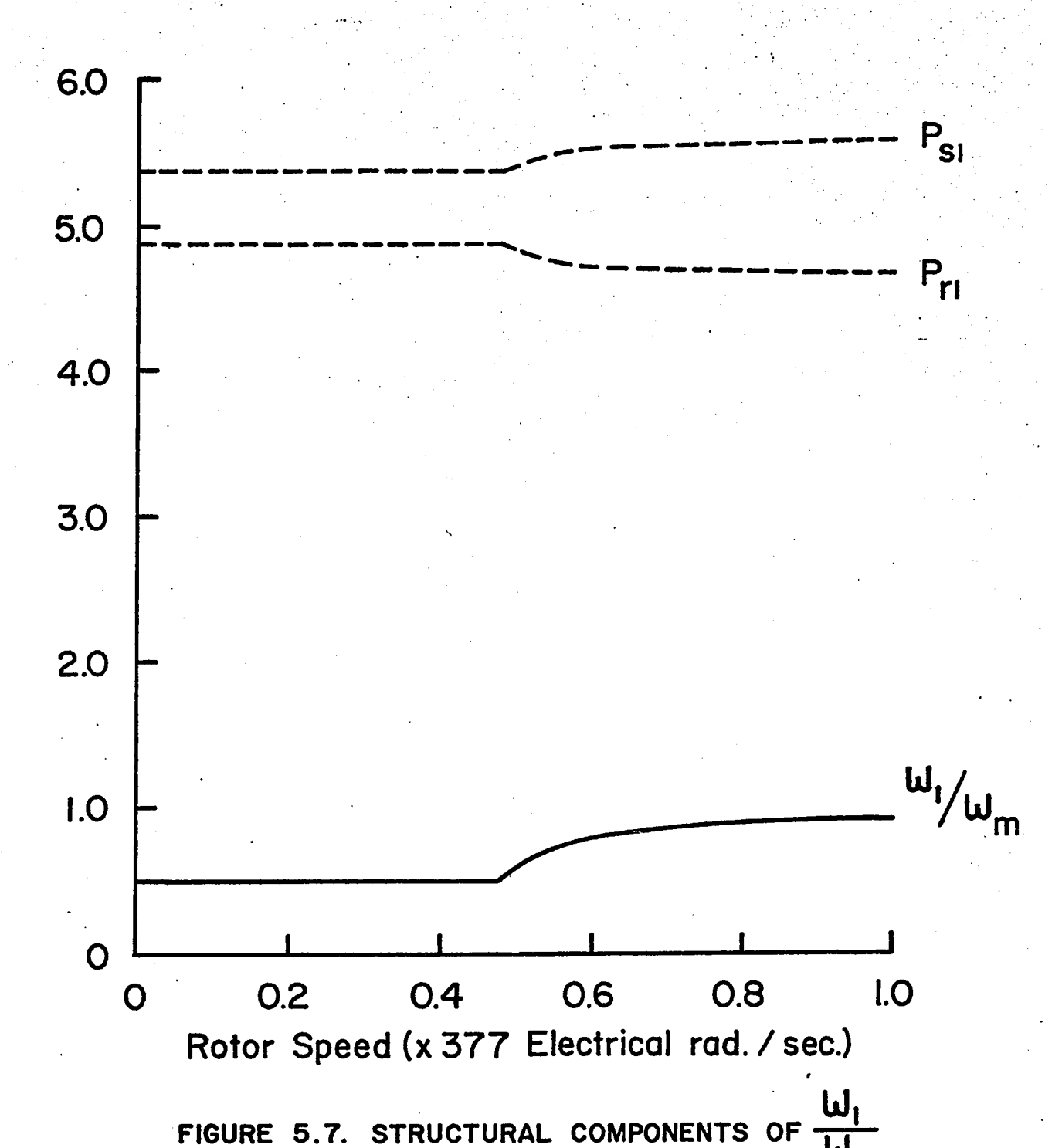
TABLE 5 - 1

		
	Stator Mode	Rotor Mode
g 2 sk	$\frac{L^2}{L^2 + M^2}$	$\frac{M^2}{L^2 + M^2}$
₹2 rk	$\frac{M^2}{L^2 + M^2}$	$\frac{L^2}{L^2 + M^2}$
$\omega_{\mathbf{k}} = (\text{Eq. } 535)$	0	ω _m
•		

The derivation of Equation 5-50 is based on physical arguments on the properties of the space vector. In Appendix D, the same results will be derived from the definitions of the eigenvector. This provides a useful check against faulty intuition.

5-11-1 Natural Frequency Variation with Speed

Figure 5-7 and Figure 5-8 show plots of the components of Equation 5-56 which correlate with the natural frequency variations with speed in Figure 5-2. $P_{rk} \text{ and } P_{sk} \text{ defined in Equation 5-57 and Equation 5-58 are normalised quantities}$ (with respect to ω_m) and they bear information as to the relative contributions of $\frac{37}{rk}$



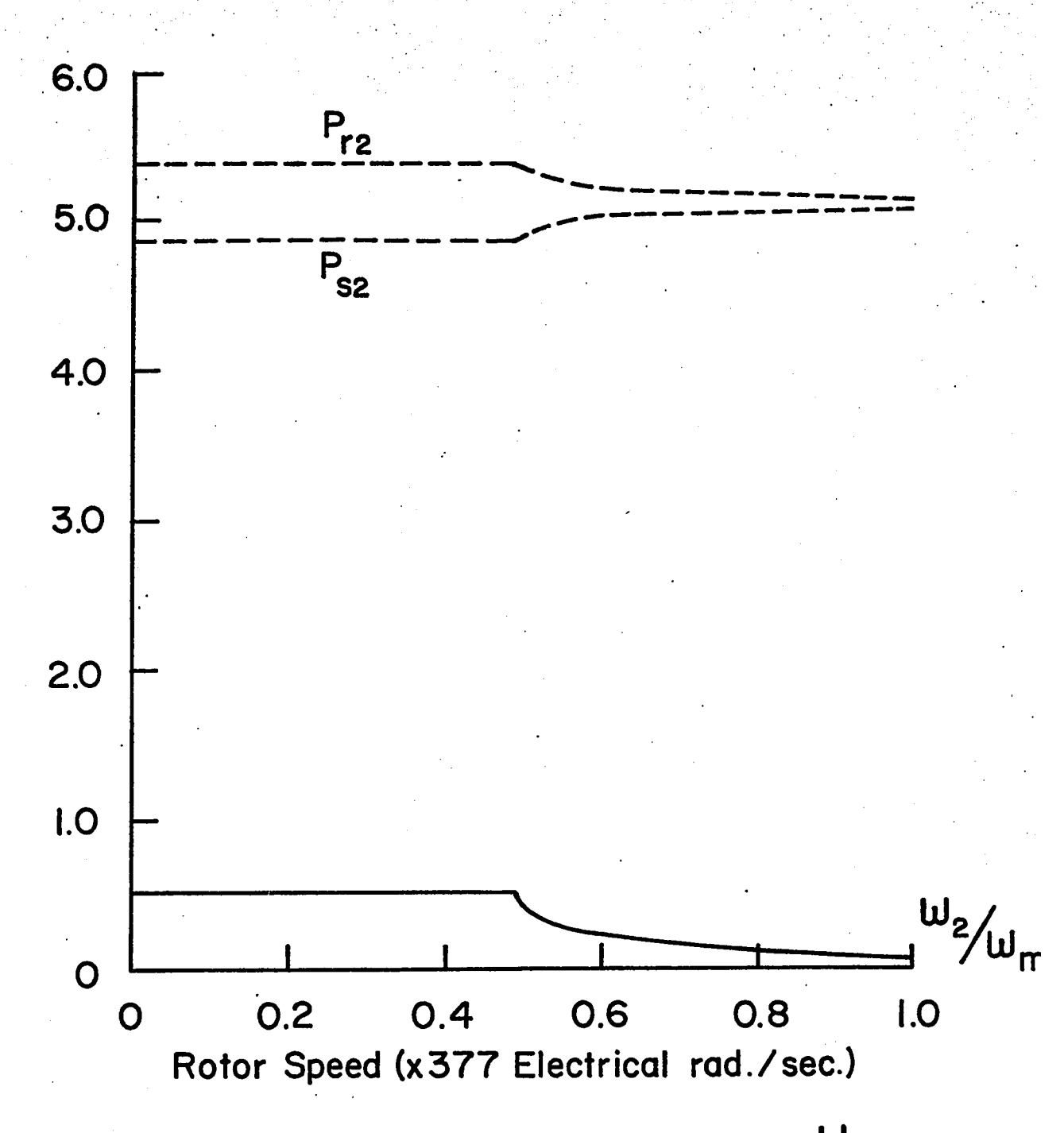


FIGURE 5.8. STRUCTURAL COMPONENTS OF $\frac{\omega_2}{\omega_m}$

and ${\mathfrak F}_{sk}$. The normalised frequency $\frac{\omega_k}{\omega_m}$ is of course the difference between

P_{rk} and P_{sk}.

CHAPTER VI

INDUCTION MOTOR STABILITY

6-1 Introduction

The basic problem in stability analysis of the induction motor is to establish whether the steady-state solution to Equation 2-1 is a stable equilibrium point, i.e. will the motor return to its steady state after the occurrence of a small system disturbance? Furthermore, if it is a stable equilibrium point, how large a disturbance will it tolerate?

The first question can be answered by eigenvalue analysis of the small perturbation linearised equations about an equilibrium operating point. But this method has the short-coming that the stability is guaranteed only for an infinitesimally small region where the small perturbation assumptions hold.

In order to answer the more difficult question of stability with large perturbations, it is necessary to use the Second or the Direct Method of Liapunov to grapple with the system nonlinearity. This method consists of generating a "Liapunov function" and using the Liapunov function to map the region of asymptotic stability around the stable equilibrium point. Unfortunately, à priori, the Liapunov function is not known and much ingenuity has to be exercised in guessing the Liapunov function which can describe the stability boundary exactly. Furthermore the Liapunov function gives only a sufficient condition for stability. This means that if the conditions for the stability are not satisfied, it does not necessarily follow that the

point is unstable, but simply that perhaps a better Liapunov function can be proposed.

The objectives of this chapter are therefore to apply these methods to the stability of the induction motor. Firstly the eigenvalue subroutines are applied to the linearised equations of the induction motor to determine the stability of the operating point. Subsequently the Direct Method is used to explore the stability boundary around a stable equilibrium point. Because of the dimensions (5th order) of the system, the Liapunov functions investigated are restricted to the quadratic functions.

6-2 Induction Motor Equation for Stability Study

Throughout this stability study, the synchronously rotating frame is chosen because the steady-state currents for a balanced voltage supply Equation 2-15 are d.c. currents and consequently the system equations are autonomous. Equation 2-13 can be rewritten as

$$\underline{\mathbf{e}}_{X\delta} = [L] \mathbf{p}_{iX\delta} + [R]_{iX\delta} + [G \omega_{m}]_{iX\delta}$$
 6-1(a)

and

$$J_1 p \omega_m + f_1 \omega_m + T_L = n M (i_{\chi}^s i_{\delta}^r - i_{\delta}^s i_{\chi}^r)$$
 6-1 (b)

where

$$\begin{bmatrix} L \end{bmatrix} = \begin{bmatrix} L^{s} & 0 & M & 0 \\ 0 & L^{s} & 0 & M \\ M & 0 & L^{r} & 0 \\ 0 & M & 0 & L^{r} \end{bmatrix} = \begin{bmatrix} R^{s} & 0 & 0 & 0 \\ 0 & R^{s} & 0 & 0 \\ 0 & 0 & R^{r} & 0 \\ 0 & 0 & 0 & R^{r} \end{bmatrix}$$

6-2

and
$$[G \omega_{m}] = \begin{bmatrix} 0 & L^{s} \omega_{f} & 0 & M \omega_{f} \\ -L^{s} \omega_{f} & 0 & -M \omega_{f} & 0 \\ 0 & M (\omega_{f} - n \omega_{m}) & 0 & L^{r} (\omega_{f} - n \omega_{m}) \\ -M(\omega_{f} - n \omega_{m}) & 0 & -L^{r} (\omega_{f} - n \omega_{m}) & 0 \end{bmatrix}$$

Before the methods of Liapunov can be applied, it is necessary to remove the forcing functions \underline{e}_{δ} and T_{L} from Equation 6-1. This can be done by solving for the steady-state solutions of the operating point and translating the system equations to a new origin at the operating point.

For a specified supply voltage $\underline{E}_{\delta\delta}$ and a load T_L , the operating point is obtained by solving for the d. c. currents $\underline{I}_{\delta\delta}$ and the constant speed $\overline{\omega}_m$ from the steady-state versions of Equation 6-1, i.e.

$$\underline{E}_{\delta\delta} = [R] \underline{I}_{\delta\delta} + [G\overline{\omega}_{m}] \underline{I}_{\delta\delta}$$
 6-3(a)

$$f_1 \overline{\omega}_m = n M (I_{\delta}^s I_{\delta}^r - I_{\delta}^s I_{\delta}^r) - T_L$$
 6-3(b)

Defining a new set of variables x

Equation 6-1 can be expressed as

$$p \underline{x} = [A] \underline{x} + \underline{f}_n$$
 6-5

where [A] is a 5×5 constant matrix and \underline{f}_n is a 5×1 column consisting of sums of quadratic products of x's. The importance of Equation 6-5 is that the system dynamics are now expressed in terms of the free motion of the state and the Liapunov Methods are directly applicable to such a formulation.

The constant [A] matrix is most informative if it is examined in its 4 - partitioned parts.

$$[A] = \begin{bmatrix} H_{11} & H_{12} \\ H_{21} & H_{22} \end{bmatrix}$$
6-6

The 4×4 [H₁₁] matrix is none other than the constant speed equation in Equation 4-5.

6-7

The 1 \times 1 [H $_{22}$] matrix relates the viscous friction f $_1$ and the moment of inertia J $_1$

$$[H_{22}] = \begin{bmatrix} -\frac{f_1}{J_1} \end{bmatrix}$$
 6-8

$$[H_{12}] = \frac{n}{L^{s}L^{r}-M^{2}} \begin{bmatrix} -M(MI_{\delta}^{s}+L^{r}I_{\delta}^{r}) \\ M(MI_{\delta}^{s}+L^{r}I_{\delta}^{r}) \\ -L^{s}(MI_{\delta}^{s}+L^{r}I_{\delta}^{r}) \\ L^{s}(MI_{\delta}^{s}+L^{r}I_{\delta}^{r}) \end{bmatrix}$$

$$= \frac{n}{L^{s}L^{r}-M^{2}} \begin{bmatrix} -M(MI_{\delta}^{s}+L^{r}I_{\delta}^{r}) \\ M(MI_{\delta}^{s}+L^{r}I_{\delta}^{r}) \end{bmatrix}$$

and
$$[H_{21}] = \frac{n M}{J_1} [I_{\delta}^r - I_{\delta}^r - I_{\delta}^s + I_{\delta}^s]$$

$$6-10$$

The nonlinear part of Equation 6-5 is a 5×1 column

$$\frac{f}{-n} = \begin{bmatrix} \frac{f}{-k} \\ \frac{f}{-l} \end{bmatrix}$$
 6-11

where
$$\frac{f}{k} = \frac{n \times_5}{L^s L^r - M^2}$$

$$- M (M \times_2 + L^r \times_4)$$

$$- M (M \times_1 + L^r \times_3)$$

$$- L^s (M \times_2 + L^r \times_4)$$

$$L^s (M \times_1 + L^r \times_3)$$

and
$$\underline{f}_1 = \frac{n M}{J_1} (x_1 x_4 - x_2 x_3)$$
 6-13

6-3 <u>Small Signal Linear Approximation</u>

The nonlinear dynamic equation in Equation 6-5 is written as the sum of a linear principal part $[A] \times and$ the nonlinear part f_n . Since the nonlinearities consist of quadratic sums of the state variables, it is possible to approximate it for small signals by reductions to Equation 6-14 which is equivalent to it from point of view of stability.

$$p \times = [A] \times 6-14$$

6-4 Stability of the Operating Point

The linear criterion of stability [40] is: "the equilibrium of Equation 6-14 is asymptotically stable if all the eigenvalues of [A] have negative real parts".

The Nyquist [55 - 57], the root-locus [24] and many standard techniques of linear theory are available to ascertain the system stability based on this criterion.

The method used in this investigation is to evaluate the eigenvalues of the matrix [A] by the DAL4 eigenvalue subroutine discussed in Section 4-6. The eigenvalue method gives a more detailed picture of the dynamics of the operating

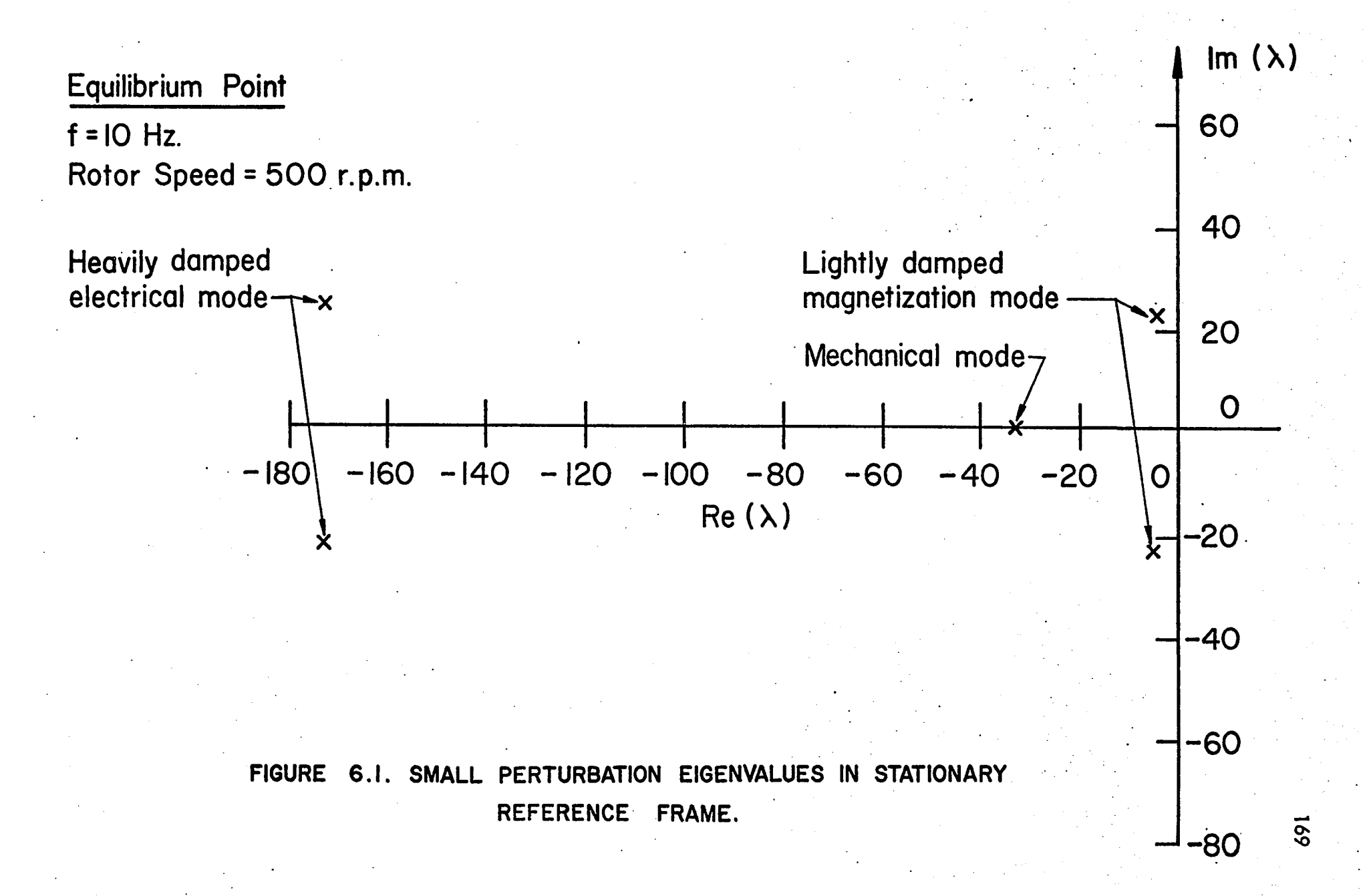
point than the Nyquist and the root-locus methods. Thus, the real parts of the eigenvalues bears information not only with respect to the system stability but also to the order of damping of the system. This has much importance in induction motor stability investigation where often-times the operating point is in fact stable but lightly damped [24].

6-5 Stability of Operating Points Over Speed Range

As an example, the stability of the operating points of an induction motor controlled by variable frequency is investigated. The motor parameters are listed in Appendix G with the additional information that $J_1=0.006~{\rm kg-m}^2$ f₁ = 0.01 Nw-m-sec. /rad. The supply voltages referenced to the synchronously rotating frame are: $E_{\chi}^{s}=\frac{240\times f}{60}$, $E_{\delta}^{s}=0$. Since a variable frequency supply voltage is used, the slip and $\omega_{\rm f}$ in the [A] matrix must always be referred to the supply.

The procedures for the solution are as follows:

- (a) For a specified frequency f, operating speed $\overline{\omega}_m$, and voltage \underline{E}_{δ} , the steady-state currents \underline{I}_{δ} are solved from the simultaneous linear equations in Equation 6-3(a).
- **(b)** Using $\overline{\omega}_{m}$ and \underline{l} δ , the dynamic matrix [A] is formed.
- (c) The DAL4 eigenvalue subroutine is used to find the eigenvalues of [A].



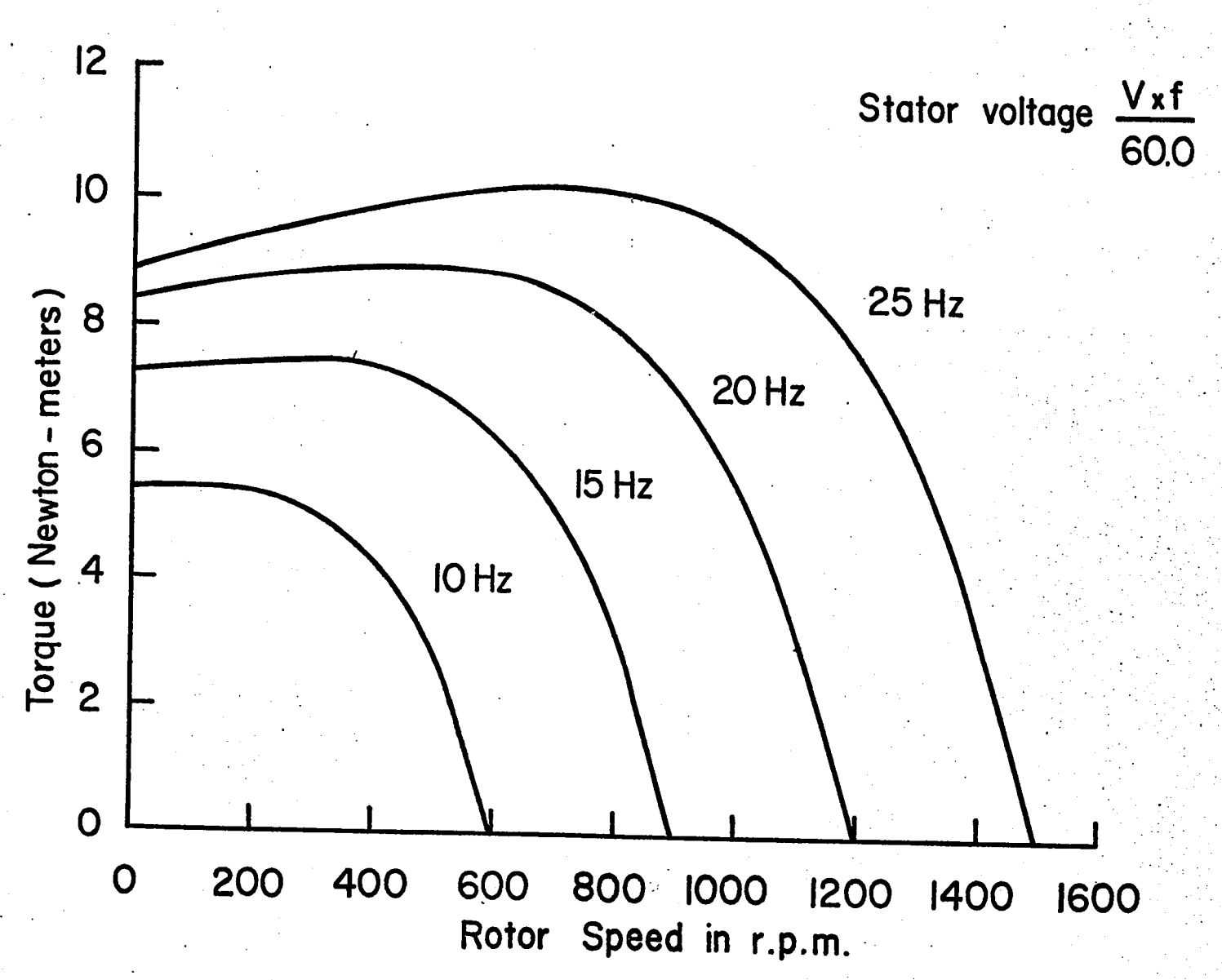


FIGURE 6.2. INDUCTION MOTOR TORQUE SPEED CHARACTERISTICS OF DIFFERENT SUPPLY FREQUENCIES

Corresponding to the 5×5 [A] matrix there are 5 eigenvalues. Of these there are two complex conjugate pairs and a fifth real eigenvalue. Since the [A] matrix yields the eigenvalues in the synchronous reference it is necessary to reduce them to a stationary reference frame (see Section 4-9) which besides being physical serves as a common basis for comparing eigenvalues for different frequency operating points.

Figure 6-1 shows the 5 eigenvalues in the stationary reference frame for an operating point defined by f=10 Hz and $\omega_m=500$ r.p.m. Since all the eigenvalues are on the left-half of the complex plane, the operating point is stable.

Figure 6-2 shows the torque-speed curves for the speed ranges for supply frequencies from 5 Hz to 25 Hz. An operating point in the torque-speed curve is defined by the frequency and the rotor speed. The dynamic properties of these operating points are displayed in Figures 6-3, 6-4 and 6-5. Figures 6-3(a), 6-4(a) and 6-5(a) show the real parts of the eigenvalues; and Figures 6-3(b) and 6-4(b) show the imaginary parts expressed in Hertz in the stationary reference frame.

Figures 6-3 and 6-4 are the plots for the two complex eigenvalue pairs which will be identified with the electrical modes of Chapters IV and V. In this particular motor, the real parts are always negatively damped. However as Nelson, Lipo and Krause have shown [25] instability arising from negatively damped electrical modes can occur in some machine parameter combinations, especially with very small rotor inertia J_1 .

The only instability occurs for the fifth real eigenvalue which can be identified with the mechanical equation of motion. Comparing the damping factor



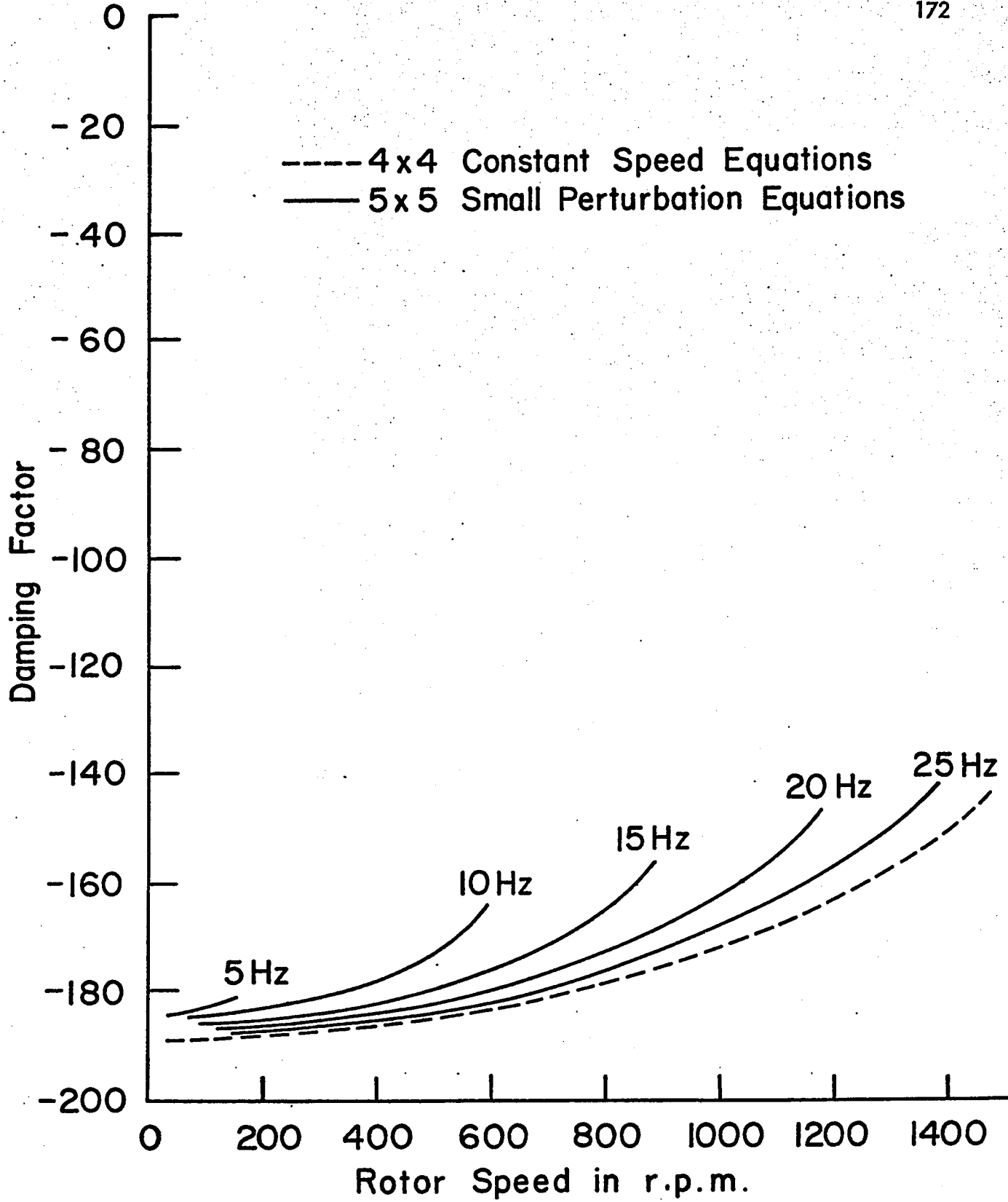


FIGURE 6.3(a). DAMPING FACTOR OF HEAVILY DAMPED ELECTRICAL MODE AS FUNCTION OF OPERATING POINT.

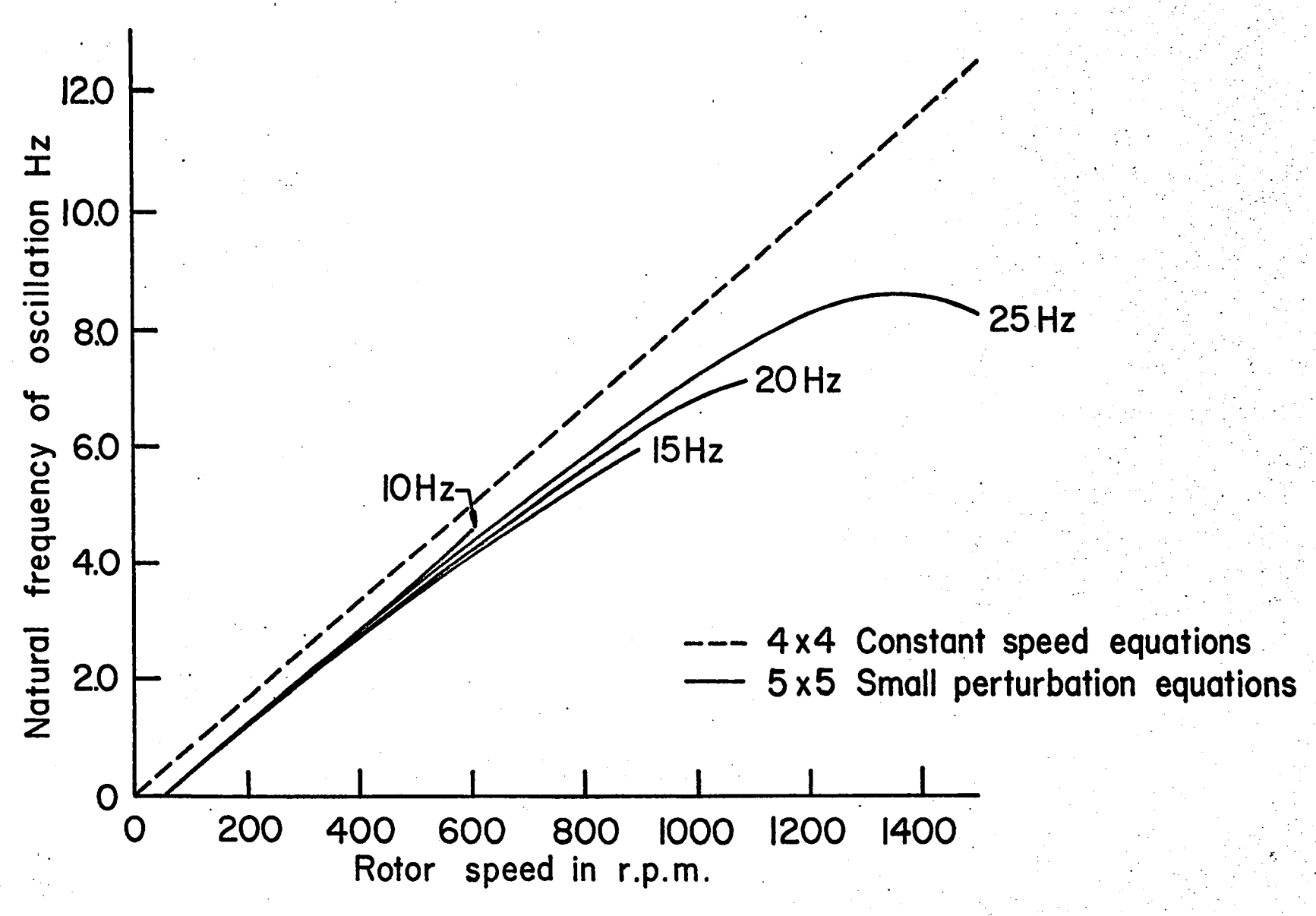


FIGURE 6.3 (b). NATURAL FREQUENCY OF HEAVILY DAMPED ELECTRICAL MODE AS FUNCTION OF OPERATING POINT.

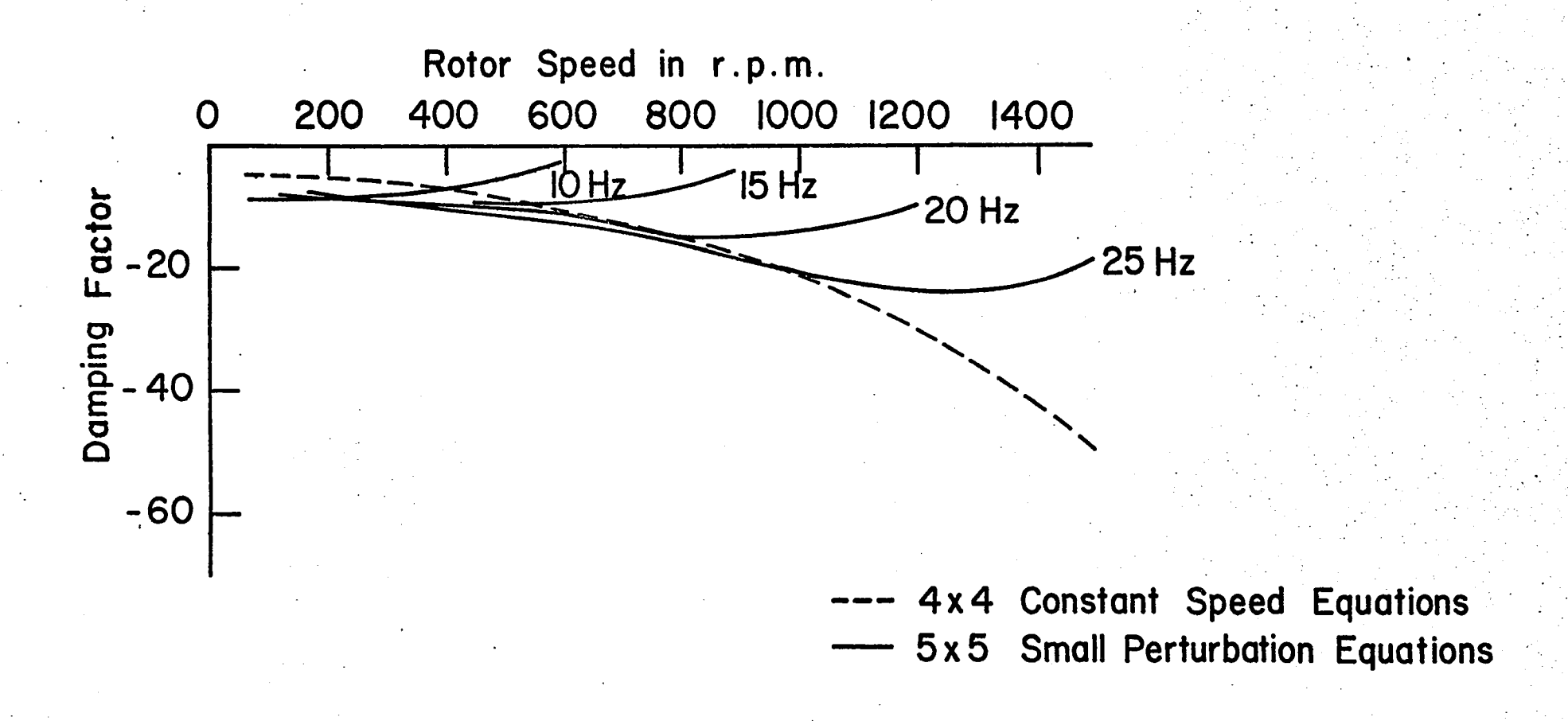


FIGURE 6.4 (a). DAMPING FACTOR OF LIGHTLY DAMPED MAGNETIZATION MODE AS FUNCTION OF OPERATING POINT.

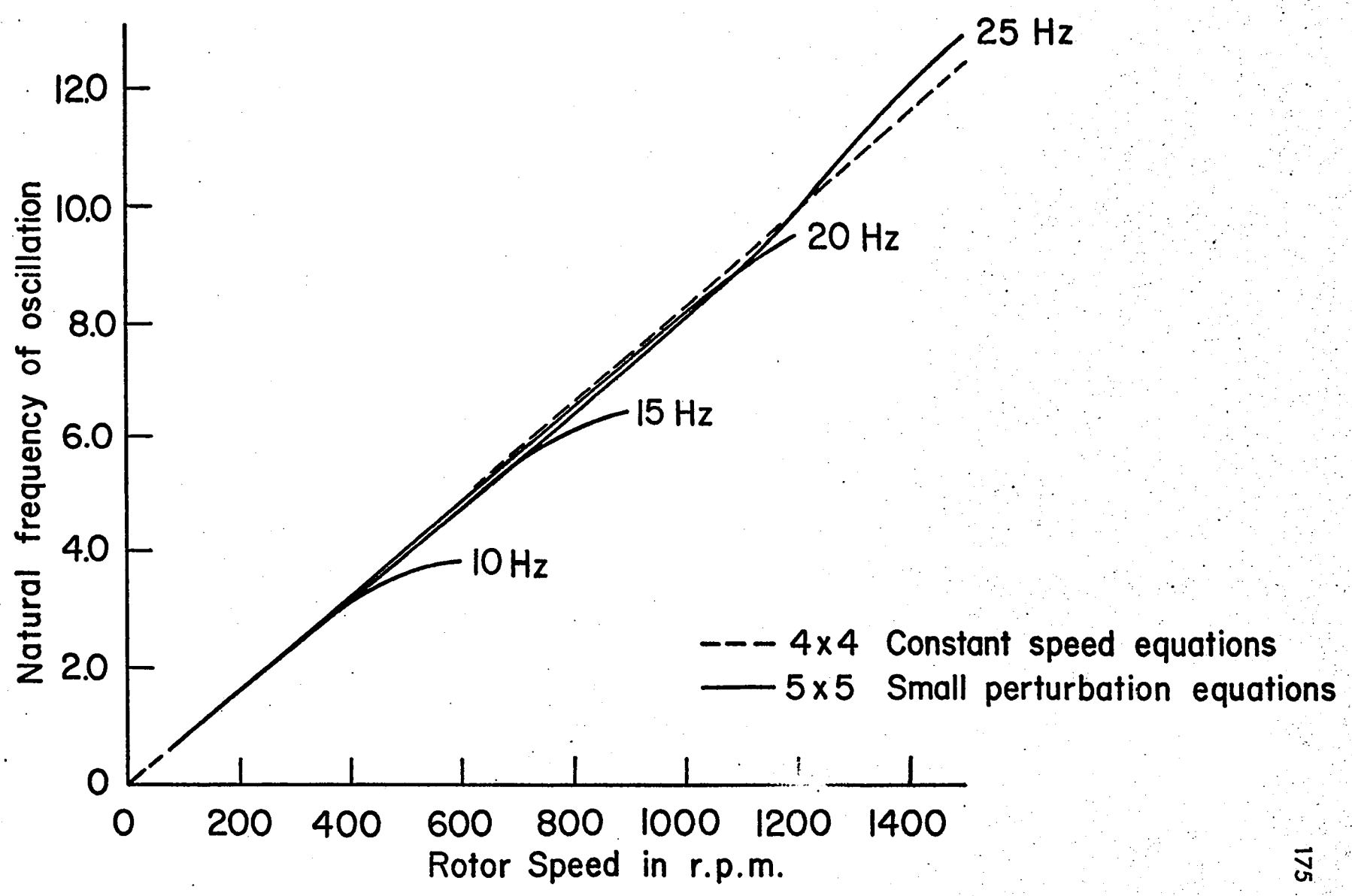


FIGURE 6.4 (b) NATURAL FREQUENCY OF LIGHTLY DAMPED MAGNETIZATION MODE AS FUNCTION OF OPERATING POINT.

of Figure 6-5 with the torque-speed curves of Figure 6-2, it can be concluded that the negative damping and instability occurs on the operating region to the left of the peak of the torque-speed curves. Instability of this kind which is associated with a positive accelerating torque speed ratio $(\frac{\Delta T}{\Delta \omega})$ is well known in traditional induction motor theory and is predictable from the static torque-speed curve.

6–6 Eigenvalues Identification

6-6-1 The Mechanical Mode

The fifth eigenvalue is related to the mechanical equation of motion.

Firstly, it can be stated that when the system is electromechanically uncoupled, the linearised mechanical equation becomes

$$J_1 p \times_5 + f_1 \times_5 = 0$$
 6-15 and the damping factor is $\sigma_5 = -\frac{f_1}{J_1}$

In the general case, besides this damping due to viscous friction, there is electromechanical damping which is approximately related to slope of the torque speed curve. The fifth row of Equation 6-14 which is

$$J_1 p x_5 + f_1 x_5 = n M (l_8^r x_1 - l_8^r x_2 - l_8^s x_3 + l_8^s x_4)$$
 6-16

can be approximated by

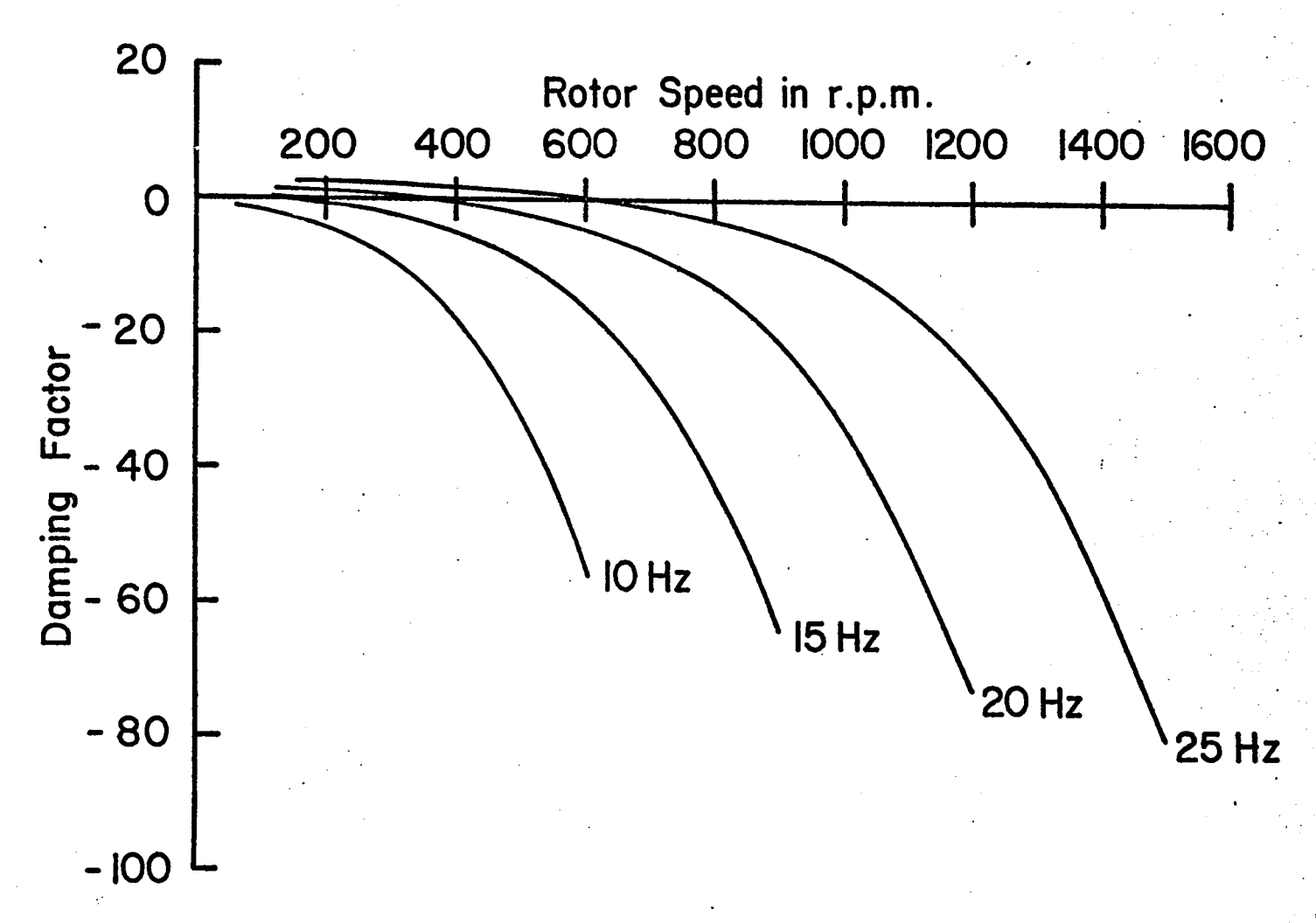


FIGURE 6.5. DAMPING FACTOR OF MECHANICAL MODE AS FUNCTION OF OPERATING POINT.

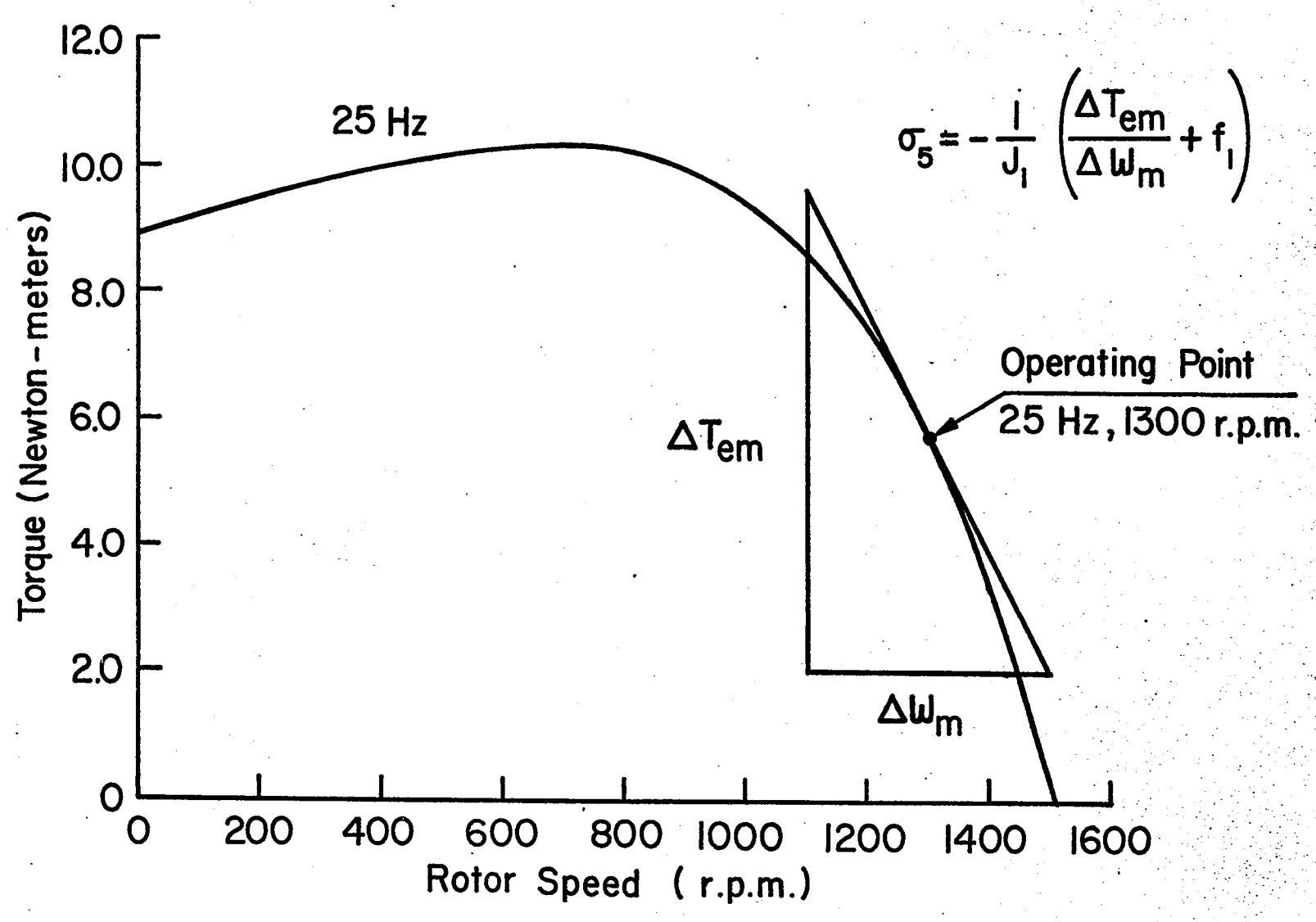


FIGURE 6.6. ESTIMATE OF MECHANICAL DAMPING FACTOR FROM TANGENT OF TORQUE SPEED CURVE

$$J_1 p \times_5 + f_1 \times_5 \approx \frac{\Delta T}{\Delta \omega_m} \times_5$$
 6-17

where the acceleration torque-speed ratio $\frac{\Delta T}{\Delta \omega}$ is defined in Figure 6-6 and the mechanical damping factor is approximately

$$\sigma_5 \approx \frac{1}{J_1} \left(\frac{\Delta T}{\Delta \omega_m} - f_1 \right)$$
 6-18

As a numerical check of Equation 6-18, the operating point defined by $\omega_{\rm m}=1350~{\rm r.p.m.}$, f = 25 Hz in Figure 6-2 has a slope :

$$\frac{\Delta T}{\Delta \omega} = -0.243$$
 newton metre sec. / rad.

Since $J_1 = 0.006$, $f_1 = 0.01$, Equation 6-18 gives

$$\sigma_5 = -42.2$$

The eigenvalue routine DAL4 has a solution $\sigma_5 = -47.7$.

Another good check comes from relating the peaks of the torque speed curve of Figure 6-2 with the speed at which $\sigma_5=-\frac{f_1}{J_1}$ in Figure 6-6.

6-6-2 The Electrical Modes

In Figures 6-3 and 6-4, the speed variations of σ_1 , σ_2 , ω_1 and ω_2 of the short-circuited motor of Chapters IV and V are plotted in dashed lines

beside the damping factors and oscillating frequencies of the excited induction motor operating points. From these plots and from arguments based on continuity the complex eigenvalues of the 5×5 [A] – matrix can be identified with the modes of the 4×4 matrix of Equation 4-5.

The connection is apparent if it is noted that the sub-matrix $[H_{11}] = [A_{\delta}]$ and when the motor is unexcited and with the stator windings short-circuited, Equation 6-6 is reduced to

The eigenvalues of this matrix are those of [A $_{\zeta\delta}$] and $\lambda_5=-\frac{f_1}{J_1}$.

However, as the stator windings are excited and as the excitation currents $\frac{1}{180}$ increase, the column sub-matrix $[H_{12}]$ and $[H_{21}]$ grow, the eigenvalues of Equation 6-19 become numerically perturbed. The eigenvalues of Equation 6-6 can thus be thought of, as being continuously shifted by the continuous growth of the elements in the off-diagonal sub-matrices. From Equations 6-9 and 6-10, the extent of this numerical perturbation would depend on the operating-point currents $\frac{1}{180}$ and the moment of inertia $\frac{1}{180}$.

In this context, Figures 6-3 and 6-4 can be viewed as a perturbation of the short-circuited modes by the steady-state currents $\frac{1}{8}$. The successive shifts



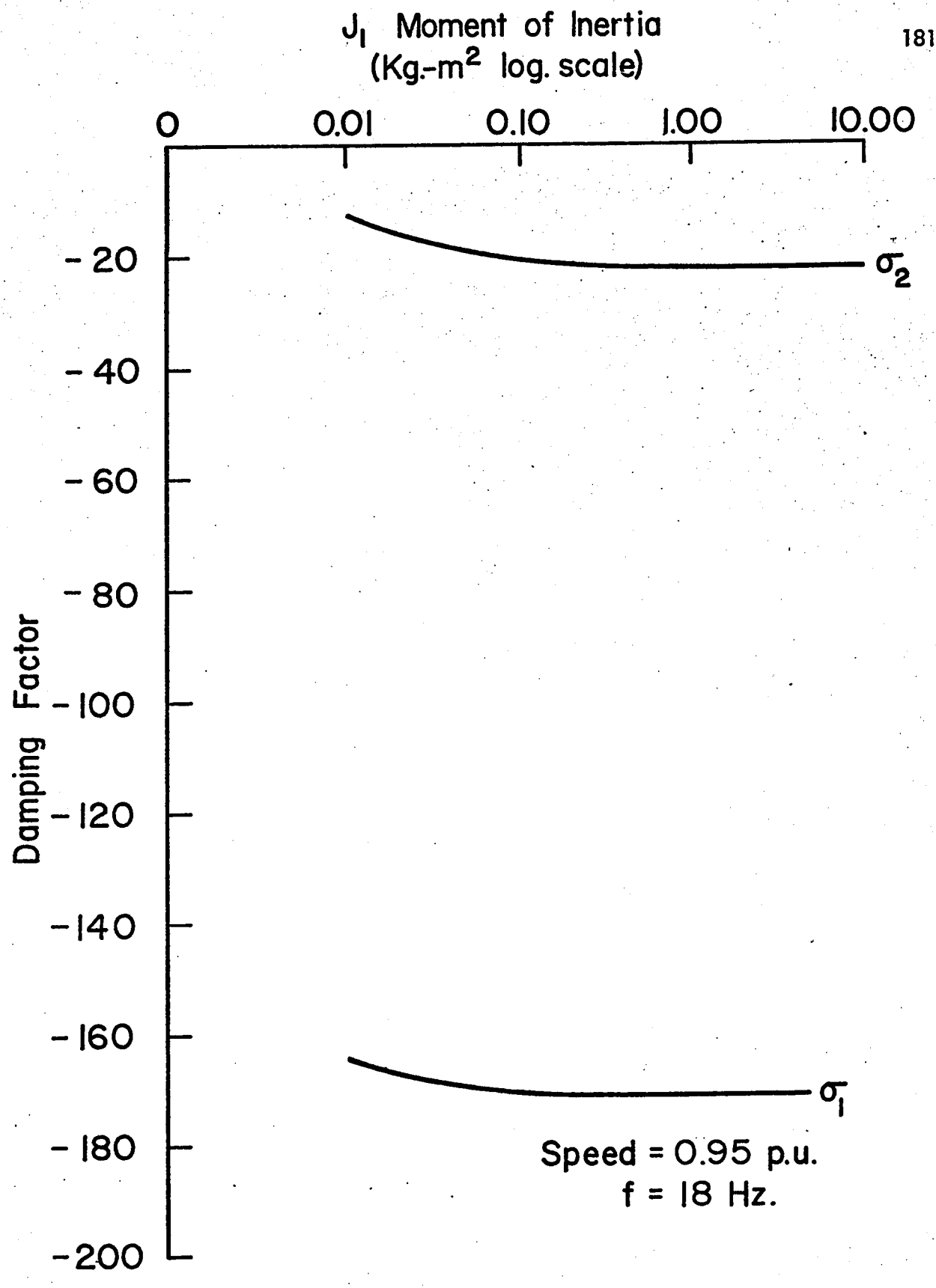


FIGURE 6-7 (a) DEPENDENCE OF THE DAMPING FACTORS OF THE ELECTRICAL MODES ON THE MOMENT OF INERTIA

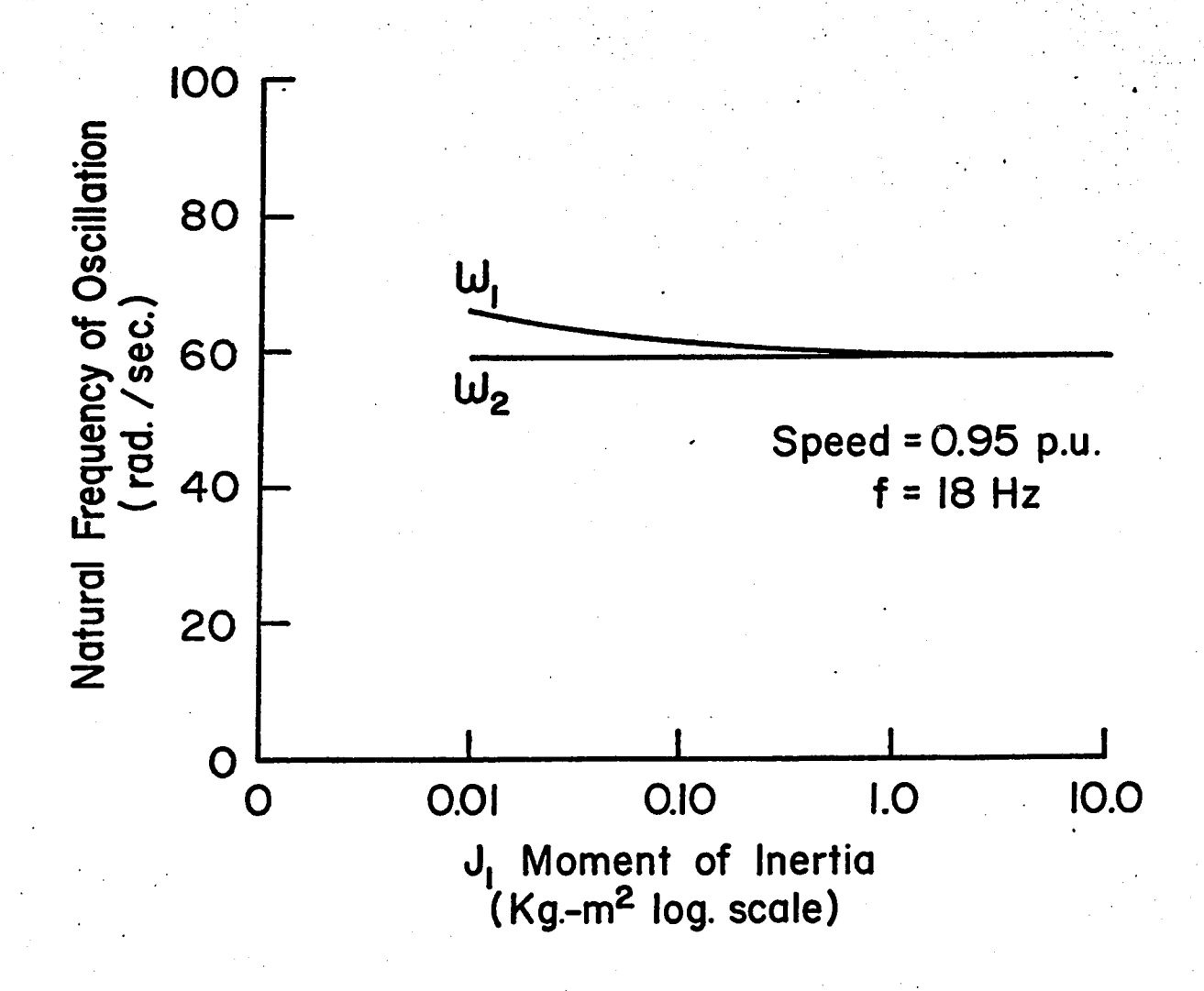


FIGURE 6.7 (b). DEPENDENCE OF THE NATURAL FREQUENCIES
OF OSCILLATION OF THE ELECTRICAL MODES ON THE MOMENT OF INERTIA

from the dashed-line by supply frequency changes is minimum for the oscillating frequencies in Figures 6-3(b) and 6-4(b). The mode associated with the mutual inductance whose damping factor is shown in Figure 6-4(a) becomes less lightly damped when excited by a 10 Hz supply. This fact is significant in this stability investigation.

For a given motor, the moment of inertia is the other factor which contributes to the electrical eigenvalue shifts. Figures 6-7(a) and (b) show the real parts of the two electrical modes as a function of J_1 , which is presented in a logarithmic scale. This result shows that the mechanical parameters are only very lightly coupled to the electrical damping factors.

6-7 The Direct Method of Liapunov

The linear stability criterion of Section 6-4 is valid only for small signal disturbances. In practice it is necessary to be assured that the region of asymptotic stability around the equilibrium is extensive so that the motor will return to the operating point after a sizeable system disturbance. In such considerations, the nonlinear terms for an no longer be negligible and the stability investigation must deal with Equation 6-5 in toto. The Direct Method of Liapunov is well suited to handle stability problems of nonlinear systems.

The Direct Method is very well treated in many standard control engineering textbooks [59 - 60] and it is only necessary here to restate the method and the pro-

perties of the Liapunov function. Basic to this method is the construction of the Liapunov function $V(\underline{x})$ which a priori is not known. This Liapunov function is then used with respect to the system equations to map out the region of asymptotic stability.

The Liapunov function $V(\underline{x})$ must be a positive definite scalar function with the following properties:

(a) V and its first partial derivatives are together continuousin a certain domain D which contains the origin.

(b)
$$\vee (\underline{x}) = 0$$
 for $\underline{x} = \underline{0}$

and

$$V(x) > 0 \qquad \text{for} \quad \underline{x} \neq 0 \qquad \qquad 6-21$$

For V (x) to be a Liapunov function of the induction motor, then its time derivative along the trajectory of the system Equation 6-5 is negative definite, i.e.

$$W(\underline{x}) = p V(\underline{x})$$

$$= \sum_{j=1}^{5} \frac{\partial V}{\partial x_{j}} p x_{j} < 0$$
6-22

in the domain D.

A systematic method of constructing a Liapunov function for Equation 6-5 is possible by the method of Zubov [62, 64 - 65] provided that the [A] matrix has negative real parts for all the eigenvalues. Since the nonlinearity part

f in Equation 6-5 consists simply of quadratic product terms, a Liapunov function made up of an infinite series of homogeneous terms can be proposed

$$V(\underline{x}) = V_2 + V_3 + \dots V_m + \dots$$
 6-23

and the coefficients of the series terms solved from a recursive relationship. This infinite series would describe exactly the boundary of the region of asymptotic stability. In practice the infinite series is approximated by a truncated series to the mth order of the homogeneous term. Unfortunately, as Undril [66] has pointed out, the size of the set of simultaneous equations which must be solved to obtain the truncated series increases rapidly with the order of the series and the dimension of the system equations. For the 5 - variable system of the induction motor, Table 6-1 shows the number of simultaneous equations which must be solved, in order to generate a Liapunov function truncated at the mth order [66].

TABLE 6 - 1.

Order of Homo- geneous Series m =	2	3	4	5	6	8	10	12	14
Number of Simul- taneous Equations	15	35	70	126	210	495	1001	1820	3060

Thus dimensionality is an inherent difficulty in applying Zubov's method to the induction motor. Furthermore as Margolis and Vogt [64] have pointed out there is no knowledge as to what order m would yield the optimum approximation to the stability boundary. They have shown examples where a higher order approximation can describe a more conservative stability region than a lower order approximation.

In the face of these difficulties, the investigation using the Direct Method will be restricted to Liapunov Functions of the quadratic form.

6-8 Total Energy as a Liapunov Function

Since the Liapunov function is a generalization of the energy concept, and the Direct Method is an extension of the intuitive notion that a stable equilibrium is associated with decreasing energy of the system, it is natural to consider a Liapunov function which consists of the sum of the storage energy associated with the perturbed variables, i.e.

where
$$\begin{bmatrix} B \end{bmatrix} = \frac{1}{2} \begin{bmatrix} L^{S} & 0 & M & 0 & 0 \\ 0 & L^{S} & 0 & M & 0 \\ M & 0 & L^{\Gamma} & 0 & 0 \\ 0 & M & 0 & L^{\Gamma} & 0 \\ 0 & 0 & 0 & 0 & J_{1} \end{bmatrix}$$
 6-24

and
$$[B] = [B]^T$$
 6-26

Equation 6-24 satisfies the partial derivative continuity requirements and also Equations 6-20 and 6-21.

Susbstituting Equations 6-5 and 6-25 into Equation 6-22

$$W(\underline{x}) = pV(\underline{x})$$

$$= \underline{x}^{T} [A]^{T} [B] \underline{x} + x^{T} [B] [A] \underline{x} + \underline{f}_{n}^{T} [B] \underline{x} + \underline{x}^{T} \underline{B} \underline{f}_{n}$$

$$6-27$$

A very important result is that the last two terms containing the nonlinear part f_n vanish when they are expanded algebraically, i.e.

$$\underline{\mathbf{f}}_{\mathbf{n}}^{\mathsf{T}} [\mathbf{B}] \underline{\mathbf{x}} + \underline{\mathbf{x}}^{\mathsf{T}} [\mathbf{B}] \underline{\mathbf{f}}_{\mathbf{n}} = \mathbf{0}$$
 6-28

Hence

$$W(\underline{x}) = \underline{x}^{T} [C] \underline{x}$$
 6-29

where
$$[C] = [A]^T [B] + [B] [A]$$

$$= \frac{1}{2} \begin{bmatrix} -2R^{S} & 0 & 0 & -nM\omega_{m} & nMI_{S}^{r} \\ 0 & -2R^{S} & nM\omega_{m} & 0 & -nMI_{S}^{r} \\ 0 & nM\omega_{m} & -2R^{r} & 0 & nL^{r}I_{S}^{r} \\ -nM\omega_{m} & 0 & 0 & -2R^{r} & -nL^{r}I_{S}^{r} \\ nMI_{S}^{r} & -nMI_{S}^{r} & nL^{r}I_{S}^{r} & -nL^{r}I_{S}^{r} & -2f_{1} \end{bmatrix}$$

When [C] is a negative definite matrix then Equation 6-22 is satisfied and the V(x) is indeed a Liapunov function. Furthermore the domain D extends to all space and the operating point is asymptotically stable in the large (ASIL). The proof for this very strong condition of stability is possible because the energy Liapunov function causes the contribution of the nonlinear term $\frac{f}{n}$ to be zero as Equation 6-28 shows.

A computer test for the negative definiteness of [C] is to show that the successive principal minors of – [C] to have positive determinants [67]. A more instructive test consists of completing the squares for Equation 6-29. Thus $W(\underline{x})$ is negative definite if for any six real numbers b_1 , b_2 ... b_6 the following inequalities are satisfied.

$$b_{1}^{2} + b_{3}^{2} - 2 R^{s} < 0$$

$$b_{2}^{2} + b_{4}^{2} - 2 R^{s} < 0$$

$$\left(\frac{n M \omega_{m}}{b_{2}}\right)^{2} + b_{5}^{2} - 2 R^{r} < 0$$

$$\left(\frac{n M \omega_{m}}{b_{1}}\right)^{2} + b_{6}^{2} - 2 R^{r} < 0$$

$$\left(\frac{n M \omega_{m}}{b_{1}}\right)^{2} + b_{6}^{2} - 2 R^{r} < 0$$

$$\left(\frac{n M \omega_{m}}{b_{3}}\right)^{2} + \left(\frac{n M \omega_{m}^{r}}{b_{4}}\right)^{2} + \left(\frac{n L^{r} \omega_{b}^{r}}{b_{5}}\right)^{2} + \left(\frac{n L^{r} \omega_{b}^{r}}{b_{6}}\right)^{2} - 2 f_{1} < 0$$

6-9 Asymptotic Stability in the Large in Induction Motors

Firstly, it can be said that any asymptotically stable operating point is in general not ASIL for the induction motor. For example, Figure 6-8 shows a load curve which intersects the torque-speed curve at points M and N. The point M is an asymptotically stable equilibrium point; but from steady-state arguments, the region of asymptotic stability around it is not global. This is because the system on being displaced to an operating point to the left of N would continue to decelerate to $\omega_{\rm m} = -\infty$, never to return to M.

As such it is not surprising that [C] in Equation 6-30 is negative definite only under very restricted conditions. In particular using the algebraic inequalities of Equation 6-31 it can be concluded that for the system to be ASIL the dissipative elements R^s , R^r and f_1 in the diagonal of [C] matrix must dominate the off-diagonal terms. This, of course, corresponds to the physical notion that it is always possible to make a system very stable provided sufficient dissipation is added. It should also be noted that ASIL is more likely to occur at low operating speeds since the terms in M_{cont} in Equations 6-30 and 6-31 would be small and would be dominated by the dissipative terms.

Thus in the numerical example of Section 6-5, the induction motor operating at 540 r.p.m. from a 10 Hz supply would be ASIL if the stator and the rotor resistances are increased to $R^{S} = R^{\Gamma} = 4.18$. This is because from Equation 6-30

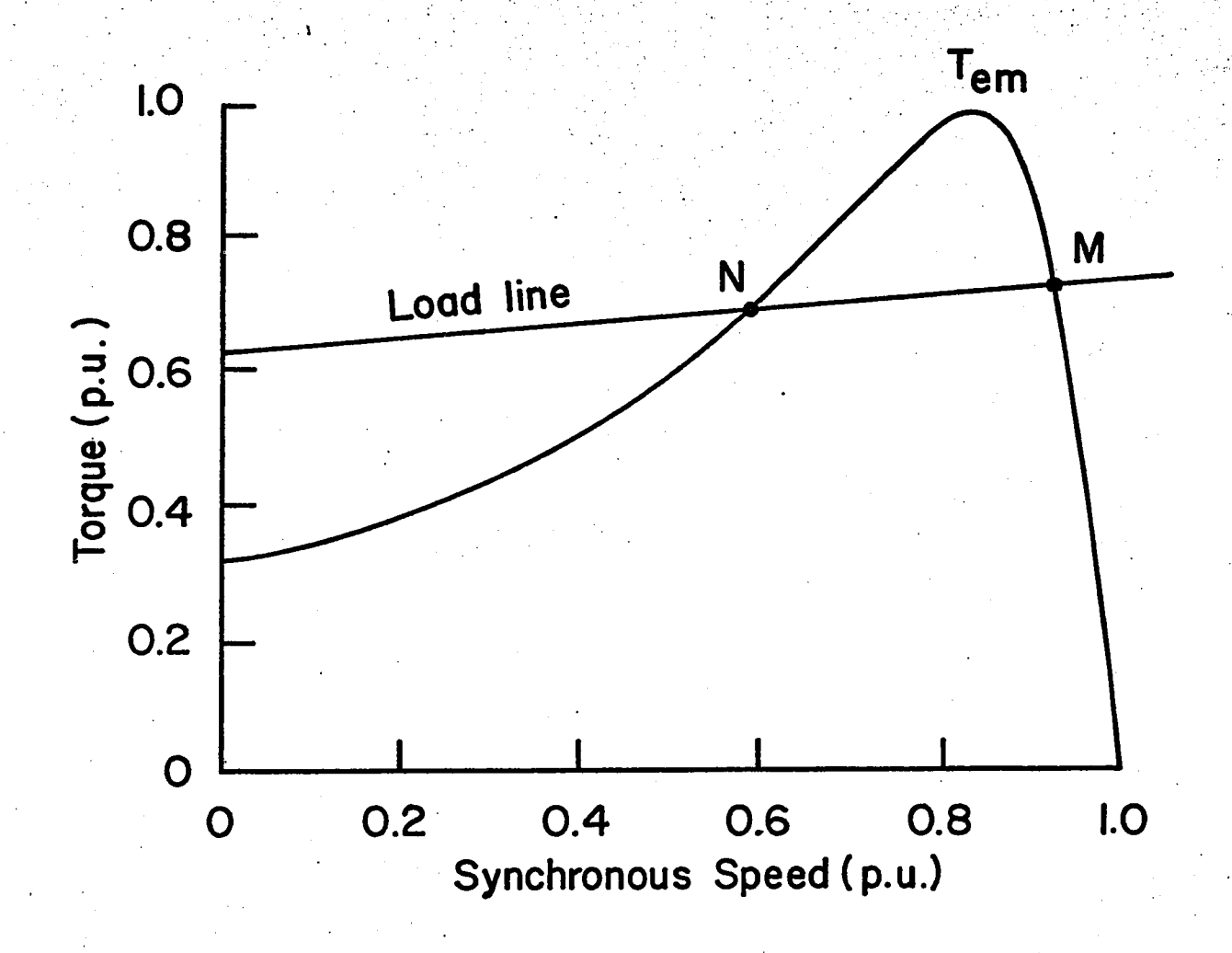


FIGURE 6.8. OPERATING POINTS M, N DEFINED BY INTERSECTION OF MOTOR TORQUE SPEED CURVE & LOAD LINE

[c] = -	4.18	0	0	3.0	-0.018
	0	4.18	-3.0	0	-0.034
	0	-3.0	4.18	0	-0.019
	3.0	0	0	4.18	-0.036
	-0.018	-0.034	-0.019	-0.036	0.01
j.					_1

6-32

is negative definite.

The increase of the rotor resistance has the effect of shifting the peak of the torque speed curve of Figure 6-8 to the region of negative speed and consequently the motor curve will not intersect the load curve again at N, thus offering the possibility of ASIL.

Although the motor can be proved to be ASIL by increasing the dissipative elements, the steady state performance characteristics deteriorates.

Since the Total Energy Liapunov Function can only prove ASIL, it cannot be used with those operating points where a bound to the asymptotic stability region is suspected to exist. In such cases a different quadratic Liapunov Function can be constructed mathematically.

6-10 Stability Bounds from Quadratic Liapunov Functions

When the equilibrium of Equation 6-5 is asymptotically stable, a quadratic Liapunov function [63] can always be constructed for the linear part, i.e.

Equation 6-14. The proposed quadratic Liapunov function is of the form

$$V(\underline{x}) = \underline{x}^{\mathsf{T}} [V] \underline{x}$$
 6-33

where [V] is an unknown matrix and $[V]^T = [V]$.

The total derivative, using Equation 6-22 and Equation 6-14 is

$$W(\underline{x}) = \underline{x}^{T} [P] \underline{x}$$
 6-34

where
$$-[P] = [A]^{T} [V] + [V] [A]$$
 6-35

[P] is a positive definite matrix, if $V(\underline{x})$ is to be a Liapunov function of Equation 6-14. Equation 6-35 represents a system of n(n+1)/2 linear equations from which the unknown elements of [V] can be solved from any arbitrary positive definite matrix [P].

In investigating the stability bounds of the equilibrium point, the total time derivative of Equation 6-22 is formed from the constructed Liapunov function Equation 6-33 and the complete nonlinear system equation, Equation 6-5. When $W(\underline{x})$ is negative throughout the whole space, ASIL can be concluded. Whenever $W(\underline{x}) = 0$, for $\underline{x} \neq 0$ the conclusion of ASIL cannot be made. But according to Hahn [61], "so long as one of the hypersurfaces $V(\underline{x}) = \text{constant lies completely in the interior of the domain determined by } W(\underline{x}) = 0$, then it belongs to the domain of attraction of the origin".

The quadratic Liapunov functions appear to have applicability to the case of the induction motor. It is proposed to apply the principles to the induction motor discussed

in Section 6-5. The operating point chosen is defined by the frequency = 60 Hz and operating speed $\overline{\omega}_{\rm m} = 3240 \, \rm r.p.m$. The objective is to investigate whether the hypersurface $V(\underline{x}) = V_{\rm o}$ of the quadratic Liapunov function is adequate in estimating the stability region around the operating point. The method is implemented along the following steps:

Step 1. Formation of the Positive Define [P] - matrix

The simplest form of a positive definite matrix is a diagonal matrix in which all the diagonal elements are real and positive, e.g.

Appendix E shows how other positive definite matrices can be formed by rotational transformations.

Step 2. Formation of Liapunov [V] - matrix

The [A] - matrix for the induction motor operating at 60 Hz, 3240 r.p.m. and viscous friction $f_1 = 0.0$ is:

6-37

Appendix F shows the details of how [V] can be solved from Equation 6-35. The solution of the 15 simultaneous equations for the 15 unknowns in [V] yields

6-38

Step 3. Asymptotic Stability Domain Estimate

With the [V] matrix determined in Equation 6-38, the Liapunov function of Equation 6-33 is used in conjunction with the original nonlinear equation, Equation 6-5 to form the total time derivative of Equation 6-22 which becomes:

$$W(\underline{x}) = -\underline{x}^{T} [P] \underline{x} + 2\underline{x}^{T} [V] \underline{f}_{n}$$
 6-39

Since $\frac{f}{n}$ consists of quadratic terms, the last term in Equation 6-39 is a cubic scalar. As such for an infinitesimally small region around the origin, $W(\underline{x})$ is negative and because the negative definite term $-\underline{x}^T[P]\underline{x}$ dominates the higher order terms. This is the Direct Method justification for the stability analysis based on linearization through small signal assumptions in Section 6-5.

But for large signal perturbations, $W(\underline{x})$ can become positive whenever $2 \times^T [V] \underline{f}_n$ is positive and dominates over the negative quadratic term in Equation 6-39. Thus, for example, in the case of the motor operating at M in Figure 6-6 it is found that for a number of Liapunov functions constructed in the manner specified above, the point N lies on $W(\underline{x}) = 0$ and all points to the left of N have positive values of $W(\underline{x})$.

However, the domain of asymptotic stability is guaranteed only for the closed region inside the surface $V(\underline{x}) = V_0$ which contacts the surface $W(\underline{x}) = 0$ from the inside. To find V_0 , the problem becomes one of minimization and can be stated as:

Find the minimum of $V(\underline{x}) = \underline{x}^T[V] \underline{x}$ which lies on $W(\underline{x}) = 0$.

6-10-1 <u>Minimization of Liapunov Function</u>

The minimization of $V(\underline{x}) = \underline{x}^T [V] \underline{x}$ under a constraint $W(\underline{x}) = 0$ can be reduced to the problem of minimization of a new unconstrained function

$$Z(\underline{x}) = V(\underline{x}) + \mu W(\underline{x})^2$$
 6-40

where μ is a constant which ultimately must tend to infinity.

The optimization of multivariable functions such as Equation 6-40 are discussed fully in Reference [68]. In this study, the IBM FMFP subroutine [49] has been used to find the local minimum of Equation 6-40 by the method of Fletcher and Powell [69]. The technique of using the minimization subroutine consists of (a) making an initial guess of the local minimum, (b) estimating a trial value of μ and (c) using the FMFP subroutine to locate the local minimum. When the approximate local minimum is found, μ is increased and a better estimate is found on an iterative process for each successively increased value of μ .

It is found that for a large number of trial initial values, the FMFP converges towards the origin. This leads to a conclusion that the Liapunov Function using Equation 6-38 can only guarantee a very small region of asymptotic stability.

6–10–2 Merit of Quadratic Liapunov Function

The [V] - matrix of Equation 6-38 indicates why it contributes to form such a poor Liapunov Function for estimating the stability region. For example at $x_2 = x_4 = x_5 = 0$,

$$V(\underline{x}) = \begin{bmatrix} x_1 & x_3 \end{bmatrix} \begin{bmatrix} 2.116 & 2.114 \\ 2.114 & 2.116 \end{bmatrix} \begin{bmatrix} x_1 \\ x_3 \end{bmatrix}$$
 6-41

It is important to note that 2.116 and 2,114 differs only at the fourth significant place and the contours of Equation 6-41 are long thin ellipses which are hardly distinguishable in single precision from those of

$$V (\underline{x}) = 2.114 (x_1 + x_3)^2$$

which describe a family of straight lines.

Likewise at $x_1 = x_3 = x_5 = 0$

$$V(\underline{x}) = \begin{bmatrix} x_2 & x_4 \end{bmatrix} \begin{bmatrix} 2.117 & 2.11\overline{5} \\ 2.115 & 2.117 \end{bmatrix} \begin{bmatrix} x_1 \\ x_5 \end{bmatrix}$$
 6-43

have contours which are also long thin ellipses.

Because the Direct Method of Liapunov gives a sufficiency condition of stability only, the minuscule region of asymptotic stability of Equation 6-38 is more likely to reflect on the poorness of the method. After all the induction motor at 60 Hz operation at low slip operation is generally known to be highly stable. Although many different positive definite [P] matrices have been tried, each of which yielding the same poor results, there is an infinity move which could have been tested. As such the de-merit of the quadratic Functions can only be concluded for the specific examples studied.

CHAPTER VII

PARAMETRIC SENSITIVITY

7-1 Introduction

In addition to calculating the torque patterns and solving for the eigenvalues, the engineer is interested in the influence of machine parameters on the system performance. Thus one is concerned that the stability of an equilibrium point is not critically sensitive to slight changes in the system components. From a synthesis point of view, one is interested in knowing which parameters to change in order to design for a particular torque transient.

Because numerical techniques have been used throughout there is no explicit inter-relationship between the numerical solutions and the system parameters.

However, by developing the concepts of parametric sensitivity coefficients and evaluating them numerically, it is possible to provide this important supplementary information.

This investigation consists of defining and developing an efficient method of calculating the eigenvalue sensitivity coefficients of the induction motor. In this chapter, the motor parameters, R^{S} , R^{Γ} etc. will be denoted by the numerically indexed symbols p a_{i} (i=1,2...).

7-2 <u>Eigenvalue Sensitivity</u>

In Chapter VI, the [A] matrix is determined by a specification of $(pa_1, pa_2, \ldots, pa_i, \ldots, pa_n)$ and the operating point state solutions. Basically, the engineer is interested in the effect of changes in the Kth eigenvalue

for a small change in the jth parameter. This information is embodied in the notion of the eigenvalue sensitivity which is defined as

$$\frac{\partial \lambda_{k}}{\partial p \, a} = \lim_{\Delta p \, a \to 0} \frac{\Delta \lambda_{k}}{\Delta p \, a}$$

$$7-1$$

7–3 Calculation of Eigenvalue Sensitivity

The eigenvalue sensitivity $\frac{\partial \lambda_i}{\partial pa_i}$ can, of course, be calculated by forming a new [A] matrix for the parameters (p a_1 , p a_2 ... p a_i + Δp a_i , ... p a_n), computing the eigenvalues λ_i + $\Delta \lambda_i$ (i = 1, 2, ... 5), and using the limiting definition Equation 7-1 to approximate the sensitivity coefficients.

The re-computation of eigenvalues to obtain the sensitivity coefficients of each of the n-parameters is time consuming and the following method described by Van Ness, Boyle and Imad [70], and Faddeev and Faddeeva [71] is more economical. This method requires the evaluation of the eigenvalues and the eigenvectors of the [A] matrix and its transpose [A]^T only once. Essentially the economy is achieved by recognizing certain basic properties of the matrix [A] and $[A]^T$. For example, $[A]^T$ has identical eigenvalues as [A] but the eigenvectors \underline{U}_k of [A] are different from $\underline{\hat{U}}_k$ of $[A]^T$. From the definition of eigenvectors:

$$[A] \underline{U}_k = \lambda_k \underline{U}_k$$

$$[A]^{\mathsf{T}} \hat{\underline{\mathsf{u}}}_{\mathsf{k}} = \lambda_{\mathsf{k}} \hat{\underline{\mathsf{u}}}_{\mathsf{k}}$$
 7-3

The eigenvalue sensitivity coefficient is obtained by differentiating Equation 7-2 partially with respect to p a.

$$\frac{\partial [A]}{\partial p a_{i}} \underline{U}_{k} + [A] \frac{\partial}{\partial p} a_{i} \underline{U}_{k} = \lambda_{k} \frac{\partial \underline{U}_{k}}{\partial p a_{i}} + \frac{\partial \lambda_{k}}{\partial p a_{i}} \underline{U}_{k}$$
 7-4

Premultiply Equation 7-4 by \underline{U}_{k}^{T}

$$\hat{\underline{U}}_{k}^{T} \quad \frac{\partial [A]}{\partial p a_{i}} \quad \underline{U}_{k} + \hat{\underline{U}}_{k}^{T} \quad [A] \quad \frac{\partial \underline{U}_{k}}{\partial p a_{i}} = \lambda_{k} \quad \hat{\underline{U}}^{T} \quad \frac{\partial \underline{U}_{k}}{\partial p a_{i}} + \frac{\partial \lambda_{k}}{\partial p a_{i}} \hat{\underline{U}}_{k}^{T} \quad \underline{U}_{k}$$
7-5

but from Equation 7-2

$$\lambda_{k} \underbrace{\hat{U}_{k}^{T}}_{b} \underbrace{\frac{\partial}{\partial pa_{i}}}_{i} U_{k} = \underbrace{\hat{U}^{T}}_{b} [A] \underbrace{\frac{\partial}{\partial pa_{i}}}_{i} U_{k}$$
 7-6

Substituting Equation 7-6 for the first term of the right hand side gives, Equation 7-1

$$\frac{\partial \lambda_{k}}{\partial p \alpha_{i}} = \frac{\hat{U}_{k}^{T} \frac{\partial [A]}{\partial p \alpha_{i}} \hat{U}_{k}}{\frac{\hat{U}_{k}}{\hat{U}_{k}}}$$
7-7

From Equation 7-7 it can be seen that at every operating point it is only necessary to solve for the eigenvectors \underline{U}_k and $\hat{\underline{U}}_k$ of [A] and $[A]^T$. As the sensitivities of the different parameters are considered, it is only necessary to compute $\frac{\partial [A]}{\partial p \, a_i}$ by numerical differentiation.

It is found that it is physically more meaningful to consider eigenvalue sensitivity in terms of percentage changes of parameters. Hence in the numerical examples following, the eigenvalue sensitivity index $\Delta \lambda_{kj}$ has been used for 1% parameter changes, i.e.

$$\Delta \lambda_{kj} = \frac{\partial \lambda_k}{\partial p a_j} \times 0.01 p a_j$$
 7-8

7-4 Numerical Example

As an example, the eigenvalue sensitivity indices of the motor in Chapter VI will be developed here. The operating point is defined by $\omega_{\rm f}$ = 10 Hz and $\omega_{\rm m}$ = 540 r.p.m. for which

Table 7-1 and Table 7-2 list the eigenvalues and the corresponding eigenvector components for the [A] matrix and the transpose [A] matrix respectively which are solved by the subroutine DAL4.

TABLE 7 - 1

[A] - MATRIX

- 3.63 ± 39.4 0.144 ± 0.206	- 169 ± 37.7 - 0.485 ± j 0.157	- 0.410
0.144 ± j 0.206	- 0.485 ± i 0.157	0.400
	1 21.00.	- 0.409
0.154 + j 0.389	- 0.0378 ± j 0.455	- 0.142
- 0.067 - i 0.321	0.481 + 0.154	- 0.387
- 0.245 ± j 0.319	0.0431 + j 0.455	0.182
). <i>7</i> 01	0.257	0.793
	0.067 + 0.321 0.245 ± 0.319	0.067 + 0.321 $0.481 + 0.154$ $0.245 + 0.319$ $0.0431 + 0.455$

TABLE 7 - 11

[A]T - MATRIX

	<u>(</u> i)	(ii)	(iii)
Eigenvalue λ	- 3.63 ± j 39.4	- 169 ± i 37.7	- 0.410
Eigenvectors Û ₁	0.181 ± j 0.481	0.117 - i 0.467	- 0.165
\hat{u}_{2}	-0.418 ± j 0.251	0.515 + j 0.0582	0.664
Û ₃	0.170 ± j 0.482	-0.0259 + j 0.423	- 0.230
$\hat{\mathbf{u}}_{4}$	-0.413 ±j 0.253	0.528 - i 0.195	- 0.684
Û ₅	0.0306	0.044	0.104

Each of the matrices $\frac{\partial [A]}{\partial p a_i}$ (i = 1, 2, ... n) can be computed numerically from :

$$\frac{\partial [A]}{\partial p a_i} \approx \lim_{\Delta p a_i \to 0} \frac{\left[A (p a_i + \Delta p a_i)\right] - [A]}{\Delta p a_i}$$
7-10

The matrix $[A(pa_i + \Delta pa_i)]$ is constructed by infinitesimally incrementing the jth parameter only. Besides the explicit terms of pa_i in [A], it should be noted that the steady-state solutions $\frac{1}{2} \sqrt{8}$ have also to be solved for the parameter change. Generally, Equation 7-10 is a sparse matrix, e.g.

$$\frac{\partial [A]}{\partial R^{S}} = \begin{bmatrix} -96.6 & 0 & 0 & 0 & 5.47 \\ 0 & -96.6 & 0 & 0 & 5.84 \\ 92.0 & 0 & 0 & 0 & -5.74 \\ 0 & 92.0 & 0 & 0 & -6.14 \\ 7.05 & -6.59 & 17.3 & 3.66 & 0 \end{bmatrix}$$
7-11

or

$$\frac{\partial [A]}{\partial f_1} =
\begin{bmatrix}
0 & 0 & 0 & 0 & 0 \\
0 & 0 & 0 & 0 & 0 \\
0 & 0 & 0 & 0 & 0 \\
0 & 0 & 0 & 0 & 0
\end{bmatrix}$$
7-12

However, Equation 7-10 can be a full matrix as in the case of the inductance parameters, e.g.

$$\frac{\partial [A]}{\partial M} = 10^{3} \times \boxed{ -17.8 } -112. 17.8 -112. -10.1$$

$$112. -17.8 112. 17.8 1.27 7-13$$

$$17.8 112. -17.8 112. 10.1$$

$$-112. 17.8 -112. -17.8 -1.29$$

$$0.737 1.05 0.009 1.55 0.0$$

Table 7-III lists the eigenvalue sensitivity indices for +1% change in the motor parameters which are calculated from Equation 7-8 and Equation 7-7. It should be noted that the eigenvalues and the eigenvectors are calculated only once and these are presented in Tables 7-1 and 7-2. The information of eigenvalue sensitivity with respect to each parameter is borne by matrices such as shown in Equation 7-11 to Equation 7-13 and these are readily computed.

7-5 Significance of Eigenvalue Sensitivity Indices

Table 7-III summarizes in an economical format 40 items of quantitative information with respect to the 5 eigenvalues and the 8 system parameters. By inspection, the damping factors of all the modes are most sensitive to the mutual inductance M. This result corresponds to the physical interpretation developed in Chapter V where it is shown that the mutual inductance M plays a dominant role in the transient characteristics at low speeds.

TABLE 7 - III

EIGENVALUE SENSITIVITY INDICES Δλ_{kj}

		•	Electri	cal Modes	Mechanical Mode			
i	Para	ameters / Eigenvalues	-3.63 ± j 39.3	- 169 ± 37.7	- 41.0			
1	R ^s	(1.0 ohm)	-0.0117 - 0.131	- 1.11 ±; 0.149	0.327			
2	R ^r	(1.0 ohm)	-0.0178 ± 0.0818	- 1.01 - j 0.238	0.005			
3	ls.	(0.0053 H)	-0.0119 ± j 0.0029	0.964 ± 0.0284	- 0.0168			
4	l ^r	(0.0053 H)	-0.0113 - j 0.0045	0.966 ± i 0.0474	- 0.231			
5	М	(0.106 H)	0.510 ± 0.0275	- 38.6 - j 1.51	0.762			
6	J	(0.006 newton-m-sec	²) -0.00546 - j 0.0571	÷ 0.171 ÷ ; 0.0129	0.371			
7	f	(0.01 newton-m-sec)	-0.00237 ± i 0.0004	0.001 <i>5</i> 8 ± ; 0.00048	0.015			
8	Ezs	(40 volts)	0.0159 ±; 0.113	0.340 ± j 0.0252	- 0.712			

At 540 r.p.m. the lightly damped mode ($\lambda = -3.63 \pm j 39.3$) has been identified approximately with the mutual inductance and the positive sign before the sensitivity index +0.510 bears this out. Likewise, the heavily damped electrical mode ($\lambda = -169 \pm j 37.7$) has real positive sensitivity indices (+0.964 and +0.966) with respect to the leakage inductances I^S and I^T and this again correlates with the identification of this mode with the leakage inductances.

Examining the mechanical mode for instance, the parameters in order of importance are: M, E $_{8}$, J_{1} , R^{s} It should be noted that an increase in E $_{8}$ dampens the mode while an increase in M, J and R^{s} have the reverse effect of decreasing the damping. The sensitivity indices confirms an earlier statement that: although the electrical parameters can affect the mechanical mode significantly, the mechanical parameters J_{1} , J_{1} do not influence the electrical modes seriously.

It should be stressed that the eigenvalue sensitivity coefficients and indices so developed, are restricted to small parameter changes only. When the effects of large parameter changes are desired, it is necessary to solve for the eigenvalues for the changed parameters in the manner described in Chapter VI.

CHAPTER VIII

SUMMARY AND CONCLUSIONS

8-1 Summary

This thesis has been a theoretical study of the transient torque and the stability of the balanced, symmetrical polyphase induction motor operating from a balanced single-frequency voltage supply. The study has been organized on a subject basis beginning with a review of the different reference frame formulations of the motor equations and an assessment of the methods for solving the transient torque patterns. This has been followed by the development of the modal methods to solve the linear constant speed equations; the application of the eigenvalue method to determine local stability; the use of the Direct Method of Liapunov to explore the stability region and finally the investigation of the effects of parameters on performance through sensitivity studies.

The results of this study have been organized around the central theme of the constant speed modes: with the eigenvalues providing the rational basis of torque components classification, and the eigenvectors bearing the information as to how each of the modes is coupled to the excitations. In this context, the phenomena of controlled nonsimultaneous switching is simply an example of mode suppression. Although the accelerating transient is strictly a nonlinear problem, it has been possible to correlate the torque patterns with the dependence of modes on the rotor speed. Furthermore by mode identification, the results from stability studies have been unified with the studies on the switching transients.

Because the modes constitute the central and unifying theme in the dynamic studies, this thesis has devoted much research to clarifying their characteristics and physical nature especially in regard to their variations with rotor speed. By a combination of methods: using approximate sub-primitive models, probing the characteristic equation, and exploiting the properties of the eigenvectors, a theory of the induction modes complete with physical interpretation has been developed.

Throughout this thesis, physical explanations have been developed using space-vectors representing the airgap m.m.f's. This has proved to be pictorially satisfying as well as theoretically fruitful, especially in explaining the phenomenon of supersynchronous speed and in representing the physical modes.

8-2 Conclusions

The conclusions listed below include those results which are felt to be of particular significance and are believed to be extensions of existing knowledge in induction motor studies.

Extension of Mathematical Methods

The modal analysis has been introduced to solve the linear constant speed transient. The power and scope of this computeraided analysis enable the initial value problems to be included with the solution of the voltage excitation problems.

- The eigenvalue method has been applied to test for the induction motor stability of the equilibrium points.
- 3. The Direct Method of Liapunov has been applied to investigate the region of asymptotic stability using quadratic Liapunov Functions. It is found that whenever the total energy of the induction motor can be shown to be a Liapunov function, then the equilibrium point is asymptotically stable in the large.
- 4. Eigenvalue parameter sensitivities has been investigated. A method is introduced which calculates the eigenvalue sensitivity coefficients efficiently by exploiting the properties of the eigenvectors of the [A] matrix and its transpose.
- The usefulness of the m.m.f. space-vector representation as
 both a mathematical tool and a physical interpretation has been
 demonstrated.
- 6. The method of sub-primitive approximation has been developed to investigate the properties of the induction motor in the limiting speed condition.

Extension of Induction Motor Theory

- shown to provide the basis for the characterizing and classification of switching torque components. Although the imaginary parts (natural frequency) of the eigenvalues have been shown to change with the chosen velocity of the common reference frame (Doppler effect), nevertheless the torque components in the classification remain invariant.
- The eigenvectors have been shown to yield information as to how the modes are coupled to the voltage excitations and the initial value currents.
- 3. The application of controlled nonsimultaneous switching has been explained in terms of mode suppression by cancelling the voltage excitation with an appropriate set of initial-value currents.
- 4. The eigenvectors have been proved to bear rotating symmetry. This rotating property has permitted the representation of a physical induction motor mode and the derivation of many important results.

 The free motion of an independently excited mode has been viewed in terms of the airgap m.m.f's., rotating with the angular velocity of the natural frequency and spiralling to zero as the magnitudes are damped out.

- 5. In the investigation on the speed dependence of the electrical modes the following conclusions have been drawn.
 - (i) The sum of the damping factors of the two complex modes is a constant for all rotor speeds.
 - (ii) The sum of the natural frequencies is equal to the rotor speed expressed in electrical radians per second.
 - (iii) At rotor standstill, the induction motor modes are the same as the nonoscillatory modes of the transformer.
 These are the lightly damped magnetization mode and the heavily damped leakage inductance mode.
 - (iv) At high rotor speeds, the induction motor modes approach those of the lossless subprimitive. These are the stator mode and the rotor mode which are related to maintaining the constant flux linkage theorem at the stator and the rotor windings respectively. Consequently these modes are identifiable with the natural frequencies $\omega_1 = 0$ and $\omega_2 = \omega_m$.
 - (v) The speed dependence of the modes can be viewed as the continuous transition from the transformer modes at standstill to the lossless modes at infinite speed. The details of this transformation has been followed by the m.m.f space-vector diagram representing the modes in the sequences shown in Figure 5-5.

(vi) The changes of modes with speed are accompanied by changes in the damping factors and the natural frequencies. Thus the lightly damped magnetization mode becomes more heavily damped because of the collapse of the magnetization m.m.f. vector 3 with speed increase. Correspondingly the leakage inductance mode becomes less heavily damped because of the negative dissipation.

To study these changes in detail, a formula has been derived which expresses the damping factor in terms of how quickly the energy in the storage elements become dissipated in the lossy parameters. Because the mode currents can be related to the eigenvectors, it has been possible to analyze the composition of energy storage and power dissipation for a mode and correlate a physical understanding for the speed changes of the damping factor.

brium point of the induction motor is characterized by 5
eigenvalues. The two complex conjugate pairs have been
identified as the same electrical modes of the constant speed
equations. The fifth real eigenvalue relates to the mechanical
equation of motion and can be approximated from the static
torque-speed curve. Instability in the mechanical mode occurs
when operating on the ascending portion of the torque-speed curve.

Instability due to the electrical modes has not been found in the specific motor parameters studied although the magnetization mode becomes lightly damped at low frequency operation.

- 7. The eigenvalue sensitivity studies has given a quantitative evaluations which correlate with the physical interpretation of modes.

 For example, at low speed operation, the magnetization mode dominates and this has expressed itself as the highest sensitivity of the damping factor with respect to the mutual inductance.
- 8. The concept of instantaneous airgap power has been defined and its usefulness demonstrated. The association of airgap power with the instantaneous angular velocity of the resultant airgap m.m.f. explains the transient phenomenon of supersynchronous rotor speed and at the same time comprehends the traditional association with the supply frequency.

8-3 Suggestions for Future Work

The areas for further investigation based on this thesis are:

(a) The treatment of coincident eigenvalues from the modal view-point and investigation of the physical significance.

- (b) Stability investigation for unbalanced supply and / or supply with harmonic content.
- (c) Further development of Liapunov functions for the induction motor.

APPENDIX A

INDUCTION MOTOR POWER EQUATION

The power equation can be derived from Equation 2–10 by forming the scalar product

which yields

$$\begin{split} e_{d}^{s} & i_{d}^{s} + e_{q}^{s} i_{q}^{s} = R^{s} (i_{d}^{s^{2}} + i_{q}^{s^{2}}) + R^{r} (i_{d}^{r^{2}} + i_{q}^{r^{2}}) \\ & + f_{1} \omega_{1}^{2} + T_{L} \omega_{m} + n M \omega_{m} (i_{d}^{s} i_{q}^{r} - i_{q}^{s} i_{d}^{r} + p [\frac{1}{2} I^{s} (i_{d}^{s^{2}} + i_{q}^{s^{2}}) \\ & + \frac{1}{2} I^{r} (i_{d}^{r^{2}} + i_{q}^{r^{2}}) \\ & + \frac{1}{2} M \{ (i_{d}^{s} + i_{d}^{r})^{2} + (i_{q}^{s} + i_{q}^{r})^{2} \} + \frac{1}{2} J_{1} \omega_{m}^{2}] \end{split} \quad A - 1 \end{split}$$

This can be written in space-vectors defined in Equations 2-19 to 2-21 as

$$e_d^s i_d^s + e_q^s i_q^s = R^s \mathcal{F}_s^2 + R^r \mathcal{F}_r^2 + f_1 \omega_m^2 + T_L \omega_m$$

+ n M
$$_{s}^{3}$$
 $_{r}^{3}$ sin $(0'_{s} - 0'_{r})$ ω_{m} + p $(\frac{1}{2} I^{s} 3'_{s}^{2} + \frac{1}{2} I^{r} 3'_{r}^{2} + \frac{1}{2} M 3'_{m}^{2})$

$$+\frac{1}{2}J_1\omega_m^2)$$

APPENDIX B

INSTANTANEOUS AIRGAP POWER

It is demonstrated that the instantaneous airgap power $P_{ag} = \frac{T_{em} \frac{g}{m}}{n}$. The power equation of the induction motor will be examined in two successive stages.

Stator Power

The first two lines of Equation 2–10 can be written as

$$e_{d}^{s} i_{d}^{s} + e_{q}^{s} i_{q}^{s} = R^{s} \mathcal{F}_{s}^{2} + p \frac{1}{2} I^{s} \mathcal{F}_{s}^{2} + i_{d}^{s} M p (i_{d}^{s} + i_{d}^{r})$$

$$+ i_{q}^{s} M p (i_{q}^{s} + i_{q}^{r}) \qquad B-1$$

 R^{s} $3\frac{2}{s}$ and $\frac{1}{2}I^{s}$ $3\frac{2}{s}$ are the stator resistance dissipative loss and the magnetic energy stored in the stator leakage inductance respectively. Hence from the energy balance considerations, the last two terms consist of power which is (a) transferred to the rotor and (b) in part stored in the mutual inductance M. In order to identify these components, the vector representations of Figure 2-5 and the definition in Equations 2 - 19 to 2 - 21 will be made.

$$i_{d}^{s} M p (i_{d}^{s} + i_{q}^{s}) + i_{q}^{s} M p (i_{q}^{s} + i_{q}^{r})$$

$$= M \left[\Im_{s} \sin \emptyset_{s} p (\Im_{m} \sin \emptyset_{m}) + \Im_{s} \cos \emptyset_{s} p (\Im_{m} \sin \emptyset_{m}) \right]$$

$$= M \left(\Im_{s} \cos (\emptyset_{s} - \emptyset_{m}) p \Im_{m} + \Im_{s} \Im_{m} \sin (\emptyset_{s} - \emptyset_{m}) \mathring{\emptyset}_{m} \right) \quad B - 2$$

Substituting Equation B-2 back into Equation B-1 and substituting for the torque term of Equation 2-23 (b), the stator power balance equation is:

$$e_{\mathbf{d}}^{\mathbf{s}} i_{\mathbf{d}}^{\mathbf{s}} + e_{\mathbf{q}}^{\mathbf{s}} i_{\mathbf{q}}^{\mathbf{s}} = R^{\mathbf{s}} \mathfrak{F}_{\mathbf{s}}^{\mathbf{2}} + p \left(\frac{1}{2} I^{\mathbf{s}} \mathfrak{F}_{\mathbf{s}}^{\mathbf{2}}\right) + M \mathfrak{F}_{\mathbf{s}} \cos (\emptyset_{\mathbf{s}} - \emptyset_{\mathbf{m}}) p \mathfrak{F}_{\mathbf{m}} + \frac{T_{\mathbf{em}} \emptyset_{\mathbf{m}}'}{n}$$

$$+ \frac{T_{\mathbf{em}} \emptyset_{\mathbf{m}}'}{n}$$

$$B - 3$$

Rotor Power

Likewise, the power associated with rotor can be written by forming the scalar product with the third and fourth rows of Equation 2 – 10.

$$0 = R^{r} \mathcal{F}_{r}^{2} + p \left(\frac{1}{2} I^{r} \mathcal{F}_{r}^{2}\right) + M \mathcal{F}_{r} \cos \left(\emptyset_{m} - \emptyset_{r}^{2}\right) p \mathcal{F}_{m}$$

$$+ \omega_{m} T_{em} - \frac{T_{em} \mathscr{G}_{m}^{2}}{n}$$

$$B - 4$$

From the trigonometric relationships of Figure 2 - 5 (c),

$$\mathcal{F}_{r} \cos \left(\mathcal{O}_{m} - \mathcal{O}_{r} \right) + \mathcal{F}_{s} \cos \left(\mathcal{O}_{s} - \mathcal{O}_{m} \right) = \mathcal{F}_{m}$$

$$B - 5$$

and hence when Equation B-3 to Equation B-4 are added, the terms

$$M \quad \mathcal{F}_{s} \quad \cos \left(\mathcal{O}_{s}' - \mathcal{O}_{m}' \right) p \quad \mathcal{F}_{m} + M \quad \mathcal{F}_{r} \quad \cos \left(\mathcal{O}_{m}' - \mathcal{O}_{r}' \right) p \quad \mathcal{F}_{m} = p \left(\frac{1}{2} M \quad \mathcal{F}_{m}^{2} \right)$$

$$B - 6$$

and the sum yields the complete power equation, Equation A - 2. It is noted that

the term $\frac{T_{em} \frac{9}{m}}{n}$ has opposite signs in Equation B - 3 and Equation B - 4 and cancels out. Therefore from physical considerations, $\frac{T_{em} \frac{9}{m}}{n}$ is the airgap power.

APPENDIX C

EIGENVECTOR ROTATIONAL PROPERTY

Assertion

If O_k + $i\omega_k$ is the eigenvalue of $[A_{dq}]$ in Equation 4-2, then the corresponding eigenvector can be written in the form $\underline{U}_k = \underline{U}_r + i [\Phi] \underline{U}_r$ where $[\Phi]$ is defined in Equation 5 - 36.

Proof

its form

From definition, the eigenvector $\underline{U}_k = \underline{U}_r + i \underline{U}_i$ satisfies the equation

$$[A_{dq}] \underline{U}_{k} = (\delta_{k} + i \omega_{k}) \underline{U}_{k}$$
 C-1

In practice the 8 unknown components in \underline{U}_k are solved for the set of 8 simultaneous linear algebraic equations which is obtained by equating the real and the imaginary parts of Equation C-1, i.e.

C - 2

However [Ada] has basic rotation symmetric properties because of

$$[A_{dq}] = \begin{bmatrix} m & n & p & r \\ -n & m & -r & p \\ \hline t & x & y & z \\ -x & t & -z & y \end{bmatrix}$$

Equation C-3 expresses $\begin{bmatrix} A_{dq} \end{bmatrix}$ in algebraic components m, n etc., to emphasize the rotational symmetry in each partition. Because of the special form of Equation C-3 the following substitution is made for Equation C-2

$$\underline{U}_{i} = [\Phi] \underline{U}_{r}$$
 C-4

in which case Equation C-2 reduces to

$$[[A_{dq}] - O_k[1] + \omega_k[\Phi]] \underline{U}_r = 0 \qquad C-5$$

. and

$$[[A_{dq}][\Phi] - O_k[\Phi] - \omega_k[I]] \underline{U}_r = 0 \qquad C-6$$

Hence it is required to show that the same 4 numbers in $\underline{U}_r^T = [U_1, U_2, U_3, U_4] \text{ satisfy both Equation C - 5 and Equation C - 6 simultaneously.}$ Equation C - 5 expands to

$$\begin{bmatrix} m - 6_k & n - \omega_k & p & r \\ - (n - \omega_k & m - 6_k & -r & p \\ t & x & y - 6_k & z - \omega_k \\ - x & t & - (z - \omega_k) & y - 6_k \end{bmatrix} \begin{bmatrix} U_1 \\ U_2 \\ U_3 \\ U_4 \end{bmatrix} = \begin{bmatrix} 0 \\ 0 \\ 0 \\ 0 \end{bmatrix}$$

$$C - 7$$

and Equation C - 6 expands to

$$\begin{bmatrix} n - \omega_k & -(m - \mathring{\bigcirc}_k) & r & -p \\ m - \mathring{\bigcirc}_k & n - \omega_k & p & r \\ x & -t & z - \omega_k - (y - \mathring{\bigcirc}_k) \\ t & x & y - \mathring{\bigcirc}_k & z - \omega_k \end{bmatrix} \begin{bmatrix} U_1 \\ U_2 \\ U_3 \\ U_4 \end{bmatrix} = \begin{bmatrix} 0 \\ 0 \\ 0 \\ 0 \end{bmatrix}$$

By inspection, Equation C – 8 is the same set of simultaneous equations as Equation C – 7 except for the interchange of the first and the second rows, and the interchange of the third and fourth rows. This proves that $\underline{U}_k = \underline{U}_r + i \begin{bmatrix} \Phi \end{bmatrix} \underline{U}_r$ is indeed the eigenvector of Equation C – 3.

APPENDIX D

MODE OSCILLATING FREQUENCY

The natural frequency of oscillation ω_k is expressed explicitly in terms of the induction motor parameters and the components of the eigenvector \underline{U}_k .

From definition of eigenvector

$$[A_{dq}] \underline{U}_{k} = (\delta_{k} + i \omega_{k}) \underline{U}_{k}$$
D-1

but from Appendix C

$$\underline{U}_{k} = \underline{U}_{r} + i \left[\Phi \right] \underline{U}_{r}$$

Premultiply D-1 by the transpose of the complex conjugate of U_k , i.e.

$$\underline{U}_{k}^{*} = \underline{U}_{r} - i [\Phi] \underline{U}_{r}$$

and this yields the scalar product

$$\underline{U}_{k}^{*T} [A_{dq}] \underline{U}_{k} = (6_{k} + i\omega_{k}) \underline{U}_{k}^{*T} \underline{U}_{k}$$
D-4

$$\left(\underline{U}_{r}^{\mathsf{T}} - i \underline{U}_{r}^{\mathsf{T}} [\Phi]^{\mathsf{T}} \right) [A_{\mathsf{dq}}] \left(\underline{U}_{r} + i [\Phi] \underline{U}_{r} \right) = (\mathcal{O}_{k} + i \omega_{k}) \left(\underline{U}_{r}^{\mathsf{T}} - i \underline{U}_{r}^{\mathsf{T}} [\Phi]^{\mathsf{T}} \right) \\
\left(\underline{U}_{r} + i [\Phi] \underline{U}_{r} \right) \qquad \mathsf{D} - \mathsf{5}$$

Equating the imaginary parts of Equation D-5

$$\underline{U}_{r}^{\mathsf{T}} \left[A_{\mathsf{dq}} \right] \left[\Phi \right] \underline{U}_{r} - \underline{U}_{r}^{\mathsf{T}} \left[\Phi \right]^{\mathsf{T}} \left[A_{\mathsf{dq}} \right] \underline{U}_{r} = \omega_{\mathsf{k}} \left(\underline{U}_{r}^{\mathsf{T}} \underline{U}_{r} + \underline{U}_{r}^{\mathsf{T}} \left[\Phi \right]^{\mathsf{T}} \left[\Phi \right] \underline{U}_{r} \right) - \mathcal{O}_{\mathsf{k}} \left(\underline{U}_{r}^{\mathsf{T}} \left[\Phi \right] \underline{U}_{r} - \underline{U}_{r}^{\mathsf{T}} \left[\Phi \right] \underline{U}_{r} \right)$$

But from the property of $[\Phi]$ in Equation 5 – 36, it can be shown that

$$\underline{U}_{r}^{T} \left[\Phi \right]^{T} \underline{U}_{r} = 0 \qquad \qquad D-7$$

$$\underline{U}_{r}^{\mathsf{T}} \left[\Phi \right] \underline{U}_{r} = 0 \qquad \qquad \mathsf{D} - \mathsf{8}$$

and
$$\underline{U}_r^T [\Phi]^T [\Phi] \underline{U}_r = \underline{U}_r^T \underline{U}_r$$
 D-9

Substituting Equation D - 7 to Equation D - 9 into Equation D - 6, the coefficients of σ_k become zero and ω_k can be expressed explicitly as follows

$$\omega_{k} = \frac{\underline{U}_{r}^{T} \left[A_{dq}\right] \left[\Phi\right] \underline{U}_{r} - \underline{U}_{r}^{T} \left[\Phi\right]^{T} \left[A_{dq}\right] \underline{U}_{r}}{2 \underline{U}_{r}^{T} \underline{U}_{r}} \qquad D-10$$

Equation 5 – 52 follows from substituting the matrix $[A_{dq}]$, \underline{U}_r and "normalizing" \underline{U}_r^T \underline{U}_r = 1.

E - 2

E - 3

APPENDIX E

A METHOD OF CONSTRUCTING THE POSITIVE DEFINITE [P] MATRIX

A systematic method of generating the [P] matrix is through the formula:

$$[P] = [E_1] [E_2] \dots [E_n] [K] [E_n]^T \dots [E_2]^T [E_1]^T$$

$$E - 1$$

where

$$\begin{bmatrix} \mathsf{K} \end{bmatrix} = \begin{bmatrix} \mathsf{k}_1 & & & \\ & \mathsf{k}_2 & & \\ & & \mathsf{k}_3 & \\ & & & \mathsf{k}_4 & \\ & & & & \mathsf{k}_5 \end{bmatrix}$$

and where $k_i > 0$ for $i = 1, 2, \dots 5$.

Each $[E_n]$ is of the form

$$\begin{bmatrix} E_n \end{bmatrix} = \begin{bmatrix} 1 & 0 & 0 & 0 & 0 \\ 1 & 0 & \cos \theta_n & 0 & \sin \theta_n & 0 \\ 0 & 0 & 1 & 0 & 0 \\ 1 & 0 & -\sin \theta_n & 0 & \cos \theta_n & 0 \\ 0 & 0 & 0 & 0 & 1 \end{bmatrix}$$

i.e. $[E_n]$ is a 5×5 unit matrix with the following changes

$$E_{ii} = E_{ii} = \cos \theta_n$$

F-4

$$E_{ij} = -E_{ji} = \sin \theta_{n}$$

where θ_n is any arbitrary angle.

Using Equation E-1, \underline{x}^T [P] \underline{x} is a function of a hyper-ellipsoid in 5 - dimensional space. The values of k_i in Equation E - 2 specify the relative magnitudes of the principal axes for the ellipsoid. The matrices $[E_n]$ rotate the ellipsoid at an angle θ_n in the plane of the ith and jth axes. By varying k_i and θ_n , a positive definite matrix [P] is generated from which the quadratic Liapunov Function is constructed using Equation 6 - 35.

F-2

APPENDIX F

SIMULTANEOUS EQUATIONS FOR SOLVING

QUADRATIC LIAPUNOV FUNCTIONS

The symmetric [V] matrix of Equation 6-35 consists of 15 unknowns

$$\nu_1$$
, ν_2 ... ν_{15}

$$\begin{bmatrix}
v_1 & v_2 & v_3 & v_4 & v_5 \\
v_2 & v_6 & v_7 & v_8 & v_9 \\
v_3 & v_7 & v_{10} & v_{11} & v_{12} \\
v_4 & v_8 & v_{11} & v_{13} & v_{14} \\
v_5 & v_9 & v_{12} & v_{14} & v_{15}
\end{bmatrix}$$

The positive definite <code>[P]</code> matrix in Equation 6 – 36 is specified by the elements <code>p_1</code> , <code>p_2</code> ... <code>p_{15}</code> in

$$[P] = \begin{bmatrix} P_1 & P_2 & P_3 & P_4 & P_5 \\ P_2 & P_6 & P_7 & P_8 & P_9 \\ P_3 & P_7 & P_{10} & P_{11} & P_{12} \\ P_4 & P_8 & P_{11} & P_{13} & P_{14} \\ P_5 & P_9 & P_{12} & P_{14} & P_{15} \end{bmatrix}$$

The unknown values of the [V] matrix are solved using the relationship of Equation 6 – 35 which is expanded to a 15 – order simultaneous equation as shown in Equation F – 3, where a_{ij} are the elements of Equation 6 – 5.

°21	^a 31	a ₄₁	^a 51								• .			1	ν 1	₹ p
a ₁₁ +a ₂₂	^a 32	a ₄₂	α ₅₂	^a 21	^a 31	a ₄₁	^a 51								ν 2	2
^a 23	a11 ^{+a} 33	^a 43	^a 53		^a 21			^a 31	^a 41	^a 51					3	2
^a 24	a ₃₄	a ₁₁ +a ₄₄	a ₅₄			^a 21			^a 31		a ₄₁	^a 51			ν 4	2 p
^a 25	^a 35	^a 45	a ₁₁ +a ₅₅	5	٦		^a 21			^a 31	•	a ₄₁	a ₅₁		ν 5	2P
^a 12				a ₂₂	α ₃₂	^a 42	^a 52						-		ν 6	. P.
^a 13	^a 12			^a 23	^a 22 ^{+a} 33	3 ^a 43	^a 53	^a 32	a ₄₂	a ₅₂	•				ν 7	2 _{P7}
a ₁₄		^a 12		^α 24	^a 34	^a 22 ^{+a} 44	^a 54		a ₃₂	·	^a 42	a ₅₂			ν 8	2 p ₈
^a 15			a ₁₂	°25	^a 35	^a 45	^a 22 ^{+a} 55			α ₃₂	·	a ₄₂	a ₅₂		ν 9	2 _P
	^a 13				°23			a ₃₃	^a 43	a ₅₃	ì				ν 10	. p ₁
	^a 14	^a 13			^a 24	^a 23		a ₃₄ .	^a 33 ^{+a} 44	a ₅₄	a ₄₃	α ₅₃	:		ا11 ا	2p
	^a 15		^a 13		^a 25		^a 23	^a 35	a ₄₅	^a 33 ^{+a} 55		a ₄₃	a ₅₃		ا 12	2p
		^a 14			•	^a 24			^a 34		a ₄₄	a ₅₄	· .		.υ 13	. p.
٠.		a ₁₅	a ₁₄		ı	^a 25	^a 24	·	^a 35	^a 34	a ₄₅	a ₄₄ +a ₅₅	a ₅₄		بر. 14	2p.

APPENDIX G

INDUCTION MOTOR PARAMETERS

A typical induction motor whose parameters are listed below, have been used throughout in the numerical examples

$$R^{S} = R^{\Gamma} = 1$$
 ohm.

$$L^{s} = L^{r} = 0.1113$$
 henry.

$$M = 0.106 \text{ henry.}$$

$$n = 1$$

REFERENCES

- [1] Kron, G., "The Application of Tensors to the Analysis of Rotating Electrical Machinery", General Electric Review, 1938, 36, pp. 181 et seq.
- [2] Lyon, W.V., "Transient Conditions in Electric Machinery", Trans.
 A.I.E.E., February 1923.
- [3] Park, R.H., "Two-Reaction Theory of Synchronous Machines II", Trans.

 A.I.E.E., 1933, pp. 352 355.
- [4] Stanley, H.C., "An Analysis of the Induction Motor", Trans. A.I.E.E., 1938, 57, pp. 751.
- [5] Gibbs, W.J., "Tensors in Electrical Machine Theory", Chapman and Hall, London, 1952.
- [6] Adkins, B., "The General Theory of Electrical Machines", Chapman and Hall, London, 1957.
- [7] White, D.C. and Woodson, H.H., "Electromechanical Energy Conversion", John Wiley, New York, 1959.
- [8] Gilfillan, F.S. and Kaplan, E.L., "Transient Torques in Squirrel Cage Induction Motors with Special Reference to Plugging", Trans. A.I.E.E., 1941, 60, pp. 1200 1209.
- [9] Lyon, W.V., "Transient Analysis of Alternating-Current Machinery",

 John Wiley, N.Y., 1954, pp. 297 298.
- [10] Maginniss, F.J. and Schultz, N.R., "Transient Performance of Induction Motors", Trans. A.I.E.E., 1940, 59, pp. 603.

- [11] Weygandt, C.N. and Charp, S., "Electromechanical Transient Performance of Induction Motors", Trans. A.I.E.E., 1946, 65, pp. 1000 1009.
- [12] Blom, J.F., "The Transient Behaviour of a Three-Phase Induction Motor Studied with an Analogue Computer", Ingenieur, 1959, 71, pp. E 61.
- [13] Blom, J.F., "The Influence of the Switch on the Transients of the Three-Phase Induction Machine", ibid., 1963, 75, pp. E 181.
- [14] Hughes, F.M. and Aldred, A.S., "Transient Characteristics and Simulation of Induction Motors", Proc. I.E.E., 1964, 111, (12), pp. 2041.
- [15] Slater, R.D., Wood, W.S., Flynn, F.P. and Simpson, R.: 'Digital Computation of Induction Motor Transient Torque Patterns,' Proc. 1.E.E., 1966, 113, (5), p. 819.
- [16] Smith, I.R. and Sriharan, S.: 'Transient Performance of the Induction Motor', ibid., 1966, 113, (7), p. 1173.
 - [17] Smith, I.R. and Sriharan, S.: 'Induction-motor Reswitching Transients', ibid., 1967, 114, (4), p. 503.
 - [18] Howard E. Jordan: 'Digital Computer Analysis of Induction Machines in Dynamic Systems', IEEE Trans. Power Apparatus and Systems, vol. 86, p. 722, June 1967.
 - [19] Wahl, A.M. and Kilgore, L.A., "Transient Starting Torques in Induction Motors", Trans. A.I.E.E., 1940, 59, pp. 603 607.

- [20] Chidambara, M.R. and Ganapathy, S., "Transient Torques in 3 Phase Induction Motors During Switching Operations", Trans. A.I.E.E., 1962, 59, pp. 47 53.
- [21] Enslin, N.C., Kaplan, W.M. and Davies, J.L.: 'Influence of Transient Switching Currents and Fluxes on the Torque Developed by a Squirrel-cage Induction Motor', Proc. I.E.E., 1966, 113, (6), p. 1035.
- [22] Slater, R.D. and Wood, W.S.: 'Constant-speed Solutions Applied to the Evaluation of Induction-motor Transient Torque Peaks', ibid., 1967, 114, (10), p. 1429.
- [23] Lyon, W.V., "Transient Analysis of Alternating Current Machinery", John Wiley, New York, 1954, pp. 240 266.
- [24] Rogers, G.J., "Linearised Analysis of Induction-Motor Transients", Proc. I.E.E., 1965, 112, (10), pp. 1917 1926.
- [25] Nelson, R.H., Lipo, T.A. and Krause, P.C., "Stability Analysis of a Symmetrical Induction Machine", I.E.E.E. Paper No. 69 TP 137-PWR, presented at Winter Power Meeting, New York, January 26-31, 1969.
- [26] Fallside, F. and Wortley, A.T., "Steady-state Oscillation and Stabilization of Variable-frequency Inverter-fed Induction Motor Drives",

 Proc. I.E.E., vol. 116 (6) 1969, pp. 991 999.
- [27] Burridge, R.E. and Barton, T.H., "Investigation of a Power Synchro System –
 Analysis and Experimental Results", Paper No. 69 TP 724 PWR,
 presented at the IEEE Summer Power Meeting, Dallas, Texas, June
 1969. To be published in IEEE Trans. on P.A.S.
- [28] Ager, R.W., "Transient Overspeeding of Induction Motors", Trans. A.I.E.E., 1941, 60, pp. 1030 1032.

- [29] Wood, W.S., Flynn, F.P. and Shanmugasundaram, A.: "Transient Torques in Induction Motors, due to Switching of the Supply", Proc. I.E.E.

 1965, 112, (7), p. 1348 1354.
- [30] Discussion on "Transient Effects in Induction Motors", Proc. I.E.E., 1968, 115, (1), p. 128.
- [31] Fitzgerald, A.E. and Kingsley, C. Jr., "Electric Machinery", McGraw-Hill, New York, 1952, pp. 324 333.
- [32] Barton, T.H. and Dunfield, J.C., "Polyphase to Two-Axis Transformation for Real Windings", IEEE Trans. on Power Apparatus and System, vol. PAS 87, No. 5, May 1968, pp. 1342 1346.
- [33] Barton, T.H., "A Generalized Theory of Electromechanical Energy Conversion", McGill University.
- [34] Robertson, S.D.T. and Hebbar, "A Digital Model for Three Phase Induction Machines", IEEE Paper No. 69 TP 6 PWR presented in Winter Power Meeting, New York, January 26 31, 1969.
- [35] Hancock, N.N., "The Parameters used in Matrix and Tensor Analysis of Electrical Machines", Int. J. Electrical Engineering Education, vol. 5, p. 590, Pergamon Press 1967.
- [36] Clarke, E., "Circuit Analysis of A.C. Power Systems", vol. 1, John Wiley, New York, 1943.
- [37] White, D.C. and Woodson, "Electromechanical Energy Conversion", John Wiley, New York, 1959, pp. 259 265.
- [38] ibid., pp. 265 278.
- [39] ibid., pp. 300 304.

- [40] Wiederholt, L. F., Fath, A.F., and Wertz, H.J.: 'Motor Transient Analysis on a Small Digital Computer', IEEE Trans., P.A.S., vol. 86, July 1967, pp. 819.
- [41] Hilderbrand, F.B., "Introduction to Numerical Analysis", McGraw-Hill, New York, 1956, pp. 233 239.
- [42] ibid., pp. 199 202.
- [43] Ralston, A. and Wilf, H.S., "Mathematical Methods for Digital Computers", Wiley, New York, 1960, pp. 110 120.
- [44] ibid., pp. 95 109.
- [45] Prabhashanker, K. and Wasyl Janischewsyj, 'Digital Simulation of Multi-machine Power Systems for Stability Studies', IEEE Trans. P.A.S., vol. 87, January 1968, pp.73.
- [46] Chen, M.S. and Duesterhoeft Jr., "Digital Computation of Transients in Synchronous Machines with Capacitive Loads", IEEE Trans., P.A.S., April 1964, pp. 369 376.
- [47] I.B.M. System 360 Scientific Subroutine Package (360A CM 03X)

 Version III, Programmer's Manual, H20 0205 3, pp. 333 336.
- [48] ibid, pp. 337 343.
- [49] ibid, pp. 221 225.
- [50] Stanton, N. K., Talukdar, S. N., "New Integration Algorithms for Transient Stability Studies", IEEE Paper No. 69 TP 646 PWR, presented at IEEE Summer Power Meeting, Dallas, Texas, June 22 27, 1969.

- [51] Zadeh, L. A. and Desoer, C. A., "Linear System Theory: The State

 Space Approach", McGraw-Hill, New York 1963, pp. 311 322.
- [52] De Russo, P. M., Roy, R. J. and Close, C. M., "State Variables for Engineers", John Wiley, New York, 1965, pp. 344 349.
- [53] Guillemin, E. A., "Theory of Linear Physical Systems", John Wiley, New York, 1963, pp. 159 213.
- [54] SHARE, Program Library Short Write Up SDA 3385.
- [55] Lipo, T.A. and Krause, P. C., "Stability Analysis of a Reluctance –
 Synchronous Machine", IEEE Transactions on Power Apparatus and
 Systems, vol. 86, July 1967, pp. 825 834.
- [56] Lipo, T.A. and Krause, P.C., "Stability Analysis for Variable Frequency Operation of Synchronous Machines", IEEE Transactions on Power Apparatus and Systems, vol. 87, January 1968, pp. 227 233.
- [57] Lipo, T.A. and Krause, P.C., "Stability Analysis of A Rectifier –
 Inverter Induction Motor Drive", IEEE Transactions on Power Apparatus
 and Systems, vol.88, January 1969, pp. 55 56.
- [58] Wilkinson, J. H., "The Algebraic Eigenvalue Problem", Clarendon Press
 Oxford 1965, Chapter 2, Perturbation Theory.
- [59] Lasalle, J. and Lefschetz, S., "Stability by Liapunov's Direct Method with Applications", New York, Academic Press 1961.
- [60] Hahn, W., "Theory and Application of Liapunov's Direct Method", (Translation from German), Englewood Cliffs, N.J., Prentice Hall, 1963.
- [61] ibid., pp. 35, Chapter 3, Section 11, Bounds for Initial Values..
- [62] ibid., pp. 78, Chapter 4, Section 21, Zubov's Method of Construction.

- [63] ibid., pp. 26, Chapter 3, Section 8, Construction of a Liapunov Function for a Linear Equation with Constant Coefficient.
- [64] Margolis, S.G. and Vogt, W.G., "Control Engineering Applications of V. I. Zubov's Construction Procedure for Liapunov Functions", IEEE Trans. Automatic Control, vol. AC-8, April 1963, pp. 104 113.
- [65] Yu, Y.N. and Vongsuriya, K., "Nonlinear Power System Stability Study by Liapunov Function and Zubov's Method", IEEE Trans. PAS 86, December 1967, pp. 1480 1484.
- [66] Undrill, J.M., discussion on [65], IEEE Trans., PAS 86, December 1967, pp. 1485.
- [67] Korn and Korn, "Mathematical Handbook For Scientists and Engineers", MaGraw-Hill, New York, 1968, 13. 5 6.
- [68] Wilde, D.J., Beightler, C.S., "Foundations of Optimization", Prentice-Hall, 1967.
- [69] Fletcher, R. and Powell, M.J.D., "A Rapid Descent Method for Minimization", Computer Journal, vol. 6, ISS. 2, 1963, pp. 163 – 168.
- [70] Van Ness, J.E., Boyle, J.M. and Imad, F.P., 'Sensitivity of Large,
 Multiple-Loop Control Systems', IEEE Trans. on Automatic Control,
 vol. AC-10, July 1965, p. 308.
- [71] Faddeev, D.K. and Faddeeva, V.N., "Computational Methods of Linear Algebra," San Francisco, California, Freeman 1963, pp. 228 229.